Ontogenetic Change in Primate Pelvic Morphology:

The Hominoid Ilium.

Thesis submitted in accordance with the requirements of the University of Liverpool for the degree of Doctor in Philosophy

By

Richard Leslie Abel

5th May 2006

Abstract

The growth and development of the hominoid *os ilium*, both cortical (external) and trabecular (internal), was studied from a comparative point of view. *Os ilia* representing *Homo sapiens* (modern human), *Pan troglodytes* (common chimpanzee), *Gorilla gorilla* (gorilla), and *Cercopithecus* sp. (old world monkeys) were analysed. Ontogenetic allometric changes in external iliac morphology, and external-internal combined (hominoids only), were assessed using landmark based geometric morphometric methods. External landmarks were digitised directly from bones and internal landmarks were taken from radiographs. The internal landmarks described the position of two trabecular bundles (struts): a posterior one, spanning the auricular surface and acetabulum and an anterior one, passing from the anterior iliac crest towards the acetabulum and/or ischium. Analyses of ontogenetic changes in bone density distribution (which utilised data taken from high resolution computed tomography) revealed that the iliac struts appeared soon after birth. Probably as a result of selective loss of bone from the posterior portion of the iliac fossa. After infancy, the position of the iliac trabecular struts changed with respect to external morphology. This finding is consistent with the notion that trabecular bone is more plastic than cortical tissue. Trabecular tissue may exhibit greater plasticity because (1) after infancy cortical tissue loses some capacity to model in response to applied loads, but trabecular bone maintains the ability to model throughout ontogeny (2) cortical tissue is more functionally and/or phylogenetically constrained. In support of this it was found that the African apes and cercopithecines share common ontogenetic allometries, calculated from external landmarks, which are distinct from that of modern humans. The results of this study have implications regarding the manner in which fossil remains are investigated. Comparative and developmental

studies of external bony morphology may be more appropriate for inferring phylogeny, whilst studies of trabecular morphology might be better suited for reconstructing locomotor behaviour.

Contents

List of Figures

List of Tables

Acknowledgments

I would like to thank my supervisor Prof. G. Macho of the University of Roehampton. I would also like to thank Dr M. Günther of the University of Liverpool (Liverpool, UK) for allowing me to borrow a microscribe. Thank you to Professor R. Foley, Dr Marta Lahr for allowing access the collection at the Leverhulme Centre for Human Evolutionary Studies (Cambridge, UK). Thanks to M. Bellatti for her help and support at the Duckworth laboratory. Thanks also to Dr H Schutkowski for allowing access to the collections at the Department of Archaeological Sciences, University of Bradford (Bradford, UK) and D. Weston for help with the specimens. Also thanks to J. Harrison and M. Harman of the Powell Cotton Museum (Birchington, Kent) for allowing access to the primate collection. Many thanks to Dr D Scutt of the Medical Imaging Unit at the University of Liverpool (Liverpool UK) for operating radiographic equipment. Also, thanks to Professor JA Gallagher for logistical support.

This work is supported by the NERC Ref. NER/S/A2001/06485

Part I: Analysing Growth and Development of the Hominoid Ilium

Chapter 1. Principals of Scaling, Relative Growth and Allometry

1.1. Overview

The pelvis is situated between the trunk and the lower limbs (Figure 1.1a) and consists of the *os sacrum* and two *ossa coxae* (Figure 1.1b). This thesis explores the development of the hominoid pelvis from a comparative point of view. The study considers both cortical (external) and trabecular (internal) morphology. This study aims to:

- determine whether external pelvic morphology of the hominoids changes during ontogeny
- infer the ancestral pattern of ontogenetic change in external iliac morphology of the hominoids using a cercopithecoid outgroup comparison and make phylogenetic inferences about the species
- infer whether trabecular structure changes during ontogeny, in relation to external morphology
- infer whether external and internal iliac morphology grow and develop independently during ontogeny
- infer whether the growth and development of cortical and trabecular iliac tissue is affected by external (i.e. hormonal) and/or internal (i.e. mechanical) stimuli
- infer whether external or internal morphology is more plastic (i.e. responsive to mechanical loading environment) during ontogeny

A cross sectional study was used to compare the growth and development of the ilium among the hominoids (internal) and cercopithecoids (external).Cortical morphology was characterised using measurements taken directly form bones.

Measurements of internal structure were collected from radiographic images and micro-computed tomographic reconstructions. Ontogenetic change in external and internal morphology was assessed in two ways (1) shape and structure were compared across developmental stages and (2) changes in shape associated with increases in size were studied (i.e. allometry).

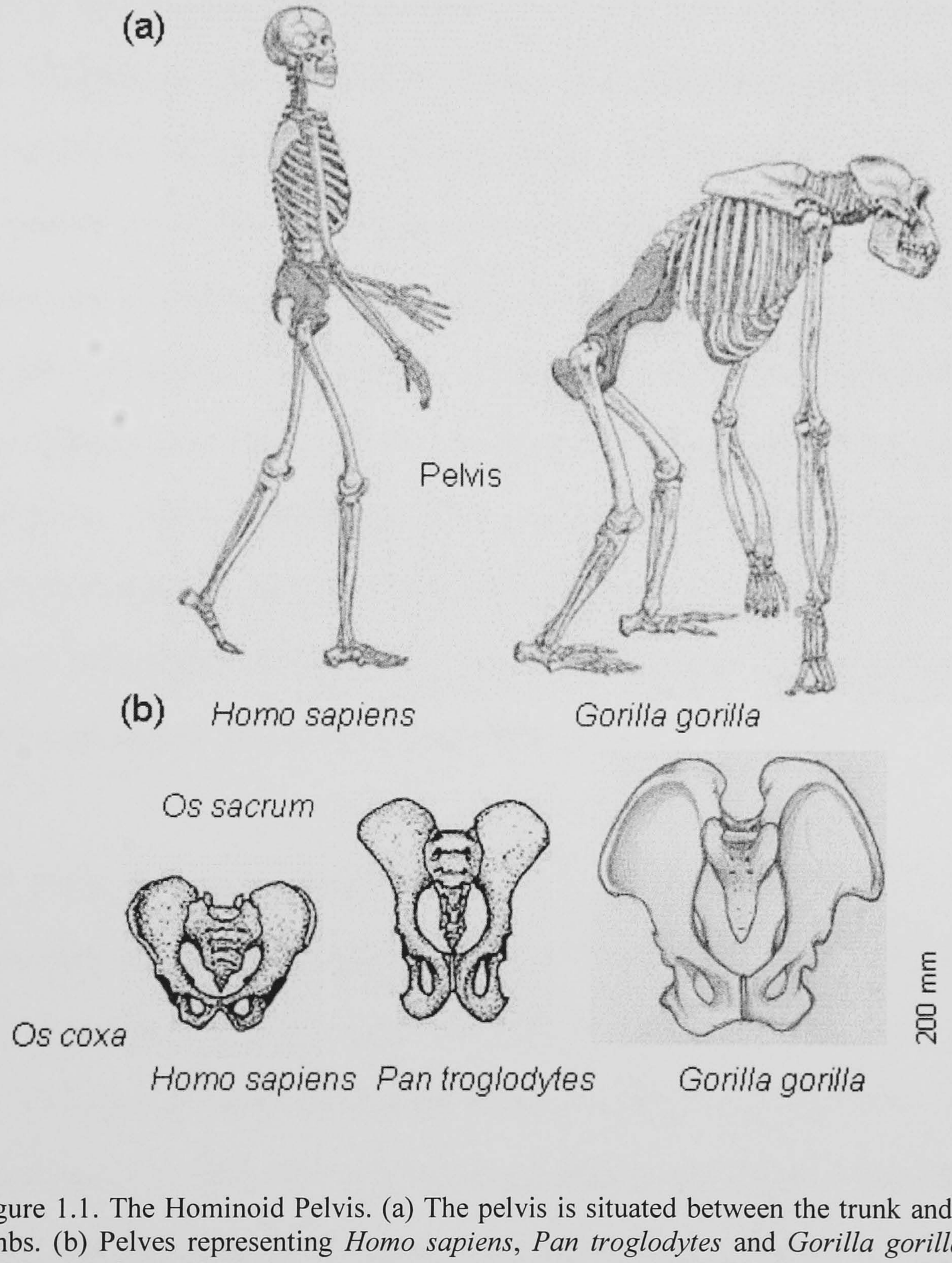

Figure 1.1. The Hominoid Pelvis. (a) The pelvis is situated between the trunk and lower limbs. (b) Pelves representing *Homo sapiens*, *Pan troglodytes* and *Gorilla gorilla*. The pelvis consists of the os sacrum and two os coxae. Drawings adapted from http://www.gpc.edu/~pgore/students/f97/glenda/pelvis.gif.

1.2. Covariation between organismal morphology and size

There is a pervasive tendency in biology for all aspects of organismal morphology to change in tandem with increasing size (Schmidt-Nielson, 1975). The principle of adjusting bodily shape (or proportions) with increasing size may be the most important determinant of the shape of organisms (Haldane, 1927). Consequently, any study of animal morphology will require an analysis of the association with overall size. Here the term "size" is used in reference to the geometric scale of an organism (or structure) (Bookstein, 1991; Rohlf, 1990a). Thus size refers to the physical dimensions of an object and has been measured using linear, area and volumetric dimensions or combinations thereof (Klingenberg, 1996a, 1996b; Mosimann, 1970). The study of change in morphology associated with increases in organismal size has been referred to in various guises as scaling, relative growth and allometry (see Blackstone, 1987ab; Klingenberg, 1998; Levington, 1988). This chapter describes how covariation between size and morphology has been conceptualised over the last century. In particular this chapter discusses how the concept of allometry developed and changed as mathematical techniques improved.

1.3. Dubois's concept of scaling

The modern concept of allometry has its roots in the first analyses of scaling (i.e. the study of change in measured anatomical features in relation to size). At the turn of the 19th century it was thought that the brains of mammals were relatively smaller in bigger species. Dubois (1897) developed a method to discriminate between the two factors that determine brain volume (i) organismal size and (ii) the degree of encephalisation (i.e. relative brain size). Mammalian brain mass was regressed against body mass and the association expressed as a power formula.

$$e = c \cdot s^r \quad (1.1)$$

where e was brain mass, s was body mass (not including the brain), c was the coefficient of encephalisation (intercept) and r the co-efficient of relation (slope). The study was repeated by Lapaicque (1907) on brain and body mass in dogs (*Canis familiaris*). The regressions were published along with a series of lines drawn at a 45^0 slope. The lines corresponded to a situation where the absolute ratio between brain and body mass was maintained with increases in body mass.

1.4. Pezard's concept of relative growth

The modern concept of allometry stems from research based on relative growth that began at the turn of the 20^{th} century. Relative growth refers the differential rates of growth of different body parts. The first published account of relative growth was written by Pezard in 1918 (Gayon, 2000). Pezard plotted measurements of cockerel morphology against overall body size and reported that some secondary sexual characteristics of the cockerel developed in accordance with body size whilst others did not. The important conclusion was that different body parts grew at different rates during development. Pezard proposed the term "isogonic growth" to describe the situation noted by Lapaicque (1907), where the ratio between variables x (body size) and y (secondary sexual characteristics) remained constant with increasing x. The term "heterogonic growth" was used to describe any instance where the ratio of x/y changed with increasing x. For this reason Pezard has been credited with being the first person to understand the importance of increasing size (as opposed to time) during ontogeny. All that was missing from Pezard's (1907) report was the algebraic form of the equation linking the measured dimensions x and y (Gaynon, 2000).

1.5. Concepts in allometry

1.5.1. Huxley's and Teissier's concept of allometry: covariation between size and proportions

By the early 1920's it was understood that body parts grew at different rates during development. Somewhat later Champy (1924, 1929) analysed the development of secondary sexual characteristics (i.e. physical attributes, other than the sexual organs, that distinguish males from females) in insects and suggested that in relation to body size growth followed a parabolic curve of the form,

$$V = qt^2 \tag{1.2}$$

where V was the measure of secondary sexual characteristics, t was body size and q was a constant. Champy (1924) had discovered that during ontogeny the growth rate of one anatomical feature changed in relation to overall body size i.e. relative growth rates of different parts of an organism changed over time. Huxley (1924) also reported that when two linear measurements of anatomical features from an ontogenetic series of growing organisms were plotted against each other, the scatter of data points followed a curved line. Huxley (1924) proposed a power law to describe the development of chelae in the fiddler crab,

$$y = bx^{\alpha} \tag{1.3}$$

where y is the magnitude of the differentially growing dimension; x is a measure of body size, α is the slope of the regression and b is the intercept. Huxley (1932) and Huxley & Teissier (1936a, 1936b) referred to this equation as the "formula of simple allometry" and termed (α) the allometric co-efficient.

The essential theoretical feature of this formula is that the constant (α) is not a ratio of two sizes but rather a ratio of two growth *rates*. The allometric coefficient α is determined by the ratio of the specific growth rates of two anatomical features:

$$\alpha = \frac{(dy/dt)/y}{(dx/dt)/x} \qquad (1.4)$$

where d denotes a change and t denotes time (Huxley, 1932; Kowalski & Guire, 1974; Laird, 1965; Lande, 1985; Reeve & Huxley, 1945; Shea, 1985bd). Provided the ratio of the specific growth rates of the two features remains constant the allometric coefficient will also remain constant. If the specific growth rate of a feature varies during ontogeny the bivariate plot yields a curved line (Huxley, 1924; Laird 1965, Shea, 1985b).

When Huxley introduced the equation of simple allometry, he specifically referred to a process known as multiplicative growth, also known as logarithmic growth (Medawar, 1945). Huxley (1924, 1932) perceived growth as the self multiplication of a living organism. Katz (1980) reported that values of α may be related directly to the relative frequency of cell division (as supposed to cell size) between the anatomical features compared. Self multiplication slows down with increasing age (and size). The self–multiplication of a living substance results in exponential growth. Huxley (1932) surmised that the relationship between the sizes of two parts of an organism was a logarithmic one (Laird, 1965). Huxley found that the curvilinear relationship between two dimensions became linear if the two data sets were transformed to logarithms. Huxley noted that the power law could be expressed as a logarithmic equation, which takes the form,

$$\text{Log } y = \alpha \text{ Log } x + \text{Log } b \qquad (1.5)$$

Thompson (1942) re-evaluated prior studies of allometry, including those published by Huxley (1932) and demonstrated that untransformed linear equations fitted many data sets as well as power functions did,

$$y = \alpha x + b \tag{1.6}$$

The simple allometric equation described by Huxley and Teissier is useful because the relationship between two measured traits can be interpreted easily. The allometric coefficient reflects the relative changes in the proportions of structures (Figure 1.2).

The special case where $\alpha = 1$ indicates direct proportionality between the two measured traits is referred to as "isometry". When the variable on the ordinate axis gets proportionately smaller in relation to the size of the variable on the abscissa the pattern of covariation was termed "negative allometry" ($\alpha < 1$). A situation where the measurement on the ordinate axis becomes proportionately larger in relation to the measurement on the abscissa axis was termed "positive allometry" ($\alpha > 1$). In most bony morphometric data sets measurements are positively correlated with size (Klingenberg, 1998) because bones do not get smaller with increasing body size (excepting pathological conditions and degeneration in old age). It should be noted that this scheme only applies when the abscissa and ordinate axes are portrayed in the same unit of measurement. If this is not the case the values of α should be altered accordingly.

1.5.2. Gould's Allometric modes

In Huxley and Teissier's scheme allometry referred to covariation between the sizes of parts of an organism during development. Since the conception of allometry the analyses have also been applied solely to adults from one, or more, species (e.g. Steudel, 1987). This led researchers to identify several allometric modes (e.g., Cock,

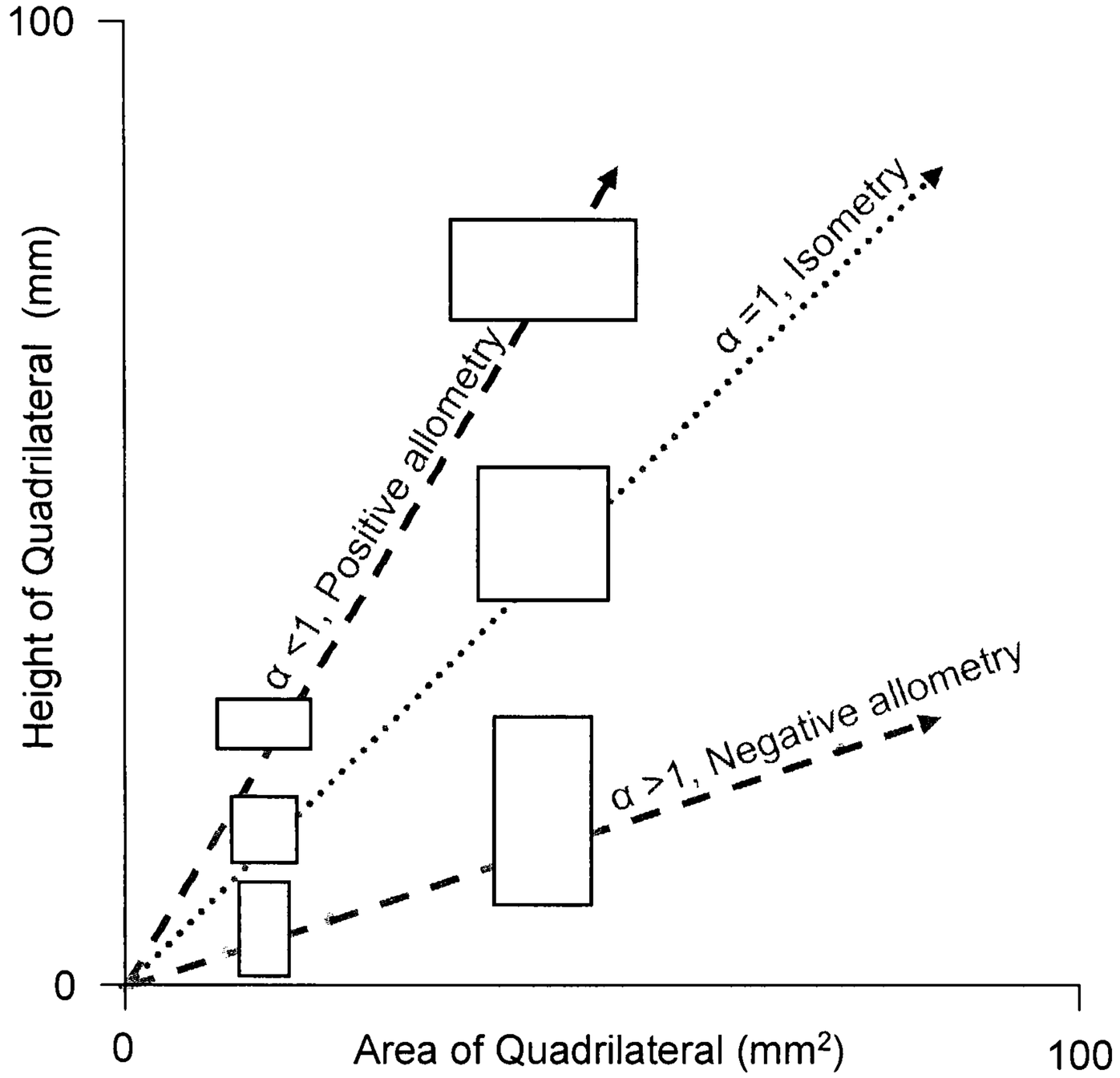

Figure 1.2. Huxley's and Teissier's (1936) concept of allometry. The term allometry refers to the pattern of ontogenetic covariation between the dimensions of two measured morphological features. Bivariate ontogenetic allometric regressions were used to calculate exponents (α) that described the association between two measured dimensions. Although allometry was primarily concerned with covariation between the sizes of parts of an organism the exponents describe changes in proportions that occur with increases in size.

1966; Gould, 1966). Three allometric modes are pertinent to this study (1) ontogenetic allometry, which refers to the relative growth of individuals; (2) intra-specific allometry, which refers to size related change in the proportions of adults within a single species (often referred to as "static" allometry) and (3) inter-specific allometry, which refers to the same phenomenon in adult individuals from related species (Fleagle, 1985) (Figure 1.3). Gould (1966, 1971) schematicised the interrelationship between the three allometric modes. Adult morphology is dependent on the pattern of growth and development during ontogeny.

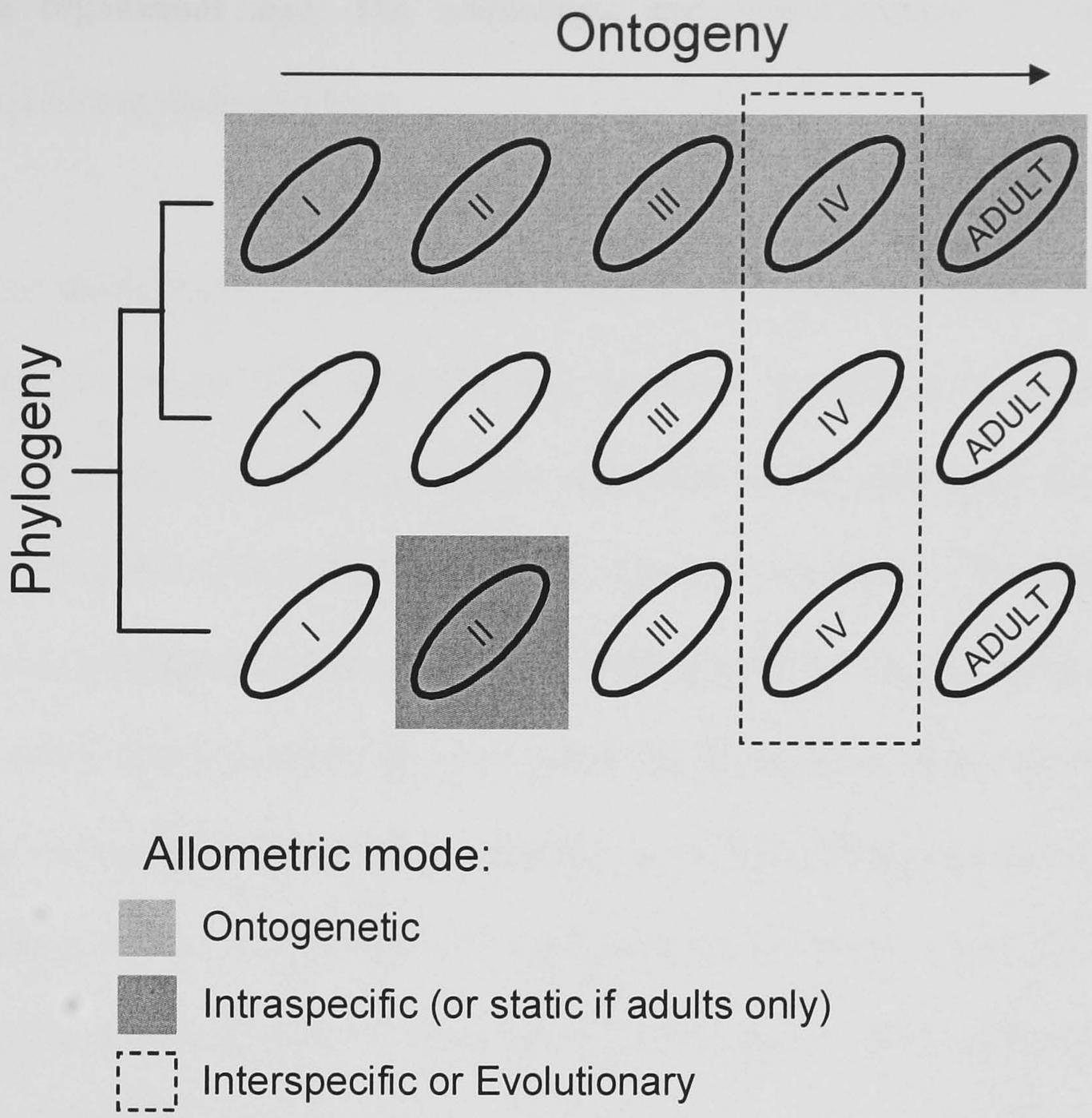

Figure 1.3. Gould's (1966) and Cock's (1966) modes of allometry. Ellipses denote developmental or growth stages e.g. size classes or dental eruption class. Allometry can be separated into three distinct modes depending on the type of data used in the analysis. (1) Ontogenetic allometry is based on an ontogenetic series of specimens from one species. (2) Intra-specific allometry is based on a set of specimens from the same developmental stage of one species. (3) Inter-specific allometry is based on sets of specimens belonging to the same developmental stage that represent two or more closely related species. Figure adapted from Klingenberg (1998).

1.5.3. Smith's comments on bivariate allometry

The type of data used in an allometric analysis will give some guide as to the methods that should be applied. Huxley and Teissier's use of logarithmic transformation in studies of growth allometry was directly related to the analysis of multiplicative, i.e. logarithmic, growth (Shea, 1985a, 1985b, 1985d). However, the majority of allometric studies have been based on intra- or inter-specific samples (Smith, 1980, 1984). In such cases a trait is not likely to vary curvilinearly with

increasing organismal size. The advantages and disadvantages of logarithmic transformation are discussed here.

Logarithmic transformation is statistically useful for two reasons (Smith, 1993). The first is that the linear form of a bivariate equation is easier to evaluate than a curvilinear regression. Bivariate allometric regression coefficients allow for the easy interpretation of the relationship between the sizes of two traits. This is lost if the regression is curvilinear (Huxley & Tessier, 1936). However, log transformation will only turn a curvilinear relationship into a linear one if relative growth *rates* are equal throughout ontogeny (Smith, 1980). Secondly, after logarithmic transformation data better conform to the assumptions of parametric statistical tests (Hoyle, 1973; Smith, 1980). Before transformation the distribution of data points often approximates the lognormal distribution (Koch, 1969). Therefore the data will be positively skewed and heteroscedastic (unequal variances). Log transformed data is more normally distributed and homoscedastic (i.e. more equal variance). There are also disadvantages to log transformation.

Transformation may reduce the amount of variance explained by the equation of a regression line. Log transformation can reduce correlation coefficients, particularly for intra-specific studies (Smith, 1984). Also, log transformed data can be utilised to study covariation in the relative proportions of two variables but not the magnitude of change in one variable in relation to the other (Smith, 1984). Furthermore, curvilinear regressions may be interesting in their own right (Shea, 1985, b, d) since they depict a change in the relative growth *rates* of two measured traits. Such changes often occur at certain life history events (Klingenberg, 1998) such as

puberty. Given the disadvantages of log transformation it is better, where possible, to use D'arcy Thompson's (1942) equation of allometry. Furthermore, in the case of ontogenetic regressions, curvilinear relationships may also be made linear by removing adults (Dainton & Macho, 1999), thereby negating the need for log transformation of the measured data.

It is reasonable to assume that in cross-sectional studies of ontogenetic allometry the change in shape observed with increasing size approximates an actual ontogenetic pathway traversed by all normal individuals of that species during the period of life investigated (Fleagle, 1985). When adults are included in the analysis this may not apply because the inclusion of adults in ontogenetic allometric regressions tends to lower the allometric co-efficient (Dainton & Macho, 1999). Underestimation of the allometric co-efficient is partly due to the curvilinear trends imparted by the inclusion of adults: allometric coefficients for intra-specific regression are usually lower than those for ontogenetic regressions (Cheverud, 1982a). Therefore, when using allometric regressions it is important to note that the inclusion of adults can dramatically affect the results and, therefore, comparisons across studies should consider the type of data chosen.

The choice of bivariate regression statistics will greatly affect the allometric co-efficient (Harvey & Pagel, 1991). Regression statistics are usually calculated using Model I regression (e.g. least squares regression) that minimises the distance squared between the y co-ordinate of a data pair and the regression line: thus assuming that measurements of the independent variable (size) are without error. However, with regard to morphological measurements the independent variable is also subject to

measurement error. If the dimensions plotted on both the abscissa and ordinate axes are subject to measurement error model I regression underestimates the allometric coefficient, unless the correlation co-efficient (r^2) is 1. Therefore, Model II regression (e.g. reduced major axis), that deals with variation in both x and y, has been suggested as a better tool for allometric studies (Ebert and Russell, 1994; Lande, 1979; Smith, 1980). If the data are to be interpreted in a biological context it is crucial the correct regression statistics be utilised.

1.5.4. Jolicoeur's multivariate generalization of allometry

The bivariate equation provides an easy method for measuring the change in the relative dimension of one part of an organism in relation to overall body size. Using the bivariate method proposed by Huxley and Teissier it is possible to assess patterns of covariation between many independent measures and one dependent measure. However, when large numbers of dimensions are considered bivariate studies of relative growth are cumbersome. Particularly when the relative growth rates of different features vary with respect to overall size. Fortunately, the approach taken by Huxley and Teissier was not restricted to pairs of measurements. Extending the concept of simple allometry to multiple measured dimensions is fairly straight forward (Klingenberg, 1996b, 1998).

Multivariate statistical methods, such as principal components analysis (PCA), were developed to assess patterns of covariation in many variables simultaneously. Jolicoeur (1963) and Jolicoeur & Mosimann (1960) proposed that PCA be utilised for assessing patterns of covariation between three or more measured bony dimensions. Using a PCA to assess patterns of covariation between multiple

dimensions has a long history in morphometry (e.g. Hotelling, 1936; Teissier, 1938). A PCA summarises the variation in the original data set in a few constructed variables, referred to as principal components (PCs). The first PC is a linear combination of the variables that account for the maximum possible variance and usually denotes overall size. Subsequent PCs account for the maximum possible variance, subject to being orthogonal to all previous component axes. The amount of variance in each measured variable accounted for by each principal component is described by the factor loadings. Using the PCA patterns of covariation between variables in large data sets can be considered simultaneously, i.e. not just one independent measure (see Figure 1.4). By plotting the PCs against one another the bivariate allometric regression is extended to include more than two variables where the regression line is in a multidimensional space defined by all of the variables (Klingenberg, 1998).

Jolicoeur (1963) proposed that the eigenvector of the first PC extracted from a covariance matrix of logarithmic variables would reflect changes in proportions with increasing size. If the first PC does represent increasing size then (a) all variables should load strongly and in the same direction along PC 1 (b) measures of organismal size (e.g. geometric mean of linear dimensions should be highly correlated with PC 1. It was very common for the first PC to account for most, if not all, of the variation in the data set e.g. 99% (Klingenberg, 1998). Consequently the patterns of covariation along PC 1 are usually related to overall organismal size.

Thus PCA provides an easy way to generalise the bivariate equation for simple allometry (Jolicoeur, 1963; Jolicoeur & Mosimann, 1960; Klingenberg, 1998). In Jolicoeur's allometric scheme isometry refers to a situation where all of the measured

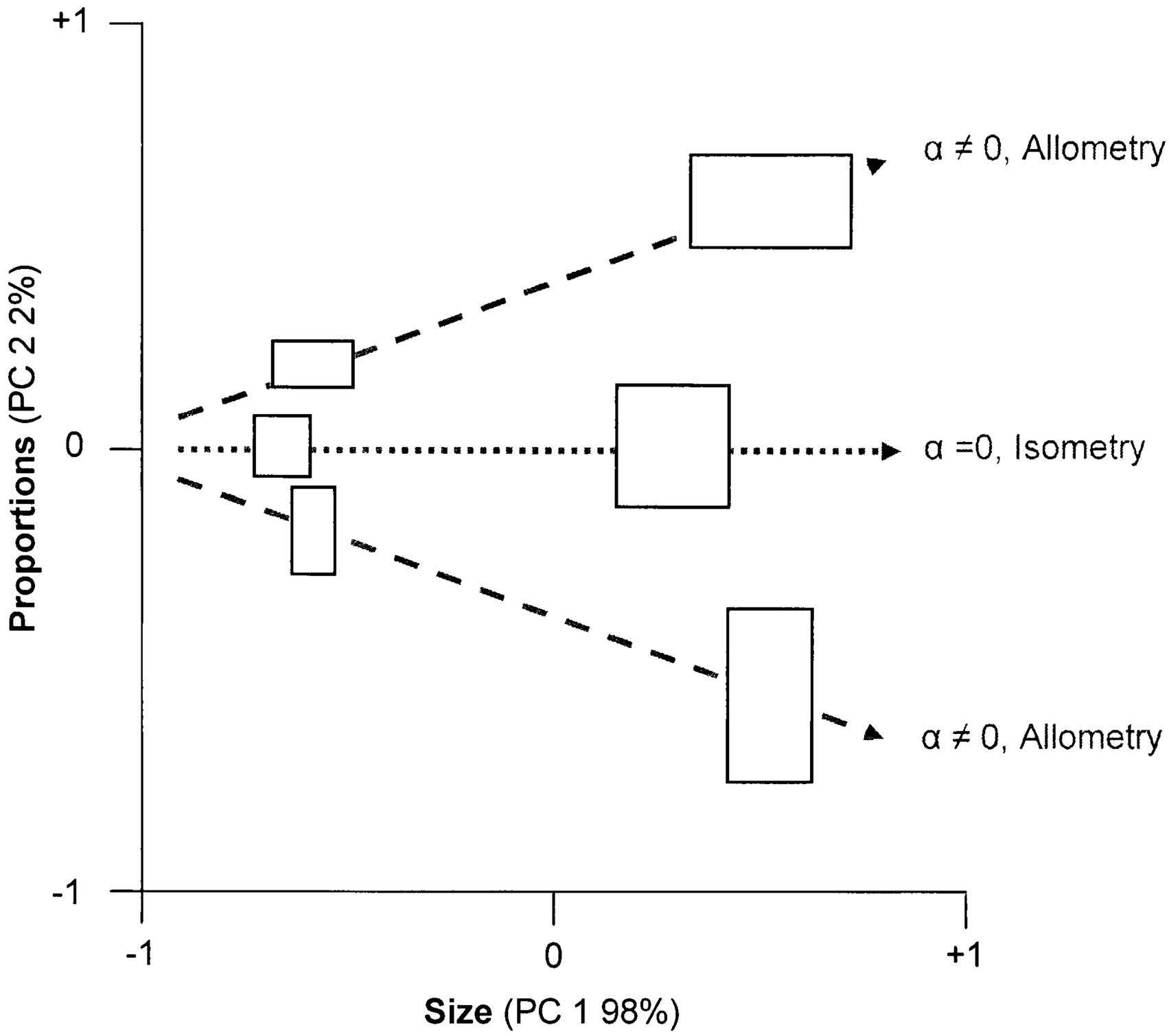

Figure 1.4. Jolicoeur's (1963) concept of multivariate allometry. A principal components analysis was used to study intra-specimen variation in size and proportions. The percentage variance pertains to the amount of variation in the original data set explained by each principal component. One of the constructed variables (i.e. principal component) usually represents overall size and, consequently, is highly correlated with measures of size (e.g. geometric mean of linear dimensions). Other PC's may describe variation in the proportions across the sample. Consequently multivariate analysis allows patterns of covariation between size and many linear dimensions to be studied simultaneously.

linear dimensions grow at the same rate (i.e. allometric co-efficient $\alpha = 0$) and allometry refers to a situation where one or more variables grow at different rates with respect to size and/or PC 1 scores (i.e. $\alpha \neq 0$). The results of the multivariate analysis can be related back to bivariate allometric analyses. The ratio of PC 1 variable loadings for two measured dimensions is identical to the value of α obtained when the two measures are plotted against each other in a bivariate regression. If a measure of the geometric mean of linear dimensions is included in the data set, then

values of α calculated from PC 1 variable loadings will be the same as values of α obtained when measured dimensions are plotted directly against the geometric mean of measured dimensions (i.e. overall body size) in bivariate regression. Hence the first PC of the covariance matrix of data could be used as a direct measure of overall organismal size in bivariate analyses of allometry.

Following Huxley and Teissier, Jolicoeur understood allometry to be the analysis of covariation among the sizes (dimensions) of parts of an organism. Of peripheral importance however was the notion of proportions. Bivariate allometry did not quantify proportional change, although a change in the relative proportions of two traits indicated a change in proportions had occurred (Klingenberg, 1998). Thus size related variation in proportions is fairly difficult to deal with in Huxley's analysis. However, Jolicoeur's method provided an easier way in which to analyse changes in proportions with increasing size (Klingenberg, 1998).

1.5.5. Mosimann's concept of allometry: covariation between size and shape

The emphasis of allometry shifted from the study of covariation between the size of two traits to the study of covariation between size and "shape" (Gould, 1966; Mosimann, 1970). In Mosimann's scheme shape was used in reference to the relative dimensions of an organism (see also Gould, 1977; Shea, 1983, 1984, 1988). Mosimann (1970) proposed a statistical definition of the new concept of allometry. Whereby allometry is an association between size and shape and isometry is their stochastic independence. Thus allometry implied some shape change associated with increased size. Conversely, isometry was the absence of size-related shape variation.

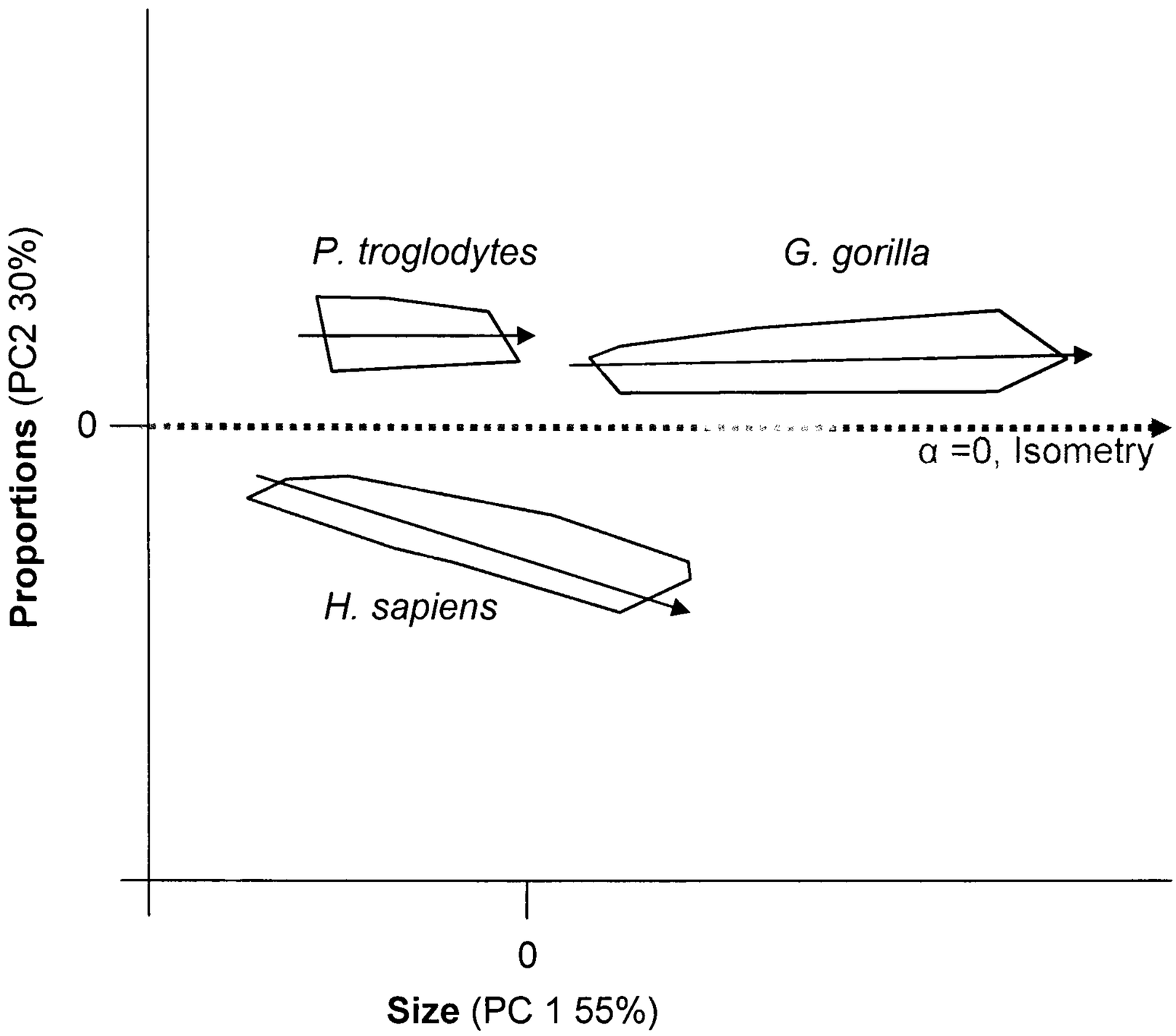

Figure 1.5. Published example of multivariate allometry. The graph depicts a principal component analysis of adult pelvic dimensions in the Hominidae. The percentage variance pertains to the amount of variation in the original data set explained by each principal component. Black arrows indicate the growth trajectory for each species. Multivariate allometric analyses are useful for determining whether (and how) the proportions of structure change with increasing size because many variables can be considered simultaneously. Figure adapted from Berge & Kazmierczak (1986).

Mosimann suggested that allometric analyses be performed in the same manner previously suggested by Huxley, Teissier and Jolicoeur. In a bivariate analysis the geometric mean of all measured variables was used as a measure of size and, in multivariate analyses, the first principal component, which is usually highly correlated with the geometric mean of linear dimensions, was utilised as a measure of size. Isometry referred to a situation in bivariate allometry where the slope equalled one (Figure 1.2). In the context of multivariate allometry, isometry is represented by a straight line at equal angles to all co-ordinate axes in the morphospace of measured traits (Figure 1.4). Following Mosimann (1970) Berge &

Kazmierczak (1986) were able to analyse static allometric change in the pelvis of adult hominoids (Figure 1.5).

The procedure allowed pelvic size related change in the proportions of three hominoid species to be compared. The study could be extended to include an ontogenetic series of non-adults. However, developments in the way morphology was recorded have since led to a new definition of shape and a better method of analysing allometry in a multivariate sense.

1.5.6. Bookstein's Geometric Morphometrics: covariation between size and geometric shape

Using traditional morphometric techniques it was difficult to record, analyse and visualise ontogenetic change of shape of complicated three-dimensional structures, such as the pelvis. This led researchers to find new ways of recording bony morphology which gave rise to new or "geometric" morphometric techniques (e.g. Bookstein, 1990, 1991; Rohlf 1990). Within the framework of geometric morphometrics organismal structures are characterised by a set of anatomical landmark co-ordinates, rather than by the distances between landmarks (Bookstein, 1991, 1993, 1996; Rohlf, 1990ab; Rohlf & Bookstein, 1990; Rohlf & Slice, 1990). The landmarks summarise the shape and spatial distribution (i.e. geometry) of the organisms under study. In geometric morphometrics shape was redefined as the geometric properties of a configuration of points that are invariant to changes in translation, rotation, and scale (Bookstein, 1990, 1991).

1.5.7. Geometric morphometric analysis of covariation between organismal size and geometry

This section discusses how landmark data can be analysed in the context of allometry. Prior to statistical analysis landmark data must be transformed so as to remove intra-specimen differences in co-ordinates that are due to being digitised at different points in space. This section details the process of superimposition whereby specimens are translated and rotated into the same plane. Once specimens are superimposed landmarks can be used in multivariate statistical analyses, which are described below. Furthermore, inter-specimen differences in landmark co-ordinate systems can be visualised using the Thin-plate spline (TPS) technique.

1.5.7.1. Procrustes superimposition

Before two biological structures can be compared statistically, and differences in geometry visualised, the landmark configuration for each measured specimen must be "superimposed". This requires that specimens be scaled to a common size measure and then normalised for translation and rotation. This ensures that the remaining differences between individuals are only shape (i.e., geometric) differences. This is achieved by using generalised least squares Procrustes superimposition (GPA) (Bookstein, 1991; Gower, 1975; Goodall, 1991; Rohlf, 1990a; Rohlf and Slice, 1990). This procedure (i) scales the specimens so that the centroid size (CS) is equal to one, (ii) and aligns the measured specimens in the same plane so that the centroid overlaps, then (iii) rotates specimens so as to minimises the distance between pairs of homologous landmarks in the grand mean configuration and each specimen. Centroid size is calculated as the square root of the sum of squared distances of a set of landmarks from their centroid or, equivalently, the

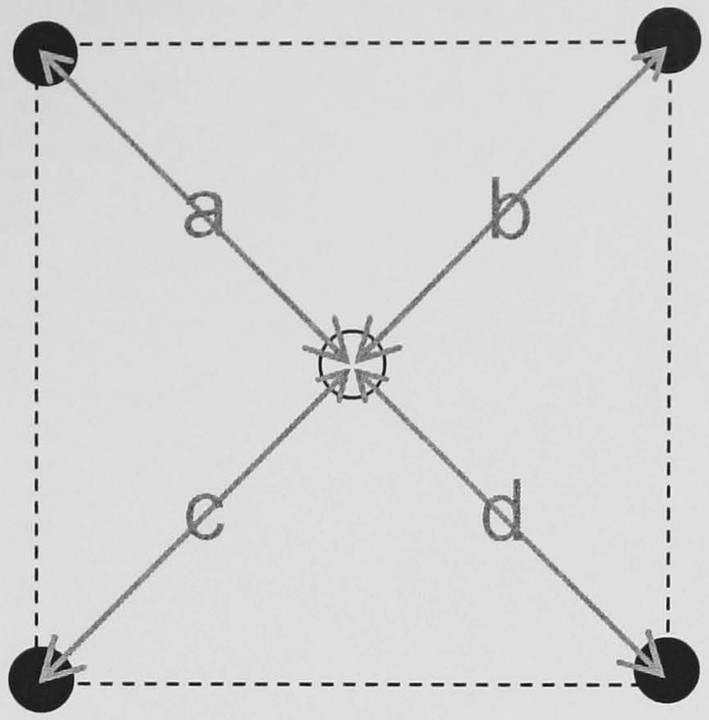

Figure 1.6. Centroid size. Centroid size is calculated as the square root of the sum of squared distances of a set of landmarks from their centroid (mean).

square root of the sum of the variances of the landmarks about that centroid in *x*- and *y*-directions (Gower, 1971; Rohlf, 1990ab) (Figure 1.6). In essence, Procrustes superimposition (also referred to as registration) minimises the distance between pairs of homologous landmarks. The minimised quantity, often called a Procrustes distance, is commonly used as a measure of the difference between pairs of biological shapes (e.g. Sneath, 1967).

1.5.7.2. Thin-Plate spline (TPS) technique

The TPS method can be used to visualise the differences between two landmark configurations, i.e. compare the shape of measured bony specimens. This ability to visualize morphological differences is invaluable, particularly when dealing with complex three-dimensional anatomical structures. The TPS function is a smooth interpolation function that computes and visualises transformations of measured

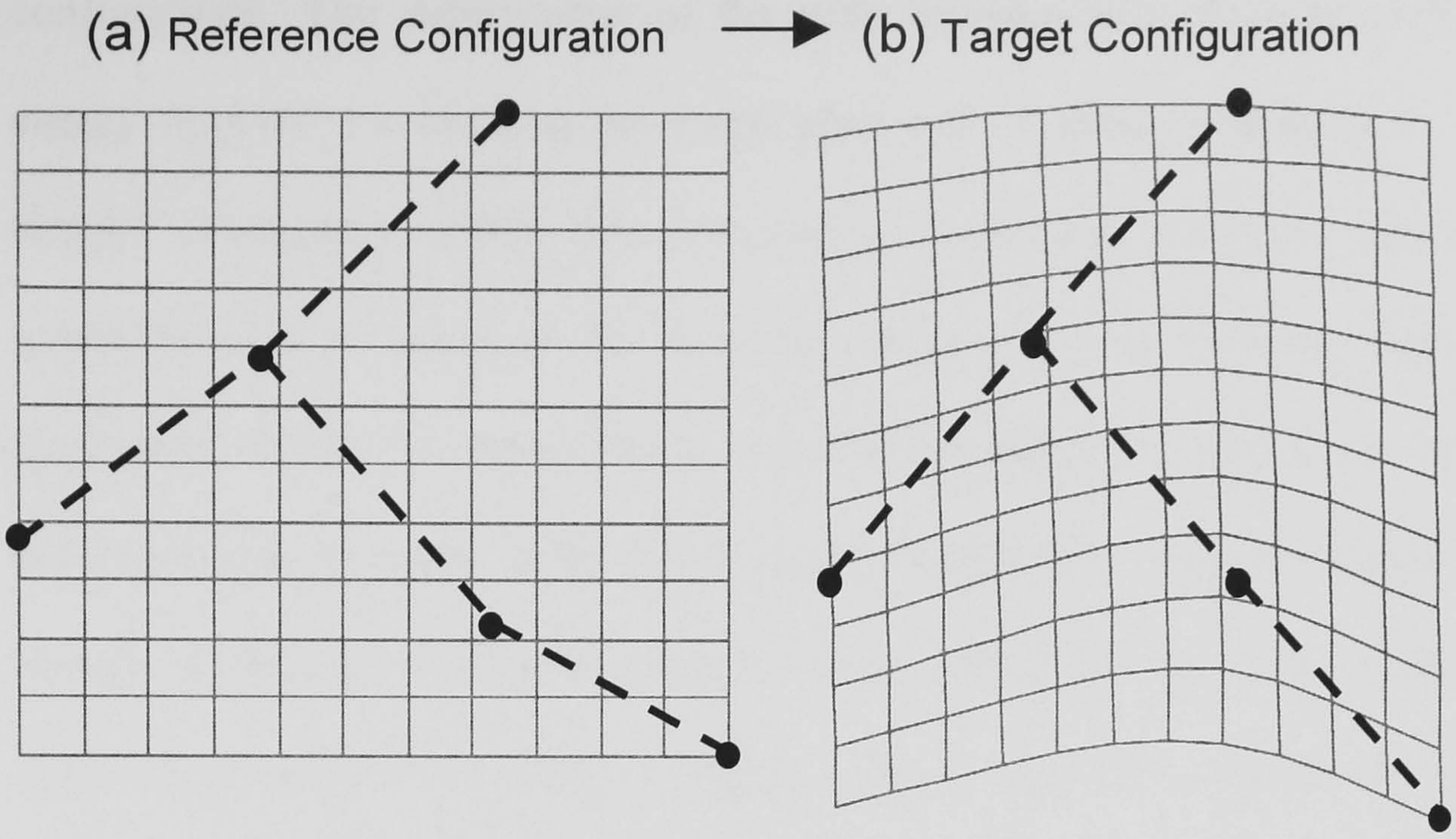

Figure 1.7. Geometric morphometrics: the thin plate spline technique is used to visualise differences in form between two landmark configurations. (a) A "reference" specimen is drawn onto an infinitely thin metal plate (depicted above as a mesh) with nails placed at each landmark. (b) A "target" specimen is superimposed onto the reference and the nails are dragged to meet the new landmark coordinates; a process referred to as "morphing". This causes a deformation in metal plate. The deformation describes inter-specimen differences in shape between the reference and target specimens. Splines are most useful for comparing the shapes of complicated structures. To aid the visualisation dashed lines demark the outline of the landmark configurations.

Cartesian co-ordinates (Bookstein, 1989; Bookstein, 1991; Frieβ, 2003) in a manner similar to D'Arcy Thompson's transformation grid (e.g. Thompson, 1917). A rectangular grid is projected over two Procrustes aligned landmark configurations and deformations of the grid are used to visually define the differences in proportions between the two specimens (Figure 1.7).

A thin-plate spline can be viewed as an infinitely thin metal plate with a set of landmarks placed on top and nailed down. This set of landmarks is referred to as the reference specimen (Rohlf, 1998). The TPS method adjusts the reference landmark configuration to match a new (target) configuration (Bookstein, 1991). This can be imagined as a second (target) landmark configuration being drawn on the metal plate and the nails being moved to match the new shape. This produces a deformation of the metal plate which is, in effect, constrained by the reference landmark

configuration. The deformation of the plate includes out of plane bending. The energy required for bending the metal plate out of plane is defined as "bending energy" (Bookstein, 1991). The homologous landmarks from two specimens are matched so as to minimise the bending energy (i.e. out of plane deformations) (Bookstein, 1991). It is important to note that the bending energy does not describe the magnitude of shape differences between specimens. This is because bending energy is affected by the distance between landmarks i.e. two closely related landmarks require more energy to move a given distance towards each other than landmarks which are far apart. The resultant deformation in the mesh describes the differences in proportions between the two specimens being analysed. In contrast to Thompson's grids the deformation can be calculated in three dimensions, rather than two. However, this is mathematically cumbersome and, in three planes, the deformations are difficult to visualise. By viewing the deformations in three planes (i.e. *x* versus *y*, *x* versus *z* and *y* versus *z*) it is possible to describe shape differences between two specimens in three dimensions. For a more detailed review of theoretical bases and calculation procedures of TPS morphometrics, see Bookstein (1989, 1991); Rohlf and Marcus (1993); Rohlf *et al,*. (1996) and Dryden & Mardia (1998).

The TPS technique has been successfully applied in a pilot study of pelvic growth and development on modern humans. Berge (1996) digitised two modern human ilia, one neonatal and one adult then used the TPS technique to compare shape (Figure 1.8). Prior to producing the splines the three-dimensional co-ordinate data was projected into two dimensions. The results of Berge's analysis are shown in Figure 1.8b. Aside from describing the differences in proportions between the two measured

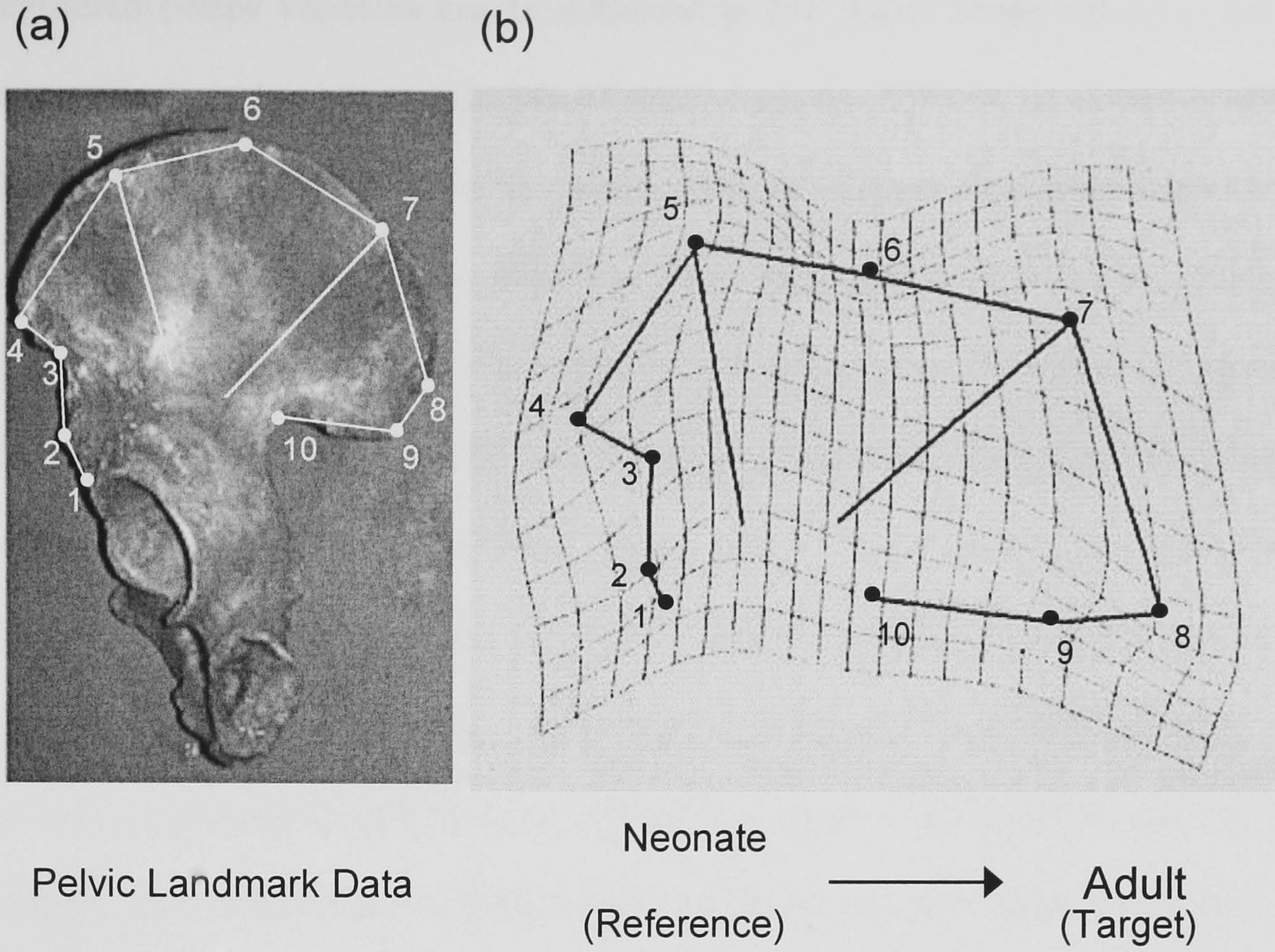

Figure 1.8. Thin plate spline comparison of the shape of modern human *os coxae*, neonate and adult. (a) *Os coxal* morphology was recorded using two-dimensional co-ordinate data. (b) Anatomical landmark data was utilised in a thin-plate spline analysis. The spline denotes a single neonatal specimen (reference) morphed onto a single adult specimen (target). Figures adapted from Berge (1996).

specimens the spline also revealed which intra-specific differences in proportions were of greatest magnitude. For example, the expansion of the dorsal iliac blade between landmarks 7-8-9, the anterior iliac blade between landmarks 4-5 and also the contraction of the iliac blade between landmarks 5-6. This is an important feature of the TPS which serves the same use as the variable loadings in PCA. It is this that allows the TPS technique to be used in conjunction with multivariate statistical analyses.

Geometric morphometric analysis is concerned with organismal size and shape variables. As well as visualization geometric morphometric analyses allow shape variables to be analysed statistically. Once landmark configurations have been

registered (shape variables can be extracted in two ways. Shape variables can be extracted either by (a) computation of relative warps (RW) by assessing a set of thin-plate transformations from the mean shape to each of the shapes under study (Bookstein, 1991) or (b) computation of Procrustes residuals from the consensus specimen (e.g. Bacon and Baylac, 1995). In both instances the shape variable are analysed by projecting the data into a tangent plane and carrying out a principal components analysis PCA (Rohlf, 1999; 2000). These procedures produce a morphospace. A morphospace is a graph produced by plotting constructed variables against one another. The shape variables (i.e. component scores) derived from a relative warp analysis (RWA) or principal components analysis (PCA) can be used as input into multivariate (and univariate) statistical analyses. Such an approach is useful because the statistical parameterisation of size and shape may be improved and, therefore, the biological interpretation of statistical observations may be enhanced.

1.5.7.2.1. Kendall's Shape space

Before shape variables that can be used in multivariate statistical analysis can be extracted from landmark data sets, measured specimens must be Procrustes fitted (i.e. registered) and then projected into Kendall's shape space (Bookstein, 1991). Once registered, landmark configurations can be represented as points in a new shape space which is of higher dimensionality than the physical space in which k landmarks were digitised (configuration space). Landmarks are digitised in p dimensions. Where p is the dimensionality of the physical space in which the specimens were digitised (two or three). Registration removes differences due to location (p dimensions), rotation ($p(p\text{-}1)/2$ dimensions) and scale (1 dimension). For two

dimensional data the new shape space of registered specimens is of dimensionality *kp*-4 and for three dimensional data, *kp*-7. This new shape space was described statistically by Kendall, (1984) and it is commonly referred to as Kendall's shape space (Bookstein, 1991). Kendall's shape space is non-Euclidean (i.e. non-linear). If variation in landmark configurations is small the relative locations of points representing specimens in Kendall's shape space are approximately independent of registration. In general the only exception to this is when the data set contains reflected specimens e.g. bones from the left and right (Rohlf, 2000). For the simplest shapes, i.e. triangles, the space can be visualised as being spherical (Figure 1.9a). For configurations with more than three landmarks the space is much more complex being both non-linear and high dimensional (Le & Kendall, 1993).

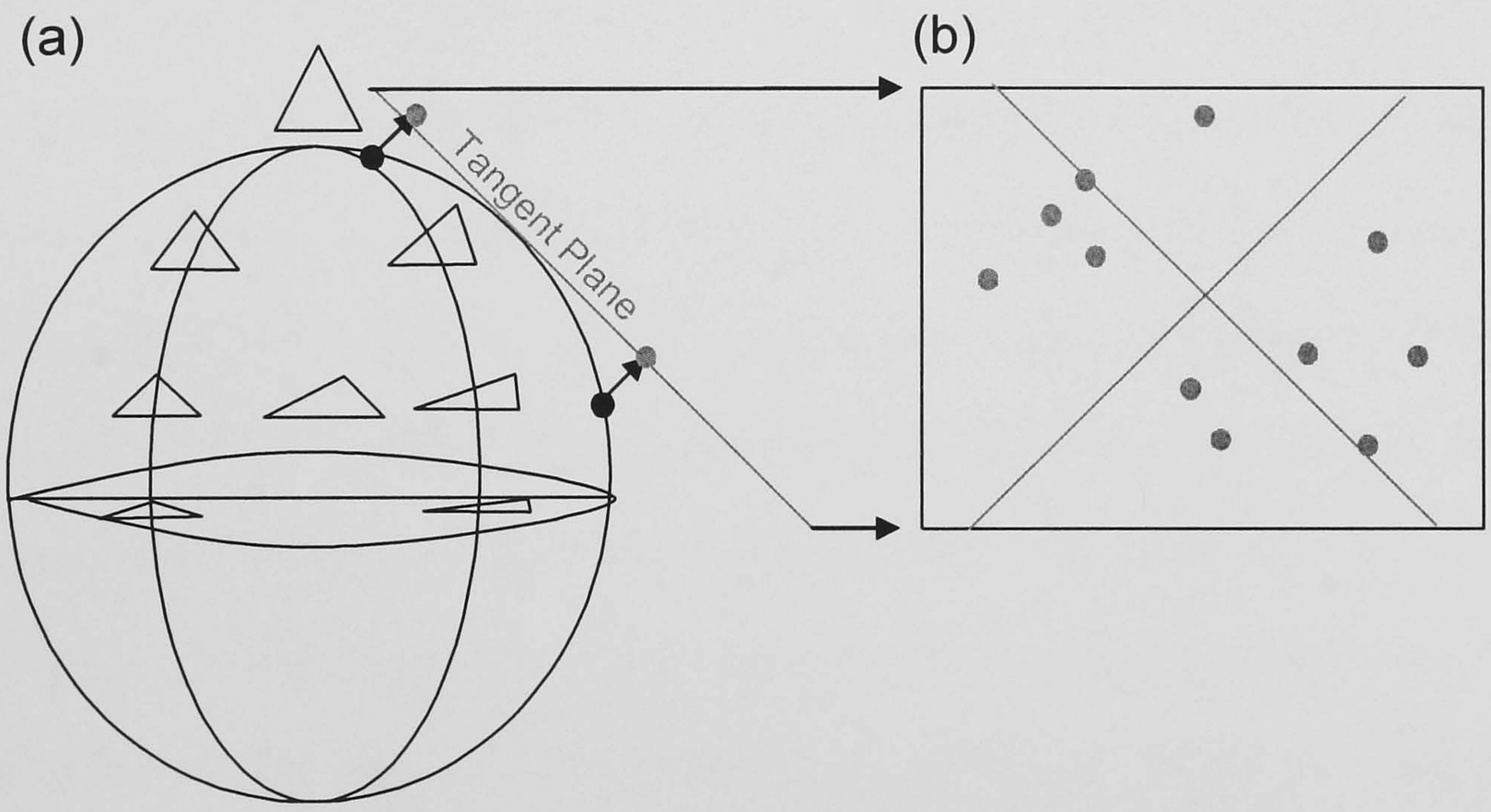

Figure 1.9. Kendall's shape space and computation of principal components. (a) An approximation of Kendall's shape space based on triangles. (b) A schematic indicating the projection of triangles (represented by points) from Kendall's shape space into a shape space tangent to the mean triangle. Black arrows denote the projection. This produces the principal components of shape variation (PC 1, PC 2). Figure (a) adapted from Kendall (1984) and (b) from Rohlf (2000).

1.5.7.2.2. Relative warp analysis of landmark co-ordinate data

Relative warp analysis is a tool for exploring within-sample variation, serving to reduce total variation in a set of co-ordinate data to a smaller number of independent dimensions, i.e. relative warps (RWs) (see Bookstein, 1991). A relative warp analysis is based on a set of registered specimens and a consensus configurations i.e. grand mean specimen (see Figure 1.10). The RWA uses the thin-plate spline technique to produce constructed variables based on differences between the landmark configuration of each specimen and the consensus. The RWA finds a function (thin-plate spline deformation) fitting all landmarks to the reference configuration. This produces principal warps (PWs) that describe shape deformations of the reference configuration at different spatial scales (see Figure 1.9). The specimen deviations from the reference configuration are called the partial warp scores (PWS). A RWA includes a PCA of the covariance matrix of the partial warp scores. This produces a new set of constructed variables, the relative warps. Hence the relative warps can be viewed as the principal components of the set of thin-plate transformations from the mean shape to each of the shapes under study. The shape (and size) of each specimen is described by the relative warp scores (RWS) which actually represent PC's of the PWS (Bookstein, 1991; Rohlf 1993, 2001b). Unless PCs were calculated using a scaling option which weighted landmarks unevenly (Rohlf, 1993). The value α is an exponent used to rescale PWs before computing their PCs, the relative warps. A scaling factor of $\alpha = 0$ and is considered to be more appropriate for systematic studies (Loy *et al.*, 1993; Rohlf, 1993; Rohlf *et al.*, 1996). Relative warps should be computed in the full shape space, i.e. including both the affine component and the non-affine components, as recommended by Bookstein (1996a and 1996b). An affine transformation is one in which parallel lines remain

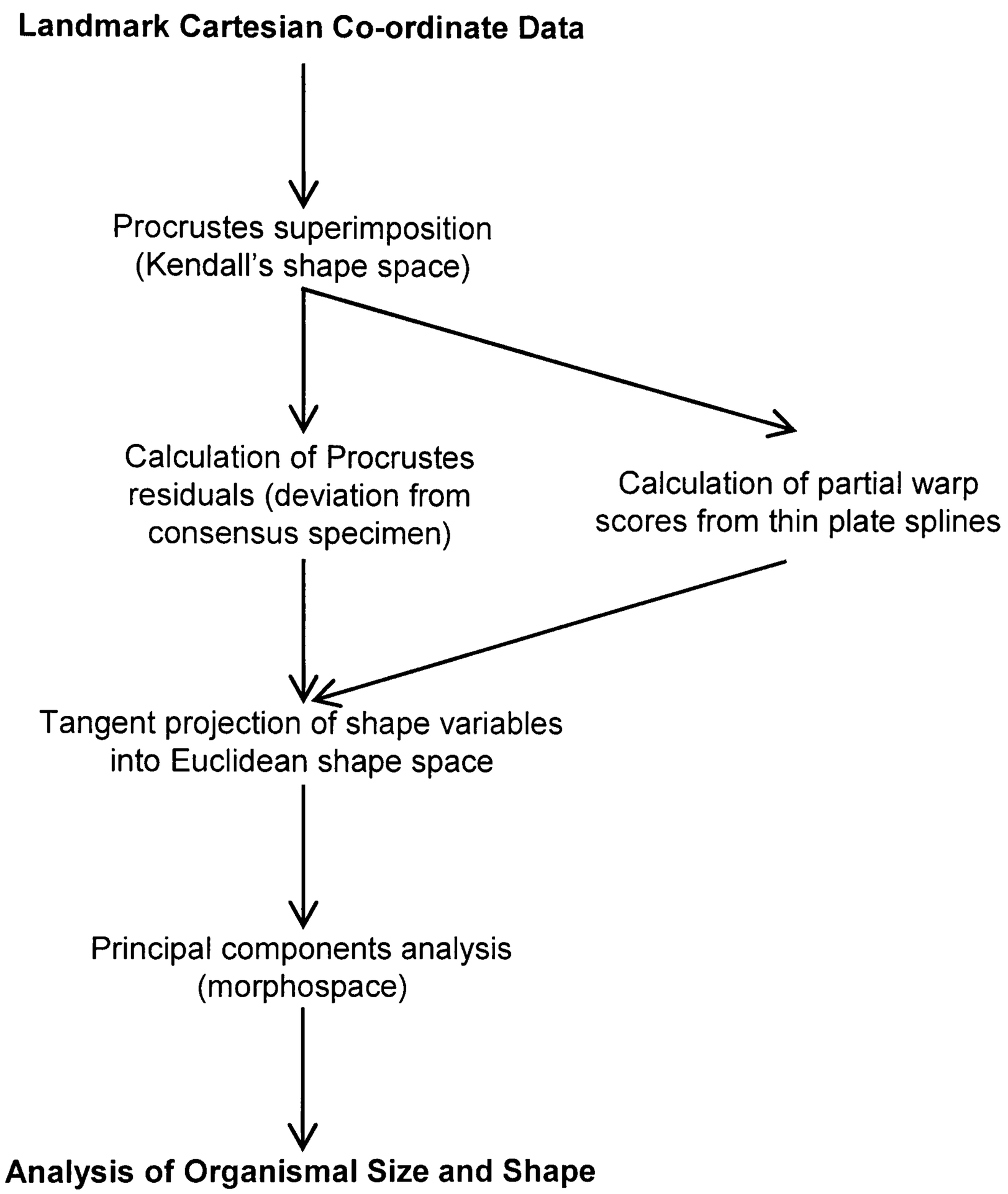

Figure 1.10. Steps for a geometric morphometric analysis of landmark co-ordinate data.

parallel. Affine transformations of a plane transform squares into parallelograms and circles into ellipses of the same shape. A non-affine transformation is one that distorts the mesh in any other fashion. This procedure usually provides effective low-dimensional ordinations (i.e. few relative warps), without requiring assumptions about the precise spatial scale of the shape changes (Bookstein, 1996a). Relative warp analyses that separate the affine and non-affine components can make

interpretation of the shape variation ambiguous if these components are correlated (Walker, 1996).

1.5.7.2.3. Principal components analysis of landmark co-ordinate data

The method for carrying out a PCA is, is some ways, similar to the RWA (see Figure 1.10) The easiest way to carry out a PCA of co-ordinate data is to project the registered specimens into the plane tangent to Kendall's shape space (Kent, 1994; Dryden & Mardia, 1993, 1998) (Figure 1.9ab). Figure 1.9b schematises principal components analysis of shape variation in the space tangenital to Kendall's shape space for triangles (Figure 1.9a). The scatter of points in the spherical shape space representing variation within a sample of triangles is shown in Figure 1.9a. The sample is projected from the spherical shape space into a Euclidean tangent plane in exactly the same way as a cartographer might project a map from a globe onto a flat sheet of paper (Figure 1.9b). The coordinates of triangles representing specimens are no longer given in terms of the sphere, but rather as coordinates in the tangent plane (Figure 1.9ab). As long as the projection has not resulted in excess distortion (as might occur if the projection encompasses a large proportion of the sphere) one can carry out useful analyses in this plane (note projected points in tangent Figure 1.9a). For higher dimensions the tangent plane to the shape sphere can be imagined as a tangent space of kp-p-p(p-1)/2-1 dimensions (Bookstein, 1991). Thus, the projected (Procrustes tangent) co-ordinates can be estimated as the kp vector of deviations from the mean of the Procrustes fitted co-ordinates (Dryden & Mardia, 1993; Goodall, 1991) i.e. Procrustes residuals. Many authors have, therefore, analysed Procrustes residuals directly using a PCA (e.g. Bacon & Baylac, 1995; Berge &

Penin 2004; Dryden & Mardia, 1998; Penin & Berge, 2001). The projection results in a $(k\text{-}1)p$ vector of tangent space shape coordinates with respect to the mean for each specimen; three dimensional data being reduced to two dimensions. Both of the vectors of tangent space coordinates are of rank $kp\text{-}p\text{-}p(p\text{-}1)\text{-}1$. A PCA can be carried out using tangent space coordinates to extract $kp\text{-}p\text{-}p(p\text{-}1)\text{-}1$ eigenvectors; which are the PCs of variation of shape.

1.5.7.2.4. The thin-plate spline technique and multivariate analysis of landmarks

A PCA or RWA produces composite variables that, when analysed, describe size related and residual changes in sets of landmarks. One of the great attributes of geometric morphometrics is that shape variation along the constructed axes of morphospace can be visualised using the TPS technique. The RWS and PCS of pairs of consecutive relative warps/principal components can be shown in scatter plots (morphospace). The morphospace describes all of the possible variation shape within a sample because isometric size has been removed. In a geometric morphometric morphospace entire landmark configurations (specimens) are represented by a single point. The patterns of shape variation (landmark configurations) along each relative warp can be visualised with thin-plate spline transformation grids (e.g. Rosas & Bastir, 2002; Frieβ, 2003). Shape changes associated with each relative warp can be visualized by regressing landmark co-ordinates against RW scores and using the regressions to construct hypothetical specimens that fall along each principal component. This is referred to a TPS regression (Rohlf, 1990ab). These hypothetical specimens can then be compared using the TPS technique so that the variation in shape along each axis can be visualised.

1.5.7.3. Bookstein's size-shape morphospace

The registration procedure (GPA) outlined above is usually carried out prior to statistical analysis. Scaling specimens does not remove geometric size (covariation between size and shape) but does remove isometric size (scale). Overall scale is an important aspect of studies which aim to interpret intra- or inter-specific differences in from biologically. This is because two organisms at the same developmental stage may have the same shape at different scale or different shape at the same scale. Shape or size differences that occur between specimens cannot be interpreted in isolation from each other. The shape spaces described for the PCA and RWA omit information on scale (Bookstein, 1991, 1996). Dryden & Mardia (1996) suggested that patterns of allometry (especially developmental) should be analysed and compared in size-shape spaces. Mitteroecker *et al.* (2004) proposed that a measure of organismal size be included in any analyses based on registered co-ordinate data so that intra- or inter-specific differences in size, shape and patterns of size shape covariation could be analysed simultaneously. It was suggested that registered co-ordinate data be augmented with the logarithm of centroid size. Typically log centroid size has the largest variance of any column (especially if registered landmarks are converted to residuals prior to analysis). Thus, the first PC will be highly correlated with size, as in traditional morphometric techniques (see Jolicoeur & Mosimann, 1960).

1.5.8. The accession of geometric morphometrics

Geometric morphometrics are used increasingly for morphometric studies because the approach provides (i) a powerful means to visualize morphological differences using thin plate spline (TPS) technique (ii) an array of methods for comparison of

shapes. The two approaches can be used independently or, importantly, in combination. When combined the statistical and visual procedures allow a greater understanding of size related shape during ontogeny and throughout phylogeny to be obtained than with traditional morphometric techniques. This chapter identified two statistical analyses that will be useful for investigating ontogenetic change in shape during growth and development. Statistical analyses can be based on (a) registered data (b) registered data supplemented with a measure of geometric scale.

Part II: External Iliac Morphology of Hominoids

Chapter 2. The Adult Hominoid Pelvis

2.1. Morphological affinities of the hominoid pelvis

Before comparing morphological growth and development among species it is useful to start by comparing adult morphology. Adulthood marks the end of development and when the differences between species are understood it becomes easier to compare growth and development. A cursory examination of the hominoid pelves reveals clear differences in morphology across species (Schultz, 1936) (Figure 1.1b). This is complicated by the fact that there are also clear differences between the sexes (Van den Broek, 1911, 1914, Tague, 1991). Many researchers have attempted to quantify interspecific differences in adult pelvic proportions and patterns of pelvic sexual dimorphism.

Comparisons of primate pelvic morphology began in the early 1900s (e.g. Straus, 1929; Wedenreich, 1914; Waterman, 1929). In the first half of the 20th century researchers assessed interspecific differences in pelvic proportions using ratio based analyses. Linear measurements were scaled according to measures that were thought to describe the size of the pelvis. The results of published inter-specific comparisons of hominoid pelvic proportions are shown in Table 2.1. Schultz (1930, 1949) and Le Gros Clarke (1955) both reviewed the findings of these studies and concluded that the morphology of modern humans contrasted with that of the African apes. Schultz (1949) went on to suggest that the pelvic topography of *G. gorilla* was closest to modern humans. Schultz (1930) and Le Gros Clarke (1955) agreed that, in relation to

os coxal size, modern humans were best distinguished from the African apes by the infero-superiorly shorter pelvis and antero-posteriorly deeper pelves.

Ratios are not ideal for studying the relative dimensions of an animal because they do not remove correlations with size (Smith, 1980, 1984). During the second half of the 20th century researchers began to employ multivariate analyses to establish the morphological affinities of the hominoids (e.g. Berge & Kazmierczak, 1986; Berge, 1998; McHenry & Corruccini, 1975; Steudel, 1981; Zuckerman *et al.,* 1973). Multivariate analyses were better than ratio based bivariate analyses because many variables could be compared across species simultaneously (Oxnard, 1978; Shea, 1985a). Two such analyses are principal components analysis (PCA) (Jolicoeur, 1963) and canonical variates analysis (CVA) (McHenry & Corrucini, 1975; Steudel, 1978). Both analyses convert a set of measured variables to a smaller set of constructed variables. The first few constructed variables usually explain most of the variance in the original data set. Normally the first two or three constructs explain virtually all of the variance in the original data set (Rohlf, 1990a). Thus multivariate analyses allow one to quantify the morphology of individuals or groups of specimens and compare them easily. Hence, it was possible to assess the overall pattern of similarity and dissimilarity in the pelvic proportions of hominoids.

McHenry & Corruccini (1975) employed CVA to investigate *os coxal* measurements collected from the hominoids, as did Steudel (1978, 1981). Morphospaces based on linear dimensions separated specimens according to size and proportions. The resulting morphospaces are shown in Figure 2.1. The group centroids of the African

Author	Numerator	Denominator	Ratio (Proportions)			Morphological Affinity
			H. sapiens	*P. troglodytes*	*G. gorilla*	
Schultz (1936)	Pelvic Height	Trunk Length	120	150	160	H < G & P
Waterman (1929)	Iliac Height	Body Length	16	24	28	H < G & P
Schultz (1936)	Iliac Height	Trunk Length	95	155	160	H < G & P
Schultz (1936)	Iliac Height	Ischial Length	60	120	80	H & G > P
Waterman (1929)	Iliac Height	Ischial Length	34	30	32	-
Waterman (1929)	Iliac Height	Innominate Length	66	69	70	-
Straus (1929)	Upper Iliac Height	Lower Iliac Height	(119-157)	100	102	H > G & P
Waterman (1929)	Iliac Breadth	Iliac Height	88	47	83	H & G > P
Schultz (1936)	Iliac Breadth	Iliac Height	290	140	210	H > G > P
Straus (1929)	Iliac Breadth	Iliac Height	(125-126)	(63-67)	(90-94)	H > G > P
Schultz (1936)	Iliac Breadth	Trunk Length	280	220	340	P < H < G
Schultz (1936)	Iliac Fossa Breadth	Trunk Length	360	365	550	H & P < G
Schultz (1936)	Auricular Surface Breadth	Trunk Length	190	80	125	H > G & P
Waterman (1929)	Anterior Superior Spine to Spina Limitans	Posterior Superior Spine to Spina Limitans	65	82	90	H < G & P
Waterman (1929)	Ischial Length	Body Length	8	11	12	H < G & P
Waterman (1929)	Ischial Length	Innominate Length	34	31	30	-

Table 2.1. Discrimination of hominoids on the basis of os coxal morphology. Published interspecific comparisons of hominoid pelvic proportions. Species defined by H =*Homo sapiens*, P = *Pan troglodytes* and G = *Gorilla gorilla*.

apes more closely approximated each other than they did to modern humans. McHenry & Corruccini (1975) analysed *os coxal* dimensions with PCA and reported the same result (Figure 2.2). Berge (1984a, 1998) also used PCA to compare hominoid morphology by analysing linear measurements. Size was suppressed by logarithmically transforming the data. Size suppression reduces the total amount of variation in measurements that is attributable to differences in size. The morphospaces are shown in Figure 2.2. All three PC's separated the hominoid species with no overlap. From these studies it was apparent that with regard to the *os coxa* (in particular Berge, 1984a; McHenry and Corruccini, 1975; Steudel, 1978, 1981) and pelvic (Berge, 1998) proportions, overall, the African apes bore more similarity to each other than either did to modern humans. Thus the findings agreed with the ratio based analyses of the early 1900s.

2.1.1. Patterns of sexual dimorphism in the hominoid pelvis

Sexual dimorphism is the existence of physical differences between males and females (other than differences in sex organs). Van den Broek (1911, 1914) was the first to suggest that modern human pelves were sexually dimorphic. This inspired other authors to ask whether pelvic sexual dimorphism was a peculiarity of modern humans and whether sex differences, if any, were comparable in the African apes (e.g. Schultz, 1940, 1949; Straus, 1927, 1929).

The first comparative study of hominoids addressing this issue reported that inter-sex differences in the relative dimensions of the upper and lower iliac height of *H. sapiens*, *P. troglodytes* and *G. gorilla* were the same (Straus, 1929). In all three species the section of the ilium between the auricular surface and the acetabulum

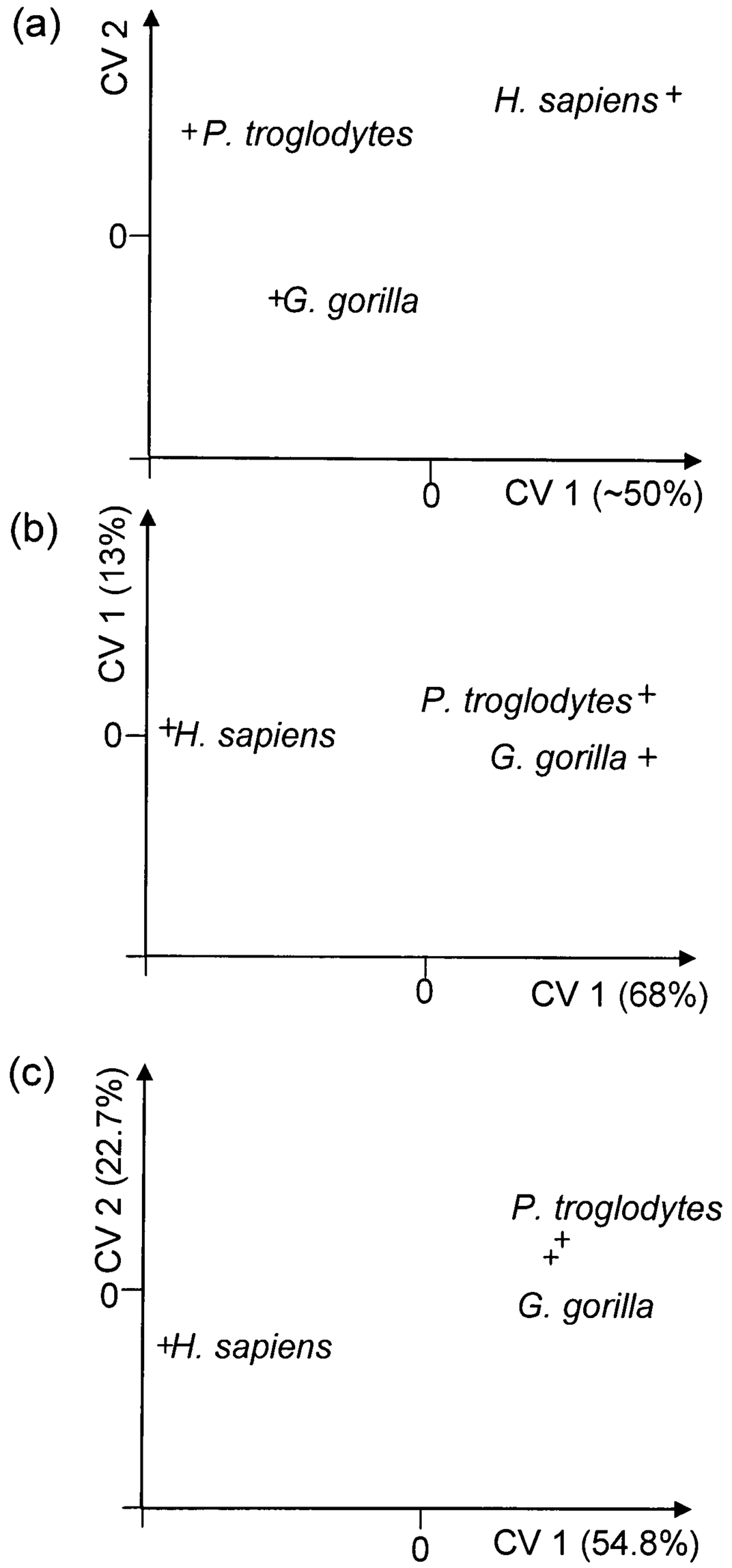

Figure 2.1 Discrimination of hominoids on the basis of *os coxal* morphology. Published canonical variates analyses comparing hominoid *os coxal* morphology (a) McHenry & Corruccini (1975) (b) Steudel (1978) (c) Steudel (1981).

was, on average, proportionally larger in females than males, i.e. in relation to the distance between the auricular surface and the iliac crest. However, the feature was only weakly dimorphic. More recent studies reported stronger evidence of hominoid sexual dimorphism. The distance between the acetabulum and the auricular surface was found to be proportionally longer in females than in males of the same size in relation to the length of the pelvis, i.e. the distance between the ischial tuberosity and the iliac crest (Berge, 1984b; Tague, 1991). It has also been reported that female hominoids possess a wider pelvic inlet transversely in relation to antero-posterior pelvic width (Leutenegger, 1973; Tague, 1991, 2005). In contrast, Schultz (1949) reported that female African apes possess a wider pelvic inlet transversely in relation to maximum pelvic breadth but that no dimorphism was present in modern humans. Females representing *H. sapiens*, *P. troglodytes* and *G. gorilla* possess a broader, shallower greater sciatic notch than males (Hager, 1996; LaVelle, 1995). Partly because of this, the female pelvis was found to be more spacious than that of the male of the same size, particularly the posterior aspect of the inlet (Berge, 1984b; Tague, 1991, 2005). In modern humans, females possessed a proportionally longer pubis in relation to ischial length (Schultz, 1949) and overall pelvic size (Berge, 1984b) than in males. In contrast, no such trend was apparent in African apes (Schultz, 1949; Berge, 1984b). As a consequence of the enlarged pubis modern human females also showed an enlarged bi-acetabular width and ventrally widened pelvis when compared to males but the female African apes did not (Berge, 1984b).

From these studies it was clear that the pattern of sexual dimorphism in the hominoids presented a mosaic where some characters displayed common patterns of

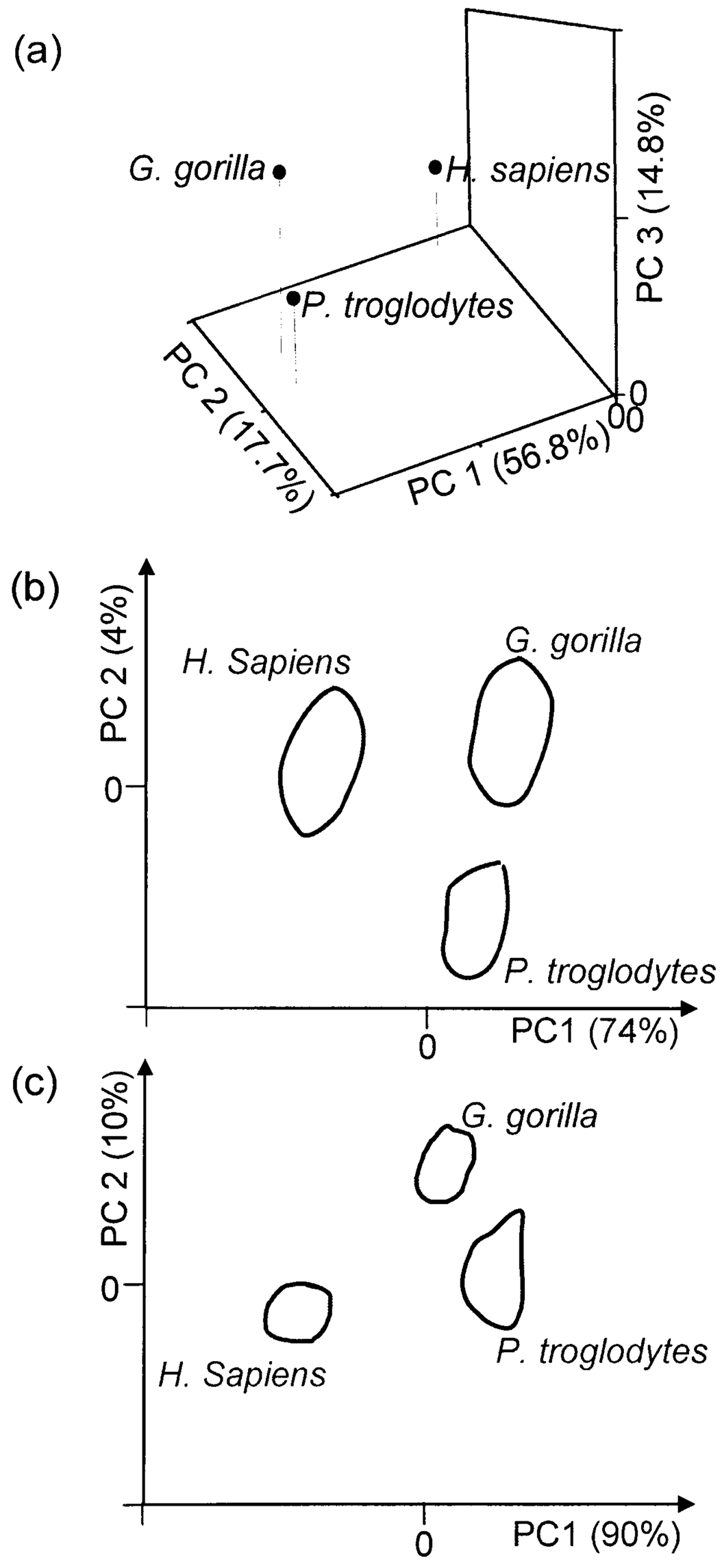

Figure 2.2. Morphological affinities of hominoid pelves. Published principal components analyses comparing hominoid pelvic morphology (a) McHenry & Corruccini (1975) (b) Berge (1984a) (c) Berge (1998). Outlines demark boundaries of data points.

sexual dimorphism whilst other dimorphisms were specific to either modern humans or African apes. Overall, the patterns of sexual dimorphism tended to distinguish the modern humans from the African apes. Tague (1991) devised a new method to compare patterns of sexual dimorphism across primates. Tague collected 14 pelvic dimensions from adult hominoids and calculated indices of sexual dimorphism for each species. The indices were ranked according to magnitude. A pairwise comparison of the ranks (Spearman Rho correlation test) revealed high correlations between all three species (Table 2.2). Thus the pattern of sexual dimorphism was reported to be comparable across the three hominoid species.

Species	*H. sapiens*	*P. troglodytes*	*G. gorilla*
H. sapiens	-		
P. troglodytes	0.80 *	-	
G. gorilla	0.87 *	0.67 *	-

Table 2.2. Spearman's rank order correlation coefficients comparing indices of pelvic sexual dimorphism (female*100/male) among hominoids. A two tailed test of significance was used* $p < 0.05$. Data from Tague (1991).

2.2. Aims

The aim of this chapter is to test two hypotheses. (1) The African apes display similar pelvic proportions to the exclusion of modern humans. (2) The African apes display a common pattern of pelvic sexual dimorphism that is distinct from that of modern humans.

2.3. Materials and methods

2.3.1. Quantifying pelvic morphology

A small sample of adult specimens representing *H. sapiens*, *P. troglodytes* and *G. gorilla* was measured for this chapter. Adults were defined as having distally fused femoral epiphyses (following Steudel, 1981). The sample is described in Table 2.3. Thirty six pelvic dimensions were measured. A visual key to the measurements is given in Figure 2.3 and a description is given in Table 2.4. Linear measurements were calculated trigonometrically from landmark co-ordinate data collected using a Microscribe model 3DX (Immersion, California). The stated precision of the Microscribe is 0.38mm. A measurement error analysis was carried out because the African ape sample size was not large enough. However, a measurement error analysis based on a larger sample in chapter 3, which included the data collected for this chapter, showed that the landmarks were both accurate and repeatable. The data analysis presented in this chapter is intended to be exploratory and exemplify some of the methods adopted in the published literature and in subsequent chapters of this thesis.

The measurements satisfied one or more of the following (i) they had been previously shown to vary across species (ii) they described the overall size and shape of the *os coxa* (iii) they described the position of the major muscle insertions in relation to the acetabulum (iv) they approximated the size of the birth canal or (v) they had previously been shown to be sexually dimorphic. Measurements that had been previously shown to vary across the sexes are iliac height (D2) (Genoves, 1959; Segebarth-Orban, 1980; Straus, 1927) the length of the pubis (D9) (LaVelle, 1995) and pelvic diameter (D27) (Steudel, 1981). Pelvic diameter (D27) approximates the sagittal diameter of the birth canal though not precisely, since the shape and size of

the sacrum are not included (Steudel, 1981). The overall size and shape of the *ossa coxae* was characterised by the measures of iliac height (D1, D2, D6 and D12-D14) iliac width (D11, D21, D15 and D35) and the length of the ischial, pubic and ischio-pubic rami (D8, D10 and D16-17). The infero-superior length (height) of the *ossa coxae* was characterised by measuring the distance separating the iliac crest from the external wall of the acetabulum (D27) the distance separating the dorsal ilium from the ischial spine and the ischial tuberosity (D18-D20 and D28) the distance separating the auricular surface and the greater sciatic notch from the ischial spine and ischial tuberosity (D30-D34) the distance separating the anterior iliac border and the pubis (D30-D31). The positions of the muscular attachments, in relation to the iliac acetabulum, were characterised by the dimensions that measure the distance between the centre of the acetabulum and the iliac crest (D1, D3, D4-D9 and D11) ischium (D8) ischio-pubic ramus (D9). The size and shape of the joint surfaces, auricular surface and acetabulum was characterised by dimensions D22-D24 and D35-D36, respectively. The approximation of the two *os coxal* joint surfaces was measured by dimensions D7 and D25-D26.

2.3.2. Assessing the morphological affinities of the hominoid pelvis

The morphological affinities of the hominoid pelvis were assessed using CVA and PCA. The constructs of the CVA maximise variation between species whilst the constructs of the PCA maximise differences between individuals. In both studies species were compared using the 95% confidence ellipses. Where confidence limits overlapped species were deemed to show comparable proportions. The multivariate analyses were carried out on the original data and, in order to make sure that the species were discriminated according to proportions and not size, the analyses were

repeated with data scaled according to the geometric mean of measured dimensions. Thus it was possible to determine whether proportions alone could be utilised to distinguish hominoid pelves. In addition to describing the overall similarity and dissimilarity of pelvic morphology among species the multivariate analyses highlighted the variables that were most important for distinguishing species. The construct loadings (canonical loadings in CVA and component loadings in PCA) are the correlation coefficients between the original and constructed variables. Analogous to Pearson's r, the squared loading coefficients equal the percent of variance in that variable explained by the construct. The linear measurements that loaded most highly in the multivariate analyses were compared across the hominoids using traditional ratio based analyses. The dimensions were scaled according to the geometric mean of all linear measures and then compared across species using one-way ANOVA with Tukey's post hoc.

Species	**Sex**	
	Male	Female
H. sapiens	15	16
P. troglodytes	6	6
G. gorilla	6	6

Table 2.3. List of adult specimens measured for analysis in chapter 2.

2.3.3. Comparing patterns of pelvic sexual dimorphism across hominoids

Patterns of sexual dimorphism were compared across *H. sapiens*, *P. troglodytes* and *G. gorilla* using a method proposed by Tague (1991). The comparison was carried out in three steps (1) indices of sexual dimorphism (female mean x 100/male mean) were calculated for the measured pelvic dimensions (2) each dimension was assigned

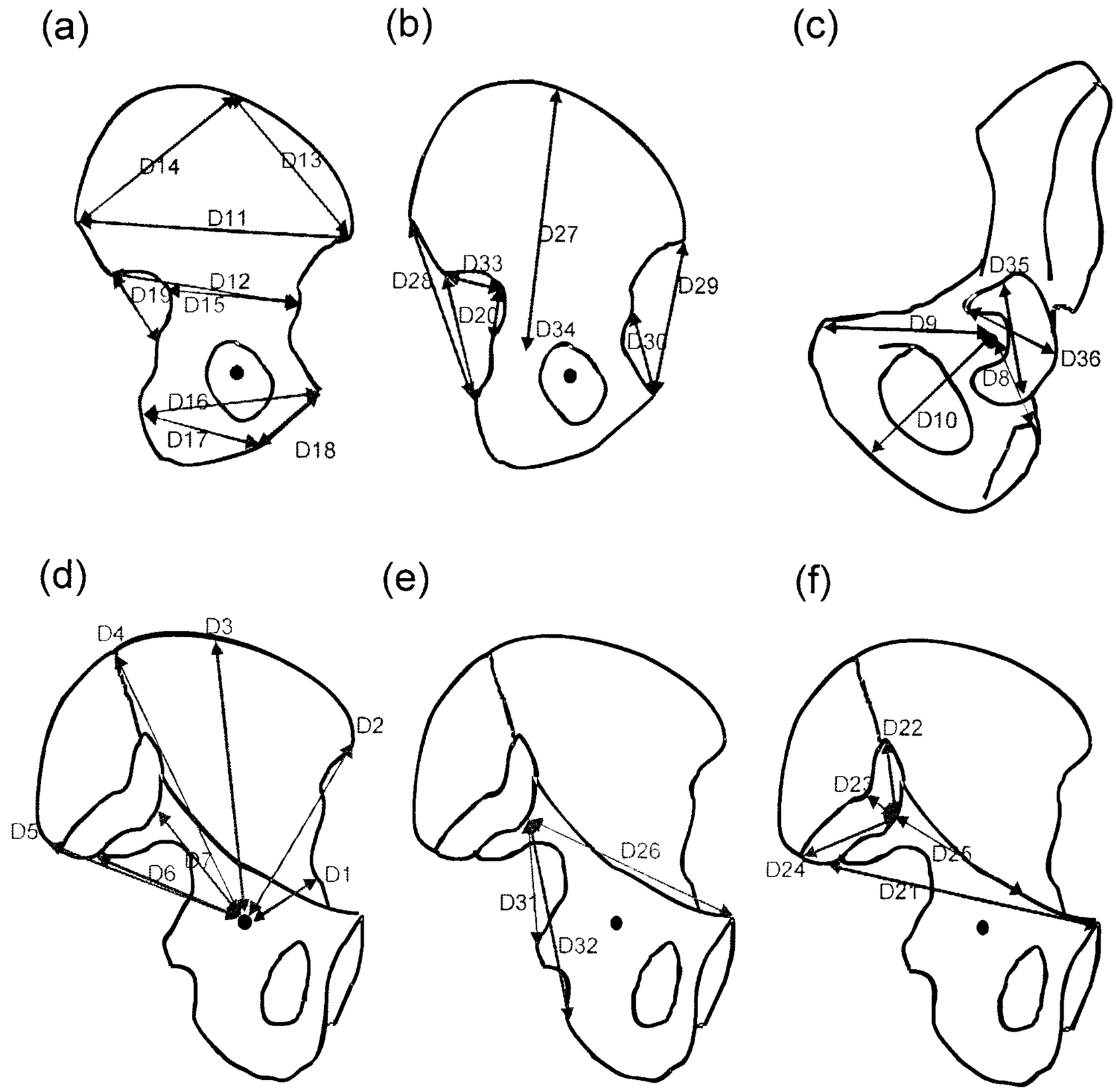

Figure 2.3. Thirty six *os coxal* dimensions were measured for this study. (a-b) lateral view (c) antero-lateral view (d-f) Medial View.

a rank according to the magnitude of sexual dimorphism and (3) a pair wise comparison of ranks was carried out using a two tailed Spearman's rank order correlation test. Spearman's correlation is a non-parametric test for the strength of the relationship between pairs of variables. Species that display a significant correlation can be deemed to show the same pattern of sexual dimorphism. A two tailed significance test was used. Spearman's correlation co-efficient (r^s) indicated the magnitude of the similarity.

Dimension		Landmarks	
No	**Name**		
D1	Anterior Iliac Height	Centre of Acetabulum	Anterior Superior Iliac Spine
D2	Iliac Height	Centre of Acetabulum	Midpoint Between Anterior and Posterior Musculature of the Iliac Crest
D3	Posterior iliac height	Centre of Acetabulum	Spina Limitans
D4	Iliac Height	Centre of Acetabulum	Posterior Superior Iliac Spine
D5	Posterior Iliac Height	Centre of Acetabulum	Posterior Inferior Iliac Spine
D6		Centre of Acetabulum	Anterior Inferior Iliac Spine
D7	Caudal Iliac Height	Centre of Acetabulum	Scalenion
D8	Ischial Length	Centre of Acetabulum	Ischial Tuberosity
D9	Pubis Length	Centre of Acetabulum	Ischio-pubic ramus
D10		Centre of Acetabulum	Pubic Symphysis
D11	Superior Iliac Width	Anterior Superior Iliac Spine	Posterior Superior Iliac Spine
D12	Inferior Iliac Width	Anterior Inferior Iliac Spine	Posterior Inferior Iliac Spine
D13	Chord Length of Anterior Iliac Crest	Anterior Superior Iliac Spine	Midpoint Between Anterior and Posterior Musculature of the Iliac Crest
D14	Chord Length of Posterior Iliac Crest	Posterior Superior Iliac Spine	Midpoint Between Anterior and Posterior Musculature of the Iliac Crest
D15	Iliac Width	Greater Sciatic Notch	Anterior Inferior Iliac Spine
D16	Ischio-pubis length	Ischial Tuberosity	Pubic Symphysis
D17		Ischial Tuberosity	Ischio-pubic ramus
D18		Ischio-pubic ramus	Pubic Symphysis

Table 2.4. Description of measured pelvic dimensions (continued on next page).

	Dimension	Landmarks	
No	**Name**		
D19	Width of Sciatic Notch	Posterior Inferior Iliac Spine	Ischial Spine
D20	Posterior Pelvic length	Posterior Inferior Iliac Spine	Ischial Tuberosity
D21	Pelvic Diameter	Posterior Inferior Iliac Spine	Pubic Symphysis
D22	Auricular Height	Scalenion	Superior Auricular Surface
D23		Scalenion	Posterior Auricular Surface
D24	Auricular Width	Scalenion	Posterior Apex of Auricular Surface
D25		Scalenion	Ilio Pubic Eminence
D26		Scalenion	Pubic Symphysis
D27	Iliac Length	Midpoint Between Anterior and Posterior Musculature of the Iliac Crest	External Acetabular wall
D28		Posterior Superior Iliac Spine	Ischial Tuberosity
D29	Anterior Pelvic Length	Anterior Superior Iliac Spine	Pubic Symphysis
D30		Anterior Inferior Iliac Spine	Pubic Symphysis
D31		Scalenion	Ischial Spine
D32		Scalenion	Ischial Tuberosity
D33		Posterior Inferior Iliac Spine	Greater Sciatic Notch
D34		Greater Sciatic Notch	Ischial Spine
D35	Acetabular Height	Superior Acetabulum	Inferior Acetabulum
D36	Acetabular Width	Anterior Acetabulum	Posterior Acetabulum

Table 2.4. Description of measured pelvic dimensions (continued from previous page).

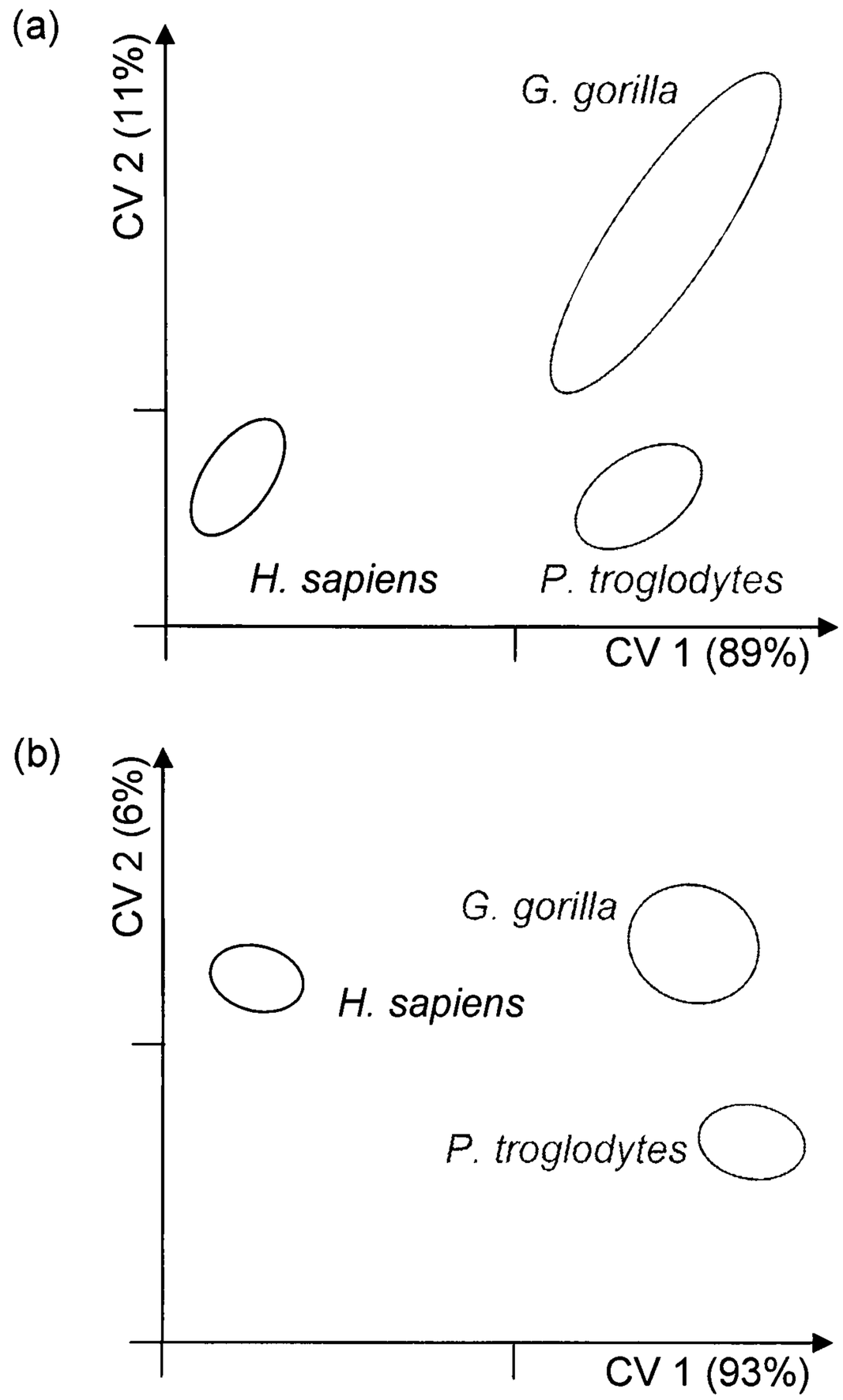

Figure 2.4. Interspecific comparison of adult hominoid *os coxal* morphology. Canonical variates analyses based on *os coxal* dimensions: ellipses represent 95% confidence limits. (a) Measured linear dimensions (b) linear dimensions scaled according to geometric mean.

2.4. Results

The separation of the confidence ellipses in the CVA analyses indicates that with regard to pelvic proportions, the African apes are more similar to each other than either is to the modern humans (Figure 2.4). The PCA morphospaces indicate that the African apes show comparable pelvic proportions which are distinct from the modern

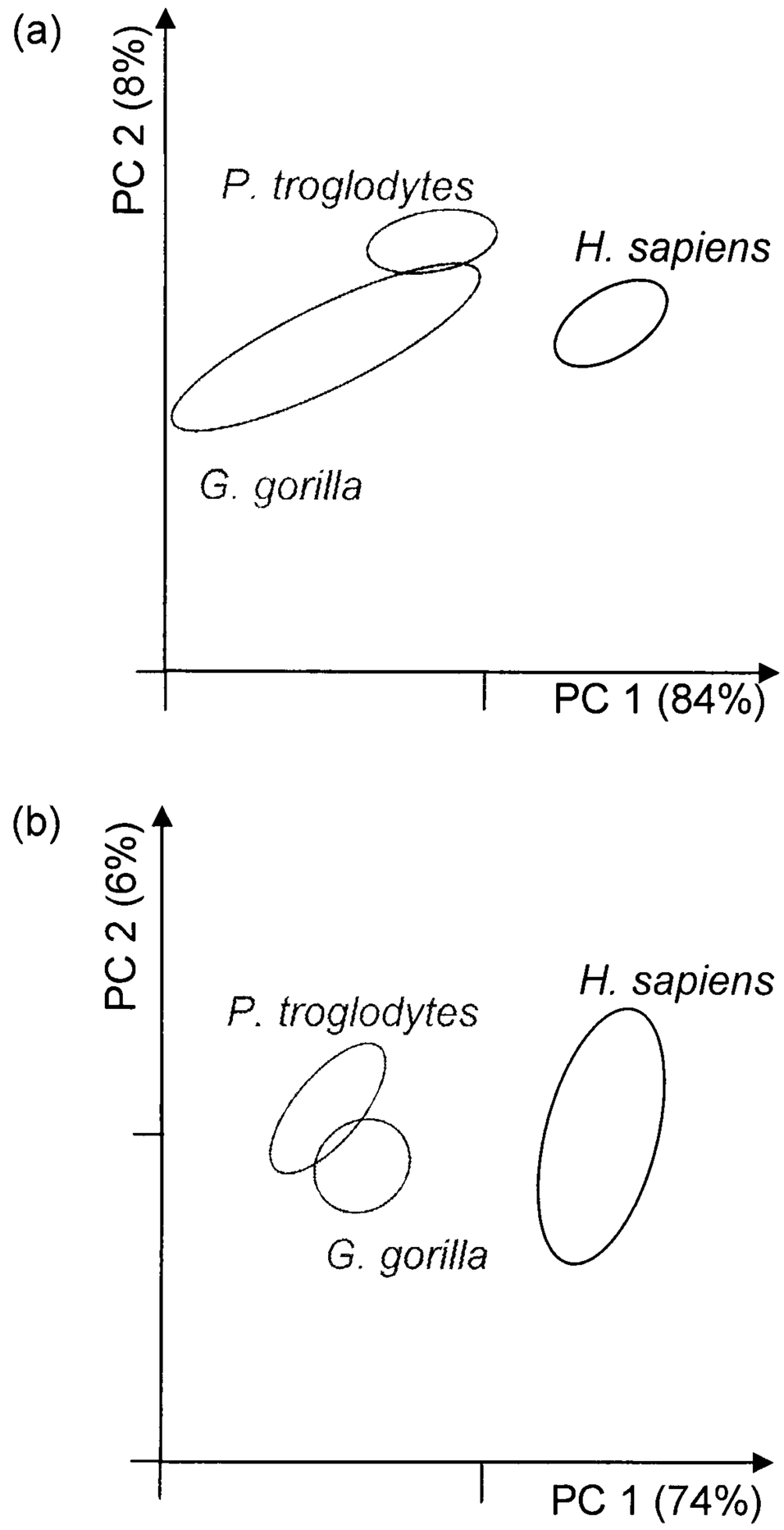

Figure 2.5. Interspecific comparison of adult hominoid *os coxal* morphology. Principal components analyses based on *os coxal* dimensions: ellipses represent 95% confidence limits. (a) Measured linear dimensions (b) linear dimensions scaled according to geometric mean.

humans. The measured dimensions that loaded most highly (0.2 - 0.5) on the first two constructs of CVA (Table 2.5) and PCA (Table 2.5) were compared among hominoids (Table 2.6). When scaled according to overall pelvic size, i.e. geometric mean of linear measurements, 10/21 dimensions distinguished modern humans from the African apes, 4/21 distinguished *H. sapiens* and *G. gorilla* from *P. troglodytes*, 7/21 distinguished all three species.

Dimension	Loading Co-efficients							
	CVA[a]		CVA[b]		PCA[a]		PCA[b]	
	CV 1	CV 2	CV 1	CV 2	PC 1	PC 2	PC 1	PC 2
D1	0.176	0.077	-0.005	-0.011	-0.223	0.039	-0.135	-0.022
D2	-0.162	-0.052	-0.010	-0.003	-0.235	-0.079	-0.083	-0.057
D3	-0.038	-0.109	0.032	0.116	-0.280	-0.016	-0.166	-0.032
D4	0.049	0.044	0.003	0.067	-0.289	0.051	-0.216	-0.044
D5	0.024	-0.074	-0.038	0.091	-0.066	0.031	0.020	0.147
D6	0.228	-0.123	-0.280	0.158	-0.099	0.047	-0.063	0.005
D7	0.337	0.188	-0.026	-0.091	-0.172	0.038	-0.134	-0.009
D8	0.063	0.046	-0.013	-0.006	-0.122	-0.070	-0.061	-0.006
D9	-0.078	-0.042	0.017	0.020	-0.043	-0.234	0.112	-0.396
D10	-0.087	0.134	-0.008	-0.106	-0.035	-0.212	0.146	0.083
D11	-0.152	0.362	-0.040	-0.389	-0.078	-0.460	0.232	-0.231
D12	-0.216	0.256	0.082	-0.279	0.045	-0.260	0.270	-0.013
D13	0.005	-0.048	0.159	0.058	0.092	-0.332	0.337	-0.019
D14	0.098	0.168	0.038	-0.186	-0.105	-0.388	0.120	-0.285
D15	-0.303	-0.109	0.339	0.230	0.003	-0.189	0.145	-0.090
D16	0.069	-0.049	-0.034	0.043	-0.101	-0.176	0.101	0.467
D17	-0.115	-0.013	0.016	-0.001	-0.043	-0.147	0.099	-0.060
D18	0.117	-0.198	-0.145	0.168	-0.063	0.031	-0.018	0.373
D19	0.153	-0.100	-0.208	0.187	-0.133	0.166	-0.120	-0.013
D20	0.127	-0.186	-0.210	0.124	-0.264	0.106	-0.236	0.070
D21	-0.066	0.286	0.075	-0.156	-0.054	-0.180	0.183	0.100
D22	0.121	0.083	-0.194	-0.076	-0.066	-0.138	0.007	-0.074
D23	0.023	-0.058	-0.060	0.012	-0.172	-0.023	-0.076	-0.078
D24	0.146	-0.036	0.048	0.061	0.053	-0.152	0.166	0.031
D25	-0.014	0.011	0.075	0.126	-0.087	0.018	0.003	-0.059
D26	-0.011	0.324	0.100	-0.220	-0.041	-0.173	0.104	-0.214
D27	0.019	0.099	-0.055	-0.058	-0.239	-0.111	-0.089	-0.063
D28	0.421	0.181	-0.379	-0.209	-0.492	0.102	-0.469	-0.100
D29	0.174	-0.020	-0.231	0.165	-0.262	0.000	-0.116	-0.315
D30	-0.026	-0.043	0.053	0.043	-0.137	-0.099	0.016	-0.279
D31	0.165	0.037	-0.271	0.032	-0.098	0.006	0.027	0.051
D32	-0.110	0.178	-0.004	-0.136	-0.306	0.061	-0.266	-0.059
D33	-0.032	-0.467	0.009	0.546	0.013	0.060	0.062	0.156
D34	-0.423	0.105	0.506	-0.019	0.042	-0.172	0.227	-0.051
D35	-0.116	-0.158	0.228	0.065	0.002	-0.129	0.114	-0.048
D36	-0.175	-0.211	0.096	0.175	0.014	-0.140	0.130	-0.029

Table 2.5. Construct loadings for CVA and PCA analyses. Symbols denote [a] test based on measured linear dimensions and [b] test based on linear dimensions scaled according to the geometric mean. The loading coefficients equal the percent of variance in a dimension that is explained by a construct, i.e. canonical variate or principal component.

Dimension	One-way ANOVA (Tukey's Post Hoc)		
	F	*p*	Post Hoc (p <0.01)
D04	192.366	< 0.001	H < P & G
D06	16.638	< 0.001	H < P & G
D07	48.347	< 0.001	H < P & G
D09	11.966	< 0.001	G > P
D10	147.830	< 0.001	G > P
D11	420.325	< 0.001	H > G > P
D12	459.737	< 0.001	H > P & G
D13	268.970	< 0.001	H > P & G
D14	64.537	< 0.001	H & G > P
D15	190.854	< 0.001	H > G > P
D18	5.479	< 0.010	G < P
D19	48.703	< 0.001	H < G < P
D20	247.841	< 0.001	H < G < P
D26	49.941	< 0.001	H > G > P
D28	758.193	< 0.001	H < P & G
D29	19.961	< 0.001	H < P & G
D31	3.969	< 0.050	H & G < P
D32	219.127	< 0.001	H < P & G
D33	62.325	< 0.001	P > H > G
D34	165.086	< 0.001	H > P & G
D35	278.505	< 0.001	H > P & G

Table 2.6. Ratio based interspecific comparison of hominoid *os coxal* proportions. Measured dimensions were scaled according to overall *os coxal* size and the ratios were compared across species using a one-way ANOVA with Tukey's post hoc. Symbols denote: H, *H. sapiens*; P, *P. troglodytes* and G, *G. gorilla*.

Indices of sexual dimorphism calculated for *H. sapiens* are not correlated with indices calculated for *P. troglodytes* (Spearman's Rho, $r^s = 0.24$ and $p > 0.05$) or *G. gorilla* (Spearman's Rho, $r^s = 0.10$ and $p > 0.05$). Indices of dimorphism calculated for *P. troglodytes* and *G. gorilla* are correlated (Spearman's Rho, $r^s = 0.45$ and $p < 0.01$). Hence the African apes appear to show a comparable pattern of sexual dimorphism that is distinct from that of modern humans (Table 2.6).

2.5. Discussion

The narrowest part of the pelvic birth canal is the pelvic inlet. The pelvic inlet of modern humans is smaller than that of the African apes in relation to the size of the fetal cranium at term (Figure 2.6). When scaled according to the transverse

dimension of the pelvic inlet the fetal cranium of modern humans is ~30-45% larger than it is in the African apes at term (see Leutenegger, 1974). Leutenegger (1974) calculated the ratio of the longest cranial dimension/transverse dimension of the pelvic inlet across *H. H. sapiens* (1.02) *P. troglodytes* (0.72) and *G. gorilla* (0.64). These results suggest that the narrowest part of the birth canal in African apes allows ample room for the fetal cranium to pass through. In contrast the fetal cranium of modern humans is too large to fit through the narrowest portion of the pelvic inlet. This has necessitated novel birthing mechanics in modern humans. In modern humans the fetus flexes (dorsally or ventrally) and rotates within the pelvic cavity (Figure 2.6) (Berge, 1984b; Rosenberg & Trevathan, 2001; Trevathan, 1988).

Given that birthing is so difficult in modern humans (Smith, 1998), obstetric function can be expected to influence pelvic morphology (Berge, 1984b; Stern & Susman, 1983). Obstetric constraints and mechanics of birthing in the African apes are similar to the exclusion of modern humans. Therefore, one might expect that patterns of sexual dimorphism will also distinguish modern humans from African apes. The interspecific comparison of patterns of pelvic dimorphism shows the African apes share a common pattern of sexual dimorphism that is distinct from modern humans. Hence it is reasonable, to suggest that obstetric requirements may influence the pelvic morphology of females and, therefore, patterns of sexual dimorphism.

The pelvis is one of the most important bones in the hominoid musculoskeletal system (Inman *et al.,* 1981). The pelvis fulfils several key functions such as providing attachments for the major locomotor muscles (Berge, 1984), transmitting loads between the trunk and lower limbs (Ries *et al.,* 1989b) and moving to maintain

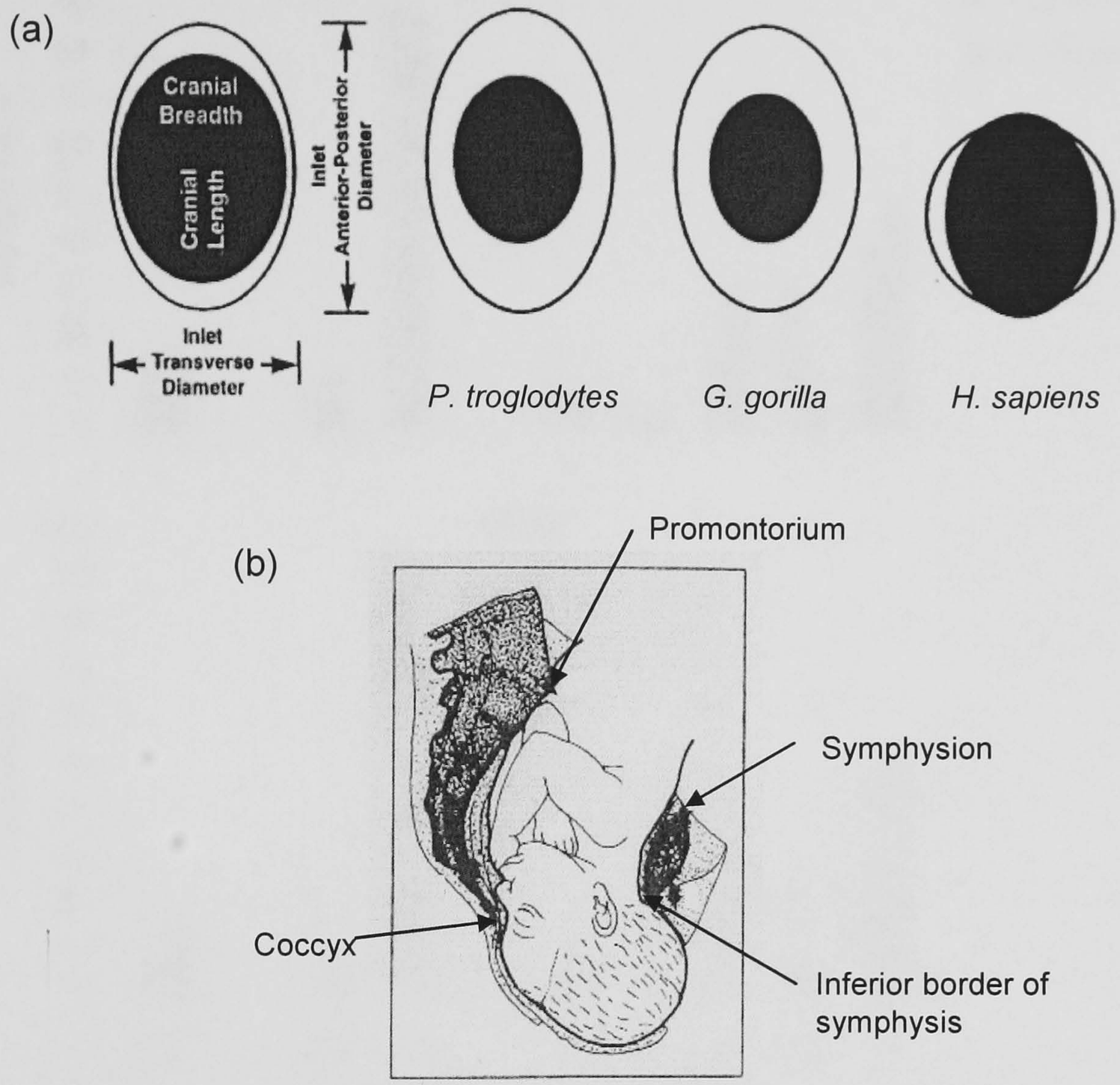

Figure 2.6. Hominoid obstetric constraints and mechanics of birthing. (a) The relationship between the size of the maternal pelvic inlet and size of the newborn head. Maternal pelvis and neonatal cranial outlines are indicted diagrammatically, but scaled so the transverse diameters of the maternal pelvic inlets are common across species. Figure modified from Rosenberg & Trevathan (2002). (b) Human obstetrical mechanics differ from the African apes in two key ways (i) flexion of the foetus and (ii) rotation of the foetus. This is illustrated by the sagittal position of the head in the pelvic outlet (between the coccyx and symphysion) and the oblique position of the shoulders within the pelvic inlet (between the coccyx and inferior border of symphysis). Figure modified from Berge (1984b).

balance (Inman *et al.,* 1981; Saunders *et al.,* 1953). It is reasonable to suggest that locomotor behaviour will also influence hominoid pelvic morphology. If this is the case one would expect hominoid locomotor behaviour and pelvic morphology to be correlated.

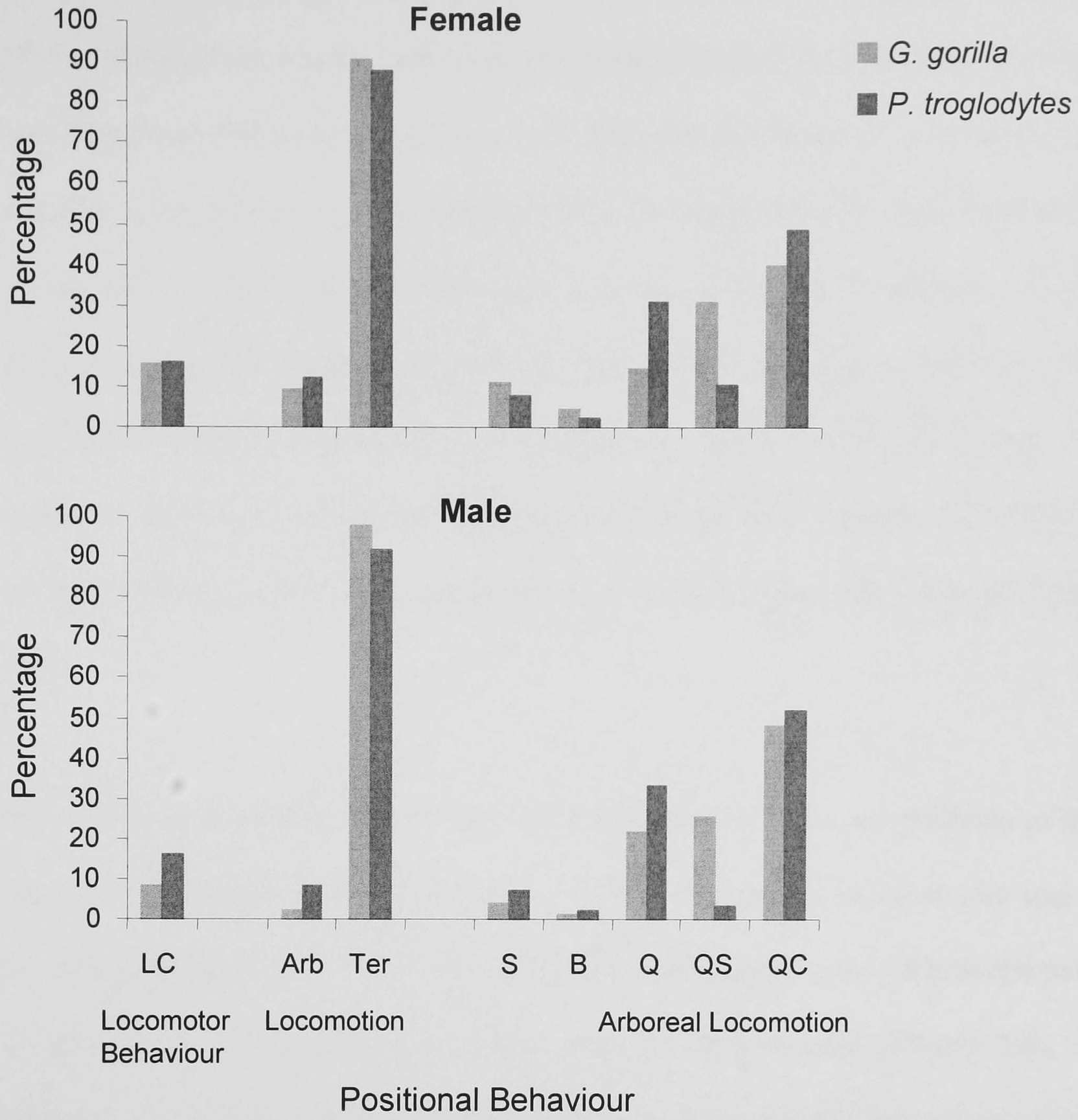

Figure 2.7. Locomotor behaviour percentages (based on continuous locomotor bout sampling) for adult African ape species. Abbreviations denote: LC, locomotion; Arb, arboreal; Ter, terrestrial; S, suspensory, B, bipedal; Q, quadrupedal; QS, quadrumanous scrambling; QC, quadrumanous climbing. Data taken from Carlson (2005).

The locomotor behaviour of adult *P. troglodytes* and *G. gorilla* is very similar (Hunt, 1992; Napier, 1976). As adults both are primarily terrestrial quadrupeds but both are partly arboreal, although *P. troglodytes* tend to be less terrestrial and more arboreal than *G. gorilla* (Figure 2.7). Furthermore, *P. troglodytes* and *G. gorilla* adopt the same locomotor behaviours when negotiating arboreal environments. Both species move through trees using suspensory, bipedal, quadrupedal, quadrumanous climbing

and quadrumanous scrambling behaviours (Carlson 2005; Doran, 1992, 1997; Hunt, 1996). Although locomotor behaviour percentages (based on continuous locomotor bout sampling) differ slightly (Figure 2.7). The smaller, lighter *P. troglodytes* tends to adopt quadrupedal walking/running whilst the larger, heavier *G. gorilla* tend to display more quadrumanous scrambling (Doran, 1997) which spreads the body weight across more branches. In contrast to the partly arboreal quadrupedal African apes adult modern humans are habitual bipeds. Modern humans do not tend to make use of the arboreal environment. If pelvic morphology and locomotor behaviour are correlated pelvic morphology should distinguish modern humans from the African apes.

Both CVA analyses indicate that the African apes bear more resemblance to each other than to modern humans. Separation of the African apes is due to size and not proportions (Figure 2.4). The results of the PCA also suggest that African ape pelvic morphology is comparable and distinct from modern humans (Figure 2.5). The measured dimensions that explained most of the variance in the data set also tended to distinguish modern humans from African apes (Table 2.6). Hence the multivariate and univariate analyses concur. The findings of this chapter agree with previous researchers that the African apes display similar or comparable pelvic shape that is distinct from modern humans (Berge, 1984a, 1998; McHenry & Corruccini, 1975; Steudel, 1978, 1981). Adult bony morphology is the product of growth and development. Therefore one might expect the pattern of pelvic growth and development to also distinguish modern humans form the African apes. Furthermore, if the notion that function affects morphology is correct the two factors should be related during ontogeny.

Part II: External Iliac Morphology of Hominoids

Chapter 3. Phylogenetic Perspectives

3.1 Comparative studies of ontogenetic allometry

According to the data presented in Chapter 2 as well as other published studies (e.g. Berge, 1984a, 1998; McHenry & Corruccini, 1975; Steudel, 1978, 1981) the adult iliac morphology differs significantly among hominoids. In theory, the morphology of adults from different species may differ because (a) the pattern of shape change that occurs with increasing age differs among species or (b) the temporal scale of development varies between species i.e. one species may grow for a longer period of time. In other words the relative growth rates of different anatomical features (Huxley & Tessier, 1936) as well as the duration of growth ultimately determine adult morphology (Alberch *et al.,* 1979; Gould, 1966; Rice, 1997). Therefore, in order to understand how or why adult hominoid ilia differ it is necessary to compare ontogenetic changes in morphology. This can be accomplished by comparing ontogenetic allometry, i.e. the changes in shape that occur in an individual during growth (i.e. increase in size). Only longitudinal data can yield an accurate description of growth (Sholl, 1950; Cock, 1966). This is because the growth of individuals within a population can vary substantially (Tanner, 1962). However, longitudinal studies are not always feasible, and it is usually only possible to study preserved specimens. Although improvements medical imaging techniques may make longitudinal studies possible in the future. Cross-sectional studies can be used to obtain information on growth, but only the average growth of a population (Cock, 1966).

3.1.1 Ontogenetic allometric trends and taxonomy

Morphological studies within a comparative framework may allow the phylogenetic relationships between species to be studied. The taxonomic relationships between species have traditionally been studied using morphological studies of affinity based on adult specimens. Species that display comparable bony shape are probably more closely related than those species that display very different shapes. However, ontogenetic studies may provide a better understanding of taxonomic relationships between species (Gould, 1966). For example, Lumer and Schultz (1941) utilised bivariate allometric regressions of tail length and trunk height to distinguish *Macaca* species. The curves for *Macaca philippinensis* (=*Macaca fasicularis*) and *Macaca sinicus* (=*Macaca radiata*) converged at adult size. This highlights the importance of considering ontogenetic allometry when comparing species and making phylogenetic inferences. Static (adult based) and ontogenetic (non-adult based) allometries are often very different and results based on static studies may be unreliable.

It is possible that species which display comparable ontogenetic allometries are likely to be more closely related than species which display divergent allometries (Bocquet, 1953; Lumer & Schultz, 1941; Olsen, 1952; Ravosa & Profant, 2000) (Figure 3.1). Albrecht (1978) analysed bivariate regressions of papionin cranial dimensions and found that inter-specific differences in *Macaca* cranial morphology were largely due to the effects of size divergence operating on shared patterns of relative growth. Profant (1995) compared patterns of ontogenetic allometry across macaques (*Macaca fasicularis*, *Macaca nemestrina*) and baboons (*Papio cynpcephalus*). With respect to basion-nasion length most patterns of relative growth were indistinguishable between the macaque species. In contrast the baboons

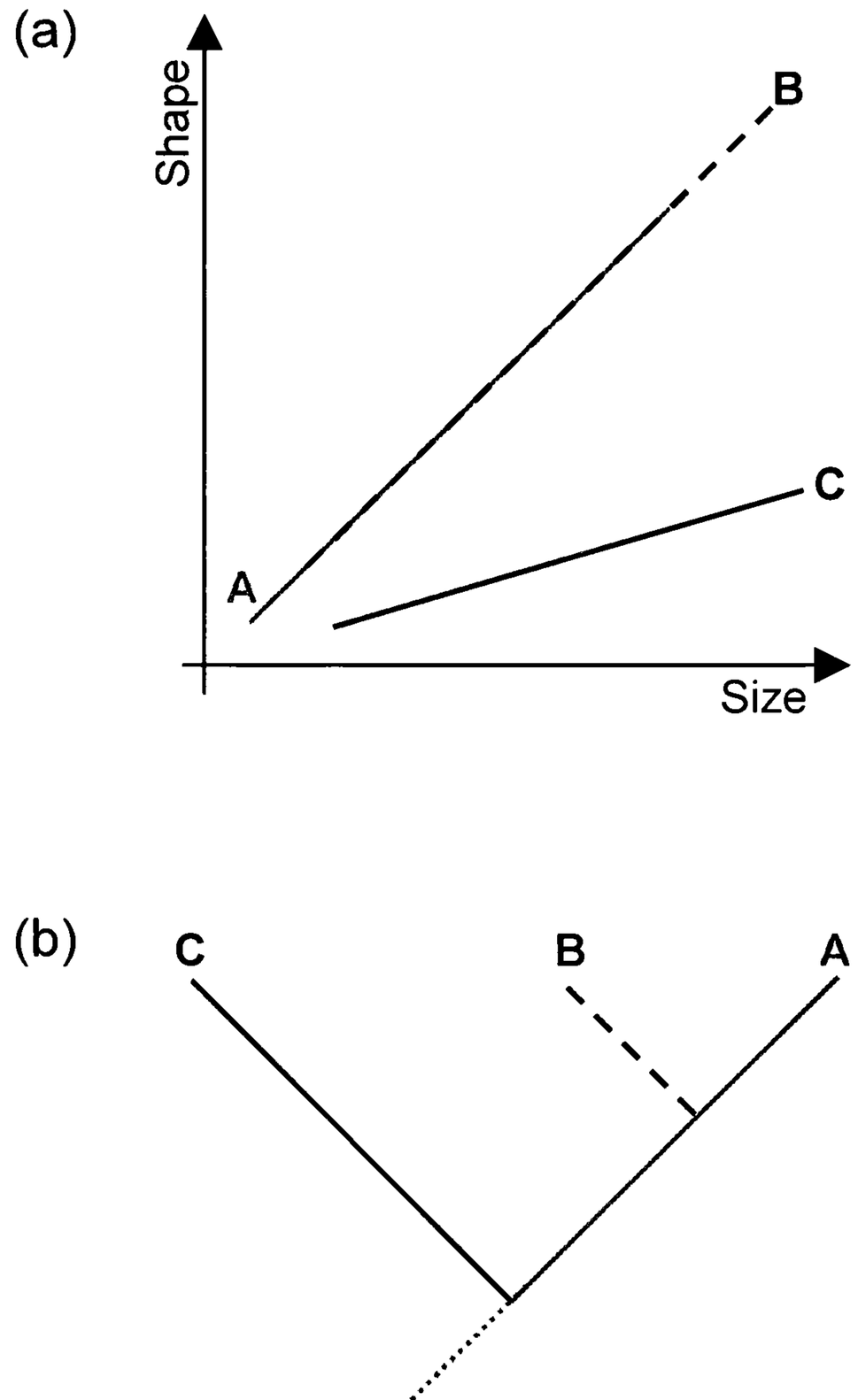

Figure 3.1. Ontogenetic allometry and phylogeny, sensu Gould (1966). A, B and C represent three species. (a) Depicts size related ontogenetic changes in proportions (b) Relative growth rates and, therefore, allometry tend to be more similar in closely related species than distantly related species. Hence allometric plots can be used to infer phylogeny.

presented a different allometric relationship. Ravosa & Profant, (2000) concluded that the macaque species were more closely related to each other than either was to the baboon. However, comparative studies of growth development may disagree depending on the type of statistical analysis used. Shea (1985d) published a multivariate PCA, combining macaques and baboons, which suggested a different relationship between the taxa too that proposed by Ravosa & Profant (2000). The first PC, which was treated as a size vector, accounted for 98% of the variation, only 2% of the variance was unexplained by non-allometric factors. The multivariate

growth trajectories for macaques and baboons were all comparable, suggesting the three species were sister taxa. Sister taxa are species derived from a common ancestor.

3.1.2 Ontogenetic allometry in the hominoid pelvis

Previous studies have shown that the pelvic morphology of adult African apes is similar to each other and distinct from modern humans (Berge, 1991a; Jungers & Hartman, 1988). Therefore, it is reasonable to suggest that the African apes may follow a similar pattern of change in pelvic shape during ontogeny, distinct from modern humans. To date, only one study has considered ontogenetic change in hominoid pelvic morphology. Berge (1998) collected 17 linear pelvic measurements (Figure 3.2) from individuals representing *H. sapiens*, *P. troglodytes* and *G. gorilla.* Ontogenetic change in pelvic proportions was analysed using a combination of bivariate and multivariate analysis of linear dimensions. Bivariate ontogenetic allometric coefficients, based on pelvic length (distance between the iliac crest and ischial tuberosity), were calculated for each species using least squares regression. Model I regression may underestimate the true value of the allometric co-efficient (α) (Ebert & Russell, 1994; Lande, 1979; Smith, 1980). Allometric coefficients and standard errors were extracted from the paper and used to calculate 95% confidence limits for each regression. This facilitated a statistical comparison of slopes across the three species. Of the 16 bivariate regressions only one differed between the African apes: the height of the ilium between the iliac crest and the centre of the acetabulum (dimension ILL in Figure 3.2). With respect to pelvic height, iliac height scaled more positively allometrically in *P. troglodytes* than *G. gorilla.* Berge reported that the African apes displayed a largely common pattern of change in

(a)

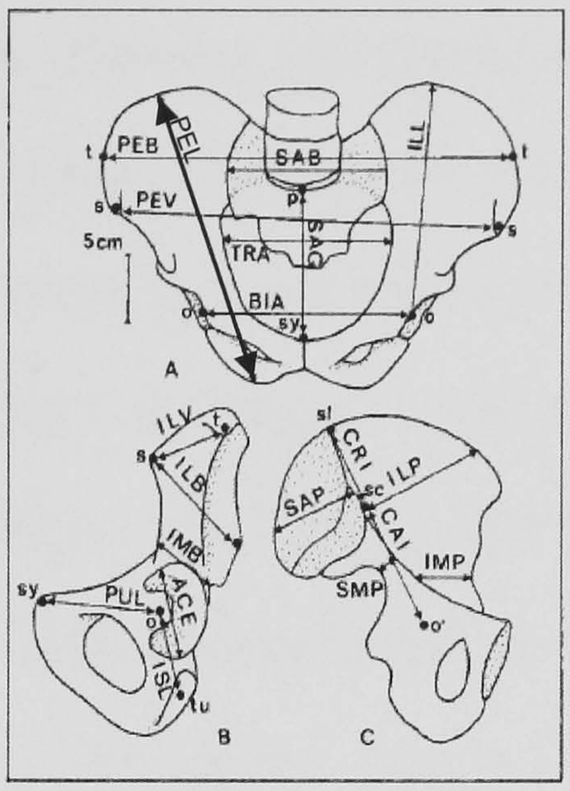

Measured Dimensions

(b)

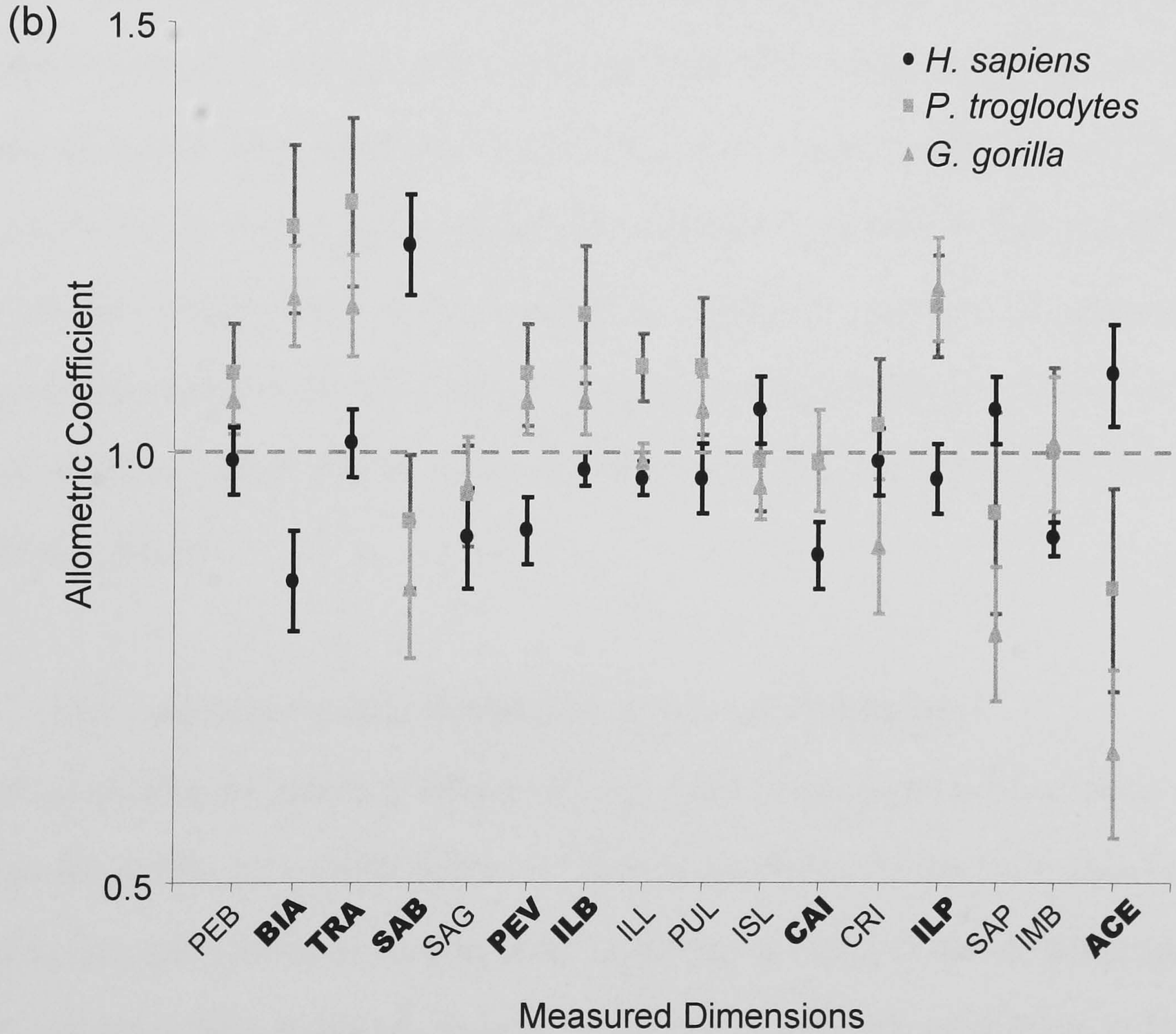

Figure 3.2. Ontogenetic allometry in the hominoid pelvis. (a) Diagram depicting measured pelvic dimensions. (b) Bivariate regression slopes for external dimensions versus pelvic length. Bold abbreviation on the abscissa axis denote measurements which distinguish the African apes from modern humans. Error bars denote mean and standard deviation. Dashed grey line indicates isometry. Line drawing and data adapted from Berge (1998).

proportions during development, i.e. relative growth rates are the same in the two species. This would explain why the adult African apes exhibit similar pelvic morphology (see Berge, 1984a; McHenry and Corruccini, 1975; Steudel, 1978, 1981). In contrast, half of the measurements scaled differently across in modern humans and African apes. The coefficients that distinguished modern humans from the African apes are highlighted in bold along the abscissa axis in Figure 3.2b. The transverse dimensions of the pelvis scaled more negatively allometrically in *H. sapiens* (BIA, TRA, and PEV). Berge attributed this to the in-curving of the anterior iliac blade that occurred during the development of modern humans, but not African apes. The sagittal dimensions of the iliac blade also scaled more negatively allometrically in *H. sapiens* (ILP, ILB) as does the width of the acetabulum (ACE) and the caudal iliac height (CAI) (see Figure 3.2). Overall, Berge reported that modern humans have a pattern of size related change in proportions that is distinct from the African apes, at least during the period of postnatal development encompassed by the sample. Following Ravosa & Profant (2000) the African apes would thus be deemed more closely related to each other than either would be to modern humans.

3.1.3 Ancestral pattern of hominoid growth and development

By considering the pattern of ontogenetic allometry in an outgroup species it may be possible to infer the ancestral pattern of hominoid growth and development (Baker & Wilisond, 2001; Jaecks & Carlson, 2001). A suitable outgroup is one (or more) taxa that branched from hominoids (ingroup) before they branched from each other. The choice of species for an outgroup is important, because it determines the assumed ancestral pattern of development, which inevitably varies across distantly related

species. Species that lie closest to the root of the ingroup are the most suitable (i.e. first clade/species to bud off before last common ancestor of ingroup). Thus, for the Hominoidea, *Pongo pygmaeus* or *Hylobates sp.* would be ideal candidates.

3.2 Aims and objectives

This chapter has two aims (1) infer the ancestral pattern of ontogenetic change in external iliac morphology of the hominoids using a cercopithecoid outgroup comparison and (2) infer for the taxonomic relationships between the Hominoidea, relative to a cercopithecoid outgroup, from ontogenetic allometric analyses of the ilium.

3.3 Materials and methods

Collecting measurements from the non-adult pelvis when the ilium, ischium and pubis are un-fused is difficult. There are several sites of secondary ossification and fusion in the pelvis. The iliac epiphyses (secondary centres of ossification) appear at the crest and the acetabulum (Delaere *et al.,* 1992; Laurenson, 1965). The pubic epiphyses appear at the acetabulum and at the body, crest and ramus of the pubis (Gray, 2000). The secondary centres of ischial ossification appear at the acetabulum, ramus of the ischium and, occasionally, the ischial tuberosity (Scheuer & Black, 2000). Ischio-pubic fusion occurs at around 7-8 years (Scheuer & Black, 2000). Three epiphyses fuse in the region of the acetabulum (Gray, 2000). The anterior acetabular epiphysis (*os acetabuli*), which separates the ilium and pubis, fuses at around 9-10 years (Ponsetti, 1978b; Zander, 1943). The posterior acetabular epiphysis (*os marginalis*), which separates the ilium and ischium, fuses at around 12-14 years (Scheuer & Black, 2000). The superior epiphysis, which forms the upper

part of the acetabulum and separates the ilium, ischium and pubis appears at around 12-14 years and may not fuse completely until 16 or 17 years (Brothwell, 1981; Scheuer & Black, 2000). The superior epiphysis frequently extends superiorly to form the lower region of the anterior iliac spine (Delaere & Dhem, 1999; Scheuer & Black, 2000). The epiphysis at the iliac crest may not fuse completely until as late as 26 years of age (Brothwell, 1981; Scheuer & Black, 2000). The pelvic elements can be reconstructed to allow measurements (see Berge, 1998). However, this relies on researchers being able to match bones from different individuals correctly. Also, when soft tissues are absent, such as the thick triradiate cartilage which separates the three elements of the *os coxa*, larger measurement errors are inevitable. Furthermore, the pelvis is often poorly preserved in the archaeological record and the pubis, ischio-pubic ramus and ischium often become broken or damaged after burial (Walker and Johnson, 1988). The ilium is the only portion of the *os coxa* which usually survives intact enough to measure. Hence, measurements of the pelvis can be difficult in adults as well as non-adults and, consequently, this study focused on the hominoid ilium only.

3.3.1 Sample and provenance

In total, 203 postnatal *os ilia* representing *Homo sapiens* (modern human), *Pan troglodytes troglodytes* (central common chimpanzee), *Gorilla gorilla gorilla* (western lowland gorilla), *Cercopithecus nictitans* (white nosed monkey), *Cercopithecus cephus* (moustached monkey) and *Cercopithecus pogonias grayi* (crested mona monkey) were included in the study. Where possible the left *os ilium* was measured. The specimens and sources are listed in Table 3.1. The modern human sample includes buried specimens from Egypt (2040-1997 BC) and Britain

(597-1450 AD and present day) (Table 3.1). Non-human primates were wild shot specimens collected from Congo, Zaire and Cameroon at the turn of the 19th-20th century; the material is held at the Powell Cotton Museum (Birchington, Kent).

Species	Source(s)	Developmental Stage					Total
		M0	M1	M2	M3	Adult	
Homo sapiens	1, 2 & 3	15	15	7	5	31	73
Pan troglodytes schweinfurthii	1 & 4	9	10	11	12	12	54
Gorilla gorilla gorilla	4	12	9	5	7	12	45
Cercopithecus nictitans	4				7	6	13
Cercopithecus cephus	4				5	3	8
Cercopithecus grayii	4				6	4	10
Total		36	34	23	42	68	203

Table 3.1. Sample size and provenance of specimens. Sources, 1 Department of Human Anatomy at the University of Liverpool; 2, The Department of Archaeological Sciences at The University of Bradford; 3, Leverhulme Centre for Human Evolutionary Studies; 4, The Powell Cotton Museum. Developmental stages defined according to molar eruption and bony fusion; M0, no permanent molars; M1, all first permanent molars; M2, all second molars; M3, all third molars; Adult, distal femoral epiphyses completely fused.

3.3.2 Defining ontogenetic series

The ontogenetic series were broken down into developmental stages on the basis of permanent molar eruption (following Berge & Penin, 2004; Penin *et al.,* 2002) and bony fusion (following Steudel, 1982). Permanent molar eruption was recorded for each measured specimen from cranial remains. Specimens were classed as to whether none or all of the first/second/third permanent molars were erupted. Assessing dental eruption was difficult because the specimens did not have any soft tissue i.e. gums. Teeth were deemed to be fully erupted when worn. As newly erupted teeth may not show wear, occluding molars were also deemed to be fully erupted. Adults were defined as having distally fused femora.

3.3.3 Hominoid outgroup analysis

Specimens representing *P. pygmaeus* or *Hylobates* were not available for this study. Three species representing the Cercopithecidae (*C. nictitans*, *C. cephus* and *C. p. grayi*) were used as an out-group. Unfortunately the cercopithecoid sample is small and biased towards adults (Table 3.1) and it must be borne in mind that static allometries often present lower allometric coefficients than ontogenetic allometries. As it would have been preferable to calculate ontogenetic allometries using only non-adults, comparison across the hominoids and cercopithecoids samples used in this study must be considered tentative. The pattern of cercopithecoid covariation between iliac size and shape was assessed using a principal components analysis based on registered landmark data. Growth trajectories for human and non-human primates were compared by eye.

3.3.4 Landmark co-ordinate data

Thirty-two external bony landmarks (Table 3.2) were digitized using the same Microscribe (model 3DX, Immersion Corporation, San Jose, California) used in chapter 2. The Microscribe was used to measure co-ordinates in three dimensions. The landmarks used in a geometric morphometric analysis are assumed to be homologous (Slice *et al.,* 1996). The attributes of two organisms are considered homologous when they are derived from an equivalent characteristic of the common ancestor and develop from the same tissues during ontogeny (McClane, 1995; Wagner, 1989; 1994). This means that structures evolved from same feature in a common ancestor (the wings of bats and the arms of humans) and that the structures arose from the same tissue in embryological development. Three landmark types with varied levels of homology were designated following Bookstein (1991). Type I

No.	Landmark Name	Description	Landmark Type
L1	Anterior Superior Iliac Spine	Anterior Superior Iliac Spine	I
L2	Anterior Iliac Crest ^{M}	Point at widest section of anterior iliac crest	II
L3	Anterior Iliac Crest ^{L}	Point at widest section of anterior iliac crest	II
L4	Iliac Tubercle ^{M}	Point along iliac crest opposite L5	III
L5	Iliac Tubercle ^{L}	Maximum apex of tubercle	II
L6	Iliac Crest ^{M}	Point along iliac crest where anterior and posterior musculature meets	I
L7	Iliac Crest ^{L}	Point along iliac crest where anterior and posterior musculature meets	I
L8	Spina Limitans ^{M}	Point along iliac crest where arcuate line meets iliac crest	I
L9		Lateral aspect of iliac crest opposite L8	III
L10	Posterior Iliac Crest ^{M}	Point at widest section of posterior iliac crest	II
L11	Posterior Iliac Crest ^{L}	Point at widest section of posterior iliac crest	II
L12	Posterior Superior Iliac Spine	Posterior Superior Iliac Spine	I
L13		Deepest point along ridge between posterior iliac spines (L12 and L14)	II
L14	Posterior Inferior Iliac Spine	Posterior Inferior Iliac Spine	I
L15	Greater Sciatic Notch	Deepest point of greater sciatic notch	II
L16	Dorsal Ilium	Point along ischial spine where the ilium and ischium meet	I
L17	Ilio-Pubic Eminence	Ilio-Pubic Eminence	I
L18	Anterior Inferior Iliac Spine	Anterior Inferior Iliac Spine	I
L19		Deepest point along ridge between anterior iliac spines (L1 and L18)	II
L20	Lateral Apex of Acetabulum ^{L}	Apex of ridge between L16 and L18	I
L21	Inferior Auricular surface	Anterior inferior apex of auricular surface	II
L22		Point where arcuate meets auricular surface (Inferior)	II
L23	Scalenion	Scalenion	II
L24		Point where arcuate meets auricular surface (Superior)	II
L25		Anterior apex of auricular surface	I
L26		Anterior projection of auricular surface inferior to L27	II
L27	Superior Auricular Surface	Superior apex of auricular surface	I
L28		Posterior projection of auricular surface inferior to L27	III
L29	Posterior Auricular Surface	Posterior indent of capsular attachment	I
L30	Posterior Apex of Auricular Surface	Posterior Apex of Auricular Surface	I
L31	Posterio-Inferior Apex of Auricular Surface	Posterio-Inferior Apex of Auricular Surface	I
L32	Intersection of Ilium, Pubis and Ischium	Intersection of Ilium, Pubis and Ischium	I

Table 3.2. Iliac landmarks digitised for this study. M = Medial L = Lateral.

landmarks are located at discrete juxtapositions of bones or bony eminences and evidence for homology is strongest. Type II landmarks are defined geometrically, for example the apex of an anatomical curve. Type III landmarks are also defined geometrically by chords or fractions of curvature, for instance, either ends of a length, or the bottom of a concavity. Thus the evidence for homology is weakest.

3.3.4.1 Measurement error analysis

When collecting data of any kind it is essential that the observer tests the accuracy and repeatability of the data for three reasons. Firstly, if data were not checked, interpretations based on the data are unreliable. Secondly, if data are found to be unreliable investigating intra-observer error can highlight weaknesses in measurement techniques so that improvements can be made. Thirdly, written reports require an estimation of measurement error. The type of error analysis must be tailored to suit the requirements of the observer and the type of analyses that are to be employed. Analyses of intra-observer error should include estimates of accuracy and repeatability (Mueller & Martorell, 1988; Jamison & Ward, 1993; Ulijaszek & Lourie, 1994).

To ensure that landmark co-ordinates were accurate and precise measured interlandmark distances were assessed in a measurement error analysis. In order to assess the accuracy of landmark data interlandmark distances calculated from digitised co-ordinates were compared to measurements taken with callipers. The callipers used were Mitutoyo Digimatic with a stated precision of 0.1mm. Landmarks were digitised using a Microscribe with a stated precision 0.38mm. The mean interlandmark distance calculated using the Microscribe should fall within one

standard error of the value measured with the callipers (see Ulijaszek & Lourie, 1994). The precision of calliper and Microscribe measured dimensions were checked first to ensure that the percentage error of measurement was less than 5%. For both calliper and Microscribe measurements it was assumed that there was no systematic error in the measurements affecting every landmark.

Six non-adult and four adult pelves representing *H. sapiens* and six non-adult and four adults representing *P. t. troglodytes* were measured repeatedly, ten times, over ten days. Also, five non-adult specimens representing *Cercopithecus sp.* were digitised repeatedly, five times on five different days. Each specimen was only digitised once each day, but the order in which specimens were digitised was randomised daily. Thirty-six dimensions were collected from the apes and eight from the cercopithecines (see Figure 1.4 and Table 3.3). The measurements were selected because they had previously been found to distinguish adult hominoids. Percentage error of interlandmark distances calculated using calliper and Microscribe measurements did not exceed 5% (Table 3.3). Furthermore, the mean interlandmark distances calculated using the Microscribe always fell within one standard error of the value measured with the callipers (Table 3.3). Landmark measurements for *H. sapiens* and *P. t. troglodytes* were therefore deemed to be accurate. It was noted that percentage error of dimensions calculated from co-ordinate data decreases with increasing distance. Percentage error was regressed against measured linear distances for *P. t. troglodytes* [a = -0.2 (-0.25, -0.15); r^2=0.74] and *H. sapiens* [a = -0.20 (-0.23, -0.17); r^2=0.76]. Since the ilia of *G. g. gorilla* are larger than those of *P. t. troglodytes* accuracy of measured dimensions should be greater. All three hominoid species were examined to ensure the 32 landmarks digitised for shape analysis were

Dimension		*Homo sapiens*			*Pan troglodytes*			*Cercopithecus* sp.		
No	Name	% Err Cal	% Err Mic	Mic Vs. Cal	% Err Cal	% Err Mic	Mic Vs. Cal	% Err Cal	% Err Mic	Mic Vs. Cal
D2	Iliac Height	2.63	2.51	NS	3.15	2.25	NS			
D3	Posterior iliac height	3.34	2.01	NS	2.70	2.58	NS			
D4	Iliac Height	3.40	3.51	NS	2.89	2.46	NS			
D5	Posterior Iliac Height	3.65	2.68	NS	2.65	2.70	NS			
D7	Caudal Iliac Height	3.80	3.32	NS	2.82	2.68	NS			
D8	Ischial Length	3.91	2.73	NS	3.15	2.84	NS			
D9	Pubis Length	3.51	2.91	NS	3.84	3.53	NS			
D11	Superior Iliac Width	4.48	3.72	NS	2.91	2.96	NS	3.27	3.24	NS
D12	Inferior Iliac Width	4.50	2.87	NS	3.15	2.96	NS	3.66	3.42	NS
D13	Chord Length of Anterior Iliac Crest	3.51	2.40	NS	3.48	2.77	NS	3.79	2.57	NS
D14	Chord Length of Posterior Iliac Crest	2.84	2.56	NS	2.70	3.15	NS	2.50	3.56	NS
D16	Ischio-pubis length	3.27	2.75	NS	2.84	3.00	NS			
D19	Width of Sciatic Notch	4.55	2.58	NS	2.99	2.91	NS			
D20	Posterior Pelvic length	3.40	2.18	NS	2.42	2.70	NS			
D21	Pelvic Diameter	3.53	3.29	NS	2.96	2.46	NS			
D22	Auricular Height	4.67	2.23	NS	2.80	3.65	NS	3.33	3.26	NS
D24	Auricular Width	3.91	3.60	NS	4.53	2.82	NS	4.53	3.11	NS
D25		3.32	3.20	NS	3.06	3.00	NS			
D26		3.67	3.13	NS	3.00	2.65	NS			
D27	Iliac Length	2.58	2.60	NS	2.51	2.16	NS	2.80	2.50	NS
D28		2.84	2.32	NS	2.94	2.70	NS			
D29	Anterior Pelvic Length	3.08	2.20	NS	3.40	2.68	NS			
D31		3.58	2.70	NS	3.13	3.03	NS			
D32		3.03	2.54	NS	2.49	2.06	NS			
D33		3.67	3.48	NS	3.82	2.84	NS	4.12	2.52	NS
D34		2.77	3.70	NS	3.60	2.84	NS			
D35	Acetabular Height	4.03	3.06	NS	3.44	3.00	NS			
D36	Acetabular Width	3.80	4.03	NS	4.20	3.08	NS			

Table 3.3. Measurement error analysis for *os coxal* dimensions calculated from digitised landmark coordinates. Abbreviations denote: %Err, percentage error of measurement; Cal, calliper measurements; Mic, microscribe measurements. NS, no significant difference between mean calliper and microscribe measurements (independent two sample t-test).

repeatable. Interlandmark distances (n = 496) calculated for the 32 landmarks digitised for shape analysis did not exceed percentage error of 5%. Landmark measurements for *H. sapiens*, *P. t. troglodytes G. g. gorilla* and *Cercopithecus* species were therefore deemed to be repeatable.

3.3.5 Geometric morphometric analysis of allometric (ontogenetic) iliac shape change

Covariation between iliac size and shape in Cercopithecoids was assessed using a PCA based on landmark data registered according to a subset of landmarks. Hominoid iliac growth trajectories were also recalculated using a PCA of landmark data registered according to a subset of landmarks and augmented with log centroid size. Procrustes superimpositions were carried out separately for each of the two analyses. In both analyses only landmarks L1-L18 (Table 3.2) was used to calculate centroid size and to register specimens. These primary landmarks best represented the overall size of the ilium. Only landmarks representing the outline of the specimens were used so that the size and relative position of joint surfaces, e.g. auricular surface, would not affect Procrustes registrations. Thus specimens were not, strictly, in Kendall's shape space. Consequently the tangent space projection and subsequent PCA of the data was incorrect. However, a comparison of PCA's based on specimens registered according to all landmarks (i.e. in Kendall's shape space) and specimens registered according to a subset of landmarks indicated that disagreement was negligible. The advantage of fitting specimens according to the outline was that splines were produced within PCA morphospaces were smoother, less complicated and more readily interpretable. Procrustes superimposition was

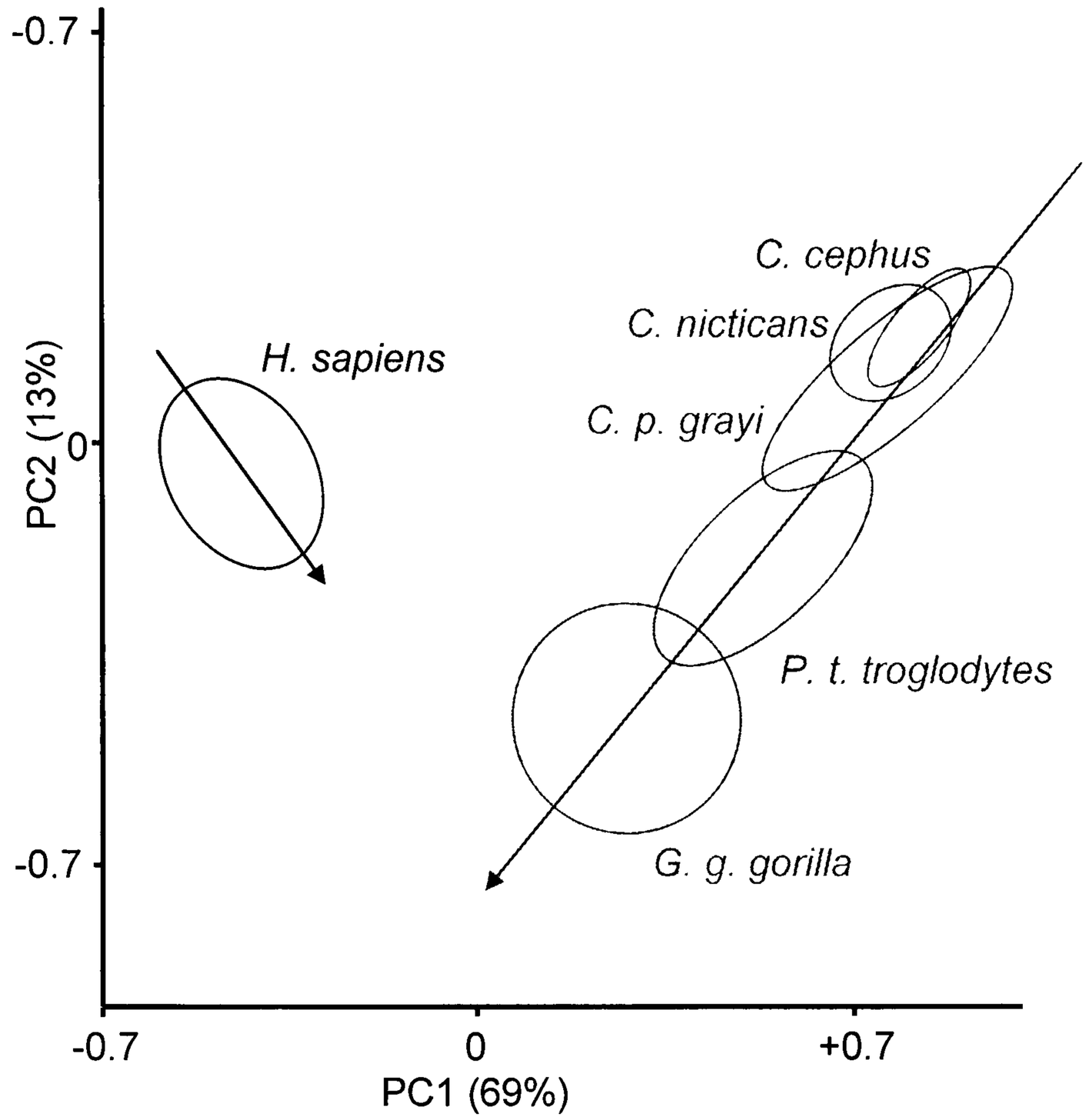

Figure 3.3. Interspecific comparison of hominoid iliac growth trajectories in size-shape space. The analysis was based on 32 iliac landmarks but specimens were registered according to a subset of 18 landmarks (see text). Ellipses denote 95% confidence limits for pooled non-adult and adult specimens. Modern human and non-human primate growth trajectories are represented by black and grey arrows respectively.

carried out using the programme MORPHEUS (Slice, 1998). The PCA's were carried out using the programme PAST V. 1.37 (http://folk.uio.no/ohammer/past).

Hominoid iliac ontogenetic allometric trajectories were quantified by calculating intercepts and slopes using the model II reduced major axis (RMA) regression technique (Clarke, 1980). Model II regression deals with measurement error in both x and y variables and is the best regression tool for bivariate allometric studies (Ebert and Russell, 1994; Lande, 1979; Smith, 1980) (see 1.4.3). Two growth trajectories were calculated for each hominid species, one based solely on non-adults and one

based on non-adults and adults pooled. Regressions were plotted in the programme PAST V. 1.37. Regression slopes and intercepts were compared following Tsutakawa and Hewett (1977) and Clarke (1980) respectively. The interdependence of *b* (intercept) and α (allometric co-efficient) required that *b* only be compared when α was comparable across groups (Gould, 1966; Tessier, 1936).

3.3.6 Thin-plate spline analysis

The thin plate spline regression (TPSRegr) technique was employed in order to visualise allometric (ontogenetic) change in hominoid iliac shape. The TPSRegr method allows the variation is shape described by one PC (e.g. size axis) to be viewed independently of shape variations described by other PC's. Landmark co-ordinates were regressed against principal component scores using the least squares method (following Rohlf, 1993). Thin-plate splines were plotted as a function of the principal component scores from the size axis.

3.4 Results

In Figure 3.3. it can be observed that, overall, the cercopithecoids showed a pattern of iliac size related shape change that is more similar to the African apes than it is to the modern humans (Figure 3.3). Furthermore, non-human primates appear to share a common growth trajectory that is distinct form modern humans. Ontogenetic allometric trajectories for *H. sapiens*, *G. g. gorilla* and *P. t. troglodytes* are compared quantitatively. Ontogenetic allometric regression coefficients and intercepts were calculated in shape space (Figure 3.3) and log centroid size-shape space (Figure 3.4). The African apes share comparable slopes and intercepts that are distinct from modern humans (Figure 3.5 and Table 3.4). A TPS analysis concurs that the African

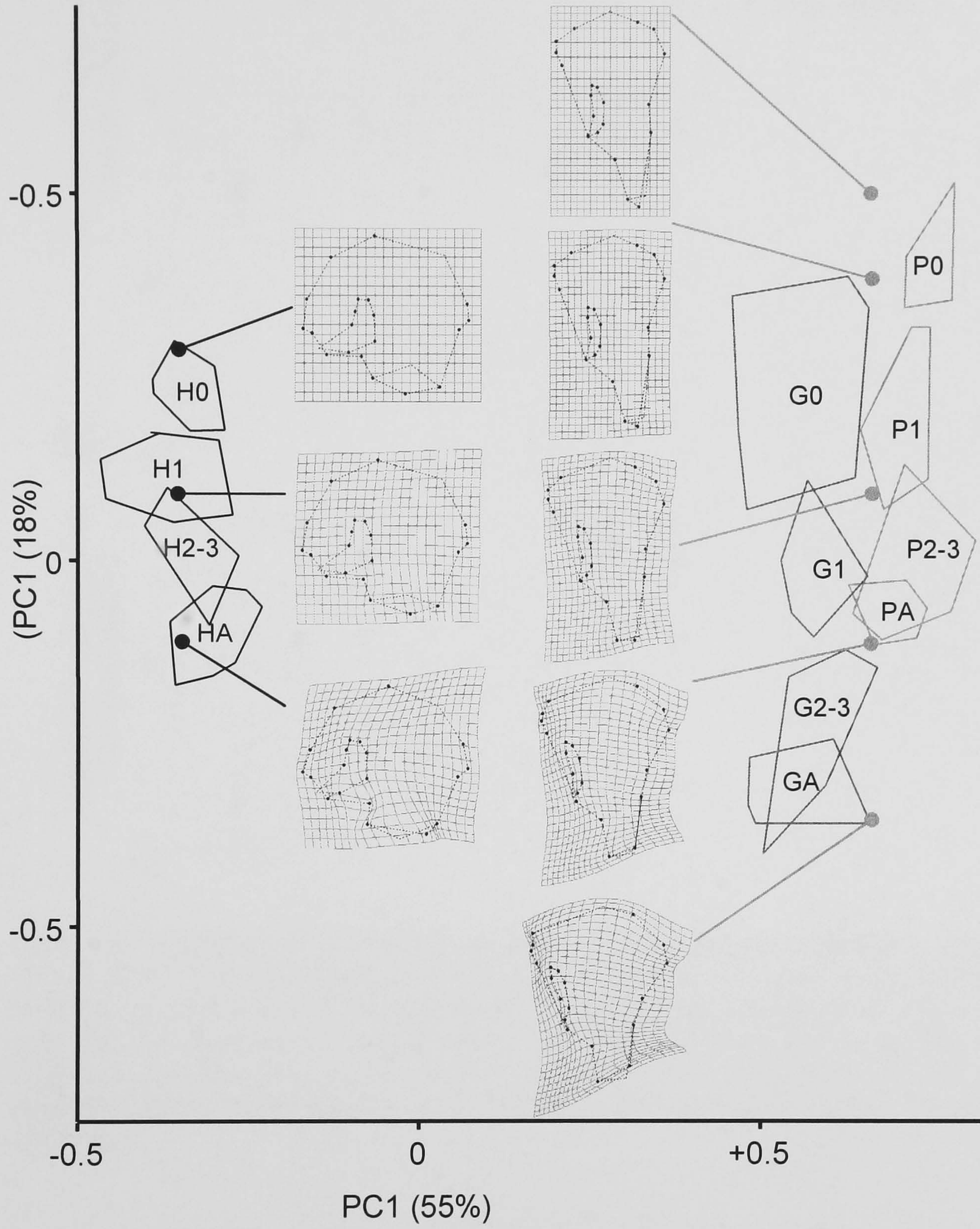

Figure 3.4. Interspecific comparison of hominoid iliac growth trajectories in size-shape space. Species denoted by H, *H. sapiens*; P, *P. t. troglodytes*; G, *G. g. gorilla*. Developmental stages defined according to permanent molar eruption are superimposed on the data. 0, no permanent molars; 1, all first permanent molars; 2, all second molars; 3, all third molars; Adult, distal femoral epiphyses completely fused. The percentage variance pertains to the amount of variation in the landmark data set explained by each principal component. Thin plate splines denote size related change in iliac shape along modern human and African ape growth trajectories.

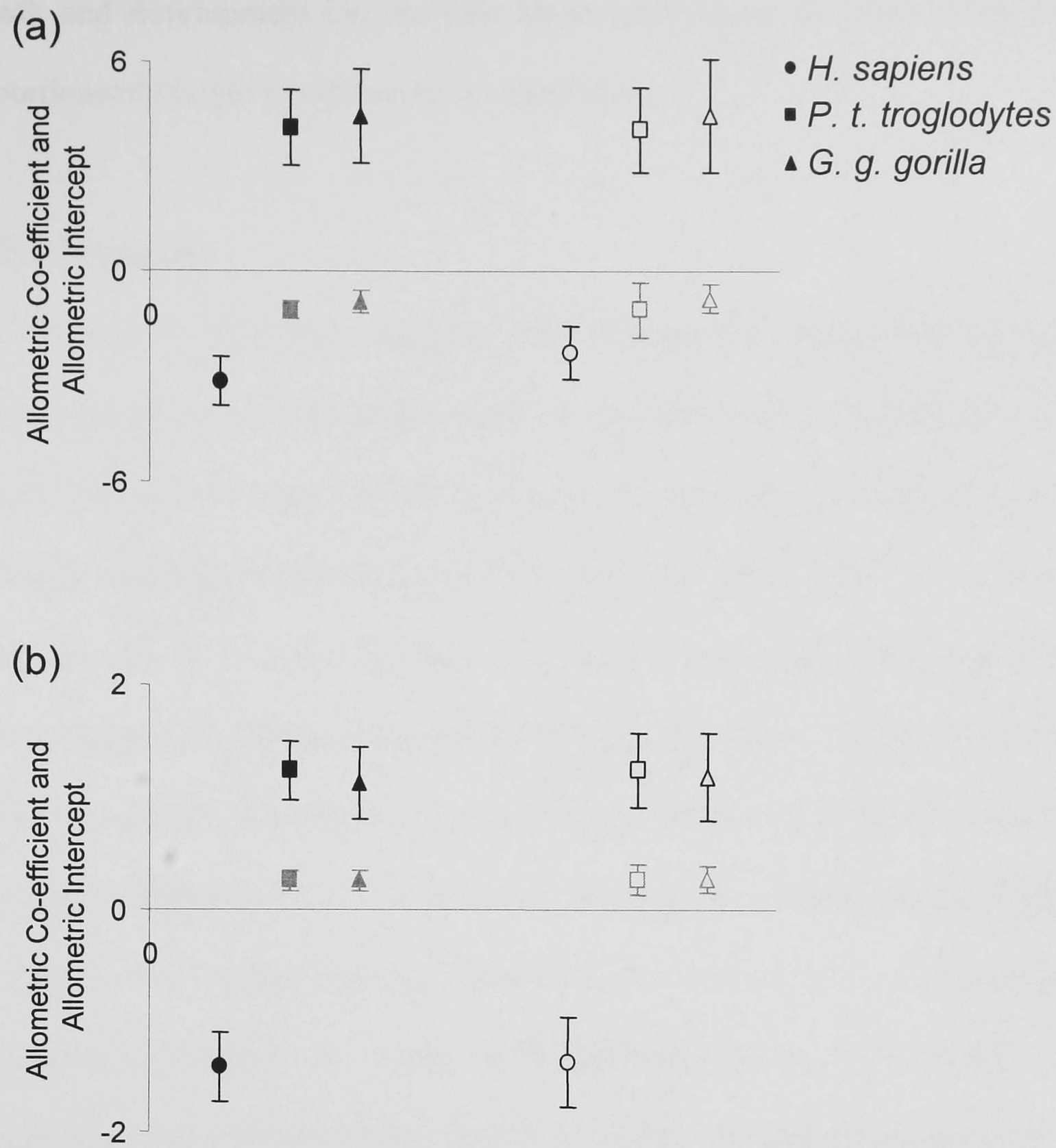

Figure 3.5. Interspecific comparison of hominoid iliac growth trajectories. Species specific RMA regression statistics were calculated from PCA's based on (a) registered landmark data augmented with log centroid size and (b) registered landmark data alone. Error bars denote mean and standard deviation. Circles denote *H. sapiens*, squares *P. t. troglodytes*, triangles *G. g. gorilla*, closed symbols non-adults only, open symbols non-adults and adults pooled, black symbols allometric coefficients, grey symbols allometric intercepts.

apes share a common pattern of ontogenetic covariation between iliac size and shape.

Ontogenetic allometric changes in hominoid iliac shape are depicted in Figure 3.4. Overall, the modern human iliac blade showed an antero-posterior "stretching" at the level of the superior iliac spines and infero-superior "squashing" during growth and development. The iliac blade of African apes showed a "mushrooming" during

growth and development i.e. the iliac blade (particularly the iliac crest) becomes proportionately larger in relation to the basal ilium.

3.5 Discussion

The findings of this study suggest that inter-specific differences between the morphology of adult African apes could be primarily due to differential extensions (or reductions) of the same growth trajectory. The geometric morphometric analyses of iliac size and shape indicates that, with respect to the first two PC's, the growth trajectories for *P. t. troglodytes* and *G. g. gorilla* have comparable intercepts and slopes (Figure 3.5). Whether considering solely non-adults, or adults and non-adults pooled, the African apes Figure 3.5 and Table 3.4. These analyses were only carried out using the first two PC's. It is possible to compare the coincidence of ontogenetic trajectories more comprehensively, across three or more PC's, by using resampling techniques (see Zelditch & Sheets, 2000). However, the analyses suggest that the African apes are ontogenetically scaled. In support of this conclusion there is a pervasive pattern of ontogenetic scaling of various bony measurements in *P. troglodytes* and *G. gorilla*. For example, Inouye (1992) reported that in relation to the diaphyseal length of the humerus, most metacarpal and phalangeal dimensions scaled in the same way in *P. troglodytes* and *G. gorilla*. Shea (1981) reported that relative growth rates of some postcranial dimensions are very similar in the African apes, e.g. leg length in relation to body mass and trunk length. Shea (1986) also noted that with respect to body mass, scapula dimensions, e.g. scapula length, scaled in the same way in *P. troglodytes* and *G. gorilla*. Shea (1985b, 1985c) further reported that cranial dimensions, as well as basicranial length and height, scale in the same way in *P. troglodytes* and *G. gorilla*. However, a more comprehensive

geometric morphometric study on cranial shape by Berge & Penin (2004) reported common patterns of shape change in *P. troglodytes* and *G. gorilla* during development but the two species were transposed.

As adults, *G. g. gorilla* possess larger ilia than *P. t. troglodytes* (Figure 3.4) and one might expect that the growth of the ilium is correlated with growth in overall body size, e.g. body mass. The African apes cease to grow in body mass at approximately the same age. Male *G. gorilla* cease growth in body mass at about 18 years, whereas *P. troglodytes* stop growing at about 15 years (see Leigh & Shea, 1996a, 1996b). Female *G. gorilla* cease growth of body mass at about 10 years and *P. troglodytes* at about 14 years (see Leigh & Shea, 1996a, 1996b). As adults, *G. gorilla* are the larger species (female 71.0-male 175.2kg) with *P. troglodytes* females only weighing only 45.8kg and males weighing 59.7kg (Smith & Jungers, 1997). According to Leigh (1996) rate of growth in body mass is higher in the *G. gorilla* than *P. troglodytes*. This may be reflected in the allometric growth trajectories of the ilia. To test this proposition, ontogenetic allometries were compared across African apes using a PCA analysis based on registered co-ordinate data augmented with log iliac centroid size.

The allometric plots indicate that *G. g. gorilla* attain a larger iliac size than *P. t. troglodytes* (Figure 3.4). After the eruption of second permanent molars *G. g. gorilla* (mean 6.77 years), reach a size and shape range which exceeds that of adult *P. t. troglodytes* (11.33 years and over) (Figure 3.4). At the time of first molar eruption in *G. g. gorilla* (mean 3.5 years), the size of the ilium is about the same as that of *P. t. troglodytes* when second molars are erupting (mean 6.74 years) (Figure 3.4). Furthermore, at the time of second molar eruption in *G. g. gorilla* (mean 6.77 years),

	Species	Slope					
		H. sapiens		*P. t. troglodytes*		*G. g. gorilla*	
		Non-Adults	Pooled	Non-Adults	Pooled	Non-Adults	Pooled
Intercept	*H. sapiens*	-		$p < 0.01$	$p < 0.01$	$p < 0.01$	$p < 0.01$
	P. t. troglodytes	$p < 0.01$	$p < 0.01$	-		NS	NS
	G. g. gorilla	$p < 0.01$	$p < 0.01$	NS	NS	-	

Table 3.4. Interspecific comparison of external iliac growth trajectories (reduced major axis regression). The African apes share comparable slopes and intercepts that are distinct from modern humans (see Figures 3.4 and 3.5). This was the case whether non-adults were studied independently or pooled with the adult sample.

the size of the ilium is about the same as that of a fully grown *P. t. troglodytes* (mean 11.33 years and over) (Figure 3.4). These findings suggest that prior to second molar eruption the ilia of *G. g. gorilla* grow almost twice as fast at those of *P. t. troglodytes*. On average newborn *G. g gorilla* weigh approximately 2.2 kg whereas *P. troglodytes* weigh approximately 1.6 kg. The gestation period in *G. gorilla* is (251-295 days) is longer than *P. troglodytes* (202-261 days). Thus the average fetal growth rate in *G. gorilla* (0.007-0.009 kg/day) is greater than in *P. troglodytes* (0.006-0.008 kg/day). This is probably an oversimplification of developmental rates since, as with postnatal development, growth rate of body mass is probably not constant. However, the findings suggest that prior to birth the rate of growth in body mass is also higher in *G. gorilla* than it is in *P. troglodytes*. Given that the body and the ilium both grow in three planes it is likely that that body mass and iliac size grow isometrically. Consequently, it is reasonable to surmise that iliac growth rate may be higher in *G. gorilla* than in *P. troglodytes* from conception through to the eruption of first permanent molars. Since prenatal growth rate is so small, postnatal growth rates might be more important for body and iliac size differences between species.

Several hypotheses have been suggested to explain the faster rate of growth in *G. gorilla* when compared with *P. troglodytes*. Leigh (1994a) reported that folivores tend to grow faster than non-folivores. Leaves make up some 40-45% of the diet in *G. gorilla* but only 10-15% in *P. troglodytes*. Inter-specific differences in growth rate may be related to diet. Elevated growth rates may confer benefits to *G. gorilla*, including metabolic advantages to early attainment of large size and early maturation of the alimentary system. The ability of *G. gorilla* to break down and digest plant food depends upon the size of the digestive tract and, therefore, overall body size.

The length of the digestive tract scales with positive allometry (with respect to body mass) during ontogeny (Leigh, 1994a). Rapid development may allow *G. gorilla* to attain a suitable size for birthing more quickly than *P. troglodytes*. However, given that *P. troglodytes* (mean 7 years) give birth one year earlier than *G. gorilla* (mean 8 years), and at a smaller body size, this seems unlikely.

As adults *H. sapiens* attain an iliac size which is similar to *P. t. troglodytes* but is smaller than that of *G. g. gorilla* (Figure 3.4). Yet the growth of modern human body mass ceases at an older age, approximately 17-20 years (Tanner *et al.*, 1966). Assuming iliac growth ceases at the same time as body mass, modern human ilia apparently grow more slowly than they do in the African apes. The slower and longer postnatal growth of the ilium in modern humans with respect to African apes is probably related to energy and nutritional requirements. Modern humans are characterised by a large brain, both absolutely and in relation to body mass (Kappelman, 1996; Leigh, 1996). In the Hominoidea the growth of the brain ceases at around the time of first permanent molar eruption (Smith, 1989). During infancy *H. sapiens* display more rapid brain growth than *P. troglodytes* (Rice, 1997). Thus growth of the modern human brain is probably more demanding in terms of energy and nutrition than in the African ape brain. The postcranium grows more slowly in modern humans than in the African apes but it grows for a longer period of time. During infancy this probably allows the modern human brain to grow more rapidly than the African ape brain. Hence growth of the brain and body (ilium) may represent a trade off.

3.5.1 Phylogenetic inferences

The conceptual framework of Ravosa & Profant (2000) allows inferences to be made regarding the phylogenetic relationships between species based on allometric slopes. The greater the similarities between the slopes of growth trajectories the more closely related two species probably are. For an alternative view see O'Higgins & Collard (2002). A comparison of papionin facial morphology, allometric vector trajectories, produced a morphology based phylogeny that was entirely different from the consensus molecular phylogeny. This may be because bones exhibit low degrees of heritability (Atchley *et al.,* 1985; Chevurud & Bulkstra, 1982; Hunter, 1990). Alternatively this may be a consequence of pleiotropic genetic effects or non-genetic influences e.g. nutrition (Atchley & Hall, 1991; Cheverud, 1982b; Herring, 1993a; Lieberman, 1992). The results form this chapter show reveal that the African apes show comparable allometric coefficients that are significantly different from modern humans (Figure 3.5). This was found to be the case whether trajectories were calculated using non-adults only or adults and non-adults pooled (Figures 3.4 & 3.5). Since the African apes share a common allometric growth trajectory the two species are probably very closely related, perhaps even sister species whereby modern humans represent a monophyletic branch of the primate lineage. While reasonable, this suggestion seems refuted by molecular studies.

Comprehensive molecular analyses of the phylogenetic relationships between species tend to conclude that the Hominoidea form a clade and that *H. sapiens* and *P. troglodytes* are sister taxa (e.g. Ruvolo, 1997; Satta *et al.,* 2000). Ruvolo (1997) compared 14 independent gene sequences across the Hominoidea and reported 11 commonalities between *P. troglodytes* and *H. sapiens*, 2 between *P. troglodytes* and

G. gorilla and 1 between *H. sapiens* and *G. gorilla*. Satta *et al.* (2000) compared 45 loci across the Hominoidea and reported that 60% support a *P. troglodytes-H. sapiens* clade, 20% *P. troglodytes-G. gorilla* and 20% for *H. sapiens-G. gorilla* split. Previous studies report that the Hominoidea share 99.9% of their genes (coding DNA). However, the (non-coding) regulatory DNA that makes up the rest of the genome varies across species. Therefore the genetic material investigated in phylogenetic studies by Ruvolo (1997) and Satta *et al.* (2000) probably included the regulatory DNA. Regulatory DNA affects gene expression and, consequently, the pattern of morphological development during ontogeny. In contrast to the published molecular reports, the morphological data on iliac development presented in this chapter indicate that the African apes are sister taxa. Several points can be proffered to explain the discrepancy.

Firstly, evolution progresses in a mosaic fashion, whereby parts of the body evolve at different times (McKinney & McNamara, 1990). Thus, the genetic material investigated by the phylogenetic studies may not have included the regulatory DNA which affects iliac pelvic growth and development. This explanation seems reasonable given that the ilium might be expected to show a slow rate of evolutionary change in comparison to other features because of functional constraint. Functional constraint refers to a situation when a character cannot change because to do so would impair its function (Arnold, 1992; Schwenk & Wagner, 2001). The ilium provides attachments for several of the muscles which power locomotion and contributes to the size of the birth canal in females. Any alterations in development, and therefore adult morphology, might affect the ability of the pelvis to function efficiently.

Secondly, growth and development of the ilium may be strongly affected by environmental stimuli, which modify gene expression by acting on regulatory DNA and genes. Experimental animal models suggest that cortical bone adapts to loading regime during ontogeny. Trabecular bone is thought to adapt to loads in response to magnitude and rate of strain (deformation). Cortical bone adapts more readily to the rate of strain rather than the magnitude of strain (Cullen *et al.,* 2001; Owan *et al.,* 1997; Turner *et al.,* 1998). In sheep the rate of periosteal modelling is higher in individuals that are exercised than those that are inactive (standing) (Lieberman, 2003). *Sus scrofa* (domestic pig) showed a thickening of cranial bones in response to increased food consistency and exercise regimes (Lieberman, 1996). There are also indirect systematic effects of exercise on bone strength and morphology (Lieberman & Crompton, 1998a, b). Given what is known about pelvic soft tissue anatomy and the development of locomotor and postural behaviour in the hominoids mechanical stimuli may well affect the development of cortical bone. A literature review comparing hominoid soft tissue morphology for features listed in the *Nomina Anatomica* was published by Gibbs *et al.* (2002). The morphology of the hominoids was broken down into discrete character states. Inter-specific comparisons of pelvic musculature (i.e. location of muscle attachments, number of muscle heads) was extracted from the paper (n = 20) (see Table 3.5). Of the features, 12/20 bore a resemblance between *P. troglodytes* and *G. gorilla*, 4/20 for *H. sapiens* and *G. gorilla*, 1/20 for *H. sapiens* and *P. troglodytes* and 2/20 were similar across all three species. Hence, soft tissue morphology of the pelvis distinguishes adult African apes to the exclusion of modern humans.

Hominoid Muscular Morphology Feature	Score			Result			Morphological Commonalities			
	0	1	2	*H*	*P*	*G*	*H-P*	*H-G*	*P-G*	*HPG*
Piriformis fused with gluteus medius	Yes	Variable	No	1	1	1				1
Origin of gluteus minimus is continuous	Yes	Variable	No	1	2	2			1	
Gluteus medius origination from fascia lata	No	Yes		0	1	1			1	
Gluteus medius is bipinnate	No	Yes		0	1	1			1	
Tensor fascia latae fused proximally with gluteus maximus	Yes	Variable		1	1	0	1			
Tensor fascia latae fused laterally with gluteus medius and minimus	Yes	No		1	0	0				1
Gluteus maximus fused with biceps femoris	Origin	No Fusion	Distal	1	0	0				1
Gluteus maximus insertion into hypotrochanteric fossa	No	Yes		0	1	1				1
Superior gemellus absent	Variable	Yes	No	0	2	0		1		
Quadratus femoris split at insertion	Yes	Variable	No	2	1	2		1		
Gracilis origin extends to whole pubic body	Yes	No		1	0	0				1
Single origin of adductor brevis	Yes	Variable	No	1	2	1		1		
Adductor brevis origination from superior pubic ramus	No	Yes		0	1	1			1	
Adductor brevis inserted between pectineus and upper part of adductor magnus	Yes	No		0	1	1			1	
Adductor magnus insertion into inferior border of quadratus femoris insertion	Yes	No		1	1	1				1
Adductor minimus absent	Yes	Variable	No	2	1	1			1	
Rectus femoris has two heads	No	Variable	Yes	2	1	1			1	
Insertion of long head of biceps femoris into iliotibial tract	No	Yes		0	1	1			1	
Semimembranous insertion into popliteal fascia and posterior wall of knee capsule via oblique popliteal ligaments	No	Yes		1	0	1		1		
Total							**1**	**4**	**12**	**2**

Table 3.5. Inter-specific comparison of hominoid pelvic soft tissue anatomy. Data collated form Gibbs *et al.*, (2002). H = *H. sapiens,* P = *P. troglodytes,* G = *G. gorilla.*

Furthermore, the pattern of ontogenetic change in locomotor and postural behaviour and, perhaps, mechanical loading is common in the African apes to the exclusion of modern humans. No data on development of locomotion is available for *P. t. troglodytes* or *G. g. gorilla* but data pertaining to their close relatives, *P. t. verus* and *G. g. beringei* has been published (see Carlson, 2005; Doran, 1992, 1997). Doran (1997) compared the ontogeny of *G. g. beringei* and *P. t. verus* using data from focal samples of continuous locomotor bouts. Doran studied *G. g. beringei* for 23 months in the Parc National des Volcans, Rwanda (Doran, 1997) and *P. t. verus* for seven months in the Tai Forest, Ivory coast (Doran, 1992a). The proportion of time spent in various locomotor behaviours, i.e. locomotor pattern, was recorded for various age categories. Doran (1997) reported that *G. g. beringei* and *P. t. verus* show a common pattern of change in locomotor patterns. However, the change was more rapid in *G. g. beringei*. Much of the intra-specific variation with age was explained by body mass. The subspecies of gorilla and chimpanzee are closely related within the respective genera. At the same or similar body mass one would expect *G. g. gorilla* and *P. t. troglodytes* to show similar locomotor patterns to their close relatives. Published data suggest that *G. g. gorilla* is more arboreal than *G. g. beringei*. Thus, it is reasonable to suggest that *G. g. gorilla* and *P. t. troglodytes* display the same pattern of change in locomotor behaviour with increasing body size. *Homo sapiens* follow the same overall pattern of ontogenetic change in locomotor behaviour, progressing from no locomotor activity to forelimb dominated pulling and grasping to quadrupedalism and bipedalism (Keen, 1993). However, whereas *P. t. troglodytes* and *G. g. gorilla* only rarely adopt bipedal postures, modern human humans become habitual bipeds. Thus, the African apes show a similar pattern of locomotor

development that is distinguished from modern humans; which suggests similarities in development of the iliac mechanical loading regime.

Part II: External Iliac Morphology of Hominoids

Chapter 4. Mechanical and Hormonal Influences on Hominoid Iliac Growth and Development: A Feedback Loop

4.1 Bone's mechanostat

Frost's mechanostat theory (1987a, 1987b, 1996, 1998, 2003) stated that cortical bone grows in response to strain, i.e. deformation (see also Kummer, 1972 and Pauwels, 1980). In line with this hypothesis, several experimental models have reported that increased loading due to exercise enhances cortical growth. Lieberman & Crompton (1998) examined the effect of increased (higher rate of) mechanical loading, i.e. exercise, on cortical growth and development in the hind limb of *Ovis aries* (sheep). One group of *O. aries* was trotted for 1hr/day for 90 days, whilst a control group was penned and did not exercise. This was repeated for three developmental categories designated according to age at the start of the experiment: juvenile (40 days old), sub-adult (265 days old) and young adult (415 days old). The exercised groups showed significantly higher subperiosteal bone deposition than penned control groups. Jee *et al.* (1991) tested whether immobilisation of growing rat hind limbs affected cortical growth and development. One hindlimb was immobilised in the flexed position using an elastic bandage, whilst the contralateral limb was allowed to move freely. The rats were sacrificed at 2, 10, 18 and 26 weeks respectively. At 18 and 26 weeks exercised limbs displayed a greater femoral cross-sectional cortical area than immobilised limbs. The results of these studies suggest that cortical bone may adapt during ontogeny in response to loading either as a result of an increase/decrease in body mass and/or the magnitude of loads induced by

muscular contractions. The extent to which this is influenced by puberty is unclear however. It would appear that changes are more marked before puberty than they are afterwards (Pearson & Lieberman, 2004). Given that the ilium provides attachments for the muscles which power locomotion, as well as playing a role in weight bearing, it is likely that changes in body mass and muscle mass will influence its growth and development. Muscle mass may be increased by hormones e.g. growth hormone (Herring, 1993b; Vogl *et al.,* 1993), which fluctuate during development and are particularly heightened during puberty (Styne, 2003). One might therefore expect that the growth trajectory will change at around the time when the pubertal growth spurt in body mass occurs.

4.2 Aims

This chapter posed two questions. (1) Do the hominoids show a shift in iliac allometric (ontogenetic) growth trajectories during ontogeny? (2) Do shifts in iliac allometric growth trajectories (if any) coincide with the onset of the pubertal growth spurt in body (and therefore muscle) mass?

4.3 Materials and methods

The postnatal sample of specimens from Chapter three was analysed. Postnatal hominoid material was subdivided according to permanent molar eruption and distal femoral epiphyseal fusion (see Table 3.1): M0, no molars erupted; M1, all first permanent molars erupted; M2, all second molars erupted; M3, all third molars erupted; A, adults defined as having completely fused distal femoral epiphyses (see section 3.3.2). The landmarks shown in Table 3.2 were used for this chapter.

4.3.1 Geometric morphometric analysis of ontogenetic allometry

Following the method outlined in Chapter 3 (see section 3.3.5) principal components analyses based on registered landmarks, augmented with log centroid size, were used to analyse ontogenetic covariation in iliac log centroid size and shape. Each species was registered and analysed separately. Specimens were grouped in the PCA morphospaces according to developmental stage. Pre-M2 and post-M2 specimens were grouped separately to determine the possible influence of puberty on iliac growth and development. The TPSRegr technique was used to evaluate shape along principal component axes.

4.4 Results

In *H. sapiens*, early development, i.e. pre-M2 eruption, is characterised by a proportional increase in length of the anterior half of the iliac crest epiphysis and a decrease is the antero-posterior width of the basal epiphyses in relation to iliac centroid size (Figure 4.1). During the later part of development, i.e. post-M2 eruption, there is a proportional increase in the length of the posterior half of the iliac crest epiphysis and the antero-posterior width of the iliac body (Figure 4.1). It seems therefore, that modern humans show an inflection the growth trajectory of the ilium at around M2 eruption (Figure 4.1).

Prior to M2 eruption in *P. troglodytes*, the iliac crest epiphysis gets proportionally longer antero-posteriorly and taller infero-superiorly, whilst the basal epiphyses get proportionally narrower antero-posteriorly, relative to iliac centroid size (Figure 4.2). After M2 eruption, the pattern of change is reversed. In *G. g. gorilla*, the pattern of iliac shape change during the early, i.e. pre-M2 eruption, and late, i.e. post-M2

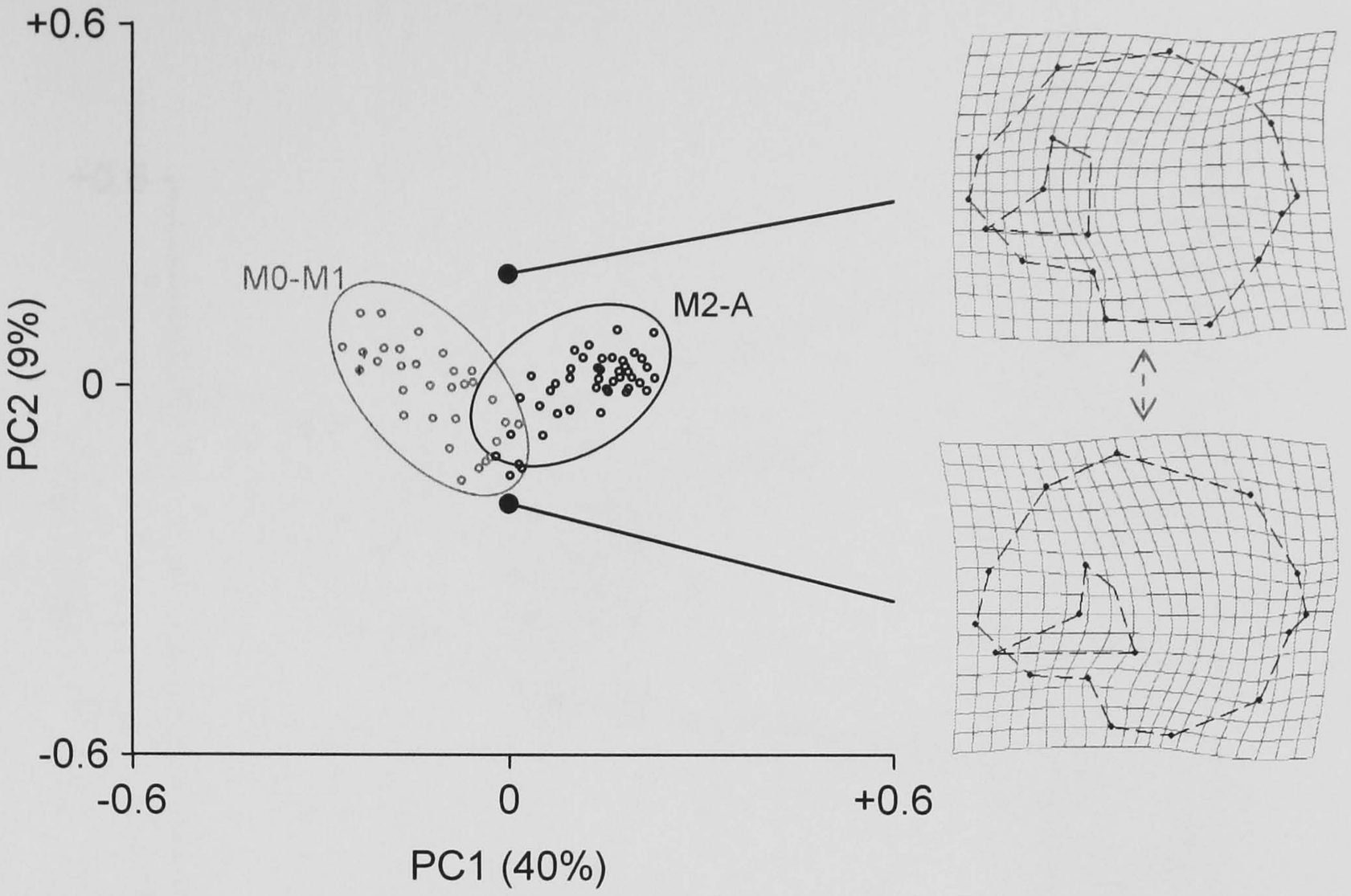

Figure 4.1. An ontogenetic series of *H. sapiens* ilia compared in size-shape space. The ellipses demark 95% confidence limits for developmental stages based on permanent molar eruption and distal femoral epiphyseal fusion; M0, permanent molars un-erupted; M1, all first molars erupted; M2, all second molars erupted; A, adults with distally fused femoral epiphyses. The thin-plate splines depict residual variation in shape along the second principal component. Dashed grey arrows denote direction of transformation.

eruption, stages is similar to that in *P. t. troglodytes* (Figure 4.3). Both *P. t. troglodytes* (Figure 4.2) and *G. g. gorilla* (Figure 4.3) show an inflection in the iliac growth trajectory at around M2 eruption, respectively.

4.5 Discussion

Homo sapiens, *P. t. troglodytes* and *G. g. gorilla* all display a pubertal growth spurt which is marked by a rapid increase in the rate of growth in body mass (Leigh & Shea, 1996a, 1996b). Pseudovelocity growth curves of hominoid body mass are depicted in Figure 4.4. The start of the highest peak demarcates the onset of the pubertal growth spurt. The pubertal growth spurt starts at around 10-13 years in *H. sapiens*, 5-7 years in *G. gorilla* and 5-7 years in *P. t. troglodytes* (see Figure 4.4).

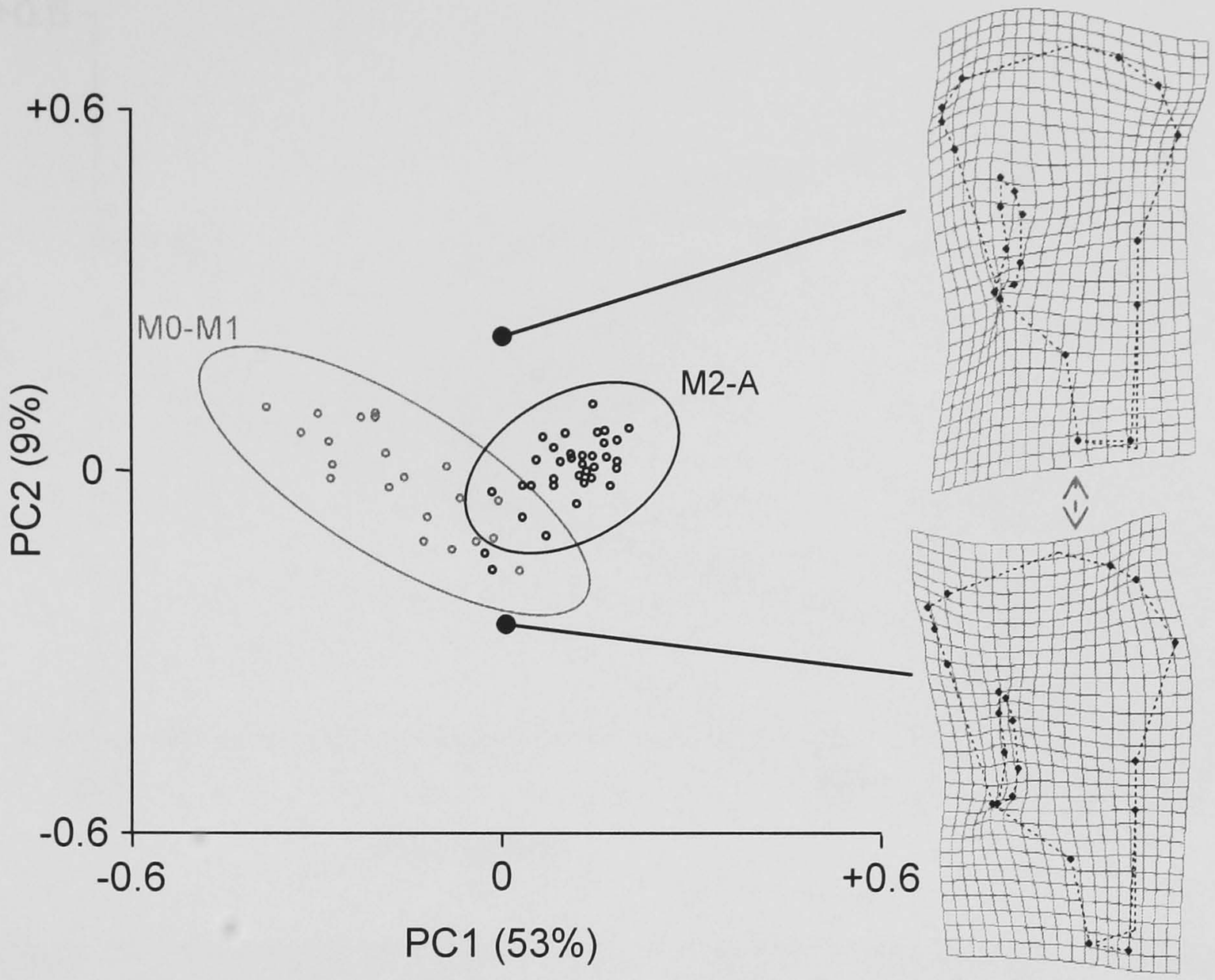

Figure 4.2. An ontogenetic series of *P. t. troglodytes* ilia compared in size-shape space. The ellipses demark 95% confidence limits for developmental stages based on permanent molar eruption and distal femoral epiphyseal fusion; M0, permanent molars un-erupted; M1, all first molars erupted; M2, all second molars erupted; A, adults with distally fused femoral epiphyses. The thin-plate splines depict residual variation in shape along the second principal component. Dashed grey arrows denote direction of transformation.

The growth curves were produced using cross-sectional data and may underestimate the rate of growth (Leigh, 1996; Tanner, 1978), but not the onset of the pubertal growth spurt. Many life history variables are correlated with dental eruption (Smith, 1991; Smith *et al.,* 1994) and pubertal growth spurt is no exception. Hence the timing of the onset of the pubertal growth spurt was compared to permanent molar eruption. Data on hominoid molar eruption times were collated from published literature for *H. sapiens* (Clements, 1953; Stones *et al.,* 1951), *G. g. gorilla* (Smith, 1994) and *P. t. troglodytes* (Anemone *et al.,* 1991, 1996; Gavan, 1967). Second permanent molar eruption times were superimposed onto pseudovelocity growth curves for body mass (Figure 4.4). The shaded grey areas on the figure indicate the age range in which

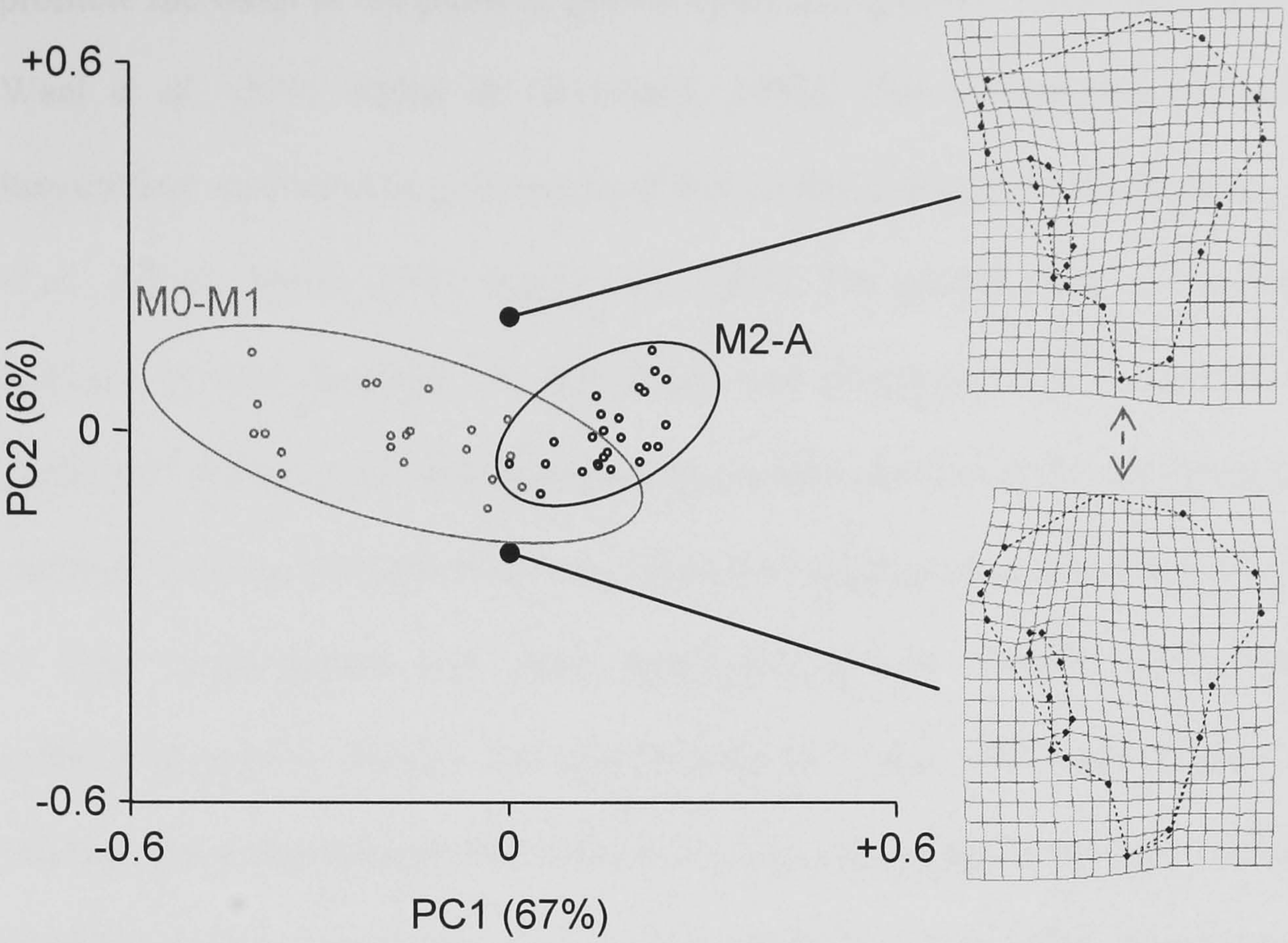

Figure 4.3. An ontogenetic series of *G. g. gorilla* ilia compared in size-shape space. The ellipses demark 95% confidence limits for developmental stages based on permanent molar eruption and distal femoral epiphyseal fusion; M0, permanent molars un-erupted; M1, all first molars erupted; M2, all second molars erupted; A, adults with distally fused femoral epiphyses. The thin-plate splines depict residual variation in shape along the second principal component. Dashed grey arrows denote direction of transformation.

second permanent molars erupt. (Figure 4.4) The eruption times appear to correspond with the pubertal growth spurt in body mass. Thus it appears as though the onset of the pubertal growth spurt is correlated with second permanent molar eruption.

At the onset of the pubertal growth spurt in modern humans there is a dramatic increase in blood hormone levels (Grumbach *et al.,* 1998) i.e. growth hormone and gonadal steroids. It is likely that such a rise also occurs in the African apes (see Coe *et al.,* 1992). A hormone is a chemical substance, formed in one organ or part of the body and carried in the blood to another organ, or part, where it alters the structure of one or more organs (Henderson, 2005). Growth hormone and gonadal steroids

promote the onset of the pubertal growth spurt (Daughaday, 1975; Delemarre-van de Waal *et al.,* 2001; Reiter & Grumbach, 1982). These hormones also affect the longitudinal growth of long bones by action on the epiphyseal growth plates (Eerden *et al.,* 2002a, 2002b, 2003; Vogl *et al.,* 2003). The growth plate is a cartilaginous template located between the metaphysis and epiphysis of a long bone. At the epiphyseal growth plate cartilaginous tissue is laid down to form a template which is replaced by bone. Growth hormones cause the columns of cartilage cells to increase in size (hypertrophy) and delay epiphyseal union, thereby accelerating and prolonging growth. Modern humans (Scheuer & Black, 2000) and African ape ilia possess four epiphyseal growth plates at the iliac crest, anterior inferior iliac spine, *os acetabuli* and *os marginalis*. Consequently, hormones that affect long bone growth may also affect the ilium. In line with this, the thin-plate spline analyses of hominoid growth and development indicate that during puberty the most significant changes in iliac morphology occur at the epiphyses. It was possible to ascertain this from the data presented in this thesis because the digitised landmarks run along the edge of the cartilage plate (where the epiphyseal line appears at fusion). After M2 eruption, modern humans are characterised by a proportional increase in the length of the posterior half of the iliac crest with respect to the anterior half and the iliac blade as a whole (PC2, Figure 4.1). In the African apes, the iliac crest becomes proportionally taller infero-superiorly and narrower antero-posteriorly, whilst the iliac body gets proportionally wider, relative to iliac size (PC2, Figures 4.2 and 4.3).

Growth hormone and gonadal steroids may also affect the pattern of iliac growth and development indirectly by increasing muscle mass (Herring, 1993b; Vogl *et al.,* 1993). In modern humans the increase in body mass during puberty is mainly

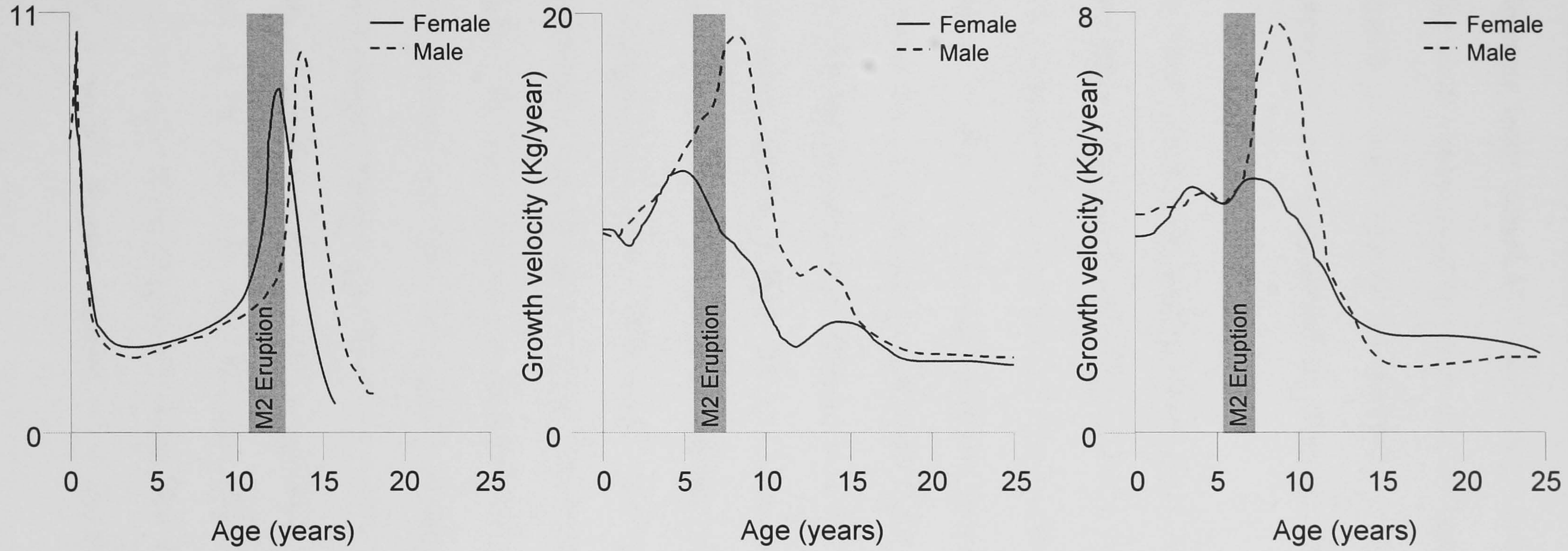

Figure 4.4. Cross-sectional growth velocity curves for body mass in (a) *H. sapiens* (adapted from Tanner *et al.,* 1966) (b) *G. gorilla* and (c) *P. troglodytes* (adapted from Leigh, 1996*)*. Superimposed grey rectangles denote eruption age range for second permanent molars. Data on hominoid molar eruption times were collated from published literature for *H. sapiens* (Clements, 1953; Stones et al., 1951), *G. g. gorilla* (Smith, 1994) and *P. t. troglodytes* (Anemone et al., 1991, 1996; Gavan, 1967).

attributable to muscular tissue (Wheeler, 1991). Attainment of large muscle (body) mass will increase loads caused by weight bearing and muscle contractions. This may alter the strain environment to which cortical bone adapts. If hominoid iliac growth responds to loads induced by muscular contraction the development of external morphology may be associated with locomotor behaviour.

The muscles which attach to the modern human ilium play a key role in locomotion and the maintenance of an erect posture (Berge, 1994). The *m. erector spinae*, which inserts on the posterior one third of the iliac crest, sustains upright posture (Latash, 1993) (Figure 4.5). The *m. quadratus lumborum* which inserts on the iliac crest anterior to the *m. erector spinae*, laterally flexes the trunk to hold the body over the stance leg during bipedal locomotion (Palastanga, 2006) (Figure 4.5). The powerful *m. gluteus maximus* and the posterior fibres of *m gluteus medius* originate on the dorsal portion of the iliac blade and power bipedal locomotion by extending and abducting the thigh (Platzer *et al.,* 2004) (Figure 4.5). It is reasonable to suggest that during puberty these muscles will get larger. The dorsal portion of the ilium and posterior half of the iliac crest may get proportionally larger in relation to overall size. Although it has been noted that muscle contractile strength is not always correlated with muscle insertion area (Burr *et al.,* 1977). At the time of second molar eruption the dorsal aspect of the ilium (i.e. everything posterior to a line joining the thinnest part of the iliac crest with the iliac body) gets proportionally larger compared to iliac centroid size (Figure 4.1). Hence the development of external iliac morphology in modern humans appears to be associated with muscle induced loading.

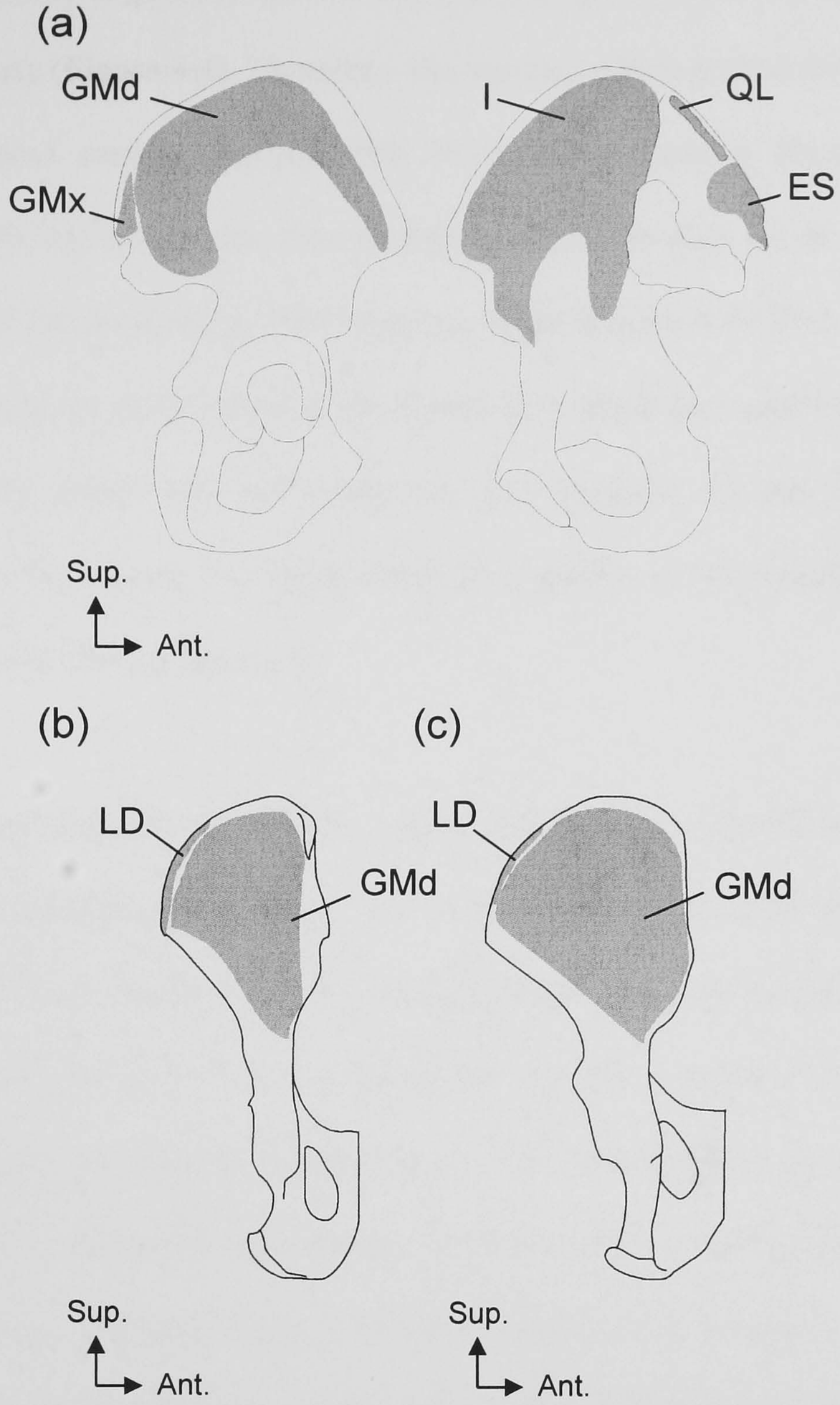

Figure 4.5. Selected muscular origins and insertions on the Hominoid pelvis. (a) *H. sapiens* (b) *P. troglodytes* (Swindler & Wood, 1982; Waterman, 1929) (c) *G. gorilla (*Waterman, 1927*)*. Abbreviation as follows: GMx, *m. gluteus maximus*; GMd, *m. gluteus medius*; I, *m. iliacus*; QL, *m. quadratus lumborum*; ES, *m. erector spinae*; LD, *m. latissimus dorsi*.

A similar association may be apparent in *P. t. troglodytes* and *G. g. gorilla*. Hunt (1994) noted that *G. gorilla* and *P. troglodytes* adopt different body postures when vertically climbing depending on body mass. Larger individuals hold their body further away from trunks. Hunt (1994) suggested that this was because climbing is

more difficult at large body size. In the African apes, body mass increases rapidly during puberty (Figure 4.4). Therefore, the muscles which extend the back and thigh, e.g. *m. gluteus medius* (Berge, 1994; Hunt, 1994; Stern & Susman 1984), and perhaps more importantly the muscles which adduct the arm, i.e. *m. latissimus dorsi* (Hunt, 1994; Larson & stern, 1986) may get larger (Figure 4.5). Post M2 eruption the insertion areas for these muscles, i.e. dorsal iliac blade and anterior iliac crest, get proportionally larger with increasing iliac size (Figures 4.2 and 4.3). Hence, the development of external iliac morphology also appears to be associated with muscle induced loads in the African apes.

More detailed analysis will probably reveal more conclusively that key stages in life history, i.e. pubertal growth spurt, can be detected in a series of isolated bones, in this case the ilium. Hormones, e.g. growth hormone and gonadal steroids, may affect the pattern of iliac growth and development through combined effects. Hormones drive pubertal increases in muscle mass (body mass) and may alter the strain environment to which the ilium adapts. Hormones may also affect the ilium directly by accelerating and prolonging longitudinal growth at the epiphyseal plates. This makes sense given that when growth hormone and gonadal steroid levels are high during puberty, the hominoid ilium shows a dramatic change in allometric growth trajectory.

Part III. Internal Iliac Morphology

Chapter 5. Trabecular Bone: A Literature Review

5.1 Organisation of trabecular bone

Thus far this study has considered the external cortical morphology of the primate pelvis. In the ilium, as in most primate bones, two types of bone can be identified macroscopically. The external shell of cortical bone surrounds trabecular bone and provides a surface for muscles to be attached. Trabecular bone is made up of trabeculae, i.e. bony rods and plates, that branch and intersect to form a three-dimensional porous network with marrow in the intervening spaces (Swartz *et al.*, 1998). The porous structure of trabecular bone confers a lower density than the solid structure of cortical bone, thereby minimising weight (Seeman, 2003). Conversely, the bony meshwork is well-suited to dissipate high compressive loads (Smit *et al.*, 1997). Bone must remain as light as possible to allow efficient locomotion (Turner, 1998) whilst maintaining sufficient strength to resist maximum mechanical stresses (Pauwels, 1980; Preuschoft, 2004). The highest loads occur primarily in posture and locomotion, simply because of the effect of body weight (or its multiple) (Preuschoft, 2004).

Microscopically, trabecular bone consists of a mineralised organic matrix. The organic matrix (osteoid) is made up of proteins, primarily type I collagen fibres, and carbohydrates, e.g. proteoglycans and glycoproteins (Hall, 1991a). The mineral component is made up of crystals of calcium phosphate salt called hydroxyapatite (Hall, 1992b). The inorganic component of the matrix provides trabecular tissue with

strength, resilience, and flexibility. Mineralization confers upon bone the property of mechanical rigidity, which complements the tensile strength and elasticity derived from bone collagen. In combination, the organic and mineral components allow trabecular bone to resist stress without breaking.

5.2 Function of trabecular bone

The primary function of trabecular bone is biomechanical. Trabecular bone resists compressive stress (Carter & Hayes, 1977a, 1977b) and plays an important role in load transmission (Swartz *et al.,* 1998). Bone must accomplish this task without breaking or being extensively damaged by applied functional loads (Ehrlich & Lanyon, 2002). Consequently, in compression trabecular bone must be strong (i.e. bear loads without bending or breaking) and stiff, i.e. able to resist deformation when loaded (Currey, 1984, 1998; Seeman, 2003).The ability of trabecular bone to resist compressive stress is dependent upon several factors including bone density that is fraction of bone per unit area or volume (Ford & Keaveny, 1996; Kleerekoper *et al.,* 1985; Turner *et al.,* 1990), trabecular connectivity and trabecular orientation (Ulrich *et al.,* 1999). This makes sense given that trabeculae are best able to resist compressive stress when the load is orientated along their long axes (Giesen *et al.,* 2003). Trabecular bone is also the primary site for mineral storage. It acts as a reservoir for calcium, phosphorous, sodium, magnesium and carbonate (Swartz *et al.,* 1998). The minerals held by trabecular bone are released through osteoclastic activity. Upon release, the minerals stored in trabecular bone can supply adequate minerals to all body cells in spite of variations in dietary intake and mineral loss, e.g. urine and perspiration. Hence, apart from its biomechanical importance trabecular bone also plays a key role in mineral homeostasis.

5.3 Trabecular growth and development

5.3.1 Osteogenesis

Iliac trabecular bone is mainly formed by a process known as endochondral ossification: the process of bone formation from cartilage. Before bone formation a prenatal cartilage Anlage (precursor) of the ilium is made by chondrification (Delaere *et al.*, 1992; Laurenson, 1965; Scheuer & Black, 2000). Chondrification is the process by which cartilage is formed from condensed mesenchyme or mesenchymal tissue (Laurenson, 1964; Hall 1992a, 1993). Mesenchyme cells differentiate into chondrocytes and secrete hyaline cartilage. Endochondral ossification begins with osteoblasts (bone forming cells) secreting osteoid into the extracellular environment. Osteoid forms a framework upon which mineralisation occurs. Osteoblasts raise the concentration of calcium and phosphate ions in the extracellular environment. Eventually, the concentration of calcium and phosphate ions becomes so high that hydroxyapatite crystals form and precipitate out of solution (Hall, 1991a). The crystals are deposited in the spaces between collagen fibres and bind to the proteins and carbohydrates in the osteoid (Hall, 1991, 1992b). Hyaline cartilage tissue is gradually replaced by bone tissue. During development the Anlagen continue to grow and are subsequently ossified in this manner, i.e. interstitial growth. The Anlagen grow at the epiphyseal growth plates which are situated close to the metaphyses of the bone (Figure 5.1a). The Anlage grows when epiphyseal chondrocytes multiply, secrete cartilage and hypertrophy (Figure 5.1b) (Beier, 2005; Nilsson *et al.*, 2005; Ohlsson *et al.*, 1992). Interstitial growth creates a chondrification front with four zones (Figure 5.1b). Close to the epiphysis is the outermost resting zone which is sparsely populated with unorganised cartilage cells. Inwardly there is a zone of proliferation where chondrocytes divide and become

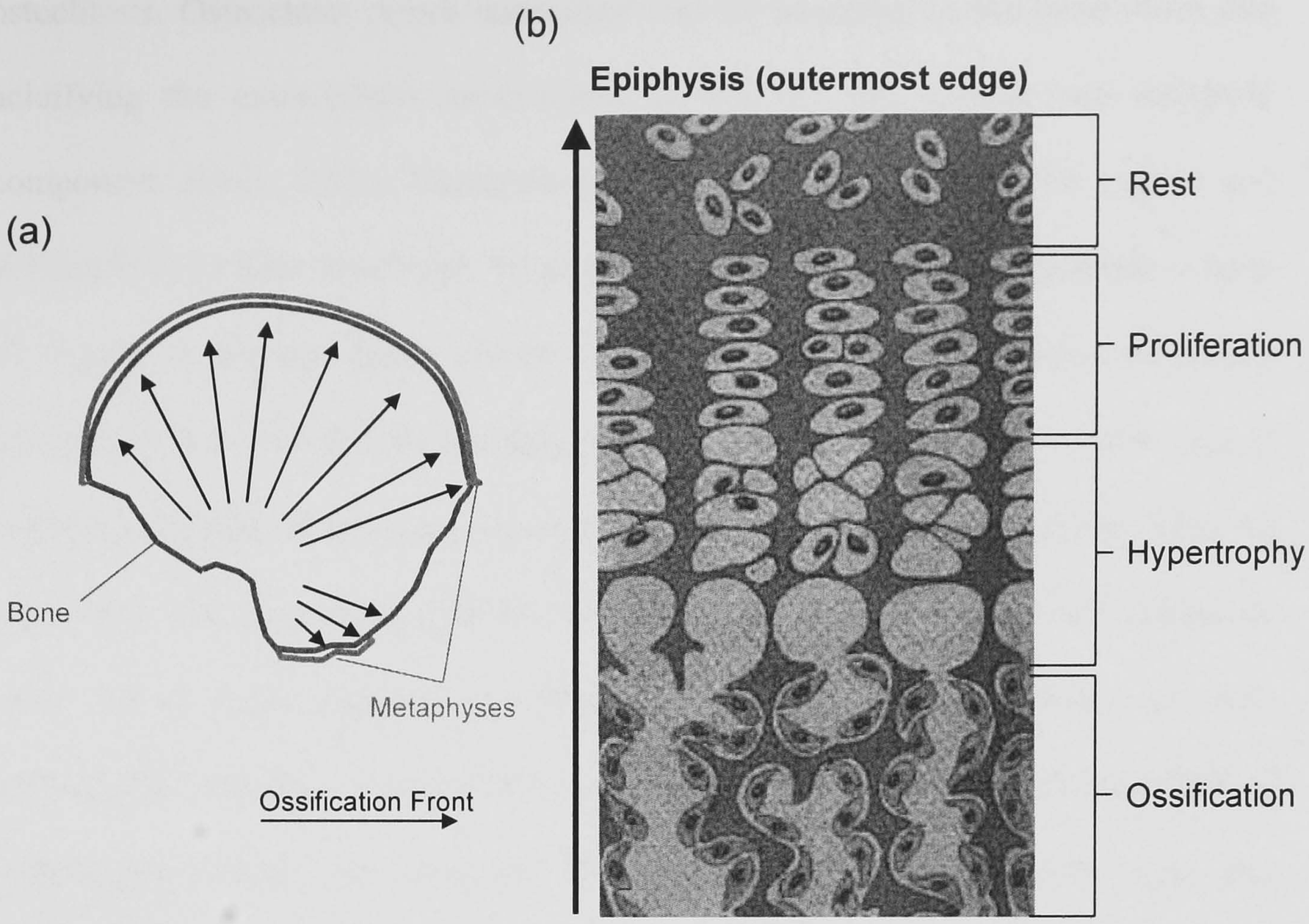

Figure 5.1. Primary (endochondral) ossification of the modern human fetal ilium. (a) a schematic representation of the fetal ilium showing the location and direction of the ossification front. (b) A close up of the chondrification front. Note that bone density decreases infero-superiorly whilst cartilage density increases. Black arrows indicate the direction of the ossification front

organised into distinct columns. This surrounds a zone where cartilage cells hypertrophy (increase in size). The innermost zone of ossification contains the bone nucleus and exposed cartilage where osteoid is deposited.

5.3.2 Modelling and remodelling

Adult trabecular morphology is achieved by modelling and remodelling of new and existing bone morphology. Modelling may be considered as uncoupled deposition and resorption of bone on different trabecular surfaces and may lead to a net gain in bone mass (Frost, 1990b). Remodelling is coupled resorption and deposition of bone at the same site (Frost, 1990b). Bone is resorbed by osteoclast cells and deposited by

osteoblasts. Osteoclasts resorb trabecular bone by attaching to the bone tissue and acidifying the extracellular environment to dissolve the organic and inorganic components (Hall, 1991b; Vaananen *et al.,* 2000). Osteoblasts deposit osteoid and mineralise it to form new bone. When new bone is laid down by osteoblasts a layer of cement is first put down. Cement lines are the boundaries between secondary osteons (new bone) and surrounding interstitial (older) bone. The cement line is collagen deficient and also less mineralized than the surrounding bone tissue (Burr *et al.,* 1988). The remodelling process leaves cement lines in cortical and trabecular tissue which have scalloped contours. The modelling process leaves no such scalloped cement lines. Frost (1990) reported that in adult modern humans 100% of 6000 cement lines in the cortex and 96.7% of cement lines in trabecular tissue had scalloped contours. The remaining 3.3% of cement lines in the trabecular tissue did not show any evidence of scalloping. Kobayashi *et al.* (2003) histologically analysed trans-iliac biopsies from the iliac crest of modern humans aged between ~50-75 years. Microscopic analysis of histological sections of trabeculae revealed that new regions of trabecular bone were bordered by smooth cement lines with no scalloping. These finding suggested that modelling of cortical bone peaks early in development and ceases at sexual maturity, whereas trabecular tissue maintains the ability to model throughout life (Frost, 1990b; Kobayashi *et al.,* 2003). However, in adults trabecular morphology is mainly altered through remodelling and changes are minor compared to modelling, which has the capacity to bring about larger changes in bone morphology.

Trabecular modelling and remodelling is thought to occur in response to several factors including mechanical loading (Ehrlich & Lanyon, 2002; Turner 1998).

Experimental animal studies have shown that during ontogeny disuse, i.e. reduced mechanical loading, is associated with bone loss (Mazess & Whedon, 1983; Takata & Yasui 2001). Weinreb *et al.* (1989) subjected two groups of pre-pubertal rats to unilateral hind-limb immobilisation between 10-42 days of life by performing a tenectomy of knee tendons or sciatic neurectomy. A histological assessment of trabecular bone volume fraction at 42 days revealed that the proximal tibial metaphyses of the immobilised limbs had lower bone density than sham operated contra-lateral limbs. Hott *et al.* (2003) also investigated the proximal tibial metaphysis of non-adult rats between 8-12 weeks. Unilateral hind-limb immobilisation was achieved using plaster casting. At 12 weeks, histomorphometric analyses revealed that immobilised tibiae possessed lower trabecular bone volume fraction than the contra-lateral tibiae. Similarly, Ito *et al.* (2002) demonstrated that disuse was associated with reduced trabecular density and a change in trabecular alignment when rats were immobilised during puberty from 8-12 weeks through unilateral sciatic neurectomy.

Animal exercise models have also been used to examine the effects of loading on trabecular tissue during growth and development. The results published to date suggest that exercise, i.e. increased mechanical loading, is associated with increased trabecular bone density, i.e. area or volume fraction (Mori *et al.,* 2003). Three studies on growing rats suggest that exercised individuals show larger increases in bone volume than sedentary controls. Hou *et al.* (1990) exercised a group of rats each day on a treadmill from pre-puberty through to adulthood (8-18 weeks). At 18 weeks histological measures of trabecular area fraction in the femoral neck were compared with an age matched sedentary control group, which they found to be significantly

lower. Iwamoto *et al.* (1999) subjected two groups of rats to treadmill exercise from 4-12 weeks, i.e. pre-puberty, and from pre-puberty through to adulthood, i.e. 4-16 weeks, respectively. At the end of each study, histological measures of trabecular bone area fraction were collated from lumbar vertebrae, proximal tibiae and distal tibiae and compared to age matched sedentary control groups. The exercised groups had significantly higher bone area fractions in the tibiae but not the vertebrae. The lack of change in vertebrae was attributed to their small role in weight bearing (Iwamoto *et al.,* 1999). Mori *et al.* (2003) subjected two groups of pubertal rats to climbing exercise between 8-10 and 8-12 weeks of development, respectively. Histological measures of trabecular bone area fraction from the proximal tibiae were compared across the exercised groups, age matched sedentary controls and a baseline control sacrificed at 8 weeks. Exercised groups showed higher bone density than baseline controls and sedentary controls, which had the lowest bone density.

The capacity of bone tissue to alter its mass and structure in response to mechanical demands has long been recognized, but the cellular mechanisms involved are not well understood. Mechanical energy is converted into electrical and/or biochemical signals (Duncan & Turner, 1995; Turner, 1998). The process by which cells convert mechanical stimuli into biochemical signals is known as mechanotransduction (Han *et al.,* 2004; Turner, 1998). It is likely that the process is mediated by more than one stimulus and multiple pathways (Pearson & Lieberman, 2005). Osteoblasts are usually implicated in strain sensing. Osteocytes (specialised osteoblasts located within bone matrix) have been identified as strain receptors and transducers. Osteocytes possess long processes, i.e. canaliculi, which radiate from the cell in all directions. Cell processes meet at junctions to allow communication between cells

(Cowin *et al.,* 1991). Together, osteocytes and bone lining cells, i.e. quiescent osteoblasts, form a connected cellular network (CCN). Several hypotheses have been suggested to explain how the CCN detects mechanical stimuli. Firstly, it has been suggested that osteocytes sense shear stresses (Weinbaum *et al.,* 1994). Mechanically induced stresses result in bone deformation, i.e. strain. Osteocytes may sense pressure changes created by bone strain in fluid-filled canaliculi (Bakker *et al.,* 2003; Cowin *et al.,* 1995). Strain rate may be an important aspect of mechanical stimulus (Jacobs *et al.,* 1998). Secondly, strains may induce stretch-activated ion channels that promote calcium influx, which in turn initiates other intracellular responses (Davidson *et al.,* 1996; Gugino *et al.,* 1989). Thirdly, bone strain itself may generate electrical potentials which are detected by osteocytes (Cowin & Moss, 2001).

5.4 Determining pelvic trabecular architecture

5.4.1 Conventional radiography

Previous studies of trabecular morphology have successfully utilised measurements of trabecular structure collected from radiographs (Martinon-Torres, 2003; Robson-Brown *et al.,* 2002). The pelvis is ideally suited for conventional radiography because of its flat shape, which minimises the effects of superimposition (Martinon-Torres, 2003). The bone appears white on the film and the density of the image, i.e. greyscale, is a function of the quantity of radiation transmitted through the object, which in turn is inversely proportional to the atomic number, density, and thickness of the bone (Scally, 1999).

5.4.2 Micro-computed tomography (μCT)

Researchers have successfully utilised computed tomographic reconstructions to take measures of trabecular morphology for comparative analyses (e.g. Ryan & Ketcham, 2002, 2005). Micro-computed tomography produces two-dimensional representations of a slice of an object based on material density, measured by X-ray transmissions (Zonneveld, 1987) and has a high enough resolution to visualise thin bony trabeculae (<100μm). The μCT slices are made up of voxels, i.e. three dimensional pixels. Each voxel is assigned a CT (grey) value derived from a linear attenuation coefficient of the material(s) being scanned (Zonneveld, 1987). When calculating grey values it is inevitable that distortion to the bone structures true make-up occurs, due to noise and partial volume averaging (Zonneveld, 1987). Partial volume averaging is the result of numerous linear attenuation coefficients (i.e. materials of different density) within a single voxel being represented by an averaged CT value (Figure 5.2). This phenomenon leads to a blurring of the bone/non-bone interface i.e. a gradient of CT values (Spoor *et al.* 1993; Zonneveld, 1987) and increases with increasing voxel size. The μCT slices can be aligned to provide a three-dimensional representation of the object under investigation. Slices from a scanned object can be stacked to produce a three dimensional reconstruction that can be resliced in any plane. It is important to note that slices, unlike radiographs, are not true images but are instead represented by voxels (or pixels) with designated CT values. However, slices or reconstructions can be thresholded in order to produce a secondary image.

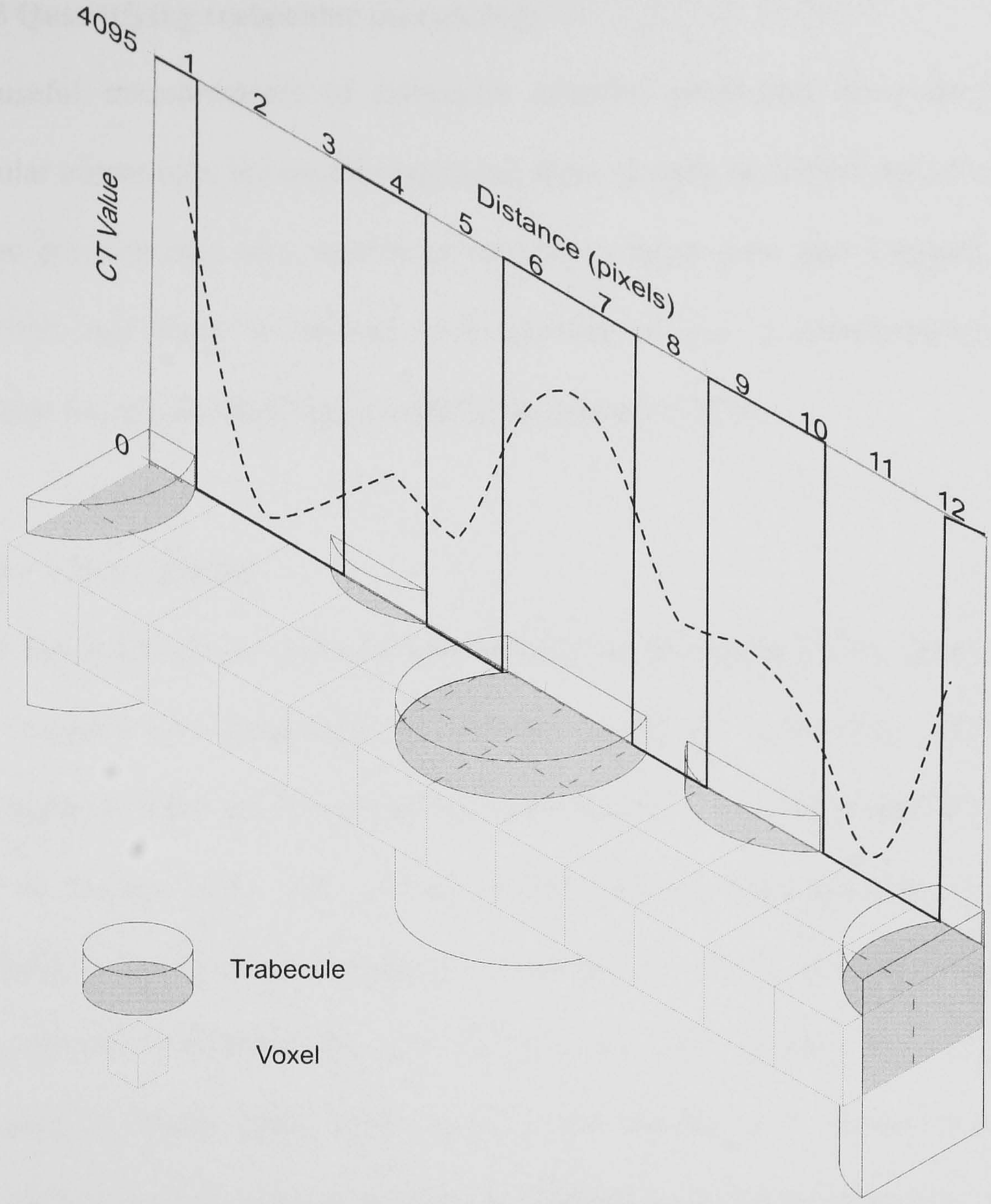

Figure 5.2. Partial volume averaging. A μCT slice is comprised of voxels. Partial volume averaging occurs when materials of different density (i.e. bone and air) occupy the same voxel. The CT value assigned to each voxel represents an average of the linear attenuation coefficients (i.e. density). This leads to a blurring of the bone non-bone boundary. Hence the actual profile along a row of voxels, solid black line on chart, is represented by a profile more like the dashed line.

5.5 Quantifying trabecular morphology

Two useful measurements of trabecular material properties, bone density and trabecular anisotropy, are usually collected. Bone density is defined here as the area of bone per unit area in a section of cancellous tissue (see also Odgaard, 1997). Trabecular anisotropy is defined as a measure of how randomly/non-randomly trabeculae are orientated (Odgaard, 1997; Whitehouse, 1974).

5.5.1 Bone density

Before measurements of trabecular bone density can be obtained from radiographs or μCT, sections bone/non-bone boundaries must be accurately determined. Determination of the bone/non-bone boundary has received a great deal of attention (Davis & Wong, 1996). The position of the bone/non-bone boundary is usually determined by setting a uniform global, i.e. whole bone, threshold value above which voxels are said to contain bone (see Banse *et al.,* 2002; Fajardo & Müller 2001; MacLatchy & Müller, 2002; Müller *et al.,* 1998; Mueller *et al.,* 1996; Tanck *et al.,* 2001). This process is often referred to as uniform thresholding. However, uniform thresholding can be inappropriate (Kuhn *et al.*, 1990; Hara *et al.*, 2002) as it incurs two main problems. Firstly, variation in bone (mineral) density across specimens affects the position of the bone/non-bone boundaries, so voxels representing non-bone may be taken as bone and vice versa (Davis & Wong, 1996; Fajardo *et al.*, 2002). Similarly, intra-specific variation in bone mineral (i.e. bone density) distribution can lead to over- or under-estimation of trabecular density. Intra-specific variation in mineralisation may be brought about by developmental or degenerative processes (see Fajardo *et al.*, 2002) as well as diagenesis and preservation (Brothwell, 1981). Secondly, radiographic artefacts may cause the threshold value to

vary across a bone. This is a particular problem when scanning whole bones. Cortical tissue is denser than trabecular tissue and attenuates X-rays more readily. Consequently, fewer x-rays (photons) penetrate right through the bone. This leads to greater resorption and diffraction of X-rays at the cortical shell, which produces inflated CT values; the CT values fall from the outer cortex to the centre of a bone purely because of artefacts. Therefore, a global uniform threshold procedure may overestimate the amount of cortical bone and/or underestimate the amount of trabecular bone in a μCT section. The error increases with the diameter of the bone. In order to determine bone and non-bone boundaries accurately a non uniform (site-specific) threshold should be applied. Only one method of non-uniform thresholding exists, the half maximum height (HMH) method (see Zonneveld, 1987). The HMH method thresholds all bone/non-bone interfaces separately. The method assumes that the bone/non-bone interface is located midway between the minimum (non-bone) and maximum (bone) CT values. The great advantage of this method is that bone/non-bone interfaces can be located within voxels. Thus the method is not as dependent on voxel size as uniform thresholding methods, although the HMH protocol is very time consuming.

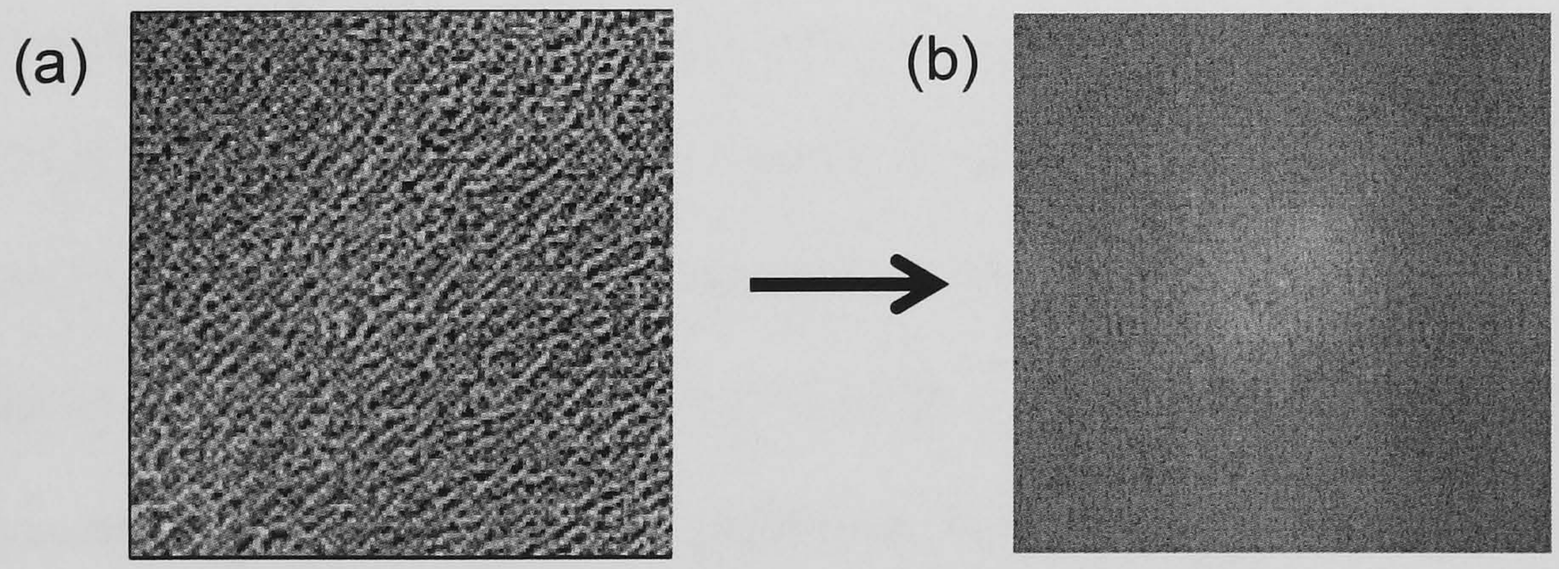

Figure 5.3. The Fast Fourier transform. (a) a radiographic image or μCT section can be transformed into (b) a secondary image using the Fast Fourier transform technique. If the original image is anisotropic the transform reveals this.

5.5.2 Trabecular anisotropy

There are two traditional methods available for calculating anisotropy in two dimensions: median intercept length (MIL) (Whitehouse, 1974) and the volume orientation (VO) method (Gundersen & Jensen, 1985; Odgaard *et al.,* 1990; Odgaard, 1997). Both methods work on the same basic principle. Firstly, the main orientation of trabecular tissue is calculated. The main trabecular orientation is defined as the direction in which most of the trabecular bone is distributed (Whitehouse, 1974; Harrigan & Mann 1984; Odgaard 1997; Odgaard *et al.,* 1997; Smit *et al.,* 1998). Secondly, the amount of bone aligned perpendicularly to the main direction is measured. Trabecular anisotropy is the ratio of the amount of bone orientated along the main direction and that perpendicular to it. Published methods differ in the way the "amount" of bone is measured. The MIL method counts the number of intersections between an imposed grid and the trabeculae at a given angle ($0\text{-}180^0$) and is normalized according to transect length (Whitehouse, 1974). The technique can be insensitive when trabeculae are not strongly aligned in any direction (Augat *et al.,* 1998; Goldstein *et al.,* 1993; Majumdar *et al.,* 1998; Whitehouse, 1975). The VO technique is based on sampling a section at a series of random points. The longest intercept through the point is measured. A second rank tensor is calculated to describe the main and perpendicular orientation (Gundersen & Jensen, 1985; Odgaard *et al.,* 1990). The methods are well-suited to histological sections. However, binary representation of the trabeculae is required before radiographic and μCT sections can be utilised for these techniques. Methods for measuring trabecular anisotropy have been developed which may be better suited to radiographic and μCT sections.

More modern techniques utilise texture analysis (TA) algorithms (e.g. Buckland-Wright *et al.,* 1994; Lespessailles *et al.,* 1998). Micro CT slices and digitised radiographs consist of matrix of pixels each with a grey level represented by an integer. The spatial variation in pixel grey values is referred to as image texture. The texture of the image bears an indirect relationship to the bony structure. Therefore an analysis of texture can reveal information about the trabecular pattern (Caligiuri *et al.,* 1993). Many techniques have been proposed to analyse texture. Algorithms measure and describe the same set of textural properties but assess different aspects of texture. The techniques used to assess bone structure (i.e. image texture) must be selected according to the biological question. In this study it is pertinent to find out whether, and how, trabecular anisotropy changes during iliac development. Methods useful for assessing anisotropy include (i) First, second and higher order statistics (e.g. auto-correlation), (ii) Topological Features (e.g. Euler features), (iii) multi scale texture analysis (e.g. fractal dimensions), (iv) textural filtering (e.g. Fourier transforms) and (v) neighbourhood grey-tone difference matrix. Topological methods are not applicable to structure without a consistent topological structure. Techniques such as auto-correlation are not discriminating; hence it is difficult to assess variation in anisotropy across specimens. Conversely multi scale texture analysis can be used to assess relationship with biological variables but data may only partially reflect the trabecular bone microarchitecture (Lespessailles *et al.*, 1998). The neighbourhood grey-tone technique is not wholly suitable for sections of trabecular tissue because it assesses tone (variation in regional brightness) rather than texture (variation in grey levels). The image intensity of radiographs/μCT sections varies greatly; hence texture dominates, as opposed to tone. Thus textural filtering techniques, such as fast Fourier transform (FFT), may be more appropriate for measuring trabecular

directionality. Techniques based around the FFT have been tried and tested (e.g. Buck *et al.,* 1998; Buck *et al.,* 2002; Lespessailles *et al.,* 1996; Oxnard & Yang, 1981; Oxnard, 1993). Furthermore, previous studies of iliac trabecular morphology have successfully utilised the fast Fourier technique (Martinon-Torres, 2003; Robson-Brown *et al.,* 2002). In accordance with previous studies the FFT technique was utilised to assess the orientation of trabeculae.

Russ (1994) described a method for obtaining measures of anisotropy from transformed images that could be applied to both radiographic and μCT sections. The FFT can be used as an image processing tool to reduce noise in an image by decomposing it into its sine and cosine components (Figure 5.3). This is accomplished by transforming the array of pixel values in a radiographic/μCT section into new array of grey values (complex numbers). The transformed pixel values are calculated by summing the cosine and sine curves. In the complex array each pixel represents a particular wave number (wavelength per distance) contained in the original image. The number of wavelengths in the transformed image corresponds to the number of pixels in the original image. Hence, the complex array (FFT section) is the same size as the original image. However, the complex array does not contain all the frequencies that formed the original image. The array contains a smaller set of wavelengths which is large enough to fully describe the original image. The reduced set is sufficient because only noise is discarded, i.e. information not described by simplified sine and cosine curves. The main advantage of measures of anisotropy collected from FFT sections over measures collected from thresholded sections is that artefacts generated by the thresholding process are avoided.

Part III. Internal Iliac Morphology

Chapter 6. Fetal Trabecular Growth and Development

During prenatal development the modern human fetus is shielded from gravitational loads in the womb. However, from about 11 weeks onwards muscles contract in a sporadic and uncoordinated manner, e.g. kicking (Delaere *et al.,* 1992; Delaere & Dhem, 1999; Scheuer & Black, 2000). If trabecular tissue adapts to mechanical loads very early in iliac development one would expect an ordered trabecular structure to have appeared soon afterwards. An ordered structure is an anisotropic one, that is an uneven distribution of bone across the iliac blade and preferentially aligned trabecular elements.

6.1 Aim

The aim of this chapter is to test the hypothesis that fetal iliac trabecular tissue of modern humans displays an ordered structure at 16 weeks i.e. uneven distribution of bone. The distribution of bone was assessed on both a macroscopic scale (bone density distribution) and microscopic scale (trabecular orientation).

6.2 Materials and methods

6.2.1 Sample

For this chapter the ontogenetic series of 137 fetal specimens was measured (Table 6.1). The specimens were obtained from the Department of Human Anatomy at the University of Liverpool (Liverpool, UK). The specimens were sourced from a Victorian workhouse at the turn of the century. Some 58 of the fetal specimens came

with associated age between 16-36 weeks. Age was determined to the nearest month on the basis of parental testimony. Prior to the start of this study the specimens had been de-fleshed using bicuspid beetles. Specimens had not been treated or preserved in any way. The specimens had been wrapped in newspaper and stored in metal tins. Thus the effects of preservation on mineralisation, if any, should be limited. Ontogenetic series were defined according to age and iliac centroid size. Centroid size was determined using the external landmarks listed in Table 3.2. The developmental stages and the number of specimens in each are given in Table 6.1.

Category	Sample Number for Age or Size Class						Total
Age (weeks)	**16**	**20**	**24**	**28**	**32**	**36**	
Sample A	7	10	10	13	11	7	58
Iliac Centroid Size (mm)	**14-24.9**	**25-29.9**	**30-34.9**	**35.39.9**	**40-44.9**	**45-50.0**	
Sample A	10	10	10	9	9	10	58
Sample B	21	26	22	23	25	20	137

Table 6.1. Prenatal iliac sample size. Specimens were sorted according to fetal age (nearest 4 weeks) and iliac centroid size class. Sample A consists of 58 aged specimens that had associated age and sample B includes all 137 measured specimens.

6.2.2 Micro-computed tomography (μCT)

Iliac trabecular tissue can be imaged non-destructively using micro-computed tomography. The resolution of μCT scans is very high in comparison to radiographs and reconstructions do not suffer the effects of superimposition. Also, due to the small size and high density of trabecular tissue in fetal ilia, μCT scans are better than conventional radiographs; low energy radiography produces images with white blobs because of the densely packed trabeculae. Hence fetal ilia were scanned with high-resolution μCT at the University of Liverpool following a protocol similar to Macho *et al.* (2005) and McColl *et al.* (2006). Ilia were scanned using a BIR Inc. ACTIS 420/600 system equipped with a tungsten x-ray target, a 250μm thick columnar

caesium iodide scintillator and a Toshiba AI5877 JP dual field image intensifier. The bones were scanned at a slice thickness of 100μm with 100μm increments and 2000 views. Voltage and current ranged from 40kV to 60kV and 160μA to 200μA respectively, giving an effective monochromatic x-ray energy of between 20 keV to 30 keV. Focal spot size was 50μm and contrast resolution was approximately 0.5%. Matrix size was 512x512 pixels, while voxel size was typically 100x100x100μm. Considering that the average trabecular thickness reported in the published literature is around 150-250μm (e.g., Whitehouse, 1974) with a range of 50-750μm (Chappard *et al.*, 1999; Byers *et al.*, 2000) the resolution chosen was considered sufficient for visualisation and measurement of iliac microstructure. Preliminary scans indicated that trabeculae radiate in fan shape manner from the iliac body to the iliac crest. Therefore, the infero-superior axis was oriented perpendicularly to the beam, thus ensuring maximum resolution (Kothari *et al.,* 1998). Micro-computed tomographic reconstructions were produced using VG Studio MAX 1.1 (maximum intensity projection reconstruction algorithm).

6.2.3 Areas of interest (AOI)

Measurements of trabecular architecture were collected from eight discrete areas of interest (AOI) in the iliac blade, as detailed in Figure 6.1. The AOI were scaled according to the size of the ilium. The edges of the AOI were equivalent to $1/5^{th}$ of the distance between the superior iliac spines. The AOI were placed according to an antero-posterior axis, connecting superior iliac spines, and a vertical axis perpendicular to, and midway along, the first axis. Anterior (A) and posterior (P) AOI were placed at the anterior and posterior superior iliac spines respectively, the

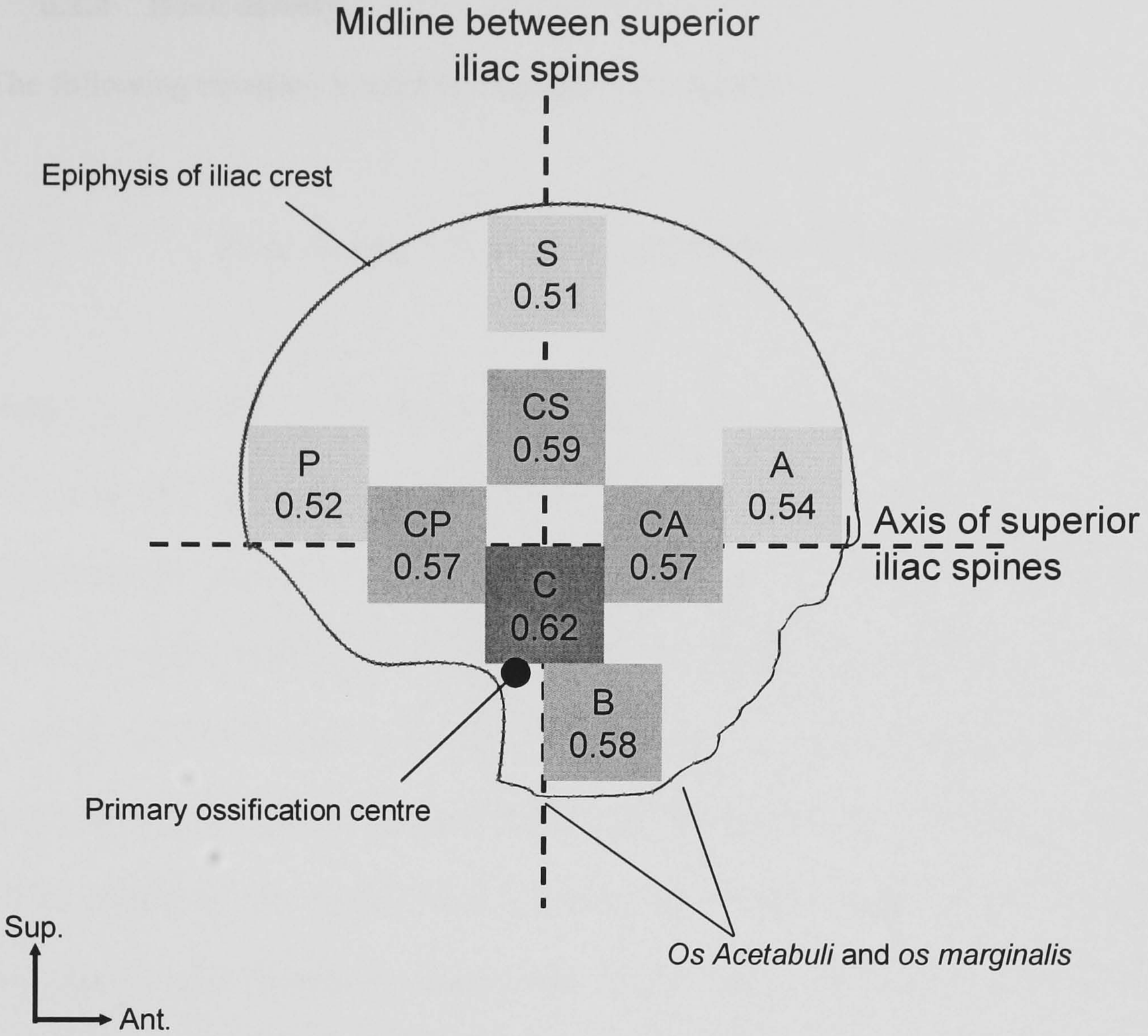

Figure 6.1. Areas of interest in the iliac blade. Letters denote regions where measures of trabecular architecture were collected: A, anterior; S, superior; P, posterior; C, central; CA, central-anterior; CS, central-superior; CP, central-posterior; B, basal. Numbers denote measured bone density (bone area fraction) in 36 week old specimens. The highest bone area fraction (AOI C) was found close to the site of primary ossification.

bases were aligned along the antero-posterior axis. A superior section (S) was centred on the infero-superior axis immediately below the iliac crest. A central AOI (C) was centred on the infero-superior axis with its superior edge placed on the antero-posterior axis. Three AOI (CA, CS and CP) were placed midway between the central AOI and the anterior, superior and posterior AOI. A basal (B) AOI was located inferior to the central AOI and immediately anterior to the infero-superior axis.

6.2.4 Bone density

The following equation is used to calculate bone density:

$$\text{Bone Density} = \text{Bone Area (pixels)}/\text{Area of AOI (pixels)} \quad (1)$$

Measurements were collected from the anterior, posterior and superior AOI for all 137 fetal ilia (Figure 6.1). Also, for 36 week old ilia only (n = 7), extra measurements were collected from the central, central-anterior, central-superior, central-posterior and basal AOI (Figure 6.1). Before measurements of bone density could be collected a binary threshold had to be applied, i.e. pixels representing bone were assigned a value of one and those representing non-bone a value of zero. A global threshold was used to determine bone/non-bone boundaries. The threshold was selected according to the distribution of grey values within a CT slice. For each AOI (Figure 6.2a) a grey value frequency distribution plot was produced (Figure 6.2b). The grey value with the lowest frequency was selected as the lower boundary and the second maximum was selected as the upper boundary (Figure 6.2b). An example of a binary threshold is shown Figure 6.2c. Since the areas of interest are so small errors incurred by the global thresholding procedure should be minimal. Furthermore, thresholding errors due to diagenetic effects on bone mineral content should be consistent across specimens given that they were preserved in the same way.

6.2.5 Trabecular anisotropy

Trabecular anisotropy was measured in all 137 specimens in the anterior, superior and posterior sections. The method used to obtain measures of anisotropy from Fast

Fourier Transforms (FFT) is described by Russ (1994). The AOI were transformed using a one-dimensional FFT algorithm. A profile plot is produced to describe variation in grey values along a row (or column) of pixels (Figure 6.2d). Then a sinusoidal curve is plotted to smooth the data (Figure 6.2d). The derived set of grey values is used to construct a new, smoothed row of pixels, i.e. grey values (Figure 6.2d). In order to transform an entire AOI the process is repeated for every row, then every column in an AOI. A 2D FFT procedure may have been better because each pixel is transformed only once, rather than a 1D FFT where each pixel is transformed twice. However, the 1D FFT is computationally simpler and is, therefore, quicker.

Measurements of trabecular anisotropy were collected from transformed AOI using the program FRACTALS (Russ, 1994). Transformed AOI were divided into segments (bins) situated around the centre of the image, each of equal arc length (Figure 6.2e). The first bin was centred on 0^0 (Horizontal). For each bin a least squares plot of *log* (magnitude)^2 versus *log* (frequency)^2 was calculated. The magnitude was the sum of pixel (grey) values in a bin. The frequency was the number of pixels (or parts of pixels) in a bin (Russ, 1990, 1994). Since the FFT array has rotational symmetry (Figure 6.2e) it was necessary to study only the first 180^0. The slopes of these plots were evaluated as a function of direction by using all of the points from bins in the first 180^0 of the FFT image. The values were viewed in a rose plot. A rose plot is an angle histogram, a polar plot showing the distribution of values grouped according to their numeric range. Each group is shown as one bin. In this study the rose plots depicted measured values of *log* (magnitude)^2 versus *log* (frequency)^2 as a function of bin angle (see Figure 6.2e). An example of a rose plot

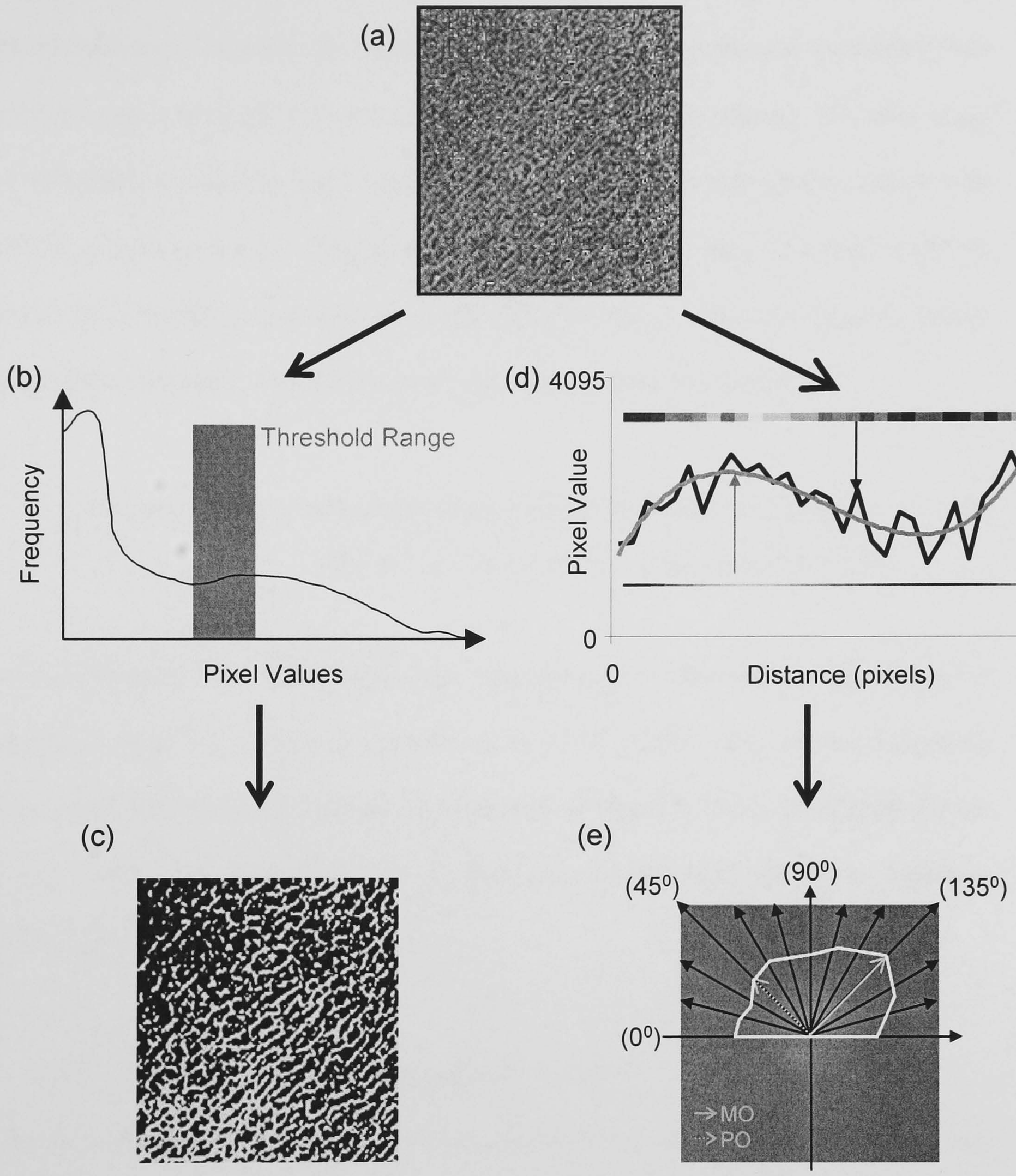

Figure 6.2. Quantifying trabecular material properties in the iliac blade. (a) Radiographic area of interest (b) Binary threshold procedure (lowest frequency used as lower boundary and second maximum set as upper boundary) (c) Binary threshold where pixels representing bone are coloured white and non-bone pixels are designated black (d) One-dimensional FFT (repeated for every row then every column). The original grey value data is smoothed. (e) Two-dimensional FFT with a rose plot superimposed on top (white line). Black arrows demarcate the bins at 15^0 intervals. Grey arrows designate the main trabecular orientation (MO) and the orientation perpendicular to the MO (PO).

(first 180^0) is given in Figure 6.2e, for simplicity only six bins (15^0 arcs) are shown. The rose plot depicted the degree of trabecular anisotropy (Figure 6.2e). For an isotropic AOI the rose plot is circular, while an anisotropic image the rose plot may have a variety of non-circular patterns. A metric value of trabecular anisotropy was read from the rose plot. This was accomplished in two steps. Firstly, the main angle of trabecular orientation was read from the rose plot i.e. the direction in which most of the trabecular bone is distributed (see MO in Figure 6.2e). The main angle of trabecular orientation falls along the angle with the highest slope of frequency versus magnitude. Secondly, trabecular anisotropy was calculated as the ratio:

$$\text{Trabecular Anisotropy} = \frac{\text{Slope of Log (Magnitude)}^2 \text{ Vs. Log (Frequency)}^2 \text{ along PO}}{\text{Slope of Log (Magnitude)}^2 \text{ Vs. Log (Frequency)}^2 \text{ along MO}} \quad (2)$$

where PO is the value of the frequency magnitude plot at the angle perpendicular to the main angle of trabecular orientation and MO is the value of the frequency magnitude plot at the main angle of trabecular orientation (Russ, 1994) (see Figure 6.2e). Values of one correspond to an isotropic structure and low values represent anisotropic structures.

6.2.6 Reproducibility of architectural measures

The precision of density and anisotropy measures was tested. Ten specimens that represented the full range of iliac size were selected. The ten specimens were measured repeatedly, five times on five separate days, in a random order. The percentage error of the measurements did not exceed 5% (Table 6.2). The measures were, therefore, deemed suitable for the study.

6.2.7 Statistical analysis of ontogenetic change in bone distribution

Mean values of structural parameters were compared across developmental classes using one-way ANOVA with Tukey's post hoc test. Associations between structural parameters and developmental stage were assessed using the χ^2 test. Correlations between measured parameters, age and iliac centroid size were assessed using Spearman's Rho test.

Architectural Measurement Variable	Area	**Percentage Error (%)**
Bone Area Fraction	A	3.6
	S	3.5
	P	4.7
Trabecular Anisotropy	A	4.1
	S	4.3
	P	4.5

Table 6.2. Estimates of repeatability for measures of trabecular tissue material properties in fetal *H. sapiens*. Measured areas of interest are labelled as follows: A, anterior; S, superior; P, posterior.

6.3 Results

Iliac bone distribution was measured between 16 and 36 weeks. At 16 weeks, fetal ilia show significantly higher bone density in the anterior and posterior AOI than the superior one (one-way ANOVA with Tukey's post hoc $F = 3.816$ $p = 0.046$; anterior versus superior $p = 0.036$, posterior versus superior $p = 0.049$). At 36 weeks fetal ilia show comparable bone density across the anterior, superior and posterior sections (one-way ANOVA; $F = 0.185$ $p = 0.631$) (Figure 6.1). Furthermore, at term bone density does not vary significantly across the iliac blade, i.e. eight measured AOI (one-way ANOVA; $F = 1.143$ $p = 0.353$) (Figure 6.1).

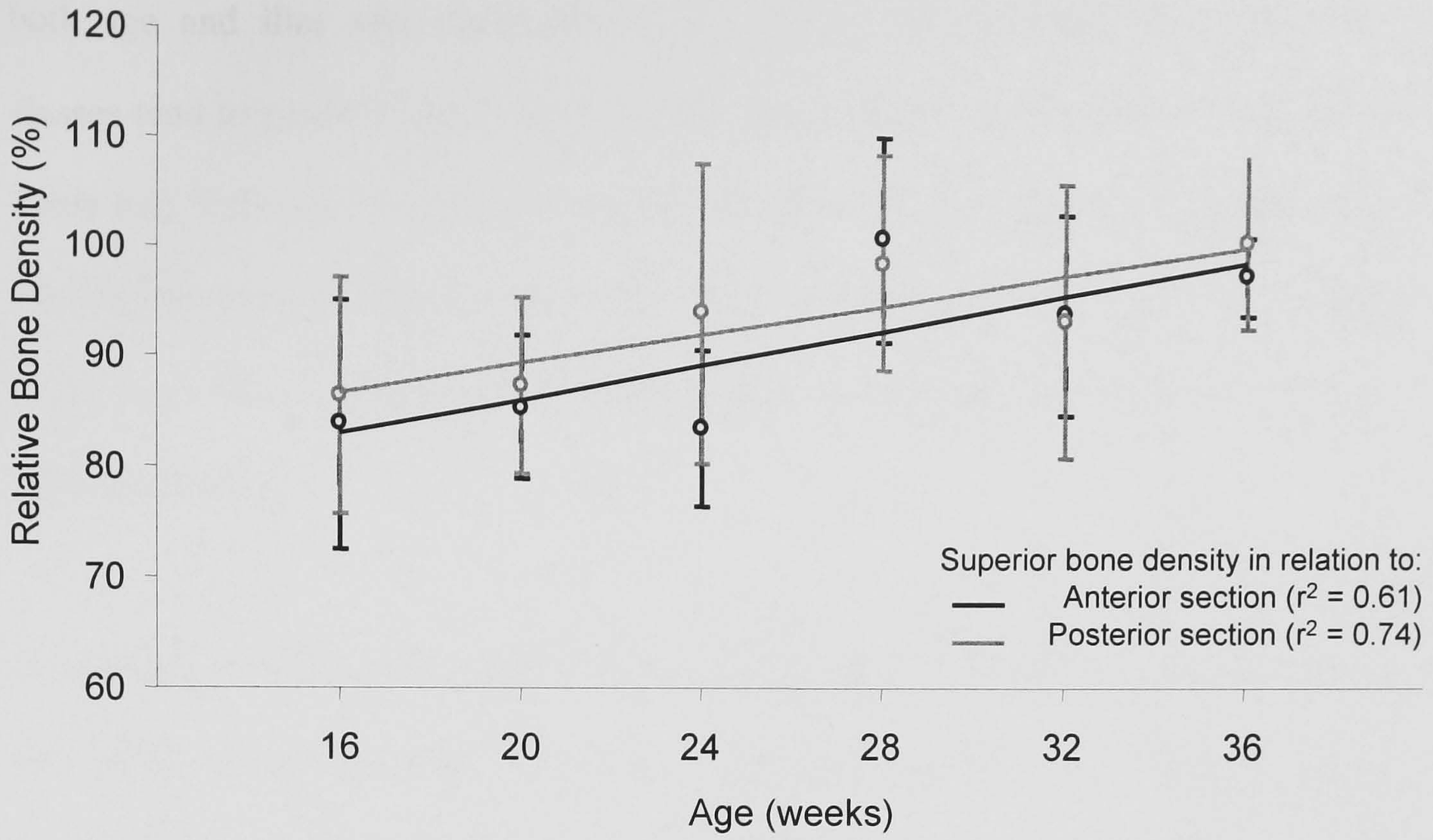

Figure 6.3. Ontogenetic change in bone density of the superior AOI: with respect to anterior and posterior areas of interest. Analysing the data in this manner standardises the specimens for exposure. The ordinate axis (relative bone density) is the proportion of bone in the superior area of interest expressed as a percentage of the density in the anterior and posterior portions of the ilium. Reduced major axis regression line. Error bars denote mean and standard deviation.

Ontogenetic changes in trabecular structure were analysed with respect to age and iliac centroid size. Anterior and posterior bone density is not associated with age or iliac size class in either sample A or B (χ^2, Table 6.3). Anterior and posterior bone densities are not correlated with age or iliac size (Spearman's Rho, Table 6.3). With one exception, mean bone density does not vary across age or iliac size classes in either the anterior or posterior AOI (ANOVA, Table 6.3). Tukey's post hoc for the one-way ANOVA reports that for sample B, the 5th largest iliac size class has a significantly higher bone density than the smallest (ANOVA, Table 6.3). Taken together these results indicate that in the anterior and posterior AOI bone density remains constant during fetal development between 16-36 weeks. In the superior AOI bone density is associated with size class in sample B but not age or iliac size class in sample A (χ^2, Table 6.3). However, bone density is positively correlated with

both age and iliac size (Spearman's Rho, Table 6.3). Furthermore, older/larger classes tend to possess higher bone density than younger/smaller classes (ANOVA, Table 6.3). Together these results suggest that superior bone density increases during fetal development between 16-36 weeks. When plotted as a function of bone density in the anterior and posterior AOI, bone density in the superior AOI increases with age (Figure 6.3).

In contrast to bone density, trabecular orientation appears to remain constant during fetal development. Trabecular anisotropy is not associated with age or iliac size class in any of the three measured AOI (χ^2, Table 6.4). Trabecular anisotropy is not correlated with either age or iliac size (Spearman's Rho, Table 6.4). Mean values of trabecular anisotropy do not vary across age or iliac size classes in either the superior or posterior AOI (ANOVA, Table 6.4). In the anterior AOI, the 28 week old class has significantly higher mean trabecular anisotropy than the 20 week class (ANOVA, Table 6.4). However, mean trabecular anisotropy is not correlated with age or size class (Spearman's Rho, Table 6.4). Taken together these results suggest that trabecular anisotropy remains constant during fetal development.

6.4 Discussion

At 16 weeks bone is not evenly distributed across the fetal ilium, the anterior and posterior AOI show higher bone density than the superior one. The mean measurement of trabecular anisotropy is about 0.6, which means that the amount of bone aligned along the primary axis is approximately two fold higher than the secondary axis. Thus, the hypothesis that modern humans may have ordered trabecular tissue from an early stage of foetal development seems to be confirmed.

Species	Area	Growth Stage	χ2 ρ	Spearman's Rho ρ	+/-	ANOVA F	ρ	Post hoc	Consensus Result
H. sapiens	A	Age	NS	NS		1.404	NS		
		Size (A)	NS	NS		1.443	NS		Constant
		Size (B)	NS	NS		4.059	***	1 > 5	
	S	Age	NS	*	+	3.676	*	1, 2 < 4	
		Size (A)	*	*	+	3.058	*	1 < 4	Increased
		Size (B)	NS	*	+	1.630	*	1 < 4	
	P	Age	NS	NS		0.123	NS		
		Size (A)	NS	NS		0.401	NS		Constant
		Size (B)	NS	NS		0.895	NS		

Table 6.3. Statistical analysis of ontogenetic change in *H. sapiens* fetal iliac bone density. Sample (A) contained 58 aged specimens and (B) contained the full set of 137 specimens. Symbols are NS = Non-significant, * = p<0.050, ** = p< 0.010, *** = p<0.001, + = positive correlation, - = negative correlation. Consensus column indicates whether analyses suggest an ontogenetic increase, decrease or constancy for bone density.

Species	Area	Growth Stage	χ2 ρ	Spearman's Rho ρ	+/-	ANOVA F	ρ	Post hoc	Consensus Result
H. sapiens	A	Age	NS	NS		2.739	*	2 > 4	
		Size (A)	NS	NS		0.872	NS		Constant
		Size (B)	NS	NS		0.139	NS		
	S	Age	NS	NS		1.357	NS		
		Size (A)	NS	NS		1.106	NS		Constant
		Size (B)	NS	NS		1.195	NS		
	P	Age	NS	NS		2.254	NS		
		Size (A)	NS	NS		0.715	NS		Constant
		Size (B)	NS	NS		2.193	NS		

Table 6.4. Statistical analysis of ontogenetic change in *H. sapiens* fetal iliac trabecular anisotropy. Sample (A) contained 58 aged specimens and (B) contained the full set of 137 specimens. Symbols are NS = Non-significant, * = p<0.050, ** = p< 0.010, *** = p<0.001, + = positive correlation, - = negative correlation. Consensus column indicates whether analyses suggest an ontogenetic increase, decrease or constancy for bone density.

Trabecular anisotropy does not change between 16-36 weeks (Table 6.4). At 36 weeks bone is evenly distributed across the iliac blade, the anterior, superior and posterior AOI show comparable bone density. Thus bone becomes more evenly distributed during fetal development i.e. less ordered. The change is mediated by an increase in superior bone density with respect to the anterior and posterior AOI (Figure 6.3). At term various AOI located around the ilium show the same bone density (Figure 6.1), hence bone appears to be evenly distributed across the entire blade.

Sporadic fetal muscular contractions are unlikely to apply evenly distributed loads across the iliac blade. Consequently, the finding that (during ontogeny) fetal iliac trabecular tissue becomes evenly distributed across the blade is not consistent with the notion that fetal bone density adapts to meet applied loads. Furthermore, in chapter 4 it was shown that the proportions of the fetal ilium change during development. Such changes can alter the line of action of muscles and the direction of loads imparted on the ilium. Trabeculae tend to align themselves along the main direction of loading (Biewener *et al.,* 1996; Ding *et al.,* 1999, 2002, 2003; Frost, 1990b). However, trabecular anisotropy does not change during fetal development (Table 6.4). Therefore, the results of this study are not consistent with the suggestion that fetal trabeculae re-orientate meet alteration in the direction of applied loads: at least not with the limited data available.

Primary iliac ossification begins in the region where the sciatic notch forms (Laurenson, 1964; Scheuer & Black, 2000). Following this, the fetal ilium grows interstitially, i.e. by endochondral ossification (Delaere *et al,* 1992; Laurenson, 1964, 1965; Uhthoff, 1990). During this process cartilage tissue is laid down at the epiphyses and is subsequently ossified (see 5.3.1). Epiphyseal growth mainly occurs at the iliac crest and iliac body (*os acetabuli* and *os marginalis*) (Figure 6.1). An ossification front probably forms between the primary ossification centre and the epiphyseal growth plates. This is consistent with the finding that early in development the anterior and posterior AOI, which are more closely situated to the primary ossification centre, contain more bone per unit area than the superior AOI. It seems as though the chondrification front is still evident at term. At term bone density did not vary significantly across the measured AOI but there does appear to

be a bone density gradient stretching from the primary ossification centre (AOI C) to the epiphyseal growth plates (AOI B, P, A and A) (See Figure 6.1). Bone density tends to decrease from AOI C→B, C→CA→A, C→CS→S and C→CP→P (Figure 6.1). Similarly, the fetal femur also shows a gradient of bone density values decreasing from the proximal epiphyseal growth plate to the diaphysis (Salle *et al.*, 1992), which is the location of the primary ossification centre (Scheuer & Black, 2000). Thus it seems that fetal trabecular bone distribution may be a product of the ossification processes.

Part III. Internal Iliac Morphology

Chapter 7. Postnatal Growth and Development of Hominoid Iliac Trabecular Tissue

Tanck *et al.* (2001) investigated the growth and development of trabecular architecture in the tibiae (epiphyses and metaphyses) and vertebrae of non-adult *Sus scrofa* (pigs) aged between 6 and 230 weeks. Three-dimensional measurements of trabecular architecture, bone volume fraction and trabecular anisotropy, were collected. At six weeks of age bone volume fraction varied across the vertebrae, tibial epiphyses and tibial metaphyses (Figure 7.1a). Furthermore, trabecular tissue was anisotropic (Figure 7.1b). Thus an ordered trabecular structure appeared at an early stage of development. Bone volume fraction increased rapidly between 6 and 100 weeks (Figure 7.1a), trabecular anisotropy increased only slowly between 6 and 56 weeks, but then rapidly between 56-104 weeks before decreasing until 230 weeks (Figure 7.1b). Tanck and colleagues (2001) suggested that trabecular structure was related to mechanical loading. The rapid increase in bone volume fraction was explained as a response to the rapidly increasing body mass of *S. scrofa*.

Like *S. scrofa*, the body mass of hominoids also increases rapidly after birth. Furthermore, the ilium is subjected to increased loading when locomotor behaviour starts. *Homo sapiens* begin to display quadrupedal crawling at about 10 months and bipedal locomotion at around 12-14 months (Keen, 1993). In *P. troglodytes* and *G. gorilla* climbing and quadrupedal behaviours first occur between 3-6 months (Carlson 2005; Doran, 1992, 1997). Given that trabecular bone adapts to loading

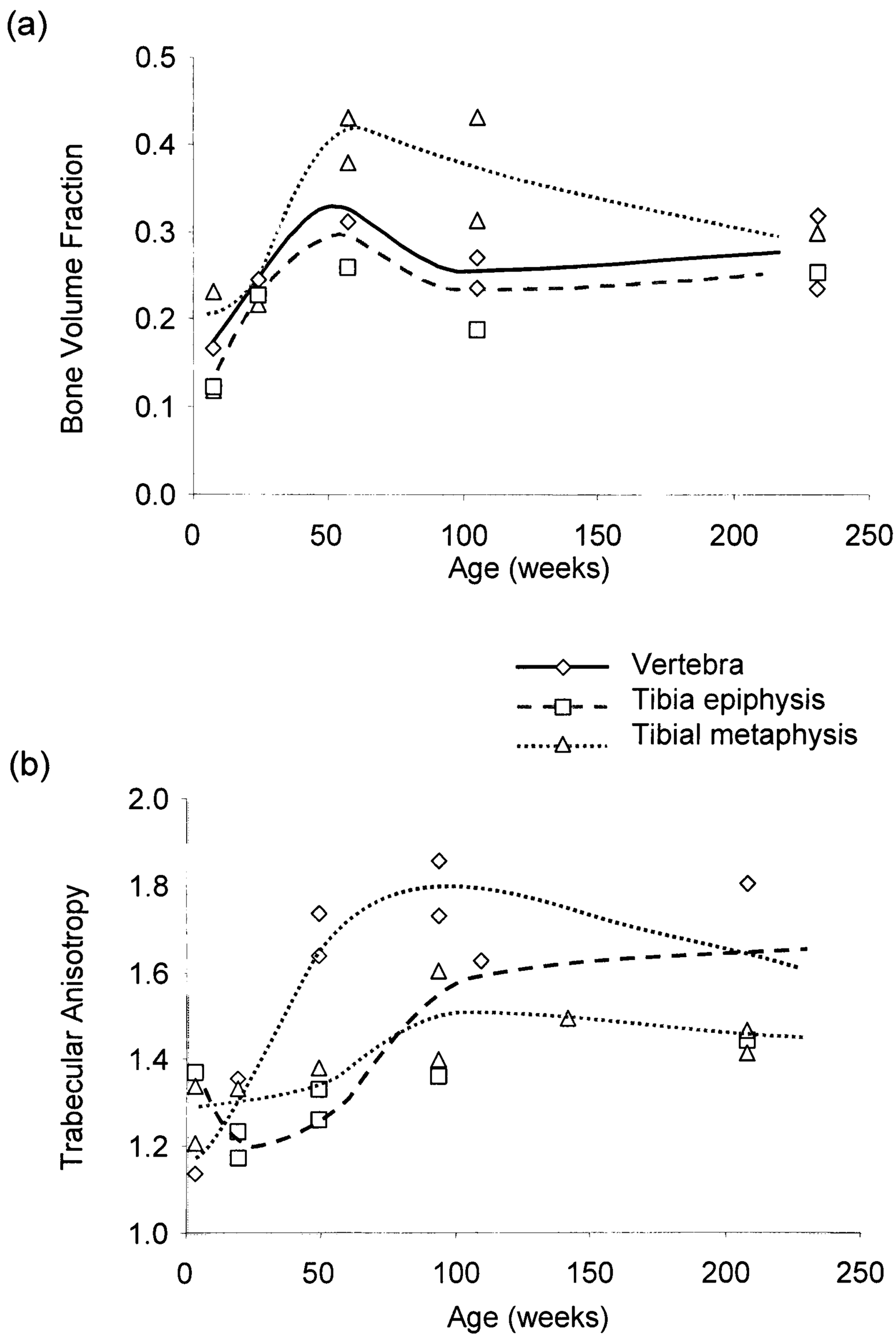

Figure 7.1. Early development of trabecular architecture in *Sus scrofa*. Ontogenetic change in (a) bone volume fraction (b) trabecular anisotropy. Modified from Tanck *et al.*, (2001).

conditions (Ehrlich & Lanyon, 2002; Turner 1998) it is reasonable to suggest that, like *S. scrofa*, hominoids will display ordered trabecular tissue from an early stage of postnatal development.

7.1 Aim

The aim of this chapter is to test the hypothesis that the hominoid ilium displays an ordered trabecular structure (i.e. uneven distribution of bone) from an early stage of postnatal development. The distribution of bone was assessed on both a macroscopic scale (bone density distribution) and microscopic scale (trabecular orientation).

7.2 Materials and methods

Measurements of internal pelvic morphology were collected from the modern human material and a subset of the African ape material described in chapters 3 and 4 (see section 3.3.1). In total 73 *H. sapiens*, 20 *P. t. troglodytes* and 19 *G. g. gorilla* specimens spanning the entire range of age and iliac size were measured and analysed (see table 7.1). The postnatal modern human sample was obtained from various sources which were preserved in different ways and Egyptian populations buried in sand and British populations buried in earth. African ape specimens were wild shot and stored in acid free paper boxes in a cool dry environment. Ontogenetic series were defined according to permanent molar eruption. Specimens from each species were classified into four categories depending on whether none (M0) or all first (M1)/second (M2)/third (M3) permanent molars had erupted (Table 7.1) see section 3.3.2. Specimens were also divided into four iliac centroid size classes (Table 7.2). The iliac centroid size classes were not equivalent across species (Table 7.2). Centroid size was calculated using the landmarks in Table 3.2.

7.2.1 Conventional radiography

As high resolution μCT scanning is very time consuming, and limited to specimens less than140mm in diameter, postnatal ilia were radiographed. Specimens were orientated in a plane defined by the anterior superior iliac spine, the posterior superior iliac spine and the ilio-pubic eminence. Radiographs were taken at a source film distance of 1.2m, with the axis of the beam centred midway between the iliac spines. Tube voltage varied from 40k to 60kVp. An Acoma DFX-50 (Tokyo Japan) and a MedCon VG. Philips Super 80D CP (Philips Medical Systems, Massachusetts, USA) were used to radiograph specimens. AGFA Structurix film was used for Acoma DFX-50. The Philips Super 80D produced digital images so no film was required. Radiographs were photographed using a Nikon Coolpix 990 camera (Tokyo, Japan). Images were converted to 4095 grey levels using the programme ImageJ (http://rsb.info.nih.gov/ij/).

Species	Sample Number for Molar Eruption Classes				Total
	M0	M1	M2	M3	
H. sapiens	13	17	7	36	73
P. t. troglodytes	5	5	5	5	20
G. g. gorilla	5	4	5	5	19

Table 7.1. Sample size of postnatal specimens measured in this chapter. The specimens are sorted according to permanent molar eruption. M0, no molars erupted; M1, all first permanent molars erupted; M2, all second molars erupted; M3, all third molars erupted.

Species	Sample Number for Iliac Size Classes				Total
H. sapiens	**125-174 mm**	**175-224 mm**	**225-259 mm**	**260-320 mm**	
	18	18	18	19	73
P. t. troglodytes	**100-169 mm**	**170-229 mm**	**230-299 mm**	**300-330 mm**	
	5	5	5	5	20
G. g. gorilla	**100-189 mm**	**190-279 mm**	**280-369 mm**	**370-460 mm**	
	5	4	5	5	19

Table 7.2. Sample size of postnatal specimens measured in this chapter. The specimens are sorted according to iliac centroid size (mm) see Figure 1.5. page 19.

7.2.2 Measurements of trabecular structure

Measurements of bone density and trabecular anisotropy were collected from radiographic areas of interest (AOI). Measurements were collected in the same manner as in the previous chapter (see sections 6.3.2.3 and 6.3.2.4). Measurements of trabecular structure were collected from an anterior, superior and posterior AOI of the iliac blade (Figure 6.1). Measures of trabecular anisotropy were gathered from Fast Fourier Transformed AOI. Binary thresholded images were used to obtain measures of bone density (bone area fraction). Specimens were thresholded following the procedure used for prenatal specimens (see section 6.3.4). The modern human material was obtained from populations preserved in different manners. Hence diagenetic processes and, therefore, mineralisation probably varied across (and within) specimens. If thresholding led to an over- or under-estimation of bone area fraction the error may be inconsistent across specimens. In contrast, the African ape specimens were all obtained and preserved in the same manner. Thus the effects of preservation on mineralisation should be comparable across specimens.

7.2.3 Reproducibility of architectural measures

The measurement procedure was selected to try and make measures of structure internally consistent. Thus the reproducibility of measurements was quantified. For this purpose ten specimens that represented the full range of size were selected from every species. Measures of bone density and trabecular anisotropy were repeatedly collected. Five measures were collected in a random order on five different days. The percentage error of bone density and trabecular anisotropy measures did not exceed 5% (Table 7.3), hence the measures were deemed to be sufficiently precise for analysis.

7.2.4 Statistical analysis of ontogenetic change in bone distribution

Ontogenetic change in iliac trabecular architecture was assessed by analysing ontogenetic change in structural parameters across developmental and growth classes. Ontogenetic series were divided according to permanent molar eruption and iliac centroid size. The classes and the number of specimens in each are given in Tables 7.1 and 7.2. Mean values of structural parameters were compared across developmental classes using one-way ANOVA with Tukey's post hoc test. Associations between structural parameters and developmental stage were assessed using the χ^2 test. Correlations between measured parameters, age, permanent molar eruption and iliac centroid size were assessed using Spearman's Rho test.

Architectural Measurement		**Percentage Error (%)**		
Variable	Area	*H. sapiens*	*P. t. troglodytes*	*G. g. gorilla*
Bone Area Fraction	A	4.8	3.2	4.4
	S	4.7	3.8	3.7
	P	4.3	3.4	4.8
Trabecular Anisotropy	A	4.6	4.6	4.3
	S	4.8	4.1	4.9
	P	4.7	4.2	4.8

Table 7.3. Estimates of repeatability for measures of trabecular tissue material properties in postnatal hominoids. Measured areas of interest are labelled as P, posterior; S, superior and A, anterior.

7.3 Results

7.3.1 Iliac bone density distribution

In the youngest developmental class (no erupted permanent molars) bone density is higher in the anterior and posterior AOI than in the superior one (Figure 7.2). Bone density values were compared across AOI using a one-way ANOVA with Tukey's post hoc. The ANOVA revealed that in all three hominoid species the anterior and posterior AOI has a higher bone density in the superior section: *H. sapiens* F =

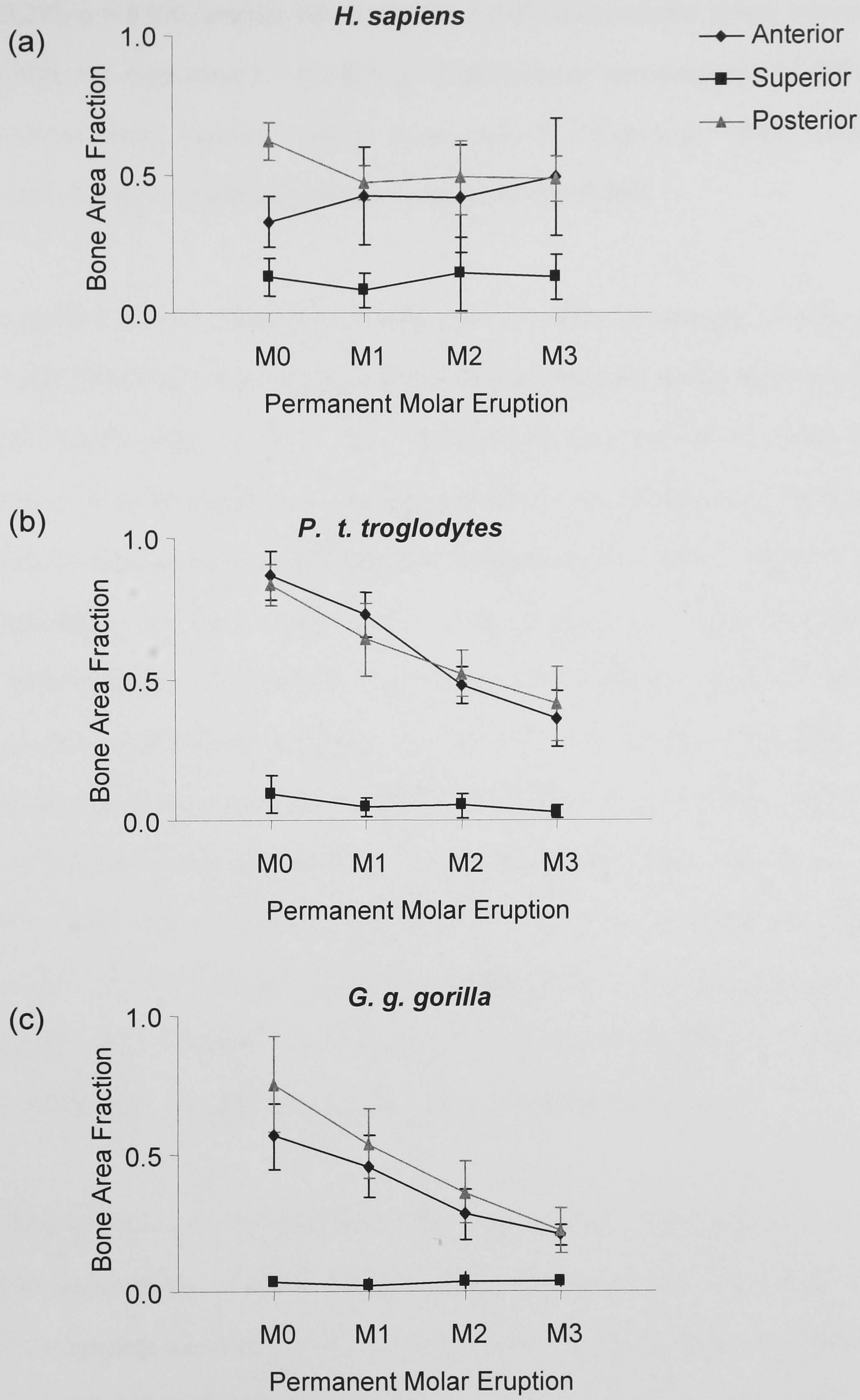

Figure 7.2. Ontogenetic change in hominoid iliac bone density. (a) *H. sapiens* (b) *P. t. troglodytes* (c) *G. g. gorilla*. Developmental stages defined according to permanent molar eruption; M0, no molars erupted; M1, first permanent molars erupted; M2, second molars erupted; M3, third molars erupted. Error bars denote standard deviation of mean.

83.271, p = 0.000 (anterior versus superior = 0.000 and posterior versus superior = 0.000); *P. t. troglodytes* F = 122.823, p = 0.000 (anterior versus superior = 0.000 and posterior versus superior = 0.000); *G. g. gorilla* F = 55.616, p = 0.000 (anterior versus superior = 0.000 and posterior versus superior = 0.000).

In modern humans, mean bone density does not differ across molar or iliac size classes (ANOVA, Table 7.4). Bone density is associated with molar eruption but not iliac growth stage (χ^2, Table 7.4). Bone density is positively correlated with permanent molar eruption but not iliac centroid size (Spearman's Rho, Table 7.4). Anterior bone density remains constant during postnatal ontogeny. Superiorly and posteriorly mean bone density does not differ across dental or iliac size classes (ANOVA, Table 7.4). Superiorly, bone density is not associated with molar eruption and iliac size class stage (χ^2, Table 7.4). Posteriorly bone density is associated with molar eruption and growth stage (χ^2, Table 7.4).Superiorly bone density is negatively correlated with molar eruption but not correlated with iliac centroid size (Spearman's Rho, Table 7.4). Posteriorly, bone density is negatively correlated with molar eruption and iliac centroid size (Spearman's Rho, Table 7.4). In summary, modern humans show a decrease in bone density in the posterior portion of the iliac blade but anteriorly and superiorly bone density remains constant (Figure 7.2).

Anteriorly and posteriorly smaller (younger) African apes have higher bone density than larger (older) individuals (ANOVA, table 7.4). Bone density is associated with molar eruption and iliac growth stage (χ^2, Table 7.4). Bone density is negatively correlated with molar eruption and iliac growth stage (Spearman's Rho, Table 7.4). Superiorly, smaller (younger) *P. t. troglodytes* have higher bone density than larger

Species	Area	Growth Stage	$\chi 2$ ρ	Spearman's Rho ρ	+/-	ANOVA F	ρ	Post Hoc	Consensus Result
H. sapiens	A	Molar	**	**	+	2.496	NS	M0 < M3	Increased
		Size	NS	NS		2.577	NS		
	S	Molar	NS	**	-	1.888	NS		Constant
		Size	NS	NS		0.290	NS		
	P	Molar	**	**	-	1.764	NS		Constant
		Size	*	*	-	1.162	NS		
P. t. troglodytes	A	Molar	**	**	-	39.630	***	M0 > M2 , M3	Decreased
		Size	*	**	-	10.539	***	1 > 3 , 4	
	S	Molar	*	*	-	1.860	NS		Decreased
		Size	*	NS		4.228	*	1 > 4	
	P	Molar	**	**	-	14.718	***	M0 > M2 , M3	Decreased
		Size	*	**	-	4.761	*	1 > 4	
G. g. gorilla	A	Molar	**	**	-	19.371	***	M0 > M2 , M3	Decreased
		Size	*	**	-	16.376	***	1 , 3 > 4	
	S	Molar	NS	*	-	0.343	NS		Decreased
		Size	*	**	-	0.139	NS		
	P	Molar	**	**	-	15.685	***	M0 > M2 , M3	Decreased
		Size	*	**	-	11.033	***	1 > 3 , 4	

Table 7.4. Statistical analysis of ontogenetic change in hominoid iliac bone density. Symbols are NS = Non-significant, * = $p<0.050$, ** = $p< 0.010$, *** = $p<0.001$, + = positive correlation, - = negative correlation. Consensus column indicates whether analyses suggest an ontogenetic increase, decrease or constancy for bone density.

(older) individuals (ANOVA, table 7.4). Bone density is associated with molar eruption and iliac growth stage (χ^2, Table 7.4). Bone density is negatively correlated with molar eruption but is not correlated with iliac growth stage (Spearman's Rho, Table 7.4). In *G. gorilla* superior bone density does not vary across molar eruption and growth classes (ANOVA, table 7.4). Bone density is associated with iliac growth stage but not permanent molar eruption (χ^2, Table 7.4). Bone density is negatively correlated with molar eruption and iliac centroid size (Spearman's Rho, Table 7.4). Together these results suggest that in the African apes' iliac bone density decreases during postnatal development (Figure 7.2).

7.3.2 Iliac trabecular anisotropy

In all four molar eruption classes hominoid trabecular tissue is anisotropic (Figure 7.3). The youngest molar eruption classes show values of ~0.70, 0.55 and 0.50 for *H. sapiens*, *P. t. troglodytes* and *G. g. gorilla* respectively (Figure 7.3). The amount of bone distributed along the main axis of orientation is approximately 1.5 to 2 fold higher than the perpendicular orientation.

In *H. sapiens* trabecular anisotropy is associated with molar and size class in all three AOIs (χ^2, Table 7.5). Trabecular anisotropy is negatively correlated with molar eruption and iliac centroid size in all three AOI (Spearman's Rho, Table 7.5). Furthermore, younger/smaller individuals possess a less anisotropic structure than older/larger specimens in all three of the measured AOI (ANOVA, Table 7.5). Together these results indicate that trabeculae become more anisotropic during ontogeny in all three measured AOI (Figure 7.3).

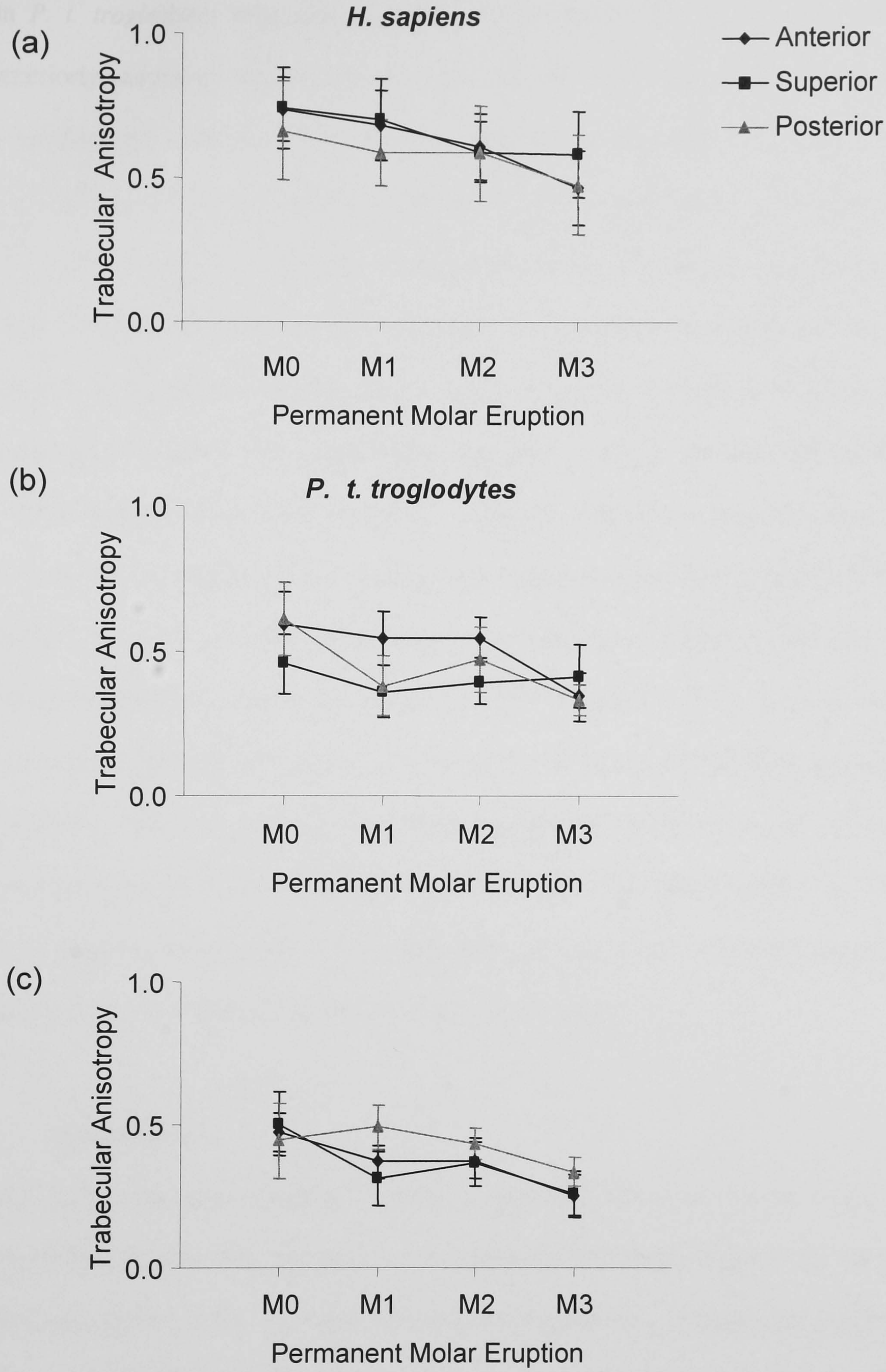

Figure 7.3. Ontogenetic change in hominoid iliac trabecular anisotropy. (a) *H. sapiens* (b) *P. t. troglodytes* (c) *G. g. gorilla*. Developmental stages defined according to permanent molar eruption; M0, no molars erupted; M1, first permanent molars erupted; M2, second molars erupted; M3, third molars erupted. Error bars denote standard deviation of mean.

In *P. t. troglodytes* trabecular anisotropy is associated with molar eruption class anteriorly and posteriorly but not superiorly. Also trabecular anisotropy is associated with iliac size class posteriorly but not anteriorly or superiorly. In *G. g. gorilla* trabecular anisotropy is associated with molar and iliac size class for all three AOI (χ^2, Table 7.5). In *P. t. troglodytes* trabecular anisotropy is negatively correlated with molar eruption and iliac centroid size class in the anterior and posterior but not superior AOI (Spearman's Rho, Table 7.5). In *G. g. gorilla* trabecular anisotropy is negatively correlated with molar eruption and iliac centroid size class for all three AOI (Spearman's Rho, Table 7.5). In *P. t. troglodytes* the mean trabecular anisotropy of anterior and posterior AOI is highest in the younger/smaller specimens (ANOVA, Table 7.5). In the superior AOI mean values of trabecular anisotropy did not vary significantly across molar or size classes (ANOVA, Table 7.5). In *G. g. gorilla* mean trabecular anisotropy of anterior AOI is highest in the younger/smaller specimens (ANOVA Table 7.5). In the posterior and superior AOI mean values of trabecular arrangement did not vary significantly across molar or size classes (ANOVA, Table 7.5). Together these results indicate that trabecular tissue becomes more anisotropic during the postnatal development of African apes (Figure 7.3).

7.4 Discussion

Prior to M1 eruption hominoids develop an uneven distribution of bone across the iliac blade (Figure 7.2). The anterior and posterior AOI show higher bone density than the superior AOIs. The hominoids also develop anisotropic trabecular alignment prior to M1 eruption (Figure 7.3). Hence the hypothesis that hominoid ilia show ordered trabecular structure from an early age seems to be confirmed.

Species	Area	Growth Stage	χ2 ρ	Spearman's Rho ρ	+/-	ANOVA F	ρ	Post Hoc	Consensus Result
H. sapiens	A	Molar	**	**	-	21.606	***	M0 > M3	Decreased
		Size	**	**	-	16.805	***	1 > 3 , 4	
	S	Molar	**	**	-	5.847	**	M0 > M3	Decreased
		Size	**	**	-	8.457	***	1 > 3 , 4	
	P	Molar	NS	**	-	5.214	*	M0 > M3	Decreased
		Size	*	**	-	4.886	*	1 > 3 , 4	
P. t. troglodytes	A	Molar	*	**	-	5.949	**	M0 > M3	Decreased
		Size	NS	**	-	3.626	*	1 > 4	
	S	Molar	NS	NS		0.727	NS		Constant
		Size	NS	NS		0.176	NS		
	P	Molar	*	**	-	4.285	*	M0 > M1	Decreased
		Size	*	*	-	1.111	NS		
G. g. gorilla	A	Molar	**	**	-	15.265	***	M0 > M3	Decreased
		Size	*	**	-	3.917	*	1 > 4	
	S	Molar	*	**	-	2.631	NS		Decreased
		Size	*	*	-	1.639	NS		
	P	Molar	*	**	-	0.265	NS		Decreased
		Size	*	*	-	0.211	NS		

Table 7.5. Statistical analysis of ontogenetic change in hominoid iliac trabecular anisotropy. Symbols are NS = Non-significant, * = p<0.050, ** = p< 0.010, *** = p<0.001, + = positive correlation, - = negative correlation. Consensus column indicates whether analyses suggest an ontogenetic increase, decrease or constancy for bone density.

In modern humans bone is evenly distributed across the ilium at term (see chapter 6). Therefore, the postnatal pattern of uneven bone distribution must have been produced by the relative decrease (selective loss) of bone from the superior AOI's, with respect to the anterior and posterior AOI. The same pattern of selective loss may have occurred in the African ape ilia. The structure of hominoid iliac trabecular tissue continues to change during postnatal development. Trabecular tissue becomes more anisotropic (Figure 7.3) whilst total bone density decreases (Figure 7.2). *Pan t. troglodytes* show a decrease in bone density in all three AOIs. *Gorilla. g. gorilla* show a decrease in bone density in the anterior and posterior AOIs, but no change superiorly. *Homo sapiens* only show a decrease in bone density in the posterior AOI, but the anterior and superior AOI show no change. These findings suggest that postnatally a relative loss, as opposed to gain, of trabecular bone leads to the formation of adult hominoid iliac morphology.

Early in hominoid development the selective loss of bone from the superior (middle) portion of the hominoid iliac blade with respect to the anterior and posterior portions leads to the formation of two trabecular struts, one anterior and one posterior. This is exemplified in an ontogenetic series of modern human radiographs published by Macchiarelli *et al.* (2001) (see Figure 7.4). Correnti (1955) and Macchiarelli *et al.*, (1999) have previously referred to these struts as the ilio-ischial and sacro-pubic bundles, respectively. Importantly, despite subsequent changes in bone density distribution the trabecular struts are maintained throughout postnatal ontogeny. If postnatal development of hominoid iliac trabecular architecture is adaptive, the structure and position of the struts should be explainable with regard to iliac function.

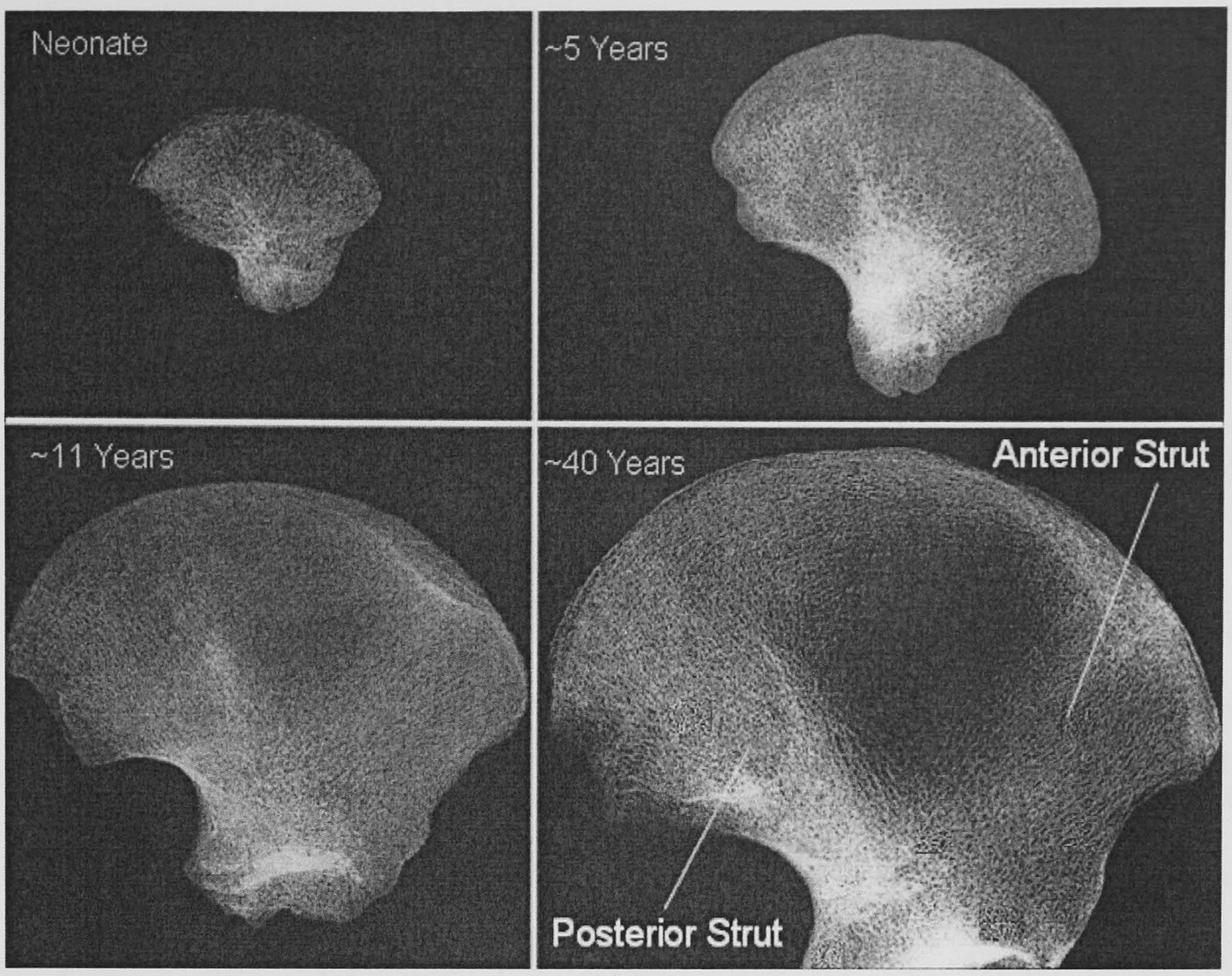

Figure 7.4. Ontogenetic change in trabecular bone distribution in modern human ilia. The fan shaped arrangement of trabeculae displayed at term is reduced to two prominent trabecular struts. Adapted from Macchiarelli *et al.*, (2001).

Part IV. The Relationship Between Internal and External Iliac Morphology

8.1 Trabecular orientation: elements and bundles

In the 19th century several scientists attempted to relate gross trabecular morphology to its mechanical, load-bearing function. Von Meyer (1867) noted the similarity between trabecular architecture and stress trajectories in the proximal femur of modern humans (Pontzer *et al.,* 2006). This led Wilhelm Roux (1881) to introduce the notion that bone was a self organising tissue, which displays evidence of functional adaptation (Martin *et al.,* 1998). This notion was further elaborated by Wolff (1892, 1896), who described three concepts of bone growth and development (Martin *et al.,* 1998): (1) bone is deposited and resorbed to achieve an optimum balance between strength and weight; (2) trabeculae in cancellous bone tend to line up with the directions of principal stresses that they experience ("Wolff's trajectorial hypothesis") and (3) both phenomena occur through self-regulating mechanisms that respond to mechanical forces acting upon bone tissues. The points are often referred to collectively as "Wolff's law of bone remodelling" (Martin *et al.,* 1998). In essence, Wolff proposed that trabecular bone will form during growth and development along orientations that correspond to principal mechanical stresses acting on the bone (Wolff, 1896; Martin *et al.,* 1998). Frost (1990b) suggested that trabeculae could re-orientate to meet applied loading directions by resorption and deposition of bone on opposite surfaces (Figure 8.1). However, reorientation of trabecular tissue has never conclusively been found to occur after a redirection of loads (Bertram & Biewener, 1991; Ruimerman *et al.,* 2005), except in pathological conditions such as osteoarthritis (e.g. Ding *et al.,* 2003; Kamibayash *et al.,* 1995). In

the absence of experimental evidence, computer simulations have been used to test whether trabeculae re-orientate to meet alternate loading directions (e.g. Ruimerman *et al.,* 2005). Ruimerman and colleagues simulated a cube of trabecular bone and applied alternate loading directions. The trabeculae realigned to new loading direction after 12 simulated years. Ruimerman *et al.* (2005) concluded that no evidence of trabecular re-orientation had been reported, because no animal experiments had continued for this long.

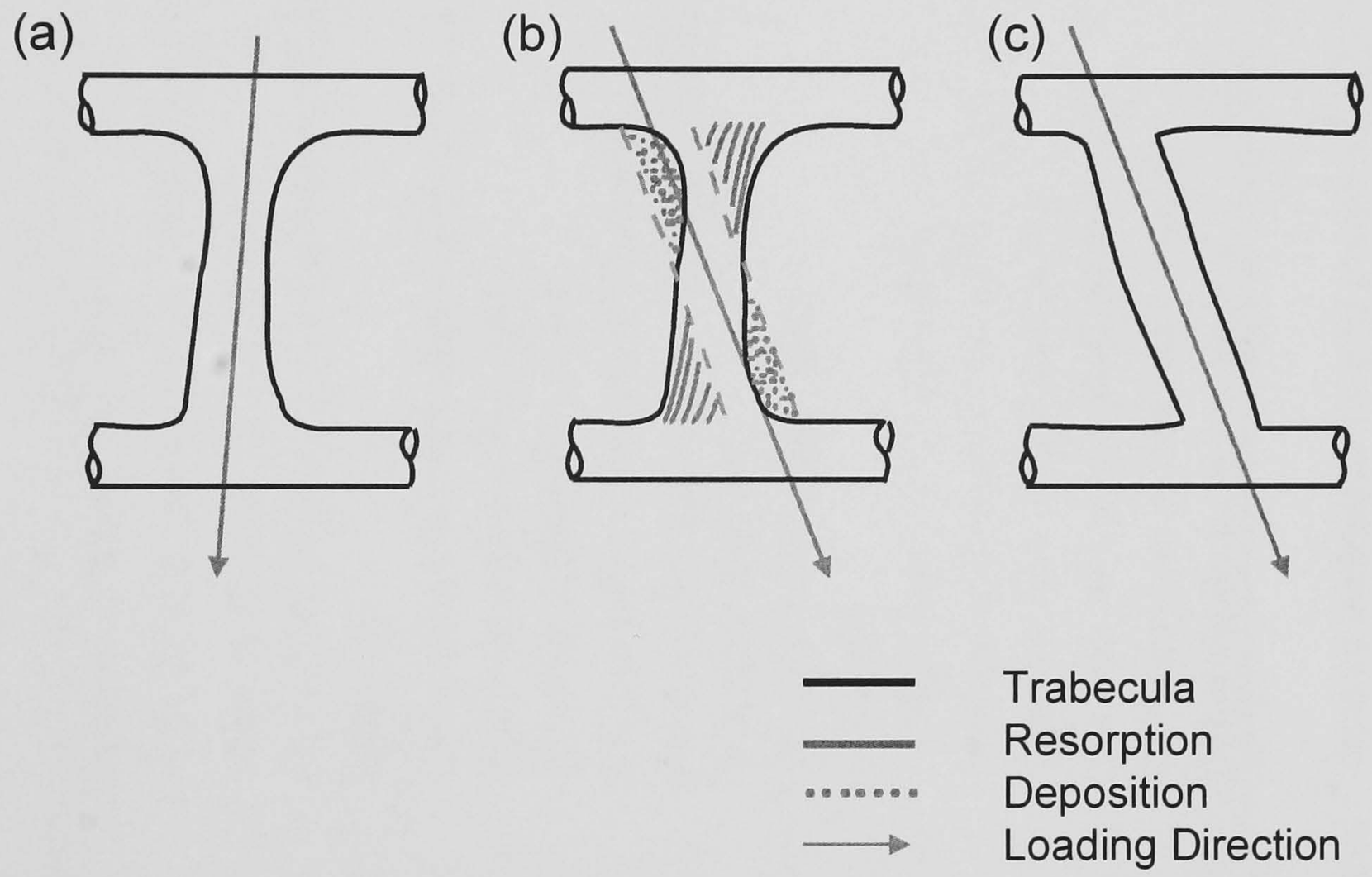

Figure 8.1. Frost (1990) hypothesised that trabecular elements can re-orientate by modelling in response to alternating loading directions. (a) Loaded trabecula (b) Alternate loading direction causes trabecula to re-orientate via modelling (c) Trabecula aligned to new loading direction. Modified from Frost (1990b).

Ontogenetic changes in orientation at the trabecular level may lead to larger scale changes in cancellous morphology which can be studied at the macroscopic level. Trabecular elements form bundles (see Correnti, 1955; Macchiarelli *et al.,* 1999). Hominoid ilia possess two main trabecular bundles or struts, one anterior and one posterior. If trabeculae re-orientate in response to alternate loading direction the struts might do as well. Thus, ontogenetic re-orientation of iliac bundles, if any, may

No.	Landmark Name	Description	Landmark Type
L1	Anterior Superior Iliac Spine	Anterior Superior Iliac Spine	I
L2	Anterior Iliac Crest [M]	Point at widest section of anterior iliac crest	II
L4	Iliac Tubercle [M]	Point along iliac crest opposite L5	III
L6	Iliac Crest [M]	Point along iliac crest where anterior and posterior musculature meets	I
L8	Spina Limitans [M]	Point along iliac crest where arcuate line meets iliac crest	I
L12	Posterior Superior Iliac Spine	Posterior Superior Iliac Spine	I
L14	Posterior Inferior Iliac Spine	Posterior Inferior Iliac Spine	I
L15	Greater Sciatic Notch	Deepest point of greater sciatic notch	II
L16	Dorsal Ilium	Point along ischial spine where the ilium and ischium meet	I
L17	Ilio-Pubic Eminence	Ilio-Pubic Eminence	I
L18	Anterior Inferior Iliac Spine	Anterior Inferior Iliac Spine	I
L23	Scalenion	Scalenion	II
L25		Anterior apex of auricular surface	I
L26		Anterior projection of auricular surface inferior to L27	II
L27	Superior Auricular Surface	Superior apex of auricular surface	I
L29	Posterior Auricular Surface	Posterior indent of capsular attachment	I
L30	Posterior Apex of Auricular Surface	Posterior Apex of Auricular Surface	I
L31	Posterio-Inferior Apex of Auricular Surface	Posterio-Inferior Apex of Auricular Surface	I

Figure 8.1. Digitised external cortical landmarks. [M] denotes landmarks form th medial aspect of the ilium.

be associated with a change in the loading direction. The ilium functions as part of an organism and not in isolation. Therefore, when inferring functional loading, the ilium (and pelvis) cannot be studied as an isolated entity, but rather as part of a system of bone and muscle. The ilium transmits loads between the sacrum and the proximal femur and possible changes in loading conditions and muscle attachments throughout ontogeny have already been highlighted (Chapters 3 and 4).

8.2 Aim

The aim of this chapter was to test the null hypothesis that iliac trabecular struts retain their position relative to external morphology throughout development.

8.3 Materials and methods

The sample used in this chapter is described in Table 7.1. Specimens representing *H. sapiens, P. t. troglodytes* and *G. g. gorilla* were classified according to permanent molar eruption: M0, no permanent molars erupted; M1, all first permanent molars erupted; M2, all second molars erupted, M3, all third molars erupted (see section 3.3.2). The four molar eruption classes were used to define an ontogenetic series for each species.

8.3.1 External and internal landmark data

In order to make a fair comparison of strut orientation across specimens of different age and size classes it was necessary to record strut orientation with respect to the cortical shell. A landmark based method was used to characterise the position of trabecular struts in relation to external morphology. Specimens were radiographed following the protocol outlined in section 7.2.1. Five trabecular landmarks

representing the posterior and anterior trabecular struts (Figure 8.2) and six external landmarks (L1, L8, L12, L14, L18 and L29 in Table 8.1) were taken from the radiographs. The cortical landmarks listed in Table 8.1 were digitised directly from bones. The cortical and radiographic data sets were combined in a two step process. Firstly, three dimensional external data were projected into the two-dimensional radiographic plane, defined by the anterior superior iliac spine, posterior superior iliac spine and the posterior apex of the auricular surface. Secondly, these three landmarks were used to position the external and radiographic data sets at contiguous points in space.

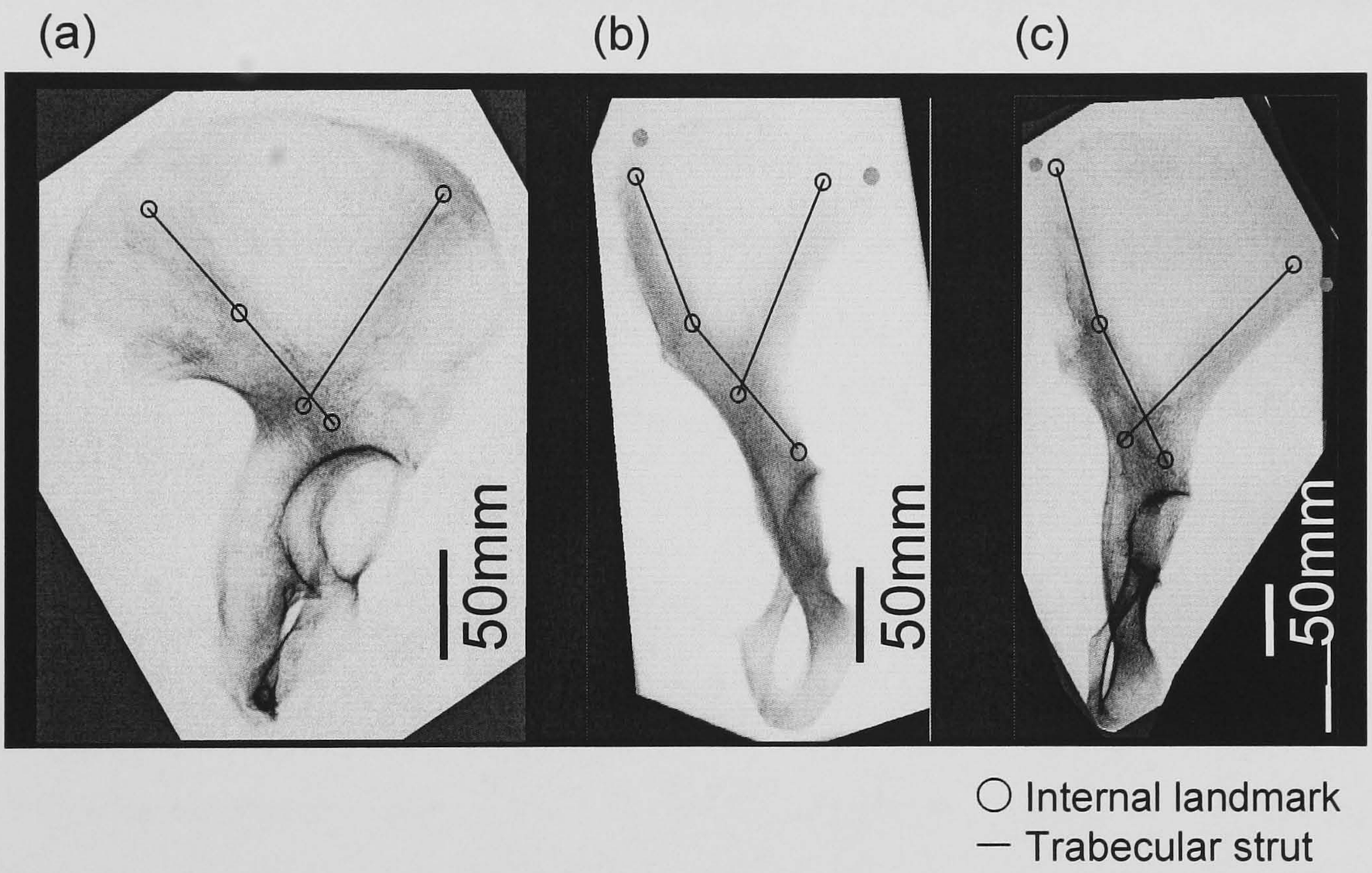

Figure 8.2. Digitised internal (trabecular) landmarks. Pelvic radiographs (a) *H. sapiens*. (b) *P. t. troglodytes and* (c) *G. g. gorilla.*

8.3.2 Measurement error analysis

Radiographic co-ordinate data was digitised twice from 10 *H. sapiens*, *G. g. gorilla* and *P. t. troglodytes* specimens. The ilia represented the full size range and were digitised in a random order. For each species repeat landmark co-ordinates were

compared using the paired Hotelling's T^2 test. Prior to analysis data was shown to be normally distributed using Mardia's multivariate normality test (Mardia, 1970) and covariance matrices were shown to be equivalent using Box's M test (see Table 8.2). No significant differences were found between repeat measures in either *H. sapiens*, *P. t. troglodytes* or *G. g. gorilla* (see Table 8.2). Hence, radiographic landmarks were deemed to be repeatable. It is worth noting that the use of Hotelling's T^2 statistic is conservative, because multivariate analyses are very powerful techniques for finding significant differences between samples.

Species	**Mardias test for normailty *p***		**Box's M *p***	**Paired Hotelling's T^2 *p***
	Skewness	Kurtosis		
H. sapiens	0.072	0.208	0.123	0.634
P. t. troglodytes	0.325	0.481	0.202	0.512
G. g. gorilla	0.388	0.156	0.308	0.758

Table 8.2. Repeat measures of radiographic coordinate data were compared to test repeatability. Ten specimens from each of three hominoid species were measured twice. Data sets were tested for multivariate normality and equality of covariance matrices before data sets were compared using the paired Hotelling's T2 test.

Another test was carried out to make sure that the external and internal data sets had been combined correctly. External landmark from the cortical and radiographic data sets were compared to ensure that there was no significant difference in co-ordinates. Three landmarks, that were digitised in both data sets, were used to accomplish this (L8, L14 and L18 in Table 8.1). If the external and radiographic samples had been combined correctly, then a paired Hotelling's T^2 test would not find any significant difference between co-ordinates in the two data sets. Prior to analysis data were shown to be normally distributed and covariance matrices were shown to be equivalent (see Table 8.3). After combining external and radiographic landmarks no

significant differences were found between bone and radiograph derived co-ordinates for either *H. sapiens*, *P. t. troglodytes* or *G. g. gorilla* (see Table 8.3).

Species	Mardias test for normailty *p*		Box's M *p*	Paired Hotelling's T^2 *p*
	Skewness	Kurtosis		
H. sapiens	0.057	0.085	0.050	0.221
P. t. troglodytes	0.056	0.481	0.202	0.101
G. g. gorilla	0.063	0.068	0.096	0.099

Table 8.3. Measurement error test for meshing of radiographic and bony landmarks. External (and internal) landmarks collected from radiographs were combined with external co-ordinates digitised directly form bones. Three landmarks collected in both data sets. The external and internal data sets were tested for multivariate normality and equality of covariance matrices before data they were compared using the paired Hotelling's T2 test.

8.3.3 Quantification of strut orientation (relative to external morphology)

Strut orientation was measured in relation to the position of external landmarks, in two-dimensions. This was accomplished by calculating angles where lines demarcating trabecular struts intersected lines connecting functionally important external landmarks (Figure 8.3). Four angles were recorded: A, orientation of the anterior strut with respect to the iliac crest (iliac tubercle, anterior superior iliac spine); B, orientation of the anterior strut with respect to the iliac body (lateral apex of acetabulum, anterior inferior iliac spine); C, orientation of the posterior strut with respect to the auricular surface (superior apex, posterior apex); D, orientation of the posterior strut with respect to the iliac body (Figure 8.3). The measured angles were compared across four permanent molar eruption classes using one-way ANOVA with Tukey's post hoc: M0, no permanent molar erupted; M1, all first permanent molars; M2, second molars; M3, all third molars erupted (see section 3.3.2).

8.3.4 Visualisation of strut position (relative to external morphology)

The thin plate spline technique was used to visualise size related (ontogenetic) changes in strut position relative to external morphology. The hominoid species were combined in a single PCA analysis based on registered landmark co-ordinate data augmented with log iliac centroid size. The TPS regression technique was used to produce splines which described changes in shape along the first PC of the PCA. Landmark co-ordinate data were regressed against PC scores separately for each species.

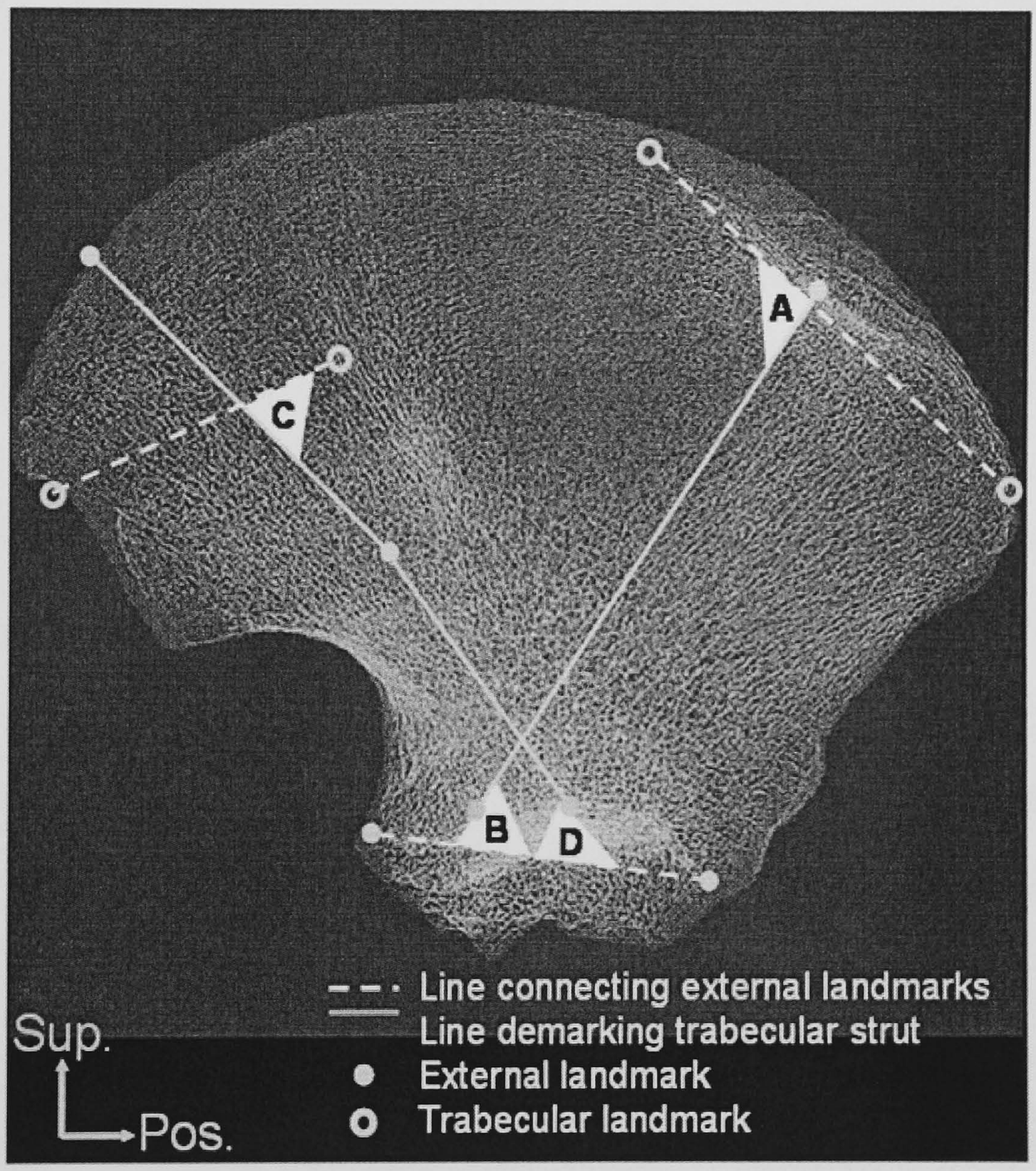

Figure 8.3. Measured angles of main trabecular bundle orientation. Open circles denote external landmarks and closed circles denote internal landmarks. Strut orientation was characterised in relation to external morphology by calculating angles where lines demarcating trabecular struts intersected lines connecting external landmarks. Triangles denote four measured angles of trabecular orientation, A, B, C and D. Radiograph form Macchiarelli *et al.* (2001).

8.4 Results

With respect to the anterior iliac border, larger *H. sapiens* ilia show a more posteriorly located anterior strut than younger individuals (Figure 8.4). The posterior strut shows an anterior rotation with increasing iliac size, in relation to external morphology (Figure 8.4). During the growth of *P. t. troglodytes* (Figure 8.5) and *G. g. gorilla* (Figure 8.6) the anterior iliac border flexes and the iliac body gets shorter infero-superiorly with respect to antero-posterior iliac width. As a result the anterior strut is located more anteriorly, in relation to the gluteal surface, in older specimens. In large African ape ilia, the posterior strut intersects the auricular surface more superiorly than in small specimens (Figure 8.5 and 8.6). In large *P. t. troglodytes* ilia the posterior strut meets the acetabulum more posteriorly than in small specimens, with respect to overall iliac morphology. In large *G. g. gorilla* ilia, the posterior strut meets the acetabulum more superiorly than in small specimens.

In all three hominoids angle A was comparable across molar eruption stages (Table 8.3 and Figure 8.7). However, angle B decreased during the development of *H. sapiens* and *G. g. gorilla* but increased in *P. t. troglodytes*. In *H. sapiens* and *G. g. gorilla*, angle B was significantly lower in the M2 and M3 stages in comparison to the M0 stage (Table 8.3 and Figure 8.7). In *P. t. troglodytes*, angle B was significantly higher in the M2 and M3 stages in comparison to the M0 stage (Table 8.3 and Figure 8.7). Angle C increased in *H. sapiens*, *P. t. troglodytes* and *G. g. gorilla*. In *P. t. troglodytes* and *G. g. gorilla*, angle C was significantly higher in the M2 and M3 stages in comparison to the M0 stage (Table 8.3 and Figure 8.7). In *H. sapiens*, angle C was significantly higher in the M3 stage in comparison to the M0 stage (Table 8.3 and Figure 8.7). Angle D decreased during ontogeny in *H. sapiens*

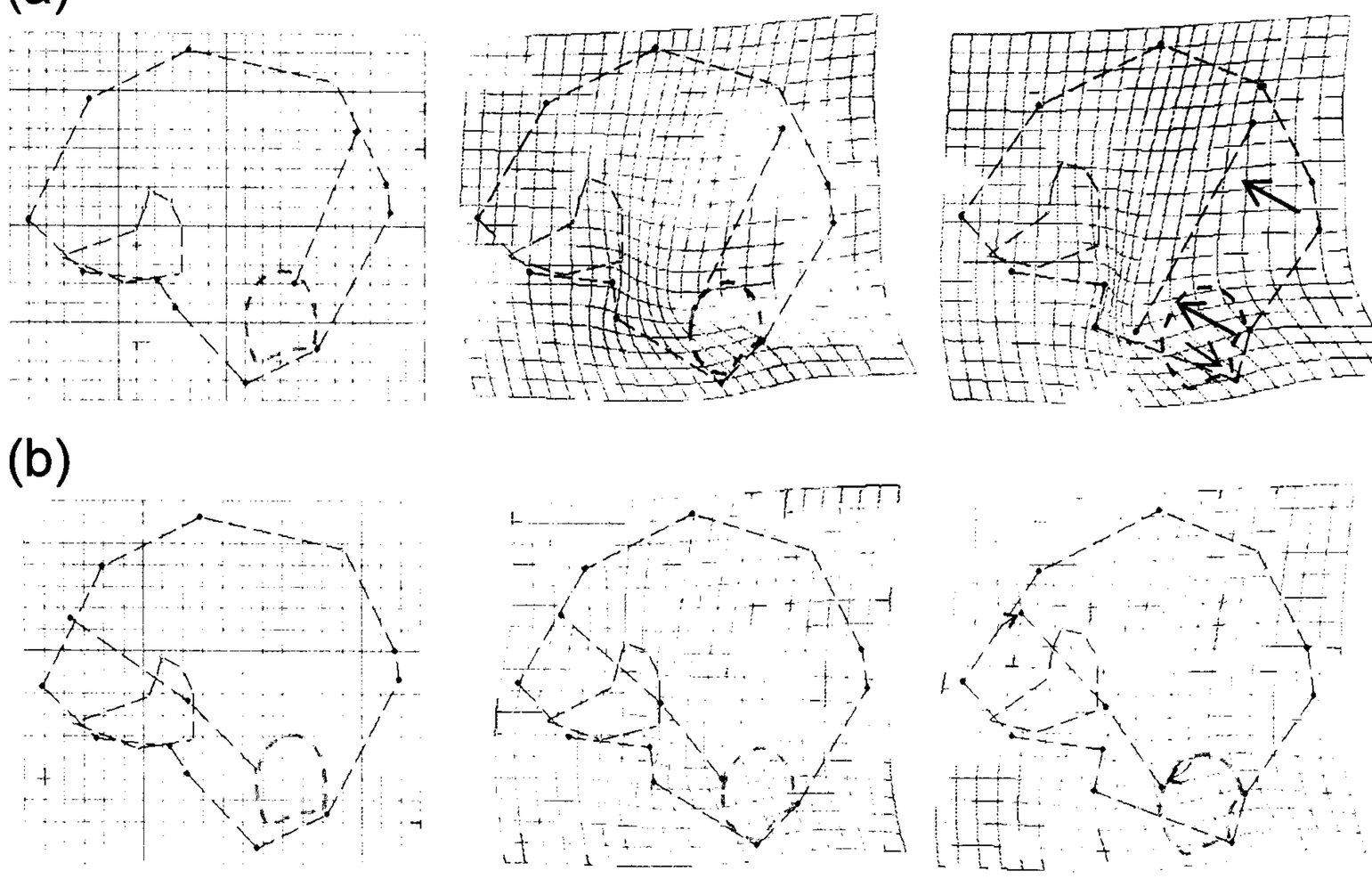

Figure 8.4. Allometric change in iliac trabecular strut orientation in relation to external morphology. *Homo sapiens* (a) anterior iliac strut and (b) posterior iliac strut. Landmarks were regressed against a measure of iliac size (second principal component of PCA analysis) using TPS regression technique. Deformations of the TPS mesh are based solely on primary landmarks but secondary landmarks are included to aid visualisation of iliac shape. Arrows indicate ontogenetic change in internal morphology relative to external. Black dashed line indicates the outline of the iliac blade and auricular surface. Grey dashed line indicates the outline acetabulum.

but increased in *P. t. troglodytes* and *G. g. gorilla*. In *G. g. gorilla*, angle D was significantly greater in M2 and M3 stages in comparison to M0 (Table 8.3 and Figure 8.7). In *P. t. troglodytes* angle D was significantly greater in M3 stage in comparison to M0 (Table 8.3 and Figure 8.7). In *H. sapiens* angle D was significantly lower in M3 stage in comparison to M0 (Table 8.3 and Figure 8.7).

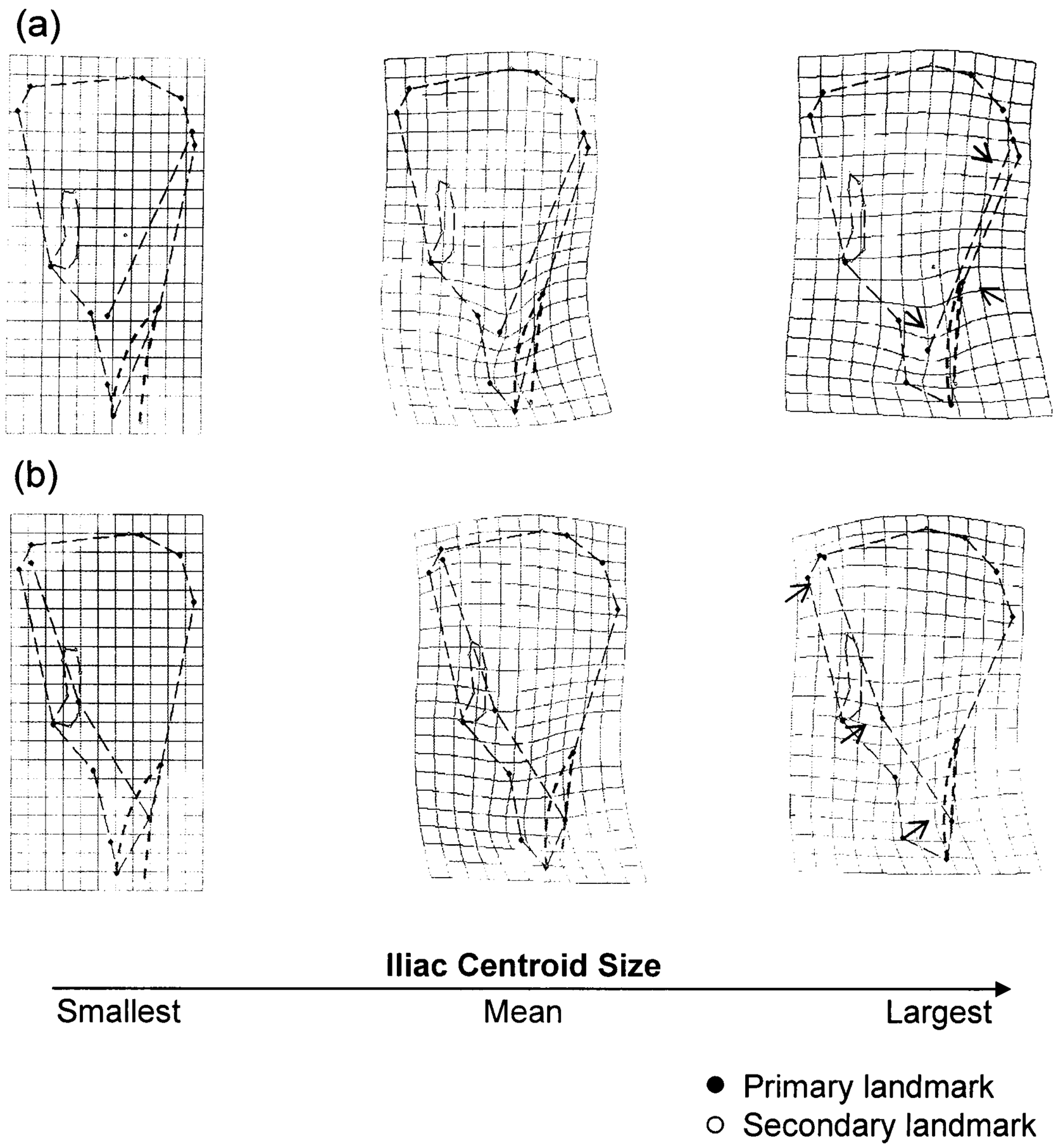

Figure 8.5. Allometric change in iliac trabecular strut orientation in relation to external morphology. *Pan. t. troglodytes* (a) anterior iliac strut and (b) posterior iliac strut. Landmarks were regressed against a measure of iliac size (second principal component of PCA analysis) using TPS regression technique. Deformations of the TPS mesh are based solely on primary landmarks but secondary landmarks are included to aid visualisation of iliac shape. Black dashed line indicates the outline of the iliac blade and auricular surface. Grey dashed line indicates the outline acetabulum.

8.5 Discussion

When assessing patterns of ontogenetic change in strut position with respect to external morphology, it is important to note the effects of superimposition. Projecting a three-dimensional shape into two-dimensions makes it difficult to asses the relative

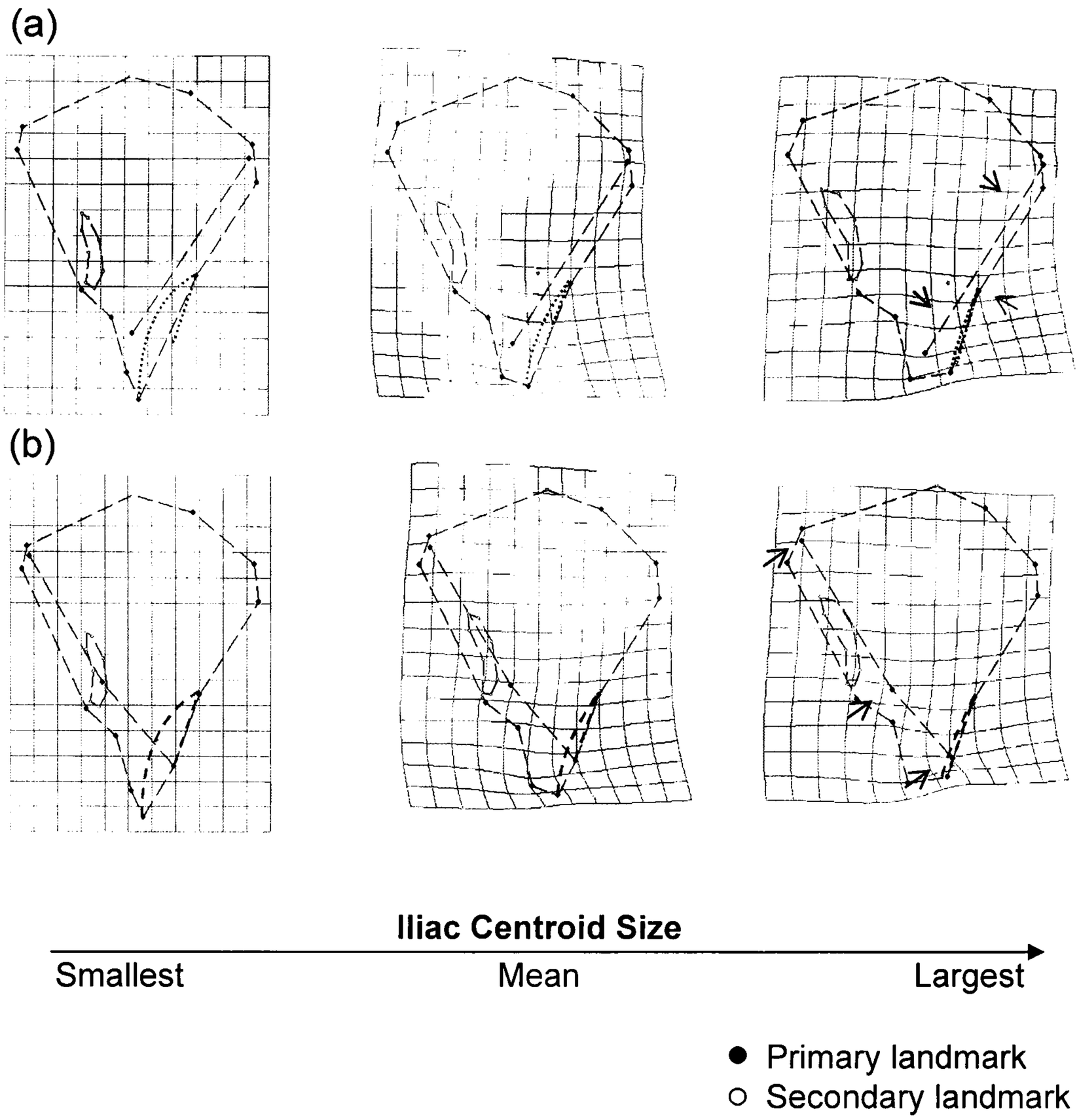

Figure 8.6. Allometric change in iliac trabecular strut orientation in relation to external morphology. *Gorilla g. gorilla* (a) anterior iliac strut and (b) posterior iliac strut. Landmarks were regressed against a measure of iliac size (second principal component of PCA analysis) using TPS regression technique. Deformations of the TPS mesh are based solely on primary landmarks but secondary landmarks are included to aid visualisation of iliac shape. Pointed arrows indicate ontogenetic change in internal morphology relative to external. Black dashed line indicates the outline of the iliac blade and auricular surface. Grey dashed line indicates the outline acetabulum.

positions of landmarks because the information in one plane is missing. Although the ilium is relatively flat some problems remain. From radiographs it is difficult to determine exactly where trabecular struts connect with the iliac cortical shell. For example, without information in the medio-lateral plane it is not possible to

determine whether the posterior strut connects with the auricular surface or the lateral cortex of the iliac blade.

The development of cortical and trabecular iliac morphology are assessed in *H. sapiens*, *P. t. troglodytes* and *G. g. gorilla* to determine whether they varied in relation to one another during ontogeny. The orientation of main trabecular struts is measured in relation to external morphology. This was accomplished by measuring angles of strut orientation where lines demarcating the bundles intersect lines connecting external landmarks (Figure 8.3). Mean measured angles are compared intra-specifically across four developmental stages, defined according to permanent molar eruption. In all three hominoids the angle between the anterior strut and the iliac body (angle B) changes significantly during ontogeny (Table 8.3 and Figure 8.7). Furthermore, the angle between the posterior strut and auricular surface (angle C) and the angle between the posterior strut and iliac body (angle D) also changes significantly (Table 8.3 and Figure 8.7). Thus the relationship between external and internal morphology appears to alter somewhat during ontogeny. Therefore, the null hypothesis that, during ontogeny, iliac trabecular struts do not re-orientate in relation to external morphology, is refuted and the alternative hypothesis is accepted. This needs some explanation.

During growth and development, trabecular tissue (Wolff, 1896; Frost, 1990b) and cortical bone (Frost, 1990b; Lieberman & Crompton, 1998) model in response to applied loads. Trabecular tissue maintains this ability throughout ontogeny (Frost, 1990b; Kobayashi *et al.*, 2003), but cortical tissue loses the ability to model after infancy (Frost, 1990b; Lieberman, 1996). Thus, trabecular tissue may be more plastic

than cortical bone. It is hypothesised that ontogenetic change in strut orientation, with respect to external landmarks, may be a response to alterations in the main direction of loading. In light of this the measured ontogenetic re-orientation of iliac trabecular struts, relative to external morphology, is interpreted with respect to presumed changes in loading direction. Ontogenetic changes in the main direction of loading are inferred from ontogenetic changes in (1) the size and position of iliac muscular insertions in relation to the ilium as a whole and (2) ontogenetic changes in locomotor and postural behaviour.

Species	**Angle**	***F***	***p***	**Post hoc versus M0 *p***		
				M1	M2	M3
H. sapiens	A	2.664	NS			
	B	48.005	0.000		0.036	0.000
	C	8.809	0.000			0.000
	D	4.346	0.007			0.039
P. t. troglodytes	A	1.132	NS			
	B	5.948	0.066		0.048	0.005
	C	3.625	0.036		0.032	0.018
	D	14.355	0.000			0.000
G. g. gorilla	A	2.546	NS			
	B	10.521	0.001		0.045	0.002
	C	4.235	0.025		0.029	0.002
	D	2.206	0.133		0.001	0.000

Table 8.4. Ontogenetic change in iliac trabecular strut orientation in the Homininae. One-way ANOVA (with Tukey's post hoc) was used to compare mean angles of orientation intra-specifically across developmental stages. Developmental stages based on permanent molar eruption; M0, no molars erupted; M1, all first permanent molars erupted; M2, all second molars erupted; M3, all third molars erupted. NS = not significant.

In modern humans the posterior iliac strut transmits weight bearing loads from the auricular surface to the acetabulum, while ground reaction forces (GRF) act in the opposite direction (Whittle, 1991). The reaction force passes from the ground

through the proximal femur to the ilium. Ontogenetic changes in the relative position of the femur and acetabulum, or acetabulum and ilium, might affect the direction in which the GRF is applied to the ilium. In modern humans, the angle formed by the supero-lateral rim of the acetabulum and the iliac blade (transverse plane) is comparable across permanent molar eruption stages ($F = 0.120$; $p > 0.05$). Hence, the orientation of the modern human acetabulum probably remains constant during development. However, the relative position of the proximal femur and ilium changes during ontogeny. The relative position of the proximal femur and acetabulum is characterised by the angle of torsion, the angle between the axis of the femoral head and neck and the condylar axis (Figure 8.8). The angle of femoral torsion decreases during growth (Shefelbine *et al.,* 2002; Svenningsen *et al.,* 1989). In newborns torsion is ~40^0, but in adults the angle is usually ~15^0 (Figure 8.8). The femoral condyles are normally aligned so that the axis lies in the coronal plane. During development the femoral head moves to point increasingly medially (Figure 8.8). The proximal femur presents a trabecular strut, which forms part of a trabecular system with the posterior iliac strut (Figure 8.8). In conjunction with decreasing torsion, the femoral trabecular strut will move to point more laterally with increasing age, assuming that it does not change position relative to the femoral cortex (Figure 8.8). In order to maintain alignment with both the auricular surface and femoral head throughout ontogeny, the posterior strut may have to rotate anteriorly (in relation to external iliac morphology). Allometric (ontogenetic) changes in external and internal iliac morphology are described in TPS based on the size axis of a PCA. With increasing iliac size the posterior strut displays a posterior rotation in relation to the iliac blade (Figure 8.4).

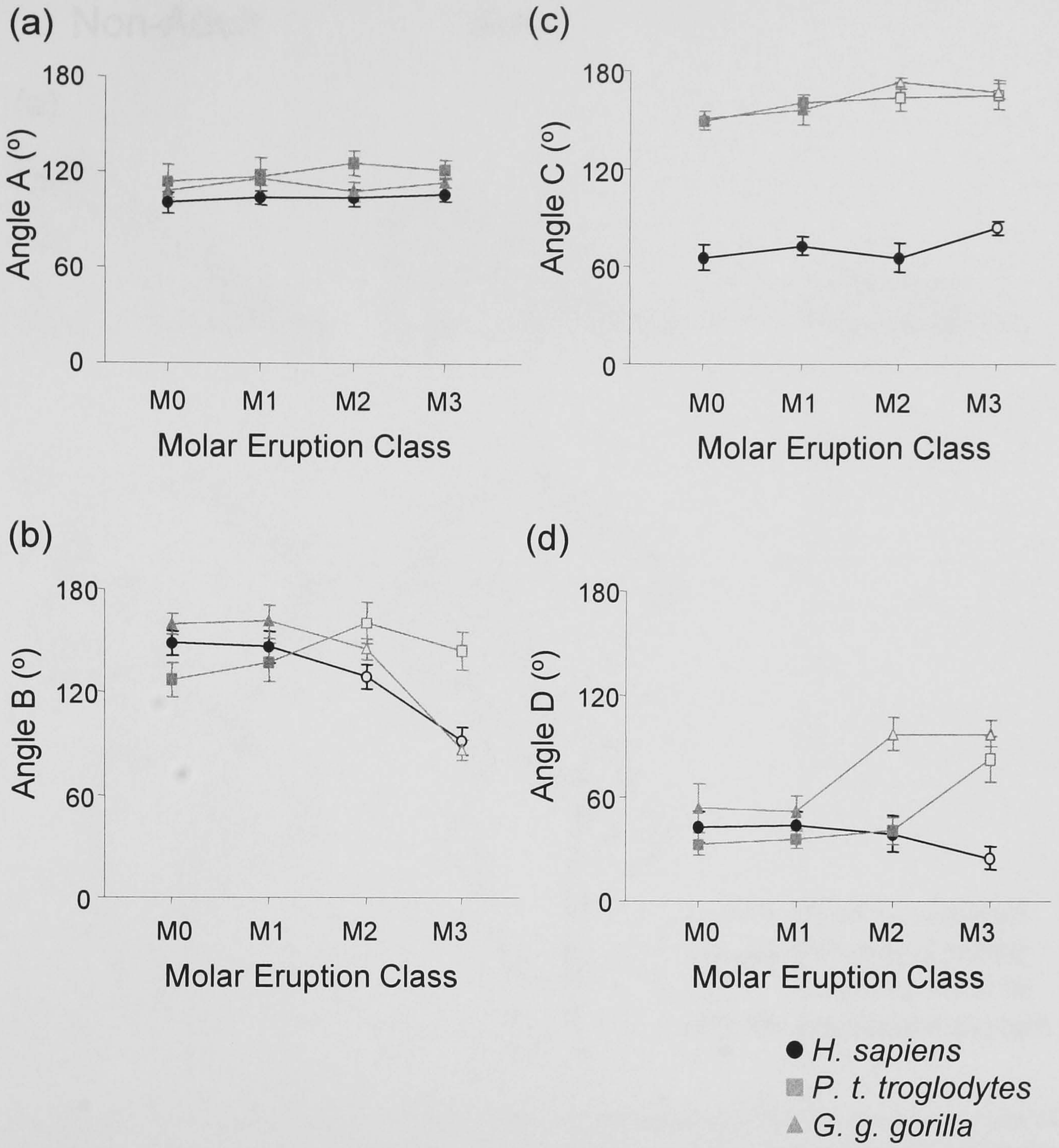

Figure 8.7. Ontogenetic re-orientation of hominoid iliac trabecular struts in relation to external morphology. (a) Angle A (b) Angle B, (c) Angel C (d) Angle D. Developmental stages based on permanent molar eruption; M0, no molars erupted; M1, all first permanent molars erupted; M2, all second molars erupted; M3, all third molars erupted. Error bars denote 95% confidence limits about mean. Open symbols indicate mean angle for that molar eruption class is significantly different from M0 class (one-way ANOVA with Tukey's post hoc $p < 0.05$). See Table 8.2 for F and p values.

Several authors have advocated the theory that in modern humans the iliac buttress resists compressive loads applied to the pelvis by gluteal contraction (e.g. Lovejoy *et al.,* 1973). The iliac buttress is formed by an incurving of the anterior iliac crest during development (Berge, 1998). When the gluteal muscles contract to abduct the

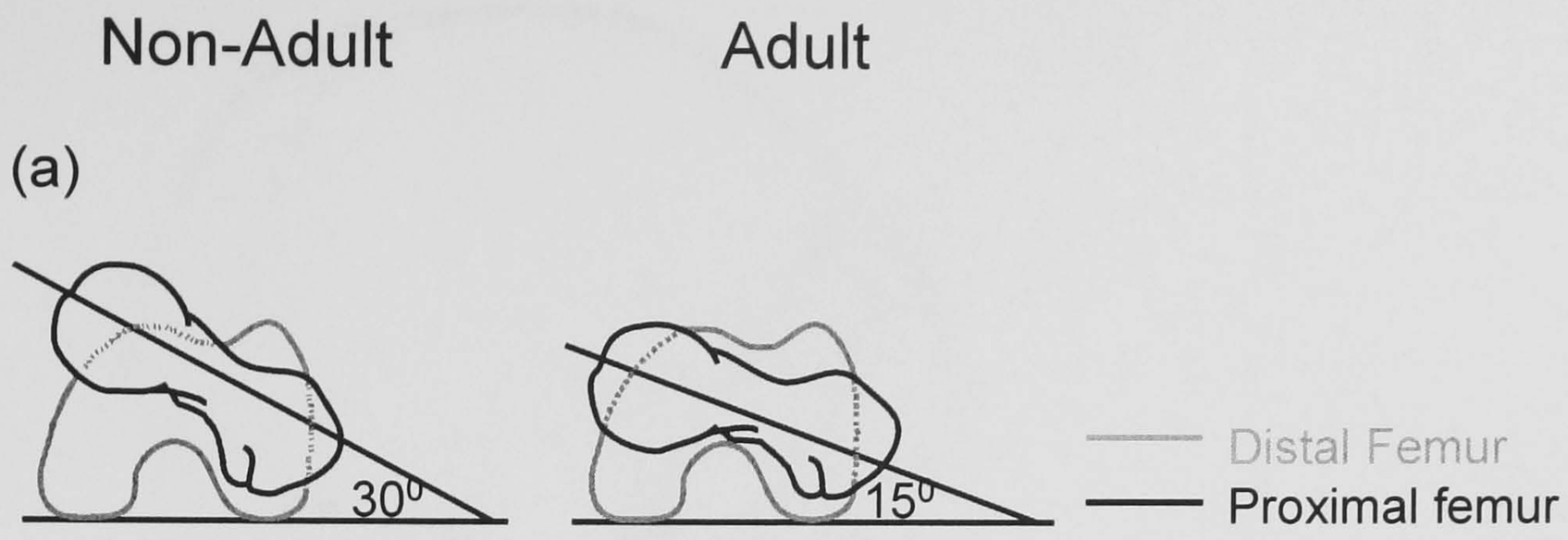

Figure 8.8. Trabecular arcades in the modern human pelvis and femur. (a) Anteversion of the modern human femur decreases during ontogeny. (b) The posterior iliac trabecular strut connects with femoral trabecular struts.

thigh a bending moment is generated in the iliac blade (Burr *et al.,* 1977). The compressive stress imparted on the blade can be expected to focus at the apex of the iliac curvature, i.e. the iliac buttress. In vitro experiments which simulated gluteal musculature contractions produced compressive forces on the lateral surface of the cortex of the iliac buttress and tensile forces on the medial one (Ries *et al.,* 1979). With increasing size the gluteal surface gets proportionately larger with respect to iliac centroid size, particularly the dorsal region (Figure 8.4). This may lead to a posterior displacement of the main axis of compressive stress, with respect to the

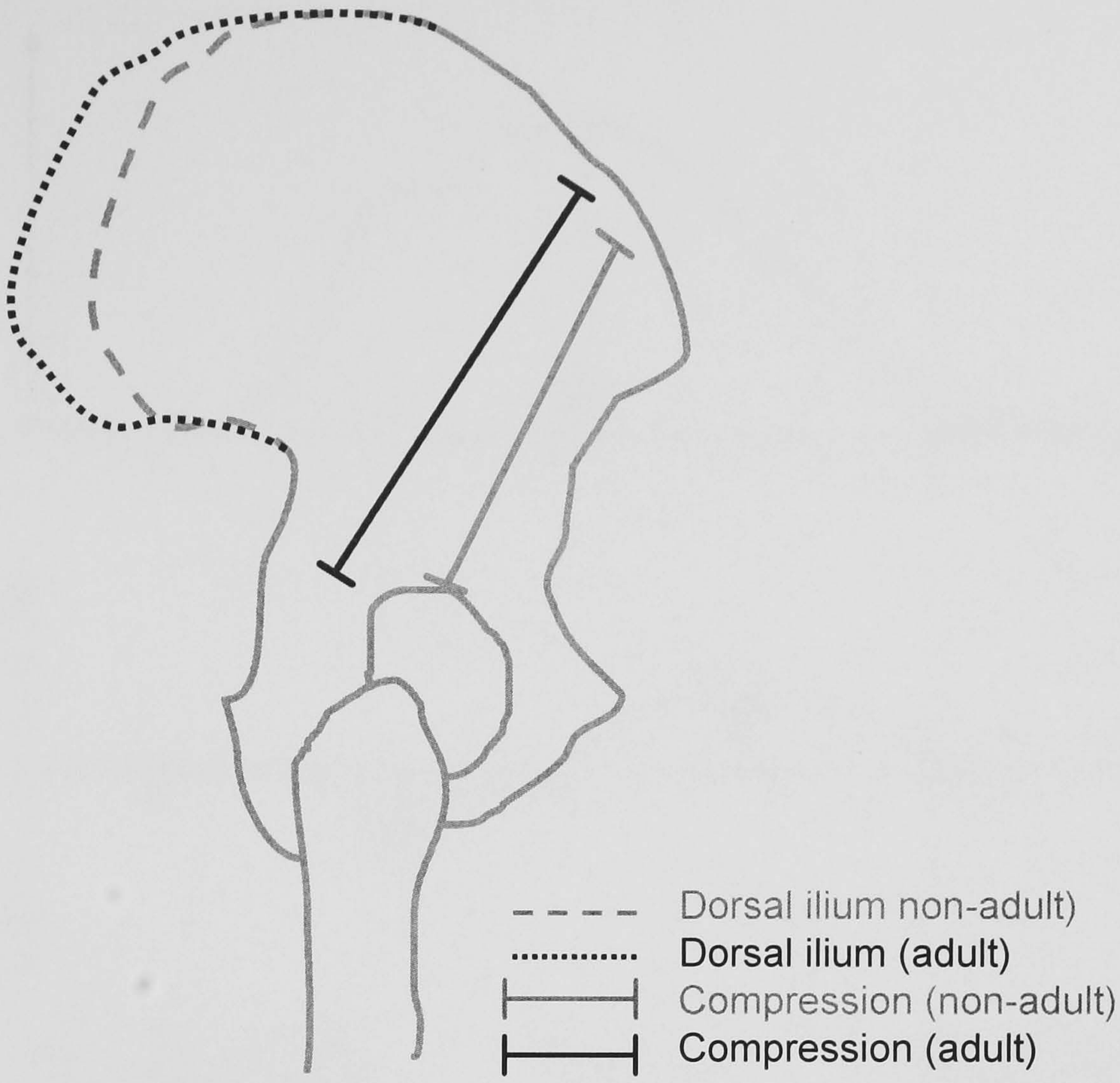

Figure 8.9. Muscle induced compressive stress in the anterior iliac blade of modern humans. Dorsal extension of posterior crest may displace muscle induced compressive forces superiorly. Flattened arrows indicate main direction of compressive stress.

anterior iliac border (Figure 8.9). In vivo strain gauge measurements of the pelvis would be required to test this supposition. In line with this, larger ilia present a buttress (iliac tubercle) and anterior strut that are located more posteriorly with respect to the anterior iliac border (Figure 8.4). Furthermore, splines indicate that with increasing size the anterior strut and iliac buttress (iliac tubercle) become more closely aligned (Figure 8.4).

Except during the earliest stages of development, *G. g. gorilla* is primarily a terrestrial quadruped (Doran, 1997). The GRF imparted on the hindlimb and pelvis during terrestrial quadrupedal locomotion can be broken down into three

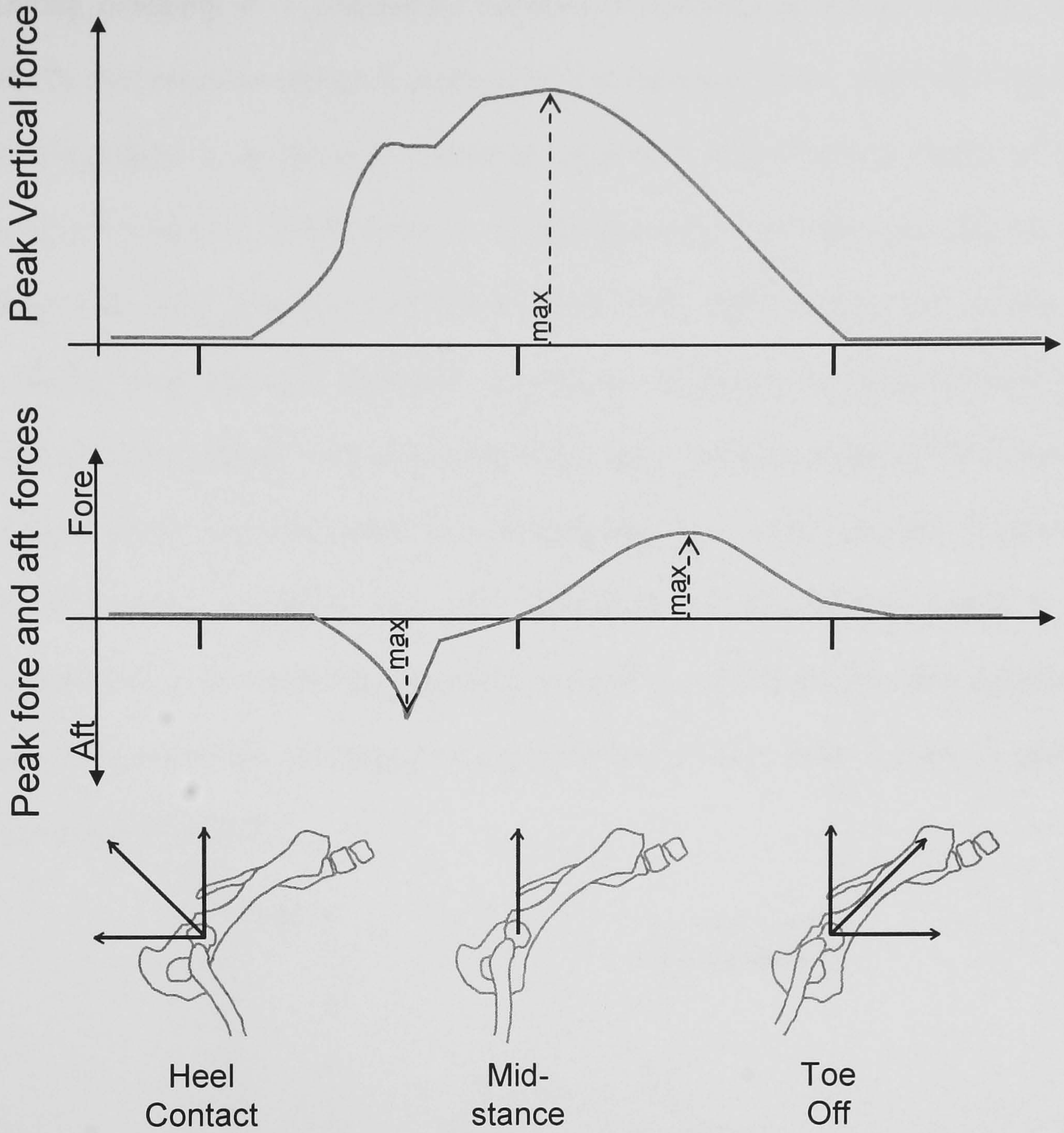

Figure 8.10. Forces acting on the hind-limb (and pelvis) of primates during quadrupedal locomotion. Adapted from Demes *et al.* (1994). Arrows indicate direction of ground reaction force.

components: vertical, fore and aft (Figure 8.10) (Demes *et al.*, 1994). Peak forces are experienced between mid-stance and toe off, when the thigh is extended (Figure 8.10). Therefore, in the functional position one might expect the brunt of the GRF to be directed towards the antero-superior portion of the acetabulum. This is consistent with the finding that in *G. g. gorilla* ilium the posterior strut, which transmits GRF from the femur to the sacrum, meets the acetabulum more antero-superiorly than in smaller specimens (Figure 8.6).

During ontogeny *P. t. troglodytes* becomes increasingly terrestrial (Doran, 1992, 1997). *Pan paniscus* (bonobo) displays greater extension of the thigh when walking quadrupedally in an arboreal context as opposed to terrestrial locomotion (Figure 8.11) (D'Août *et al.*, 2004). Since *P. t. troglodytes* adopts the same type of locomotor behaviours as *P. paniscus* (see Doran, 1992, 1993, 1997) they can reasonably be expected to do the same. Should *P. troglodytes* adopt less extended positions with increasing age, the aft component of the GRF may become increasingly prominent in relation to the fore component, i.e. force applied for a longer duration. Hence, the main direction of loading may shift towards the postero-superior aspect of the acetabulum. In line with this suggestion larger *P. t. troglodytes* ilia show a posterior strut that meets the acetabulum more postero-superiorly than it does in smaller specimens (Figure 8.5).

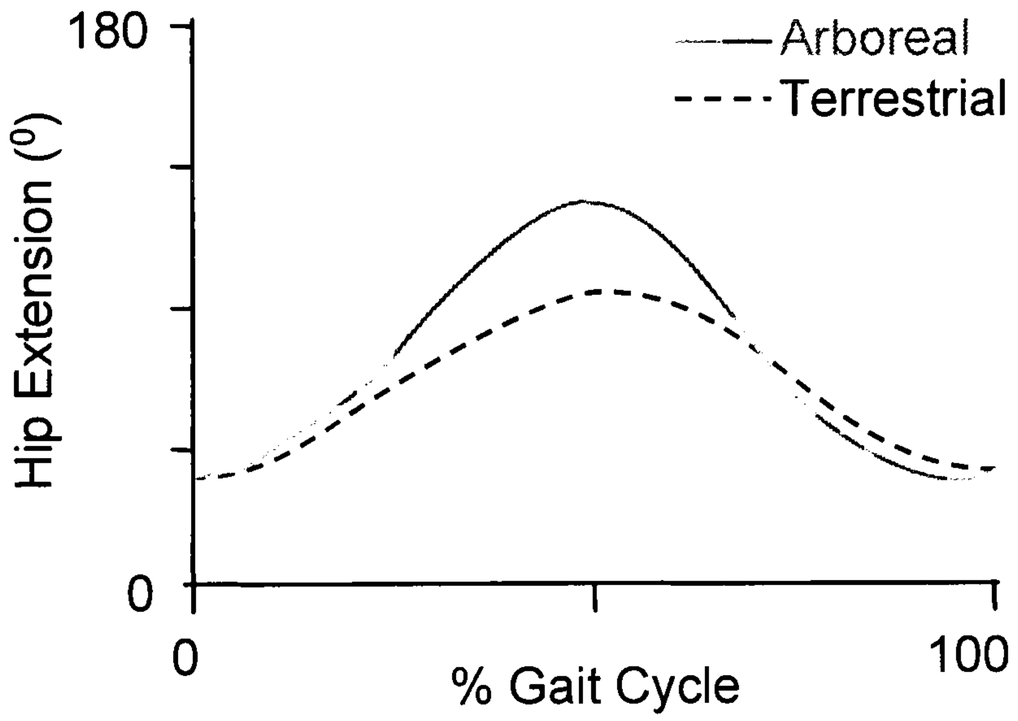

Figure 8.11. Hip extension during quadruedal locomotion on different substrates in *Pan paniscus*. Adapted from D'Aout *et al.* (2004).

In both *P. t. troglodytes* and *G. g. gorilla* the superior portion of the auricular surface gets proportionately larger, in relation to the inferior portion, with increasing iliac size (Figure 8.5 and 8.6). This may indicate that in larger individuals the loads imparted by (or upon) the sacrum are directed more antero-superiorly. In both *P. t.*

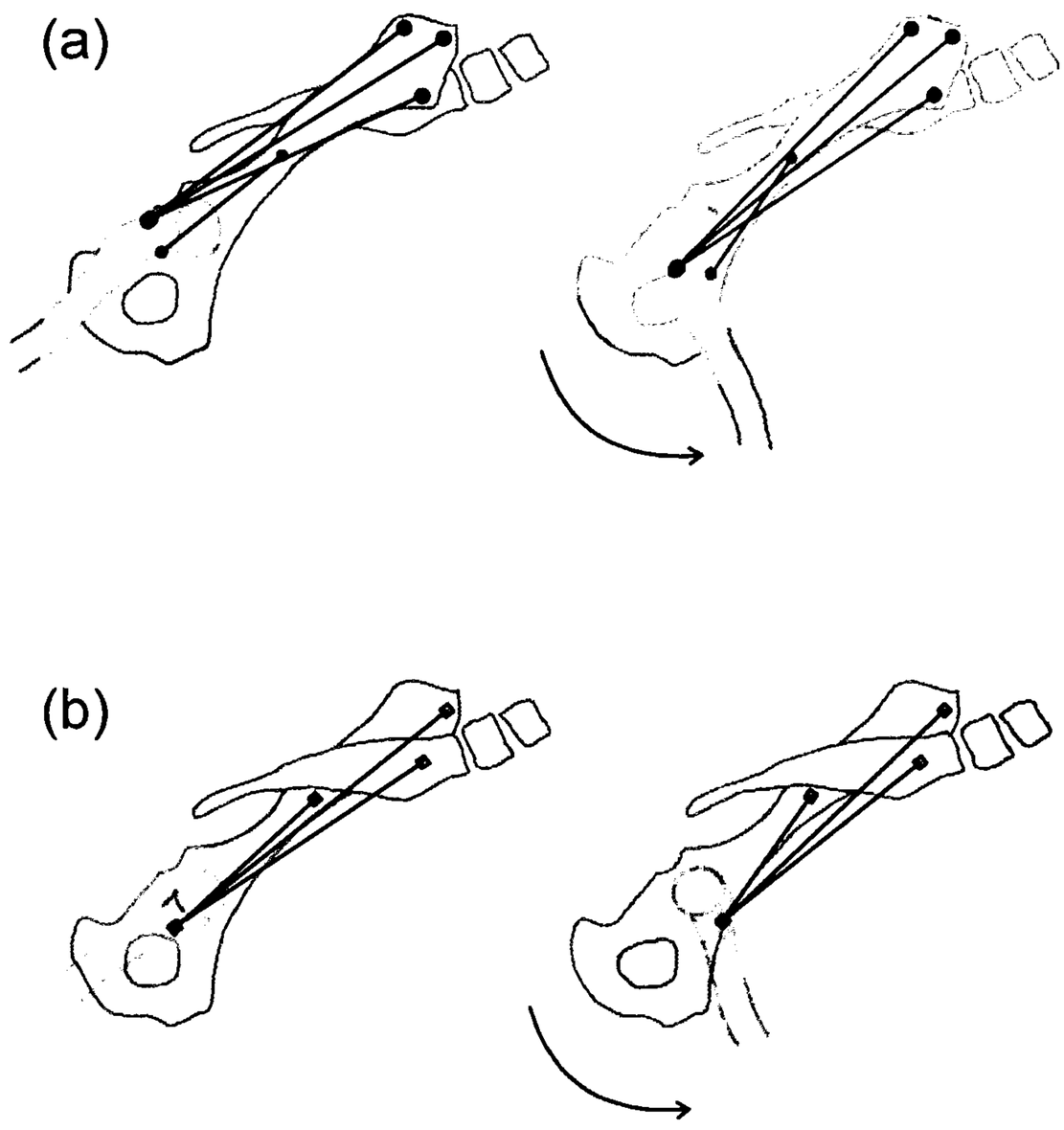

Figure 8.12. Functional position of the African ape pelvis and femur, extended and flexed postures. Open arrows indicate direction of femoral flexion. The figures depict the lines of action of muscle pull in the sagittal view. The lines of action refer to fibres of (a) the gluteals and (b) Iliacus. Muscle lines of actions are demarked by arrows. Gluteus medius is denoted by open circles, gluteus minimus by closed circles and iliacus by open squares.

troglodytes and *G .g gorilla* the superior strut intersects the auricular surface more superiorly in large ilia than in small ilia (Figure 8.5 & Figure 8.6).

In the African apes, the *m. gluteus medius* and *m. gluteus minimus* extend the thigh and *m. iliacus* flexes it. In the functional position the action lines of each muscle (posterior, central and anterior fibres) are schematically reconstructed (Figure 8.12). The action lines of the muscles are drawn as vectors connecting the proximal origin and distal insertion. If each muscle is assumed to generate a contractile force along the action line, the loads that are generated should fall antero-laterally outside the ilium (in all but the most extended postures). Therefore, the anterior iliac border may

bear a large proportion of the compressive stress imparted on the ilium by flexion and extension of the thigh. This is consistent with the finding that in large African ape ilia the anterior iliac buttress is located more anteriorly, with respect to the anterior iliac border, than it is in small specimens (Figures 8.5 and Figure 8.6).

In modern humans measured ontogenetic re-orientation of bundles in relation to external morphology correlates with presumed ontogenetic changes in the main direction of mechanical loading. During the growth and development of African ape ilia trabecular struts change position in relation to external morphology to come more into line with the presumed main direction of loading. Thus, trabecular struts may develop independently of external morphology (sensu Frost, 1990b), probably adapting to alternate loading directions so as to support the cortical shell. These changes are relatively subtle, however when viewed across the entire developmental period trends become apparent. This may lend support to Ruimerman and colleagues (2005) suggestion that trabecular modelling occurs over extended periods of time e.g. decades.

Part V. Conclusions

This study compared the iliac morphology of primates from a developmental perspective. The hominoid ilium consists of a cortical shell which surrounds trabecular tissue (Mednick, 1955; Correnti, 1955; Machiarelli *et al.,* 1996). During development cortical and trabecular tissues adapts to applied loads by modelling (Frost, 1990b; Currey, 1984; Turner, 1998). Trabecular tissue maintains the ability to model throughout development (Frost, 1990b; Kobayashi *et al.,* 2003), but cortical bone loses some capacity to model at the end of infancy (Frost, 1990b; Lieberman, 1996). The end of the infant period is marked by the eruption of first permanent molars (Smith, 1989, 1991) while eruption of the second molars occurs at about puberty. Given the decreasing potential of bone to model after first permanent molar eruption trabecular tissue may be more plastic than cortical bone and show greater morphological changes later in life. The findings of this study are consistent with this notion. Hominoid ilia present two trabecular struts, one anterior and one posterior (Figure 8.2), which develop relatively early during infancy. At, or after the eruption of first permanent molars, the struts appear to re-orientate with respect to external morphology (see Figure 8.7), whereby, the change in the position of the struts brings them into line with presumed loading directions (see Chapter 8).

The cortical shell of the ilium supports the muscles which move the arms (e.g. *m. latissimus dorsi*), trunk (e.g. *m. transversus abdominus* and *m. quadratus lumborum*) and lower limbs (e.g. *m. gluteus maximus*, m. *gluteus medius*, *m. gluteus minimus* and *m. iliacus*). The ilium also bears the weight of the trunk and transmits ground reaction forces from the proximal femur to the sacrum. A reduction in locomotor

Species	Approximate first occurence of locomotor behaviour				
	No locomotor Activity	Quadrupedalism	Bipedalism	Adult Pattern	Source
H. sapiens	0-10 months	10 months	12-14 months	7-9 years	Keen (1993)
P. t. versus	0-3 months	4-6 months	4-6 months	3 years	Doran (1992)
G. g. beringei	0-3 months	6 months	4-5 months	4 years	Doran (1997)

Table 9.1. Hominoid developmental milestones: locomotor behaviour.

efficiency could seriously impair fitness. Therefore, cortical tissue may be less plastic than trabecular bone because it is more functionally constrained, i.e. cannot change because to do so would impair its function (Schwenk & Wagner, 2001). The results presented in this thesis also provide evidence that external morphology may be phylogenetically constrained, i.e. the patterns of iliac growth and development that can evolve are limited by evolutionary history (see Richardson & Chipman 2003). This is inferred from the fact that African apes and cercopithecines (*C. p. grayi*, *C. nictitans* and *C. cephus*) share a common allometric growth trajectory, i.e. share a common pattern of covariation between iliac size and shape (see Figure 3.3).

African apes and cercopithecines adopt very similar locomotor and postural behaviour. The African apes (Carlson, 2005; Doran, 1992, 1997; Hunt, 1991) and cercopithecus species (Gebo & Sargis, 1994; Manaster, 1979; Meldrum, 1991) utilise both terrestrial and arboreal habitats and are primarily quadrupedal. Furthermore, *P. t. troglodytes* and *G. g. gorilla* may show very similar patterns of locomotor development throughout ontogeny. Although no data are available for *P. t. troglodytes* or *G. g. gorilla* data pertaining to their close relatives, *P. t. verus* and *G. g. beringei*, have been published. The two species follow the same pattern of ontogenetic change in locomotor behaviour, progressing from no locomotor activity to forelimb dominated pulling and grasping to suspensory and climbing behaviours and then quadruepdal behaviours (Table 9.1) (Carlson, 1995; Doran, 1997). It is noteworthy that, although developmental rates differ between *P. t. verus*, *G. g. beringei*, they exhibit very similar locomotor behaviour at the same body mass (Figure 9.1) (Doran, 1997). Therefore, the shared growth trajectory of the non-human

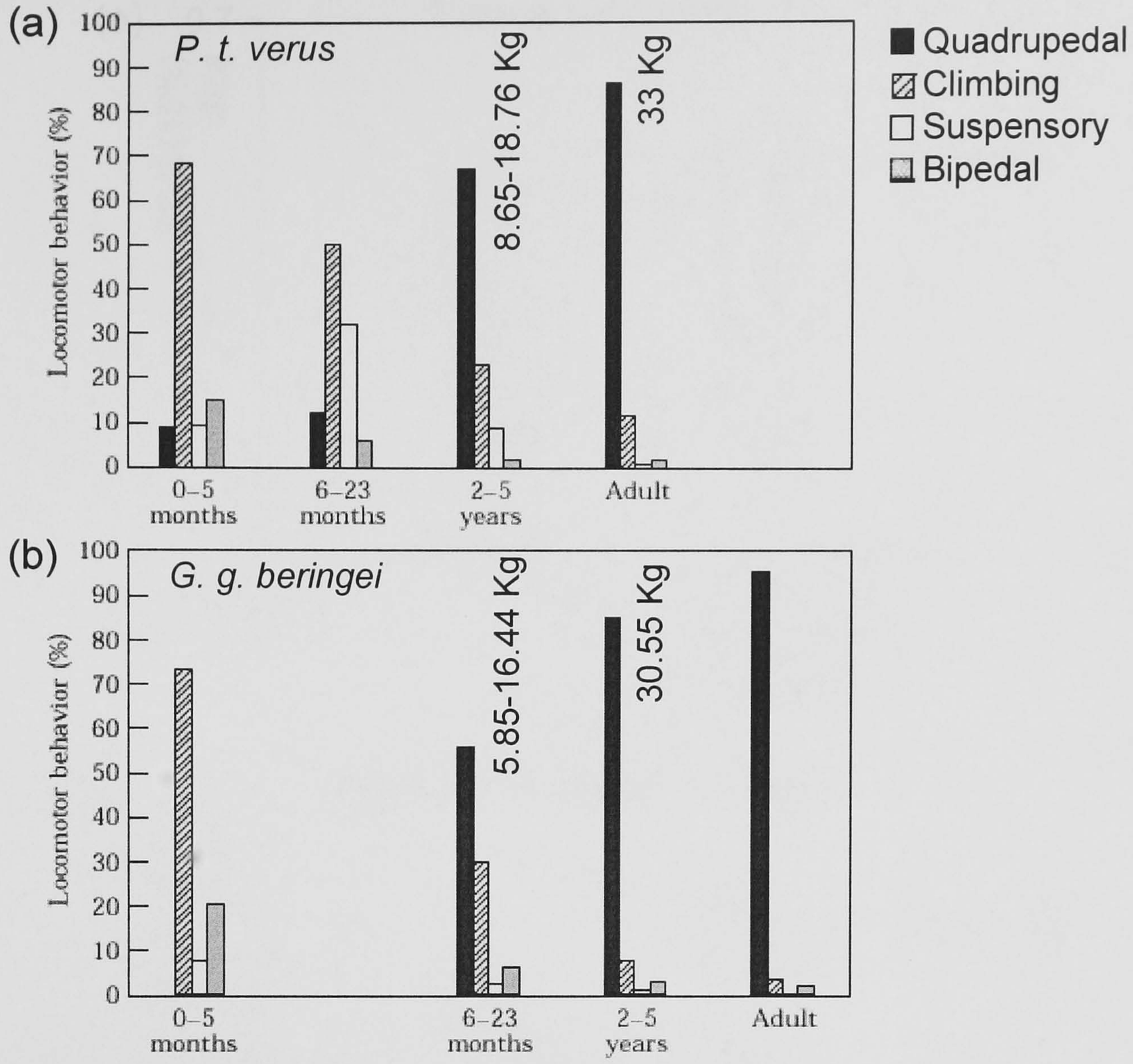

Figure 9.1. Inter-specific comparison on ontogenetic change in locomotor pattern (a) *P. t. verus* and (b) *G. g. beringei*. Mass (Kg) refers to mean body mass of developmental stage. Modified from Doran (1997).

primates, especially *P. t. troglodytes* and *G. g. gorilla* may reflect similarities in locomotor behaviour (mechanical loading).

Combined external-internal iliac growth trajectories were compared across the hominoids using a landmark based geometric morphometric study (see Table 7.1 for sample). Cortical landmarks digitised directly from bones (Table 8.1) were combined with trabecular landmarks taken from radiographs (Figure 8.2) see section 8.3.2. Since the African ape sample was small allometric trajectories were calculated by plotting 95% confidence ellipses in a size-shape morphospace generated using

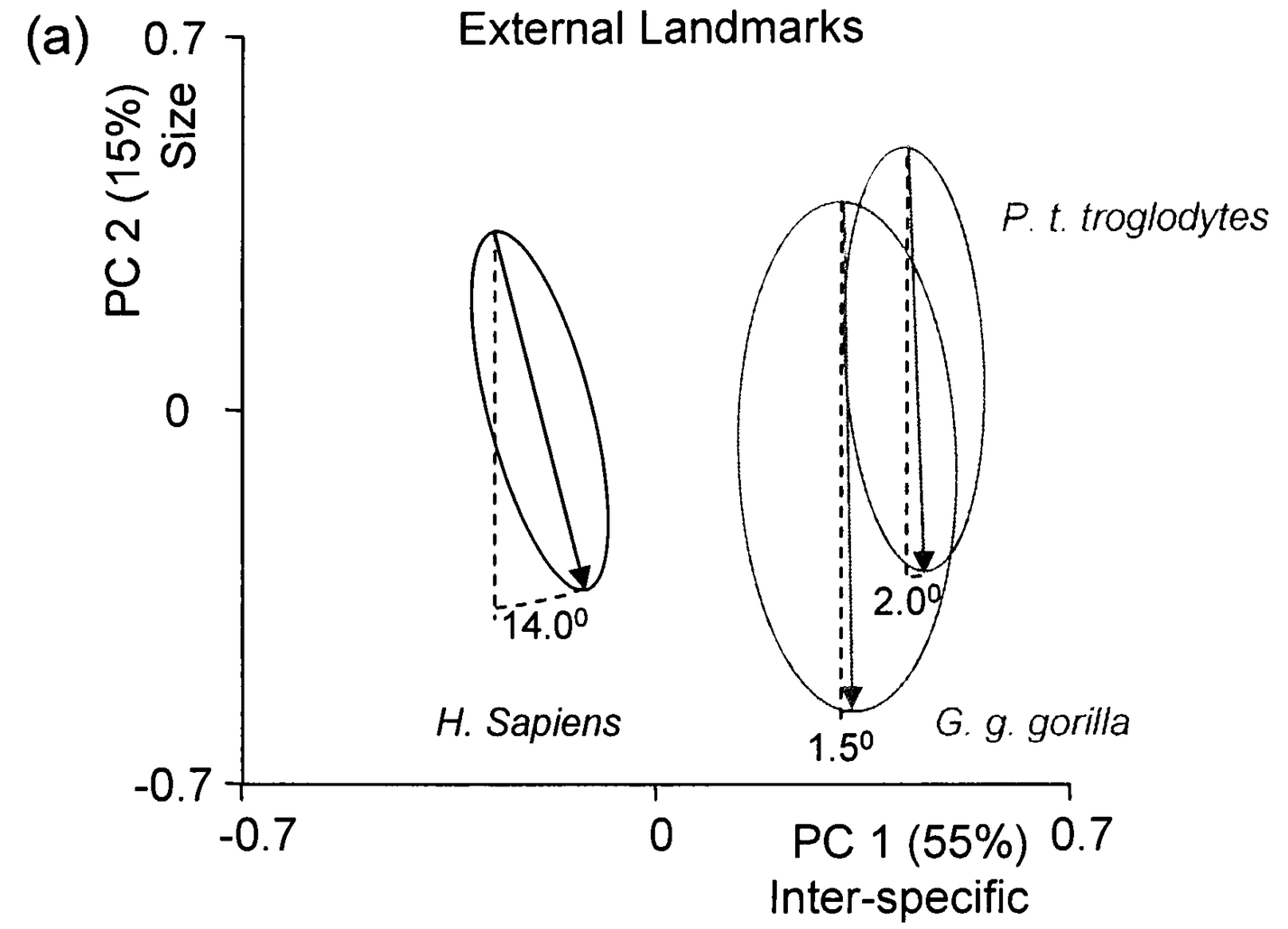

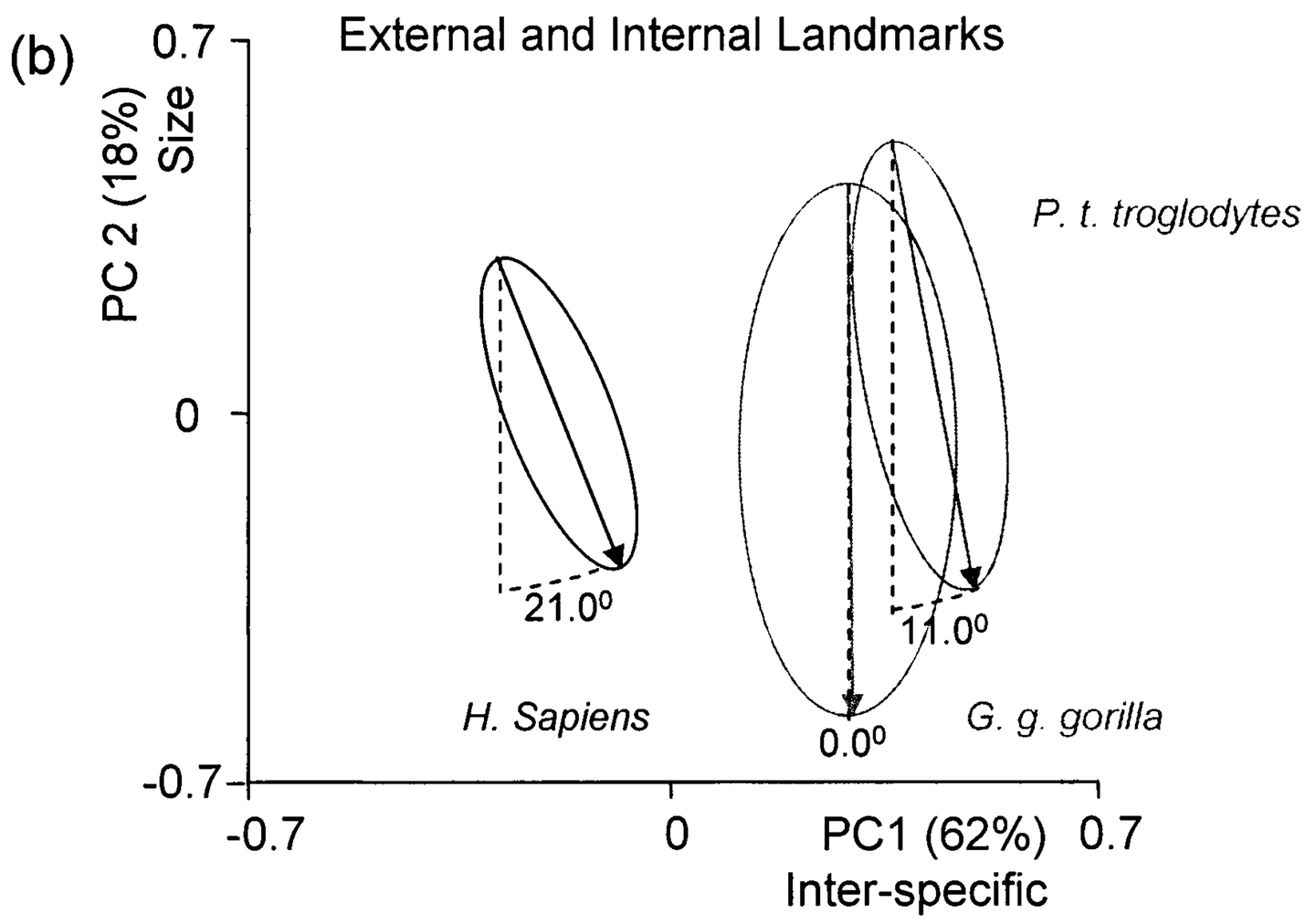

Figure 9.2. Ontogenetic change in orientation of anterior trabecular struts, in relation to external morphology, in the hominoid ilium. Principal components analysis (a) external landmarks, supplemented with iliac centroid size (b) external and internal landmarks, supplemented with iliac centroid size. Arrows indicate growth trajectory.

principal components analysis (see section 2.7.7.4). It would be better to compare the coincidence of ontogenetic trajectories more comprehensively, across three or more PC's, by using resampling techniques (see Zelditch & Sheets, 2000). However, analysing the first two PC's does assess the major effects and indicates general

trends. The results are shown in Figure 9.2. External iliac growth trajectories distinguish the African apes from modern humans. The external growth trajectories of *P. t. troglodytes* and *G. g. gorilla* differ by only 0.5^0. In contrast, the external-internal iliac growth trajectories differ by 11^0. This finding is consistent with the notion that external shape is more constrained and internal is more responsive to mechanical loading. Therefore, external shape may be more useful than trabecular morphology when inferring phylogeny from comparative studies of bony development (e.g. Ravosa & Profant, 2000). The development of trabecular morphology, on the other hand, may be more informative with regards to locomotor and postural behaviour or mechanical loading (e.g. Macchiarelli *et al.,* 1999, 2001; Rook *et al.,* 1999, 2004).

Cited Literature

Abramoff, M.D., Magelhaes, P.J. and Ram, S.J. 2004. Image Processing with Image J. Biophotonics International. 11(7):36-42.

Albrecht, G.H. 1978. The craniofacial morphology of the Sulawesi macaques: Multivariate approaches to biological problems. Contrib Primatol, 13:1-151.

Anemone, R.L., Watts, E.S. and Swindler, D.R. 1991. Dental development of known-age chimpanzees, *Pan troglodytes* (primates, pongidae). Am J Phys Anthropol, 86 (2):229-241.

Anemone, R.L., Mooney, M.P. and Siegel, M.I. 1996. Longitudinal study of dental development in chimpanzees of known chronological age: Implications for understanding the age at death of Plio-Pleistocene hominids. Am J Phys Anthropol, 99 (1):119-133.

Arnold, S. 1992. Constraints on phenotypic evolution. J Am Natur (suppl), 140 (5): 85.

Atchley, W.R. and Hall, B.K. 1991. A model for development and evolution of complex morphological structures. Biol Rev. 66:101–157.

Atchley, W.R., Plummer, A.A. and Riska, B. 1985. Genetics of mandible form in the mouse. Genetics. 111:555–577.

Augat, P., Link, T., Lang, T.F., Lin, J.C., Majumdar, S. and Genant, H.K. 1998 Anisotropy of the elastic modulus of trabecular bone specimens from different anatomical locations. Med Eng Phys, 20:124-131.

Bacon, A.M. and Baylac, M. 1995. Landmark analysis of distal femoral epiphysis of modern and fossil primates with particular emphasis on *Australopithecus afarensis* (AL 129-1 and AL 333-4). C R Acad Sci [IIA], 321:553-560.

Baker, R.H. and Wilkinson, G.S. 2001. Phylogenetic analysis of sexual dimorphism and eye-span allometry in stalk-eyed flies (Diopsidae). Evol, 55(7):1373–1385.

Bakker, B., van der Eerden, B.C., Koppenaal, D.W., Karperien, M. and Wit, J.M. 2003. Effect of X-irradiation on growth and the expression of parathyroid hormone-related peptide and indian hedgehog in the tibial growth plate of the rat. Horm Res, 59; (1):35-41.

Banse, X., Devogelaer, J.P. and Grynpas, M. 2002. Patient-specific microarchitecture of vertebral cancellous bone: a peripheral quantitative computed tomographic and histological study. Bone, 30(6):829-835.

Beier, F. 2005. Cell-cycle control and the cartilage growth plate. J Cell Physiol, 202(1):1-8.

Berge, C. 1984a. Multivariate analysis of the pelvis for Hominids and other extant primates: Implications for the locomotion and systematics of the different species of australopithecines. J Hum Evol, 13:555-562.

Berge, C. 1984b. Obstetric interpretations of the Australopithecine pelvic cavity. J Hum Evol, 13:573-587.

Berge, C. and Kazmierczak, J.B. 1986. Effects of size and locomotor adaptations on the hominid pelvis: evaluation of australopithecine bipedality with a new multivariate method. Folia Primatol, 46(4):185-204.

Berge, C. 1991. Size and locomotion-related aspects of hominid and anthropoid pelves: An osteometrical approach. Hum Evol, 6:365-376.

Berge, C. 1994. How did the australopithecines walk? A biomechanical study of the hip and thigh of *Australopithecus afarensis*. J Hum Evol, 26:259-273.

Berge, C. 1996. The evolution and growth of the Hominid pelvis. In: L.F. Marcus, M. Corti, A. Loy, G.J.P. Naylor, D. Slice, eds. Advances in morphometrics. New York and London: Plenum Press. 441-448.

Berge, C. 1998. Heterochronic processes in human evolution: an ontogenetic analysis of the hominid pelvis. Am J Phys Anthropol, 105:441-59.

Berge, C. and Penin, X. 2004.Ontogenetic allometry, heterochrony, and interspecific differences in the skull of African apes, using tridimensional Procrustes analysis. Am J Phys Anthropol, 124:124-38.

Biewener, A.A. and Bertram, J.E.A. 1991. Efficiency and optimization in the design of skeletal support systems. In: R. W. Blake, ed. Efficiency and Economy in Animal Physiology. Cambridge. Cambridge University Press. 65–82.

Biewener, A.A., Fazzalari, N.L., Konieczynski, D.D. and Baudinette, R.V. 1996. Adaptive changes in trabecular architecture in relation to functional strain patterns and disuse. Bone, 19:1-8.

Bocquet, C. 1953. Recherches sur le polymorphisme naturel des Jaara marina (Fabr.) (Isopodes asllotes). Essai de systématique evolutive. Arch Zool Exp Gen, 90:187-250.

Bookstein, F.L. 1989. Principal warps: thin-plate splines and the decomposition of deformations. IEEE trans. Pattern Analysis Machine Intelligence, 11:567-585.

Bookstein, F.L. 1990. Higher-order features of shape change for landmark data. In: Proceedings of the Michigan Morphometric Workshop. Special Publication No. 2. Ann Arbor MI, The University of Michigan Museum of Zoology. 237-250.

Bookstein, F.L. 1991. Morphometric Tools for Landmark Data. Geometry and Biology. New York. Cambridge University Press.

Bookstein, F.L. 1993. A brief history of morphometric synthesis. In: Contributions to Morphometrics. Marcus, L.F., Bello, E. and Garcia-Valdecasas, A., eds. Museo Nacional de Ciencias Naturales, Madrid. 15-40.

Bookstein, F.L. 1996a. Combining the tools of geometric morphometrics. In: LF Marcus, M. Corti, A. Loy, G. Naylor, and DE Slice, eds. Advances in morphometrics New York. Plenum. 131–151.

Bookstein, F.L. 1996b. Biometrics, biomathematics and the morphometric synthesis. Bull Math Biol, 58:313-365.

Broeck van den, J.P. 1911. Ueber Geschlechtsunterschiede im Becken bei Primaten. Arch f Anat u Physiol Anatom Abt, 163-184.

Broeck van den, J.P. 1914. Studien zur Morphologie des Primatenbeckens. Gegenbaurs Morphol Jahrb 49:1-118.

Brothwell, D.R. 1981. Digging Up Bones, (3rd edition). New York: Cornell University Press.

Buck, A.M., Price, R.I., Sweetman, I.M. and Oxnard C.E. 2002. An investigation of thoracic and lumbar cancellous vertebral architecture using power-spectral analysis of plain radiographs. J Anat, 200(5):445-56.

Buckland-Wright, J.C., Lynch, J.A., Rymer, J. and Fogelman I. Fractal signature analysis of macroradiographs measures trabecular organization in lumbar vertebrae of postmenopausal women. Calcif Tissue Int, 54(2):106-12.

Burr, D.B., Van Gerven, D.P. and Gustav, B. L.1977. Sexual dimorphism and mechanics of the human hip: A multivariate assessment. Am J Phys Anthropol, 47(2):273-278.

Burr, D.B., Schaffler, M.B. and Frederickson, R.G. 1988. Composition of the cement line and its possible mechanical role as a local interface in human compact bone. J Biomech, 21(11):939-945.

Byers, S., Moore, A.J., Byard, R.W. and Fazzalari, N.L. 2000. Quantitative histomorphometric analysis of the human growth plate from birth to adolescence. Bone, 27(4):495-501.

Caligiuri, P., Giger, M.L., Favus, M.J., Jia, H., Doi, K. and Dixon, L.B. 1993. Computerized radiographic analysis of osteoporosis: preliminary evaluation. Radiology, 186:471-474.

Carlson, K.J. 2005. Investigating the form-function interface in African apes: Relationships between principal moments of area and positional behaviors in femoral and humeral diaphyses. Am J Phys Anthropol, 127:312-34.

Carter, D.R. and Hayes, W.C. 1977a. Compact bone fatigue damage-I. Residual strength and stiffness. J Biomech, 10:325-37.

Carter, D.R. and Hayes, W.C 1977b. Compact bone fatigue damage: a microscopic examination. Clin Orthop Relat Res, 127:265-74.

Clements, E.M.B., Davies-Thomas, E. and Pickett, K.G.1953. Time of Eruption of Permanent Teeth in British Children in 1947-8. Brit. Med J, 1:1421-1424.

Champy, C. 1929. La croissance dysharmonique des caracteres sexuels accessoires. Arch Scie Phys nat Zoologie, 194-244.

Champy, C. 1924. *Sexualite et hormones*. Doin, Paris.

Chappard, D., Legrand, E., Pascaretti, C., Basle, M.F. and Audran, M. 1999. Comparison of eight histomorphometric methods for measuring trabecular bone architecture by image analysis on histological sections. Microsc Res Tech, 1, 45(4-5):303-312.

Cheverud, J.M. 1982a. Relationships among ontogenetic, static, and evolutionary allometry. Am J Phys Anthropol, 59:139-149.

Cheverud, J.M. 1982b. Phenotypic, genetic, and environmental morphological integration in the cranium. Evol. 36:499–516.

Cheverud, J.M. and Buikstra, J.E. 1982. Quantitative genetics of skeletal nonmetric traits in the rhesus macaques on Cayo Santiago. III Relative heritability of skeletal nonmetric and metric traits. Am J Phys Anthropol, 59:151–155.

Clarke, M.R.B. 1980. The reduced major axis of a bivariate sample. Biometrika. 67:441-446.

Cock, A.G. 1966. Genetical aspects of metrical growth and form in animals. Q Rev Biol, 41(2):131-190.

Coe, C. L., Savage, A. and Bromley, L.J. 1992. Phylogenetic influences on hormone levels across the primate order. Am Journal of Primat, 28:81-100.

Correnti, V. 1955. Le basi morfomeccaniche della struttura dell'osso iliaco. Riv Antrop, 42:289-336.

Corti, M. and Rohlf, F.J. 2001. Chromosomal speciation and phenotypic evolution in the house mouse. Biol J Linnaean Society, 73(1085):99-112.

Cowin, S.C., Moss-Salentijn, L. and Moss, M.L. 1991. Candidates for the mechanosensory system in bone. J Biomech Eng, 113:191-197.

Cowin, S.C. and Moss, M.L. 2001. Mechanosensory mechanisms in bone. In: Cowin SC, ed. Bone biomechanics handbook, 2nd ed. Boca Raton: CRC Press. 29-1-29-17.

Cowin, S.C., Weinbaum, S. and Zeng, Y. 1995. A case for bone canaliculi as the anatomical site of strain generated potentials. J Biomech, 28:1281-1297.

Cullen, D.M., Smith, R.T. and Akhter, M.P. 2001. Bone-loading response varies with strain magnitude and cycle number. J Appl Physiol, 91(5):1971-1976.

Currey, J. 1984. The Mechanical Adaptations of Bones. Princeton: Princeton University Press.

Currey, J. D. 1998. Mechanical properties of vertebrate hard tissues. Journal Of Engineering In Medicine. Proc Inst Mech Eng (part H), 212(6):399-412.

Dainton, M. and Macho, G.A. 1999. Did knuckle walking evolve twice? J Hum Evol, 36:171-194.

Davidson, R.M., Lingenbrink, P.A. and Norton, L.A. 1996. Continuous mechanical loading alters properties of mechanosensitive channels in G292 osteoblastic cells. Calcif Tissue Int, 59:500-504.

Davis, G.R. and Wong, F.S. 1996. X-ray microtomography of bones and teeth. Physiol Meas, 17:121-146.

Daughaday, W.H. 1975. Somatomedin levels in human beings. Adv Metab Disord, 8:159-170.

D'Aout, K., Vereecke, E., Schoonaert, K., De Clercq, D., Van Elsacker, L. and Aerts, P. 2004. Locomotion in bonobos (*Pan paniscus*): differences and similarities between bipedal and quadrupedal terrestrial walking, and a comparison with other locomotor modes. J Anat, 204 (5):353-361.

Delaere, O., Kok, V., Nyssen-Behets, C. and Dhem, A. 1992. Ossification of the human fetal ilium. Acta Anat, 143(4):330-334.

Delaere, O. and Dhem, A. 1999. Prenatal development of the human pelvis and acetabulum. Acta Orthop Belg, 65(3):255-260.

Delemarre-van de Waal, H.A., van Coeverden S.C. and Rotteveel, J. 2001. Hormonal determinants of pubertal growth. J Pediatr Endocrinol Metab (suppl. 6),14:1521-1526.

Demes, B., Larson, S.G., Stern, J.T. and Jungers, W.L. 1994. The kinetics of primate quadrupedalism: "hindlimb drive" reconsidered. J Hum Evol, 26(5/6):353-374.

Ding, M., Odgaard, A. and Hvid, I. 1999. Accuracy of cancellous bone volume fraction measured by Micro-CT scanning. J Biomech, 32:323-326.

Ding, M., Odgaard, A., Linde, F. and Hvid, I. 2002. Age-related variations in the microstructure of human tibial cancellous bone. J Orthop Res, 20:615-621.

Ding, M., Odgaard, A. and Hvid, I. 2003. Changes in the three-dimensional microstructure of human tibial cancellous bone in early osteoarthritis. J Bone Joint Surg Br, 85(6):906-912.

Doran, D.M. 1992. The ontogeny of chimpanzee and pygmy behaviour chimpanzee behaviour: a case study of paedomorphism and its behavioural correlates. J Hum Evol, 23:139-157.

Doran, D.M. 1993. Comparative locomotor behavior of chimpanzees and bonobos: The influence of morphology on locomotion. Am J Phys Anthropol, 91(1):83.

Doran, D.M. 1997. Ontogeny of locomotion in mountain gorillas and chimpanzees. J Hum Evol, 32:323-344.

Dryden, I.L. and Mardia, K.V. 1993. Multivariate shape analysis. Sankya, 55(A):460-480.

Dryden, I.L. and Mardia, K.V. 1998. Statistical shape analysis. London: John Wiley and Sons.

Dubois, E. 1897. Sur le rapport de l'encephale avec la grandeur du corps chez les Mammiferes. Bull. Soc Anthropol (4e serie), 8:337-374.

Duncan, R.L., Turner, C.H. 1995. Mechanotransduction and the functional response of bone to mechanical strain. Calci Tiss Int, 57:344-358.

Ebert, T.A. and Russell, M.P. 1994. Allometry and model II nonlinear regression. J Theor Biol, 168:367-372.

Eerden van der, B.C.J., Van de Ven, J., Lowik, C.W., Wit, J.M. and Karperien, M. 2002a. Sex steroid metabolism in the tibial growth plate of the rat. Endo, 143:4048-4055.

Eerden van der, B.C.J., Gevers, E.F., Lowik, C.W., Karperien, M. and Wit, J.M. 2002b. Expression of estrogen receptor α and ß in the epiphyseal plate of the rat. Bone, 30:478–485.

Eerden van der, B.C.J., Karperien, M. and Wit, J.M. 2003. Systemic and Local Regulation of the Growth Plate Endocrine Reviews, 24(6):782-801.

Ehrlich, P.J., Lanyon, L.E. 2002. Mechanical strain and bone cell function: a review. Osteoporos Int, 13(9):688-700.

Everett, C. O. 1952. The Evolution of a Permian Vertebrate Chronofauna. Evolution. 6(2): 181-196.

Fajardo, R.J. and Müller, R. 2001. Three-dimensional analysis of nonhuman primate trabecular architecture using microcomputed tomography. Am J Phys Anthropol, 115:327-336.

Fajardo, R.J., Ryan, T.M. and Kappelman, J. 2002. Assessing the accuracy of high-resolution X-ray computed tomography of primate trabecular bone by comparisons with histological sections. Am J Phys Anthropol, 118(1):1-10.

Fleagle, J.G. 1985. Size and adaptation in primates. In: W.L. Jungers, ed. *Size and Scaling in Primate Biology*. New York: Plenum Press. 1–19.

Ford, C.M. and Keaveny, T.M. 1996. The dependence of shear failure properties of trabecular bone on apparent density and trabecular orientation. J Biomech, 29:1309-1317.

Frieβ, M. 2003. An application of the relative warps analysis to problems in human paleontology - with notes on raw data quality. Image Anal Stereol, 22:63-72.

Frost, H.M. 1987a. Bone "mass" and the "mechanostat": a proposal. Anat Rec, 219(1):1-9.

Frost, H.M. 1987b. The mechanostat: a proposed pathogenic mechanism of osteoporoses and the bone mass effects of mechanical and non mechanical agents. Bone Miner, 2(2):73-85.

Frost, H.M. 1990a. Structural adaptations to mechanical usage (SATMU):1. Redefining Wolff's Law: The bone modeling problem. Anat Rec 226:403-413.

Frost, H.M. 1990b. Structural adaptations to mechanical usage (SATMU):2. Redefining Wolff's Law: The bone remodeling problem. Anat Rec 226:414-422.

Frost, H.M. 1990c. Skeletal structural adaptations to mechanical usage (SATMU): 3. The hyaline cartilage modeling problem. Anat Rec. 1990 Apr;226(4):423-32.

Frost, H.M. 1990d. Skeletal structural adaptations to mechanical usage (SATMU): 4. Mechanical influences on intact fibrous tissues. Anat Rec, 26(4):433-9.

Frost, H.M. 1996. A proposed general model of the "Mechanostat" (suggestions from a new skeletal-biologic paradigm. Anat Rec, 244(2):139-147.

Frost, H.M. 2003. Bone's mechanostat: a 2003 update. Anat Rec Part A, 275:1081-1101.

Frost, H.M., Ferretti, J.L. and Jee, W.S.S. 1998. Perspectives: some roles of mechanical usage, muscle strength, and the mechanostat in skeletal physiology, disease, and research. Calci Tissue Int, 62(1):1-7.

Gavan, J.A. 1967. Eruption of primate deciduous dentition: A comparative study. J Dent Res, 46:984-988.

Gayon, J. 2000. History of the concept of allometry. Am Zool, 40:748–758.

Gebo, D.L. and Sargis, E.J. 1994. Terrestrial adaptations in the postcranial skeletons of guenons. Am J Phys Anthropol, 93(3):341-371.

Genoves, S. 1959. Diferencia sexuales en el hueso coxal. University Nacional Autonoma de Mexico: Instituto de Historia, Mexico City.

Gibbs, S., Collard, M. and Wood, B. 2002. Soft-tissue anatomy of the extant hominoids: a review and phylogenetic analysis. J Anat, 200(part 1):3-50.

Giesen, E. B. W. Ding, M. Dalstra, M. van Eijden, T. M. G. J. 2003. Architectural measures of the cancellous bone of the mandibular condyle identified by principal components analysis. Calcif Tissue Int, 73(3):225-231.

Goldstein, S.A., Goulet, R. and McCubbrey, D. 1993. Measurement and Significance of Three-Dimensional Architecture to the Mechanical Integrity of Trabecular Bone. Calci Tissue Int, 53 (supp1):S127.

Goodall, C.R. 1991. Procrustes methods and the statistical analysis of shape. J. Royal Statistical Soc (B), 53:285-340.

Gould, S.J. 1966. Allometry and size in ontogeny and phylogeny. Biol Rev Cam Phil Soc, 41:587-640.

Gould, S.J. 1971. Geometric similarity in allometric growth: a contribution to the problem of scaling in the evolution of size. Am Nat, 105:113-136.

Gould, S.J. 1977. Ontogeny and Phylogeny. Cambridge. Mass. Harvard University Press.

Gower, J.C. 1971. A general co-efficient of similarity and some of its properties. Biometrics, 27:857-871.

Gower, J.C. 1975. Generalised Procrustes analysis. Psychometrika, 40:33-50.

Grumbach, M.M., Bin-Abbas, B.S. and Kaplan, S.L. 1998. The Growth Hormone Cascade: Progress and Long-Term Results of Growth Hormone Treatment in Growth Hormone Deficiency. Horm Res, 49(Suppl.2):41-57.

Gugino, L.D., Aglio, L. S., Raymond, S. A., Romero, R., Ramirez, M., Gonzalez, A. and Black, P M. 2001. Intraoperative cortical function localization techniques. Cerebral cortical surgery with functional mapping. Tech Neurosurg, 7(1):19-32.

Hall, B. K. 1991a. Bone matrix and bone-specific products. Boca Raton. CRC Press.

Hall, B. K. 1991b. The Osteoclast .Boca Raton. Boca Raton. CRC Press.

Hall, B. K. 1992a. Bone growth A. Boca Raton. CRC Press.

Hall, B. K.1992b. Bone metabolism and mineralisation. Boca Raton. CRC Press.

Hall, B. K. 1993. Bone Growth B. Boca Raton. CRC Press.

Hager, L.D. 1996. Sex differences in the sciatic notch of great apes and modern humans. Am J Phys Anthropol, 99:287-300.

Hammer, Ø., Harper, D.A.T., and P. D. Ryan, 2001. PAST: Paleontological Statistics Software Package for Education and Data Analysis. Palaeontologia Electronica 4(1): 9pp. http://palaeo-electronica.org/2001_1/past/issue1_01.htm. [Accessed 01.05.06].

Han, Y., Cowin, S.C., Schaffler, M.B. and Weinbaum, S. 2004. Mechanotransduction and strain amplification in osteocyte cell processes. Proc Nat Acad Sci U S A, 101(47):16689-16694.

Hara, T., Tanck, E., Homminga, J. and Huiskes R. 2002. The influence of microcomputed tomography threshold variations on the assessment of structural and mechanical trabecular bone properties. Bone, 31(1):107-109.

Harrigan, T.P. and Mann, R.W. 1984. Characterization of microstructural anisotropy in orthotropic materials using a second rank tensor. J Mat Sci, 19(3):761–767.

Henderson, J. 2005. Ernest Starling and 'Hormones': an historical commentary. J Endocrinol, 184:5–10.

Herring, S.W. 1993a. Epigenetic and functional influences on skull growth. In Hanken J, Hall BK (eds) The Skull, vol 1, pp 153–206. Chicago: University of Chicago Press.

Herring, S.W. 1993b. Formation of the vertebrate face: epigenetic and functional influences. Am Zool, 33: 372-483.

Hotelling, H. 1936. Relations between two sets of variates. Biometrika, 28:321-377

Hott, M., Deloffre, P., Tsouderos, Y. and Marie, P.J. 2003. S12911-2 reduces bone loss induced by short-term immobilization in rats. Bone, 33(1):115-123.

Hou, J.C., Salem, G.J., Zernicke, R.F. and Barnard, R.J. 1990. Structural and mechanical adaptations of immature trabecular bone to strenuous exercise. J Appl Physiol, 69(4):1309-1314.

Hoyle, M.H. 1973. Transformations-An introduction and a bibliography. ISR, 41:203-223.

Hunt, KD. 1991. Mechanical implications of chimpanzee positional behavior Am J Phys Anthropol, 86(4):521-536.

Hunt, K.D. 1992. Positional behaviour of Pan troglodytes in the Mahale Mountains and Gombe Stream National Parks, Tanzania. Am J Phys Anthropol, 87(1):83-105.

Hunt K.D. 1994. Body Size Effects on Vertical Climbing Among Chimpanzees. Int J Primatol, 15(6):855-865.

Hunter, W.S. 1990. Heredity in the craniofacial complex. In Enlow DH (ed), Facial Growth, pp 249–266. Philadelphia: WH Saunders.

Huxley, J.S. 1924. Constant differential growth-ratios and their significance. Nature, 114:895-896.

Huxley, J.S. 1932. Problems of relative growth. Methuen ed. London. Reprinted 1993, John Hopkins University Press.

Huxley, J.C. and Teissier, G. 1936a. Terminology of relative growth. Nature, 137:780-781.

Huxley, J.C. and Teissier, G. 1936b. Terminologie et notation dans la description de la croissance relative. Comptes Rendus Eances Soc Biol Fil, 121:934-937.

Inman, V.T., Ralston, H.J. and Todd, F. 1981. Human walking. Baltimore: Williams and Wilkins.

Ito, M., Nishida, A., Nakamura, T., Uetani, M. and Hayashi, K. 2002. Differences of three dimensional trabecular microstructure in osteopenic rat models caused by ovariectomy and neurectomy. Bone. 30(4):594-598.

Iwamoto, J., Yeh, J.K., Aloia, J.F. 1999. Differential effect of treadmill exercise on three cancellous bone sites in the young growing rat. Bone, 24(3):163-169.

Jacobs, C.R., Yellowley, C.E., Davis, B.R., Zhou, Z., Cimbala, J.M. and Donahue, H.J. 1998. Differential effect of steady versus oscillating flow on bone cells. J Biomech, 31:969-976.

Jaecks G. S. and Carlson, S.J. 2001. How phylogenetic inference can shape our view of heterochrony: examples from thecideide brachiopods Paleobiology, 27(2):205–225.

Jamison, P.L. and Ward, R.E. 1993. Brief communication: Measurement size, precision, and reliability in craniofacial anthropometry: Bigger is better. Am J Phys Anthropol, 90(4):495-500.

Jee, W.S., Li, X.J., Schaffler, M.B. 1991. Adaptation of diaphyseal structure with aging and increased mechanical usage in the adult rat: A histomorphometrical and biomechanical study. Anat Rec, 230(3):332-338.

Jensen, E.B. and Gundersen, H.J.G. 1985. The stereological estimation of moments of particle volume. J Appl Probab, 22(1):82-98.

Jolicoeur, J. 1963. The multivariate generalization of the allometry equation. Biometrics, 19:497-499.

Jolicoeur, P. and Mosimann, J.E. 1960. Size and shape variation in the painted turtle. A principal component analysis. Growth, 24:339-354.

Jungers, W.L. and Hartmann, S.E. 1988. Relative growth of the locomotor skeleton in orang-utans and other large-bodied hominoids. 347–359, In: Schwartz, J.H., ed. Orang-utan Biology, Oxford University Press.

Kamibayashi, L., Wyss, U.P., Cooke, T.D. and Zee, B. 1995. Changes in mean trabecular orientation in the medial condyle of the proximal tibia in osteoarthritis. Calcif Tissue Int, 57(1):69-73.

Kappelman, J. 1996. The evolution of body mass and relative brain size in fossil hominids. J Hum Evol, 30:243–276.

Katz, M.J. 1980. Allometry formula: a cellular model. Growth, 44:89-96.

Keen, M. 1993. Early Development and Attainment of Normal Mature Gait. J Pros Orth, 5:35-38.

Kendall, D.G. 1984. Shape manifolds, procrustean metrics and complex projective spaces. Bull Lond Math Soc, 16:81-121.

Kent, J.T. 1994. The complex Bingham distribution and shape analysis J Roy Statist Soc (B), 56:285-299.

Kleerekoper, M., Villanueva, A.R., Stanciu, J., Rao, D.S. and Parfitt, A.M. 1985. The role of three-dimensional trabecular microstructure in the pathogenesis of vertebral compression fractures. Calcif Tissue Int. 37(6):594-7.

Klingenberg, C.P. 1996a. Individual variation of ontogenies: a longitudinal study of growth and timing. Evol, 50:2412-2428.

Klingenberg, C.P. 1996b. Multivariate allometry. In: L. F. Marcus, M. Corti, A. Loy, G. J. P. Naylor and D. E. Slice, eds. Advances in morphometrics. New York. Plenum Press. 23-49.

Klingenberg, C.P. 1998. Heterochrony and allometry: the analysis of evolutionary change in ontogeny. Biological Reviews, 73:79–123.

Kobayashi, S., Takahashi, H.E., Ito, A., Saito, N., Nawata, M., Horiuchi, H., Ohta, H., Ito, A., Iorio, R., Yamamoto, N. and Takaoka, K. 2003. Trabecular minimodeling in human iliac bone. Bone, 32(2):163-169.

Koch, A.L. 1969. The logarithm in biology. II. Distributions simulating the lognormal. J Theor Biol, 23:251-268.

Kothari, M., Keaveny, T.M., Lin, J.C., Newitt, D.C., Genant, H.K. and Majumdar, S. 1998. Impact of Spatial Resolution on the Prediction of Trabecular Architecture Parameters. Bone, 22:437-443.

Kowalski, C.J. and Guire, K.E. 1974. Longitudinal data analysis. Growth, 38:131-69.

Kuhn, J.L., Goulet, R.W., Pappas, M. and Goldstein, S.A. 1990. Morphometric and anisotropic symmetries of the canine distal femur. J Orthop Res, 8(5):776-780.

Kummer, B. 1972. Biomechanics of bone. In: Fung YC, Perrone N, Anlicker M., eds. Biomechanics: its Foundations and Objectives. Englewood Cliffs, NJ: Prentice Hall. 237–271.

Laird, A.K. 1965. Dynamics of relative growth. Growth, 32:347-354.

Lande, R. 1979. Quantitative genetic analysis of multivariate evolution, applied to brain: body size allometry. Evol, 33:402-416.

Lande, R. 1985. Genetic and evolutionary aspects of allometry. In: W. L. Jungers, ed. Size and scaling in primate biology. New York. Plenum Press 21-32.

Lapicque, L. 1907. Tableau général des poids somatiques et encéphaliques dans les espèces animales. Bull Mém Soc Anthropol Paris, 5e série, 9:248–269.

Larson, S.G. and Stern, J.T. 1986. EMG of scapulohumeral muscles in the chimpanzee during reaching and `arboreal' locomotion. Am J Anat, 176:171-190.

Latash, M.L. 1993. Control of movement. Champaign, Ilinois. Human Kinetics publishers.

Laurenson, R.D. 1964. The primary ossification of the human ilium. Anat Rec, 148:209-217.

Laurenson, R.D. 1965. Development of the acetabular roof in the fetal hip; an arthrographic and histological study. J Bone Joint Surg Am, l(47):975-983.

LaVelle, M. 1995. Natural selection and developmental sexual variation in the human pelvis. Am J Phys Anthropol, 98:59-72.

Le, H. and Kendall, D.G. 1993. The Riemannian structure of Euclidean shape spaces: A novel environment for statistics. Ann. Stat, 21:1225-1271.

Le Gros Clarke, W.E. 1955. The os innominatum of the recent Ponginae with special reference to the Australopithecinae. Am J Phys Anthropol, 13:19-27.

Leigh, S.R. 1992. Cranial capacity evolution in *Homo erectus* and early *Homo sapiens*. Am J Phys Anthropol, 87:1−13.

Leigh, S.R. 1994. Ontogenetic correlates of diet in anthropoid primates. Am J Phys Anthropol, 94:499-522.

Leigh, S.R. and Shea, B.T. 1996a. Ontogeny of body size variation in African apes. Am J Phys Anthropol, 99:43-65.

Leigh, S.R. and Shea, B.T. 1996b. Size and ontogeny in African apes. Am J Phys Anthropol, 101(4):455-474.

Leigh, S.R. 1996. Evolution of human growth spurts. Am J Phys Anthropol, 101(4):455-474.

Lieberman, D.E. 1992. Making behavioral and phylogenetic inferences from hominid fossils: Considering the developmental influence of mechanical forces. Ann Rev Anthropol, 26:185–210.

McHenry, H.M. and Corruccini, R.S. 1975. Distal humerus in hominoid evolution. Folia Primatol, 23:117-44.

Lespessailles, E., Jacquet, G., Harba, R., Jennane, R., Loussot, T., Viala, J.F. and Benhamou, C.L. 1996. Anisotropy measurements obtained by fractal analysis of trabecular bone at the calcaneus and radius. Rev Rhum Engl Ed (Joint Bone Spine Diseases), 63(5):337-343.

Lespessailles, E., Roux, J.P., Benhamou, C.L., Arlot, M.E., Eynard, E., Harba, R., Padonou, C. and Meunier, P.J. 1998. Fractal analysis of bone texture on os calcis radiographs compared with trabecular microarchitecture analyzed by histomorphometry. Calcif Tissue Int, 63(2):121-5.

Leutenegger, W. 1973. Maternal-fetal weight relationships in primates. Folia Primatol, 20:280-293.

Leutenegger, W. 1974. Functional aspects of pelvic morphology in simian primates. J Hum Evol, 3:207-222.

Levington, J. 1988. Genetics, palaeontology and macroevolution. Cambridge. Cambridge University Press.

Lieberman, D.E. 1996. How and why humans grow thin skulls: Experimental evidence for systemic cortical robusticity. Am J Phys Anthropol, 101(2):217-236

Lieberman, D.E. and Crompton, A.W. 1998. Responses of bone to stress. In: Wiebel E, Taylor C , Bolis L, eds. *Principles of biological design: the optimization and symmorphosis debate*. Cambridge: Cambridge University Press. 78-86.

Lovejoy, C.O., Heiple, K.G. and Burstein, A.H. 1973. The gait of Australopithecus. Am J Phys Anthropol, 38(3):757-779.

Loy, A., Corti, M., Marcus, L.F. 1993. Landmark data: size and shape analysis in systematics. A case study on Old World Tapidae (Mammalia, Insectivira). In: L.F. Marcus, E. Bello, A Garcia-Valdecasas, eds. *Contributions to morphometrics*. Museo Nacional de Ciencias Naturales, Madrid. 213-240.

Lumer, H, and Schultz AH (1941) Relative growth of the limb segments and tail in macaques. Hum. Biol, 13:283-305.

Macchiarelli, R., Bondioli, L., Galichon, V. and Tobias, P.V. 1999. Hip bone trabecular architecture shows uniquely distinctive locomotor behaviour in South African australopithecines. J Hum Evol, 36:211-32.

Macchiarelli, R., Rook, L. and Bondioli, L. 2001. Comparative analysis of iliac trabecular architecture in extant and fossil primates by means of digital image processing techniques: implications for the reconstruction of fossil locomotor behaviours. In: L. de Bonis, G. Koufos, P. Andrews, eds. Phylogeny of the Neogene Hominoid Primates of Eurasia. London. Cambridge University Press. 60-101.

Macho, G. A., Abel, R. L., Schutkowski, H. 2005. Age changes in bone microstructure: do they occur uniformly? Int J of Osteoarch. 15(6):421-430.

MacLane, S. 1995. *Homology*. Berlin. Springer.

MacLatchy, L. and Muller, R. 2002. A comparison of the femoral head and neck trabecular architecture of *Galago* and *Perodicticus* using micro-computed tomography (μCT). J Hum Evol, 43(1):89-106.

Majumdar, S., Kothari, M., Augat, P., Newitt, D.C., Link, T.M., Lin, J.C., Lang, T., Lu, Y. and Genant, H.K.1998. High-Resolution Magnetic Resonance Imaging: Three-Dimensional Trabecular Bone Architecture and Biomechanical Properties. Bone, 22(5):445-454.

Manaster, B.J. 1979. Locomotor adaptations within the Cercopithecus Genus: a multivariate approach. Am J Phys Anthropol, 50(2):169-182.

Mardia, K.V. 1970. Measures of multivariate skewness and kurtosis with applications. Biometrika, 57:519-530.

Martin, R.B., Burr, D.B. and Sharkey, N.A. 1998. Skeletal tissue mechanics. New York: Springer-Verlag.

Martinon-Torres, M. 2003. Quantifying trabecular orientation in the pelvic cancellous bone of modern humans, chimpanzees, and the Kebara 2 Neanderthal. Am J Hum Biol, 15(5):647-661.

Mazess, R.B., Whedon. G.D. 1983. Immobilization and bone. Calcif Tissue Int, 35(3):265-267.

McColl, D.J., Abel, R.L., Spears, I.R. and Macho, G.A. 2006. Automated method to measure trabecular thickness from microcomputed tomographic scans and its application. Anat Rec A Discov Mol Cell Evol Biol. 288: 982-8.

McHenry, H.M. and Corruccini, R.S. 1975. Distal humerus in hominoid evolution. Folia Primatol, 23:117-44.

McKinney, M.L. 1990. Trends in body size evolution. In: McNamara, K. J., ed. Evolutionary trends. Tuscon: University of Arizona Press. 75–118.

Mednick, L.W. 1955. The evolution of the human ilium. Am J Phys Anthropol, 13(2):203-216.

Medawar, P.B. 1945. Size, shape and age. In: WE LeGros Clark, PB Medawar, eds. Essays on Growth and Form. Oxford. Clarendon. 157–87.

Meldrum, D.J. 1991. Kinematics of the cercopithecine foot on arboreal and terrestrial substrates with implications for the interpretation of hominid terrestrial adaptations. Am J Phys Anthropol, 84(3):273-289.

von Meyer, G.H. 1867. Die Architektur der Spongiosa. Arch Anat Phys Wiss Med, 34:615-628.

Mitteroecker, P., Gunz, P., Weber, G.W. and Bookstein, F.L. 2004. Regional dissociated heterochrony in multivariate analysis. Ann Anat, 186:463-470.

Mori, T., Okimoto, N., Sakai, A., Okazaki, Y., Nakura, N., Notomi, T. and Nakamura, T. 2003. Climbing exercise increases bone mass and trabecular bone turnover through transient regulation of marrow osteogenic and osteoclastogenic potentials in mice. J Bone Miner Res, 18(11):2002-2009.

Mosimann, J. E. 1970. Size Allometry: Size and Shape Variables with Characterizations of the Lognormal and Generalized Gamma Distributions. ASA, 65(330):930-945.

Mueller, W.H. and Martorell, R. 1988. Reliability and accuracy of measurement. In: TG Lohman, AF Roche and R Martorell, eds. Anthropometric Standardisation Reference Manual. Champaign, IL: Human Kinetics Books. 83–86.

Mueller, R., Hahn, M., Vogel, M., Delling, G. and Rueegsegger, P. 1996. Morphometric analysis of noninvasively assessed bone biopsies: Comparison of high resolution computed tomography and histologic sections. Bone, 18(3):215-220.

Muller, R., Gerber, S.C. and Hayes, W.C. 1998. Micro-compression: a novel technique for the nondestructive assessment of local bone failure. Technol Health Care, 6(5-6):433-444.

Napier, J.R. 1967. Evolutionary aspects of primate locomotion. Am J Phys Anthropol, 27:333-342.

Nilsson, O., Marino, R., De Luca, F., Phillip, M. and Baron, J. 2005. Endocrine Regulation of the Growth Plate. Horm Res, 64:157-165.

Odgaard, A. 1997. Three-dimensional methods for quantification of cancellous bone architecture. Bone 20(4):315-328.

Odgaard, A., Jensen, E.B., Gundersen, H.J. 1990. Estimation of structural anisotropy based on volume orientation. A new concept. J Microsc, 57(2):149-162.

Odgaard, A., Kabel, J., van Rietbergen B, Dalstra M, Huiskes R. 1997. Fabric and elastic principal directions of cancellous bone are closely related. J Biomech. 30(5):487-95.

O'Higgins, P. 1999. Ontogeny and phylogeny: morphometric approaches to the study of skeletal growth and evolution. In Chaplain, M. A. J., Singh, G. D. & McLachlan, J. (Eds) On growth and form: spatio-temporal patterning in biology, 373-393.. London: John Wiley.

O'Higgins, P. and Collard, M. 2002. Sexual dimorphism and facial growth in papionin monkeys. J Zool, 257:255-272.

Ohlsson, C., Nilsson, A., Isaksson, O.G. and Lindahl, A. 1992. Effect of growth hormone and insulin-like growth factor-I on DNA synthesis and matrix production in rat epiphyseal chondrocytes in monolayer culture. J Endocrinol, 133:291-300.

Owan, I., Burr, D.B., Turner, C.H., Qiu, J., Tu, Y., Onyia, J.E. and Duncan, R. 1997. Mechanotransduction in bone: osteoblasts are more responsive to fluid forces than mechanical strain L. Am J Physiol, 273; (3,1):C810-C815.

Oxnard, CE. 1978. One Biologist's View Of Morphometrics. Ann Rev Ecol Syst, 9:219-241.

Oxnard, C.E. 1993. Bone and bones, architecture and stress, fossils and osteoporosis. J Biomech, 26 (suppl. 1):63-79.

Oxnard, C.E. and Yang ,H.C. 1981. Beyond biometrics: studies of complex biological patterns. Symp Zool Soc Lond, 46:127-167.

Pagel, M.D. and Harvey, P.H. 1993. Evolution of the juvenile period in mammals. In: ME Pereira and LA Fairbanks, eds. Juvenile Primates. New York: Oxford University Press. 28-37.

Palastanga, N. 2006. Anatomy and Human Movement (5th edition), Structure and Function. London. Butterworth-Heinemann.

Pauwels, F. 1980. *Biomechanics of the locomotor apparatus*. Berlin: Springer Verlag.

Pearson, O.M. and Lieberman, D.E. 2004. The aging of Wolff's "law": Ontogeny and responses to mechanical loading in cortical bone. Am J Phys Anthropol, (suppl) 39:63-99.

Penin, X. and Berge, C. 2001. Heterochronia via procrustean superimposition: application to the skulls of Homonidae primates. C R Acad Sci III, 324:87-93.

Penin X, Berge C, Baylac M. 2002. Ontogenetic study of the skull in modern humans and the common chimpanzees: neotenic hypothesis reconsidered with a tridimensional Procrustes analysis. Am J Phys Anthropol, 118(1):50-62.

Pezard, A. 1918. Le conditionement physiologique des caracteres sexuels secondaires chez les oiseaux. Bull Biol Fr Belg, 52:1-176.

Ponseti, I.V. 1978a. Morphology of the acetabulum in congenital dislocation of the hip. Gross, histological and roentgenographic studies. J Bone Joint Surg Am, 60 (5):586-599.

Ponseti, I.V. 1978b. Growth and development of the acetabulum in the normal child. Anatomical, histological, and roentgenographic studies. J Bone Joint Surg Am, 60 (5):575-585.

Pontzer, H., Lieberman, D.E., Momin, E., Devlin, M.J., Polk, J.D., Hallgrimsson, B. and Cooper, D.M. 2006. Trabecular bone in the bird knee responds with high sensitivity to changes in load orientation. J Exp Biol, 209 (1):57-65.

Preuschoft, H. 2004. Mechanisms for the acquisition of habitual bipedality: are there biomechanical reasons for the acquisition of upright bipedal posture? J Anat, 204(5):363-84.

Profant, L. 1995. Historical allometric inputs to interspecific patterns of craniofacial diversity in the cercopithecine tribe Papionini. Am J Phys Anthropol (suppl. 20), 175.

Rao, C. R. 1964. The use and interpretation of principal component analysis in applied research. Sankhya A, 26:329-358.

Rasband, W.S., 1997. Image processing and analysis in Java. [online] Research Service Branch, J.U.S. National Institutes of Health, Bethesda, Maryland, USA. Available from: http://rsb.info.nih.gov/ij/, 1997-2006. [Accessed 15.1105].

Ravosa, M.J., David, M., Meyers, K.E. and Glander T.I. 1993. Relative growth of the limbs and trunk in sifakas: Heterochronic, ecological, and functional considerations. Am J Phys Anthropol, 92(4):499-520.

Ravosa, M.J. and Profant, L.P. 2000. Evolutionary morphology of the skull in Old World monkeys. In: P. F. Whitehead & C. J. Jolly, eds. Old World Monkeys. New York: Cambridge University Press. 237–268.

Reiter, E.O. and Grumbach, M.M. 1982. Neuroendocrine control mechanisms and the onset of puberty. Ann Rev Physiol, 44:595-613.

Remis, M. 1995. Effects of body size and social context on the arboreal activities of lowland gorillas in the Central African Republic. Am J Phys Anthropol, 97 (4):413-433.

Reeve, E.C.R. and Huxley, J.S. 1945. Some problems in the study of allometric growth. In: W.E. Le Gros Clarke and P. Medawar eds. Essays on growth and form presented to D'Arcy Wentworth Thompson. Oxford. Clarendon Press. 121-156.

Rice, S.H. 1997. The analysis of ontogenetic trajectories: When a change in size or shape is not heterochrony. Proc Nat Acad Sci U S A, 94(3):907-912.

Richardson, M.K., Chipman, A.D. 2003. Developmental constraints in a comparative framework: A test case using variations in phalanx number during amniote evolution. J Exp Zool Part B: Mol Dev Evol, 296(1):8-22.

Ries, M., Pugh, J., Au, J.C., Gurtowski, J. and Dee, R. 1989a. Cortical pelvic strains with varying size hemiarthroplasty in vitro. J Biomech, 22:775-780.

Ries, M., Pugh, J., Au, J.C., Gurtowski, J. and Dee, R. 1989b. Normal pelvic strain pattern in vitro. J Biomed Eng, 11(5):398-402.

Robson-Brown, K.A., Davies, E.N. and McNally, D.S. 2002. The angular distribution of vertebral trabeculae in modern humans, chimpanzees and the Kebara 2 Neanderthal. J Hum Evol, 43(2):189-205.

Rohlf, F.J. and Slice, D.E. 1990. Extensions of the Procrustes method for the optimal superimposition of landmarks. Syst ZAool, 39:40-59

Rohlf, F.J. 1990a. Morphometrics. Ann Rev Ecol Syst, 21:299-316.

Rohlf, F.J. 1990b. Rotational fit (Procrustes) methods. Proc of the Michigan Morphometrics Workshop, University of Michigan Museums, Ann Arbor: 227-236.

Rohlf, F.J. and Marcus, L. 1993. A revolution in morphometrics. Trends Ecol & Evol, 8:129-132.

Rohlf, F.J. 1993. Relative warp analysis and an example of its application to mosquito wings. In: (ed. L.F. Marcus, E. Bello, A Garcia-Valdecasas eds. Contributions to Morphometrics. Museo Nacional de Ciencias Naturales, Madrid. 131-159.

Rohlf, F.J., Loy, A. and Corti, M. 1996. Morphometric analysis of Old World Talpidae (Mammalia, Insectivora) using partial warp scores. Syst Biol, 45:344-362.

Rohlf, F.J. 1999. Shape statistics: Procrustes superimpositions and tangent spaces. J Classif, 16:197-223.

Rohlf, F.L. 2000. Statistical power comparisons among alternative morphometric methods. Am J Phys Anthrop, 111:463–478.

Rohlf, F.J. 2001. Comparative methods for the analysis of continuous variables: geometric interpretations. Evol, 55:2143-2160.

Rook, L., Bondioli, L., Kohler, M., Moya-Sola, S. and Macchiarelli, R. 1999. Oreopithecus was a bipedal ape after all: evidence from the iliac cancellous architecture. Proc Natl Acad Sci U S A. 96(15):8795-8799.

Rook, L., Bondioli, L., Casali, F., Rossi, M., Kohler, M., Moya-Sola, S. and Macchiarelli, R. 2004. The bony labyrinth of *Oreopithecus bambolii.* J Hum Evol, 46:349-356.

Rosas, A. and Bastir, M. 2002. Thin-plate spline analysis of allometry and sexual dimorphism in the human craniofacial complex. Am J Phys Anthropol, 117:236-45.

Rosenberg, K.R. and Trevathan, W.R. 2001. The evolution of human birth. Sci Am, 285:72-77.

Roux W. 1881. Der züchtende Kampf der Teile, oder die "Teilauslese" im Organismus (Theorie der "Funktionellen Anpassung"). Leipzig: Wilhelm Engelmann.

Ruimerman, R., Hilbers, P., van Rietbergen, B. and Huiskes, R. 2005. A theoretical framework for strain-related trabecular bone maintenance and adaptation. J Biomech, 38(4):931-941.

Russ, J.C. 1990. Surface characterization: Fractal dimensions, Hurst coefficients, and frequency transforms. J Comp-Assist Microsc 2(3):161-183.

Russ, J.C. 1994. Fractal surfaces. New York: Plenum Press.

Ruvolo, M. 1997. Genetic Diversity in Hominoid Primates. Ann Rev Anthropol, 26:515-540.

Ryan, T.M. and Ketcham, R.A. 2002. Femoral head trabecular bone structure in two omomyid primates. J Hum Evol, 43(2):241-263.

Ryan, T.M. and Ketcham, R.A. 2005. Angular orientation of trabecular bone in the femoral head and its relationship to hip joint loads in leaping primates. J Morphol, 265(3):249-263.

Salle, B.L., Rauch, F., Travers, R., Bouvier, R. and Glorieux, F.H. 2002. Human fetal bone development: histomorphometric evaluation of the proximal femoral metaphysis. Bone, 30(6):823-828.

Satta, Y., Klein, J. and Takahata, N. 2000. DNA Archives and Our Nearest Relative: The Trichotomy Problem Revisited. Mol Phyl Evol, 14(2):259-275.

Saunders, J., Inman, V.T., Eberhart, H.D. 1953. The major determinants in normal and pathological gait. Bone Joint Surg Am, 35(A):543-558.

Scally, P. 1999. Medical imaging. Oxford : Oxford University Press

Scheuer, L., Black, S. 2000. Developmental Juvenile Osteology. London. Academic Press.

Uhthoff, H.K. 1990. The embryology of the human locomotor system. Berlin Heidelberg New York : Springer.

Scheuer, L. and Black, S. 2000. Developmental Juvenile Osteology. London. Academic Press.

Schultz, A. 1930. The skeleton of the trunk and limbs of higher primates. Hum Biol, 2:203-438.

Schultz, A.1930. The skeleton of the trunk and limbs of higher primates. Hum Biol, 2:203-438.

Schultz, A. 1936. Characters common to higher primates and characters specific for man. Q Rev Biol, 11:259-283 and 425-459.

Schultz, A. 1940. Growth and development of the chimpanzee. Contrib Embryol, 170:1-63.

Schultz, A. 1949. Sex differences in the pelves of higher primates. Am J Phys Anthropol. 7:401-423.

Schwenk, K. and Wagner, G.P. 2001. Function and the evolution of phenotypic stability: Connecting pattern to process. Am Zool, 41(3):552-563.

Segebarth-Orban, R. 1980. An evaluation of the sexual dimorphism of the human innominate bone. J Hum Evol, 9:601–607.

Seeman, E. 2003 Reduced bone formation and increased bone resorption: rational targets for the treatment of osteoporosis. Osteoporos Int. (suppl 3):S2-8.

Shea, B.T. 1981. Relative growth of the limbs and trunk in the African apes. Am J Phys Anthropol, 56:179-201.

Shea, B.T. 1983b. Allometry and heterochrony in the African apes. Am J Phys Anthropol, 62:275-289.

Shea, B.T. 1985a. Bivariate and multivariate growth allometry: statistical and biological considerations. J Zool, 206:367–390.

Shea, B.T. 1985b. Ontogenetic allometry and scaling: A discussion based on the growth and form of the skull in African apes. In: Jungers, W. L. ed. Size and scaling in primate biology. New York. Plenum. 175-205.

Shea, B.T. 1985c. On aspects of skull form in African apes and orangutans, with implications for hominoid evolution. Am J Phys Anthropol, 68:329-342.

Shea, B.T. 1985d. Bivariate and multivariate growth allometry: statistical and biological considerations. J Zool Lond A, 206:367-390.

Shea, B.T.1986. Scapula form and locomotion in chimpanzee evolution. Am J Phys Anthropol, 70(4):475-488.

Shea, B.T. 1988 Heterochrony in primates. In: ML McKinney ed. Heterochrony in Evolution. New York: Plenum. 237-266.

Shefelbine, S.J., Tardieu, C. and Carter, D.R. 2002. Development of the femoral bicondylar angle in hominid bipedalism. Bone, 30(5) 765-770

Sholl, A.D. 1950. The theory of differential growth analysis. Proc R Soc Lon B, 137:470-474.

Slice, D.E., Rohlf, F. J. and Bookstein, F.L. 1996. In: Marcus, L. F., M. Corti, A. Loy, G. Naylor, and D. E. Slice, eds. Advances in Morphometrics. Proceedings of the 1993 NATO Advanced Studies Institute on Morphometrics in Il Ciocco, Italy. New York. Plenum Publishing Corp. 531-551.

Slice, D.E. 1998. Morpheus et al.: software for morphometric research. Revision 01-30-98. Department of Ecology and Evolution, State University of New York, Stony Brook, New York.

Slomianka, L., 2004. Blues histology. School of Anatomy and Human Biology - The University of Western Australia. Available from: http://www.lab.anhb.uwa.edu.au/mb140/CorePages/Bone/Bone.htm. [Accessed 01.05.06.]

Smit, T. H., Odgaard, A. and Schneider, E. 1997. Structure and function of vertebral trabecular bone. Spine, 22:2823-2833.

Smit, T.H., Schneider, E. and Odgaard, A. 1998. Star length distribution: a volume-based concept for the characterization of structural anisotropy. J Microsc, 191(3):249-257.

Smith, R.J. 1980. Rethinking allometry. J Theor Biol, 87:97-111.

Smith, R.J. 1984a. Allometric scaling in comparative biology: problems of concept and method. Am J Physiol, 246:152-160.

Smith, R.J. 1984b. Determination of relative size: the "criterion of subtraction" problem in allometry. J Theor Biol, 108:131-142.

Smith, R.J. 1993. Logarithmic transformation bias in allometry. Am J Phys Anthropol, 90:215-228.

Smith, R.J. 1998. Sexual dimorphism in primate neonatal body mass. J Hum Evol, 34:173-201.

Smith, R.J. and Jungers, W.L. 1997. Body mass in comparative primatology Journal of Human Evolution, 32(6):523-559

Smith, B. H. 1989. Dental development as a measure of life history in primates. Evol B, 43(3):683-688

Smith, B.H. 1991. Dental development and the evolution of life history in Hominidae Am J Phys Anthropol, 86:157–174.

Smith, B.H. 1994. Patterns of dental development in Homo, Australopithecus, Pan, and Gorilla. Am J Phys Anthropol, 94(3):307-325.

Spoor, C.F., Zonneveld, F.W. and Macho, G.A. 1993. Linear measurements of cortical bone and dental enamel by computed tomography: applications and problems. Am J Phys Anthropol, 91(4):469-484.

Stern, J. and Susman, R.L. 1983. The locomotor anatomy of *Australopithecus afarensis*. Am J Phys Anthropol, 60:279-317.

Steudel, K. 1978. A multivariate analysis of the pelvis of early Hominids. J Hum Evol, 7:583-595.

Steudel, K. 1981. Functional aspects of primate pelvic structure: a multivariate approach. Am J Phys Anthropol, 55:399-410.

Steudel, K. 1982. Patterns of intraspecific and interspecific allometry in Old World primates. Am J Phys Anthropol, 59(4):419-430.

Stones, H.H., Lawton, F.E., Bransby, E.R. and Hartley, H.O. 1951. Time of eruption of permanent teeth and time of shedding of deciduous teeth. Br Dent J, 90(1):1-7.

Straus, W. 1927. The human ilium: sex and stock. Am J Phys Anthropol, 11:1-28.

Straus, W. 1929. Studies on primate ilia. Am J Anat, 43:403-460.

Styne, D.M. 2003. The Regulation of Pubertal Growth. Horm Res, 60 (suppl 1):22–26.

Svenningsen, S., Apalset, K., Terjesen, T. and Anda, S. 1989. Osteotomy for femoral anteversion. complications in 95 children. Acta Orthop Scand, 60(4):401-405.

Swartz, S.M., Parker, A. and Huo, C. 1998. Theoretical and empirical scaling patterns and topological homology in bone trabeculae. J Exp Biol, 201(4):573-590.

Swindler, D.R. and Wood, C.D. 1982. Atlas of Primate Gross Anatomy: Baboon, Chimpanzee, and Man. Florida: Robert E. Krieger Publishing Company.

Tague, R.G. 1991. Commonalities in dimorphism and variability in the anthropoid pelvis, with implications for the fossil record. J Hum Evol, 21:153-176.

Tague, R.G. 2005. Big-bodied males help us recognize that females have big pelves. Am J Phys Anthropol, 127:392-405.

Takata, S. and Yasui, N. 2001. Disuse osteoporosis. J Med Invest, 48(3-4):147-156.

Tanck, E., Homminga, J., van Lenthe, G.H. and Huiskes, R. 2001. Increase in bone volume fraction precedes architectural adaptation in growing bone. Bone, 28(6):650-654.

Tanner, J.M. 1955. Growth at adolescence. With a general consideration of the effects of hereditary and environmental factors upon growth and maturation from birth to maturity, 2nd ed. Oxford: Blackwell Scientific.

Tanner, J.M. 1962. Growth at Adolescence. Oxford: Blackwell Scientific Publications.

Tanner, J.M., Whitehouse, R.H. and Takaishi, M. 1966. Standards from birth to maturity for height, weight, height velocity, and weight velocity: British children, 1965. Arch Dis Child. I. 41(219):454-471.

Teissier, G. 1938. Un essai d'analyse factorielle, les variants sexuels de Maja squinada. Biotypologie, 7:73–96.

Thieme, F.P. and Schull, W.J. 1957. Sex determination form the skeleton. Hum Biol, 29:242-273.

Thompson, D'A.W. 1917. On growth and form. Cambridge: Cambridge University press.

Thompson, D'A.W. 1942. On Growth and Form. Cambridge: Cambridge University Press.

Trevathan, W.R. 1988. Fetal emergence patterns an evolutionary perspective. Am Anthropol, 90:19-26.

Tsutakawa, R.K. and Hewett J.E. 1977. Quick test for comparing two populations with bivariate data. Biometrics. 33:215-219.

Turner, C.H., Cowin, S.C., Rho, J.Y., Ashman, R.B. and Rice, J.C. 1990. The fabric dependence of the orthotropic elastic constants of cancellous bone. J Biomech, 23:549-561.

Turner, C.H. 1998. Three rules for bone adaptation to mechanical stimuli. Bone, 23(5):399-407.

Ulijaszek, S.J. and Lourie, J.A. 1994. Intra- and inter-observer error in anthropometric measurement. In: SJ Ulijaszek and CGN Mascie-Taylor, eds. Anthropometry: the Individual and the Population. Cambridge: Cambridge University Press. 30–55.

Ulrich, D., van Rietbergen, B., Laib, A. and Ruegsegger, P. 1999. Load transfer analysis of the distal radius from in-vivo high-resolution CT-imaging. J Biomec, 32:821-828.

Vaananen, H. K., Zhao, H., Mulari, M. and Halleen, J. M. 2000. The cell biology of osteoclast function. J Cell Sci, 113(3):377-382.

Vogl, C. Atchley, W.R. Cowley, D.E. Crenshaw, P. 1993. The epigenetic influence of growth hormone on skeletal development. Growth Development and Aging, 57(3):163-182.

Wagner, G.P. 1989. The biological homology concept. Annu. Rev. Ecol. Syst, 20:51-69.

Wagner, G.P.1994. Homology: The Hierarchical Basis of Comparative Biology,

Walker, J.A. 1996. Principal components of body shape variation with an endemic radiation of threespine stickleback. In: ed. L. F. Marcus, M. Corti, A. Loy, G. Naylor and D. E. Slice, eds. Advances in morphometrics. New York: Plenum Press. 321-334.

Waterman, H. 1929 Studies on the evolution of the pelvis of man and other primates. Bull Am Mus Nat Hist, 12:585-642.

Weidenreich, F. 1913. Ueber das Hüftbein und das Becken der Primaten und ihre Umformung durch den aufrechten Gang. Anat Anz, 44S:497-513.

Weinbaum, S., Cowin, S.C. and Zeng, Y. 1994. A model for the excitation of osteocytes by mechanical loading-induced bone fluid shear stresses. J Biomech, 27:339–360.

Weinreb, M., Rodan, G.A. and Thompson, D.D. 1989. Osteopenia in the immobilized rat hind limb is associated with increased bone resorption and decreased bone formation. Bone, 10(3):187-194.

Wheeler, M.D. 1991. Physical changes of puberty. Endocrinol Metab Clin North Am, 20(1):1-14.

Whitehouse, W.J. 1974. The quantitative morphology of anisotropic trabecular bone. J Microsc, 101:153-168.

Whitehouse, W.J. and Dyson, E.D. 1974. Scanning electron microscope studies of trabecular bone in the proximal end of the human femur. J Anat, 118:417-444.

Witte, H., Eckstein, F. and Recknagel, S. 1997. A calculation of the forces acting on the human acetabulum during walking. Based on in vivo force measurements, kinematic analysis and morphometry. Acta Anat (Basel), 160(4):269-80.

Wolff, J. 1892. Das Gesetz der Transformation der Knochen. Berlin: Hirschwald Verlag.

Wolff, J. 1996. The law of bone remodelling [translated from 1892 original, Das Gesetz der Transformation der Knochen, by P. Maquet and R. Furlong] Berlin: Springer Verlag.

Zander, G. 1943. Os acetabuli and other bone nuclei: periarticular calcifications at the hip joint. Acta Radiol, 24:317-327.

Zelditch, M.L., Sheets, H.D. and Fink, W.L. 2000. Spatiotemporal reorganization of growth rates in the evolution of ontogeny. Evol, 54:1363–1371.

Zonneveld, F.W. 1987. Computed tomography of the temporal bone and orbit. Munich. Urban and Schwarzenberg.

Zuckerman, S., Ashton, E.H., Flinn, R.M., Oxnard, C.E. and Spence, T.F. 1973. Some locomotor features of the pelvic girdle in primates. Symp Zool Soc Lond, 33:71-165.

PAGE NUMBERING AS ORIGINAL

Appendix

Published papers submitted in support of the thesis.

Cited Literature

Abramoff, M.D., Magelhaes, P.J. and Ram, S.J. 2004. Image Processing with Image J. Biophotonics International. 11(7):36-42.

Albrecht, G.H. 1978. The craniofacial morphology of the Sulawesi macaques: Multivariate approaches to biological problems. Contrib Primatol, 13:1-151.

Anemone, R.L., Watts, E.S. and Swindler, D.R. 1991. Dental development of known-age chimpanzees, *Pan troglodytes* (primates, pongidae). Am J Phys Anthropol, 86 (2):229-241.

Anemone, R.L., Mooney, M.P. and Siegel, M.I. 1996. Longitudinal study of dental development in chimpanzees of known chronological age: Implications for understanding the age at death of Plio-Pleistocene hominids. Am J Phys Anthropol, 99 (1):119-133.

Arnold, S. 1992. Constraints on phenotypic evolution. J Am Natur (suppl), 140 (5): 85.

Atchley, W.R. and Hall, B.K. 1991. A model for development and evolution of complex morphological structures. Biol Rev. 66:101–157.

Atchley, W.R., Plummer, A.A. and Riska, B. 1985. Genetics of mandible form in the mouse. Genetics. 111:555–577.

Augat, P., Link, T., Lang, T.F., Lin, J.C., Majumdar, S. and Genant, H.K. 1998 Anisotropy of the elastic modulus of trabecular bone specimens from different anatomical locations. Med Eng Phys, 20:124-131.

Bacon, A.M. and Baylac, M. 1995. Landmark analysis of distal femoral epiphysis of modern and fossil primates with particular emphasis on *Australopithecus afarensis* (AL 129-1 and AL 333-4). C R Acad Sci [IIA], 321:553-560.

Baker, R.H. and Wilkinson, G.S. 2001. Phylogenetic analysis of sexual dimorphism and eye-span allometry in stalk-eyed flies (Diopsidae). Evol, 55(7):1373–1385.

Bakker, B., van der Eerden, B.C., Koppenaal, D.W., Karperien, M. and Wit, J.M. 2003. Effect of X-irradiation on growth and the expression of parathyroid hormone-related peptide and indian hedgehog in the tibial growth plate of the rat. Horm Res, 59; (1):35-41.

Banse, X., Devogelaer, J.P. and Grynpas, M. 2002. Patient-specific microarchitecture of vertebral cancellous bone: a peripheral quantitative computed tomographic and histological study. Bone, 30(6):829-835.

Beier, F. 2005. Cell-cycle control and the cartilage growth plate. J Cell Physiol, 202(1):1-8.

Berge, C. 1984a. Multivariate analysis of the pelvis for Hominids and other extant primates: Implications for the locomotion and systematics of the different species of australopithecines. J Hum Evol, 13:555-562.

Berge, C. 1984b. Obstetric interpretations of the Australopithecine pelvic cavity. J Hum Evol, 13:573-587.

Berge, C. and Kazmierczak, J.B. 1986. Effects of size and locomotor adaptations on the hominid pelvis: evaluation of australopithecine bipedality with a new multivariate method. Folia Primatol, 46(4):185-204.

Berge, C. 1991. Size and locomotion-related aspects of hominid and anthropoid pelves: An osteometrical approach. Hum Evol, 6:365-376.

Berge, C. 1994. How did the australopithecines walk? A biomechanical study of the hip and thigh of *Australopithecus afarensis*. J Hum Evol, 26:259-273.

Berge, C. 1996. The evolution and growth of the Hominid pelvis. In: L.F. Marcus, M. Corti, A. Loy, G.J.P. Naylor, D. Slice, eds. Advances in morphometrics. New York and London: Plenum Press. 441-448.

Berge, C. 1998. Heterochronic processes in human evolution: an ontogenetic analysis of the hominid pelvis. Am J Phys Anthropol, 105:441-59.

Berge, C. and Penin, X. 2004.Ontogenetic allometry, heterochrony, and interspecific differences in the skull of African apes, using tridimensional Procrustes analysis. Am J Phys Anthropol, 124:124-38.

Biewener, A.A. and Bertram, J.E.A. 1991. Efficiency and optimization in the design of skeletal support systems. In: R. W. Blake, ed. Efficiency and Economy in Animal Physiology. Cambridge. Cambridge University Press. 65–82.

Biewener, A.A., Fazzalari, N.L., Konieczynski, D.D. and Baudinette, R.V. 1996. Adaptive changes in trabecular architecture in relation to functional strain patterns and disuse. Bone, 19:1-8.

Bocquet, C. 1953. Recherches sur le polymorphisme naturel des Jaara marina (Fabr.) (Isopodes asllotes). Essai de systématique evolutive. Arch Zool Exp Gen, 90:187-250.

Bookstein, F.L. 1989. Principal warps: thin-plate splines and the decomposition of deformations. IEEE trans. Pattern Analysis Machine Intelligence, 11:567-585.

Bookstein, F.L. 1990. Higher-order features of shape change for landmark data. In: Proceedings of the Michigan Morphometric Workshop. Special Publication No. 2. Ann Arbor MI, The University of Michigan Museum of Zoology. 237-250.

Bookstein, F.L. 1991. Morphometric Tools for Landmark Data. Geometry and Biology. New York. Cambridge University Press.

Bookstein, F.L. 1993. A brief history of morphometric synthesis. In: Contributions to Morphometrics. Marcus, L.F., Bello, E. and Garcia-Valdecasas, A., eds. Museo Nacional de Ciencias Naturales, Madrid. 15-40.

Bookstein, F.L. 1996a. Combining the tools of geometric morphometrics. In: LF Marcus, M. Corti, A. Loy, G. Naylor, and DE Slice, eds. Advances in morphometrics New York. Plenum. 131–151.

Bookstein, F.L. 1996b. Biometrics, biomathematics and the morphometric synthesis. Bull Math Biol, 58:313-365.

Broeck van den, J.P. 1911. Ueber Geschlechtsunterschiede im Becken bei Primaten. Arch f Anat u Physiol Anatom Abt, 163-184.

Broeck van den, J.P. 1914. Studien zur Morphologie des Primatenbeckens. Gegenbaurs Morphol Jahrb 49:1-118.

Brothwell, D.R. 1981. Digging Up Bones, (3rd edition). New York: Cornell University Press.

Buck, A.M., Price, R.I., Sweetman, I.M. and Oxnard C.E. 2002. An investigation of thoracic and lumbar cancellous vertebral architecture using power-spectral analysis of plain radiographs. J Anat, 200(5):445-56.

Buckland-Wright, J.C., Lynch, J.A., Rymer, J. and Fogelman I. Fractal signature analysis of macroradiographs measures trabecular organization in lumbar vertebrae of postmenopausal women. Calcif Tissue Int, 54(2):106-12.

Burr, D.B., Van Gerven, D.P. and Gustav, B. L.1977. Sexual dimorphism and mechanics of the human hip: A multivariate assessment. Am J Phys Anthropol, 47(2):273-278.

Burr, D.B., Schaffler, M.B. and Frederickson, R.G. 1988. Composition of the cement line and its possible mechanical role as a local interface in human compact bone. J Biomech, 21(11):939-945.

Byers, S., Moore, A.J., Byard, R.W. and Fazzalari, N.L. 2000. Quantitative histomorphometric analysis of the human growth plate from birth to adolescence. Bone, 27(4):495-501.

Caligiuri, P., Giger, M.L., Favus, M.J., Jia, H., Doi, K. and Dixon, L.B. 1993. Computerized radiographic analysis of osteoporosis: preliminary evaluation. Radiology, 186:471-474.

Carlson, K.J. 2005. Investigating the form-function interface in African apes: Relationships between principal moments of area and positional behaviors in femoral and humeral diaphyses. Am J Phys Anthropol, 127:312-34.

Carter, D.R. and Hayes, W.C. 1977a. Compact bone fatigue damage-I. Residual strength and stiffness. J Biomech, 10:325-37.

Carter, D.R. and Hayes, W.C 1977b. Compact bone fatigue damage: a microscopic examination. Clin Orthop Relat Res, 127:265-74.

Clements, E.M.B., Davies-Thomas, E. and Pickett, K.G.1953. Time of Eruption of Permanent Teeth in British Children in 1947-8. Brit. Med J, 1:1421-1424.

Champy, C. 1929. La croissance dysharmonique des caracteres sexuels accessoires. Arch Scie Phys nat Zoologie, 194-244.

Champy, C. 1924. *Sexualite et hormones*. Doin, Paris.

Chappard, D., Legrand, E., Pascaretti, C., Basle, M.F. and Audran, M. 1999. Comparison of eight histomorphometric methods for measuring trabecular bone architecture by image analysis on histological sections. Microsc Res Tech, 1, 45(4-5):303-312.

Cheverud, J.M. 1982a. Relationships among ontogenetic, static, and evolutionary allometry. Am J Phys Anthropol, 59:139-149.

Cheverud, J.M. 1982b. Phenotypic, genetic, and environmental morphological integration in the cranium. Evol. 36:499–516.

Cheverud, J.M. and Buikstra, J.E. 1982. Quantitative genetics of skeletal nonmetric traits in the rhesus macaques on Cayo Santiago. III Relative heritability of skeletal nonmetric and metric traits. Am J Phys Anthropol, 59:151–155.

Clarke, M.R.B. 1980. The reduced major axis of a bivariate sample. Biometrika. 67:441-446.

Cock, A.G. 1966. Genetical aspects of metrical growth and form in animals. Q Rev Biol, 41(2):131-190.

Coe, C. L., Savage, A. and Bromley, L.J. 1992. Phylogenetic influences on hormone levels across the primate order. Am Journal of Primat, 28:81-100.

Correnti, V. 1955. Le basi morfomeccaniche della struttura dell'osso iliaco. Riv Antrop, 42:289-336.

Corti, M. and Rohlf, F.J. 2001. Chromosomal speciation and phenotypic evolution in the house mouse. Biol J Linnaean Society, 73(1085):99-112.

Cowin, S.C., Moss-Salentijn, L. and Moss, M.L. 1991. Candidates for the mechanosensory system in bone. J Biomech Eng, 113:191-197.

Cowin, S.C. and Moss, M.L. 2001. Mechanosensory mechanisms in bone. In: Cowin SC, ed. Bone biomechanics handbook, 2nd ed. Boca Raton: CRC Press. 29-1-29-17.

Cowin, S.C., Weinbaum, S. and Zeng, Y. 1995. A case for bone canaliculi as the anatomical site of strain generated potentials. J Biomech, 28:1281-1297.

Cullen, D.M., Smith, R.T. and Akhter, M.P. 2001. Bone-loading response varies with strain magnitude and cycle number. J Appl Physiol, 91(5):1971-1976.

Currey, J. 1984. The Mechanical Adaptations of Bones. Princeton: Princeton University Press.

Currey, J. D. 1998. Mechanical properties of vertebrate hard tissues. Journal Of Engineering In Medicine. Proc Inst Mech Eng (part H), 212(6):399-412.

Dainton, M. and Macho, G.A. 1999. Did knuckle walking evolve twice? J Hum Evol, 36:171-194.

Davidson, R.M., Lingenbrink, P.A. and Norton, L.A. 1996. Continuous mechanical loading alters properties of mechanosensitive channels in G292 osteoblastic cells. Calcif Tissue Int, 59:500-504.

Davis, G.R. and Wong, F.S. 1996. X-ray microtomography of bones and teeth. Physiol Meas, 17:121-146.

Daughaday, W.H. 1975. Somatomedin levels in human beings. Adv Metab Disord, 8:159-170.

D'Aout, K., Vereecke, E., Schoonaert, K., De Clercq, D., Van Elsacker, L. and Aerts, P. 2004. Locomotion in bonobos (*Pan paniscus*): differences and similarities between bipedal and quadrupedal terrestrial walking, and a comparison with other locomotor modes. J Anat, 204 (5):353-361.

Delaere, O., Kok, V., Nyssen-Behets, C. and Dhem, A. 1992. Ossification of the human fetal ilium. Acta Anat, 143(4):330-334.

Delaere, O. and Dhem, A. 1999. Prenatal development of the human pelvis and acetabulum. Acta Orthop Belg, 65(3):255-260.

Delemarre-van de Waal, H.A., van Coeverden S.C. and Rotteveel, J. 2001. Hormonal determinants of pubertal growth. J Pediatr Endocrinol Metab (suppl. 6),14:1521-1526.

Demes, B., Larson, S.G., Stern, J.T. and Jungers, W.L. 1994. The kinetics of primate quadrupedalism: "hindlimb drive" reconsidered. J Hum Evol, 26(5/6):353-374.

Ding, M., Odgaard, A. and Hvid, I. 1999. Accuracy of cancellous bone volume fraction measured by Micro-CT scanning. J Biomech, 32:323-326.

Ding, M., Odgaard, A., Linde, F. and Hvid, I. 2002. Age-related variations in the microstructure of human tibial cancellous bone. J Orthop Res, 20:615-621.

Ding, M., Odgaard, A. and Hvid, I. 2003. Changes in the three-dimensional microstructure of human tibial cancellous bone in early osteoarthritis. J Bone Joint Surg Br, 85(6):906-912.

Doran, D.M. 1992. The ontogeny of chimpanzee and pygmy behaviour chimpanzee behaviour: a case study of paedomorphism and its behavioural correlates. J Hum Evol, 23:139-157.

Doran, D.M. 1993. Comparative locomotor behavior of chimpanzees and bonobos: The influence of morphology on locomotion. Am J Phys Anthropol, 91(1):83.

Doran, D.M. 1997. Ontogeny of locomotion in mountain gorillas and chimpanzees. J Hum Evol, 32:323-344.

Dryden, I.L. and Mardia, K.V. 1993. Multivariate shape analysis. Sankya, 55(A):460-480.

Dryden, I.L. and Mardia, K.V. 1998. Statistical shape analysis. London: John Wiley and Sons.

Dubois, E. 1897. Sur le rapport de l'encephale avec la grandeur du corps chez les Mammiferes. Bull. Soc Anthropol (4e serie), 8:337-374.

Duncan, R.L., Turner, C.H. 1995. Mechanotransduction and the functional response of bone to mechanical strain. Calci Tiss Int, 57:344-358.

Ebert, T.A. and Russell, M.P. 1994. Allometry and model II nonlinear regression. J Theor Biol, 168:367-372.

Eerden van der, B.C.J., Van de Ven, J., Lowik, C.W., Wit, J.M. and Karperien, M. 2002a. Sex steroid metabolism in the tibial growth plate of the rat. Endo, 143:4048-4055.

Eerden van der, B.C.J., Gevers, E.F., Lowik, C.W., Karperien, M. and Wit, J.M. 2002b. Expression of estrogen receptor α and ß in the epiphyseal plate of the rat. Bone, 30:478–485.

Eerden van der, B.C.J., Karperien, M. and Wit, J.M. 2003. Systemic and Local Regulation of the Growth Plate Endocrine Reviews, 24(6):782-801.

Ehrlich, P.J., Lanyon, L.E. 2002. Mechanical strain and bone cell function: a review. Osteoporos Int, 13(9):688-700.

Everett, C. O. 1952. The Evolution of a Permian Vertebrate Chronofauna. Evolution. 6(2): 181-196.

Fajardo, R.J. and Müller, R. 2001. Three-dimensional analysis of nonhuman primate trabecular architecture using microcomputed tomography. Am J Phys Anthropol, 115:327-336.

Fajardo, R.J., Ryan, T.M. and Kappelman, J. 2002. Assessing the accuracy of high-resolution X-ray computed tomography of primate trabecular bone by comparisons with histological sections. Am J Phys Anthropol, 118(1):1-10.

Fleagle, J.G. 1985. Size and adaptation in primates. In: W.L. Jungers, ed. *Size and Scaling in Primate Biology*. New York: Plenum Press. 1–19.

Ford, C.M. and Keaveny, T.M. 1996. The dependence of shear failure properties of trabecular bone on apparent density and trabecular orientation. J Biomech, 29:1309-1317.

Frieβ, M. 2003. An application of the relative warps analysis to problems in human paleontology - with notes on raw data quality. Image Anal Stereol, 22:63-72.

Frost, H.M. 1987a. Bone "mass" and the "mechanostat": a proposal. Anat Rec, 219(1):1-9.

Frost, H.M. 1987b. The mechanostat: a proposed pathogenic mechanism of osteoporoses and the bone mass effects of mechanical and non mechanical agents. Bone Miner, 2(2):73-85.

Frost, H.M. 1990a. Structural adaptations to mechanical usage (SATMU):1. Redefining Wolff's Law: The bone modeling problem. Anat Rec 226:403-413.

Frost, H.M. 1990b. Structural adaptations to mechanical usage (SATMU):2. Redefining Wolff's Law: The bone remodeling problem. Anat Rec 226:414-422.

Frost, H.M. 1990c. Skeletal structural adaptations to mechanical usage (SATMU): 3. The hyaline cartilage modeling problem. Anat Rec. 1990 Apr;226(4):423-32.

Frost, H.M. 1990d. Skeletal structural adaptations to mechanical usage (SATMU): 4. Mechanical influences on intact fibrous tissues. Anat Rec, 26(4):433-9.

Frost, H.M. 1996. A proposed general model of the "Mechanostat" (suggestions from a new skeletal-biologic paradigm. Anat Rec, 244(2):139-147.

Frost, H.M. 2003. Bone's mechanostat: a 2003 update. Anat Rec Part A, 275:1081-1101.

Frost, H.M., Ferretti, J.L. and Jee, W.S.S. 1998. Perspectives: some roles of mechanical usage, muscle strength, and the mechanostat in skeletal physiology, disease, and research. Calci Tissue Int, 62(1):1-7.

Gavan, J.A. 1967. Eruption of primate deciduous dentition: A comparative study. J Dent Res, 46:984-988.

Gayon, J. 2000. History of the concept of allometry. Am Zool, 40:748–758.

Gebo, D.L. and Sargis, E.J. 1994. Terrestrial adaptations in the postcranial skeletons of guenons. Am J Phys Anthropol, 93(3):341-371.

Genoves, S. 1959. Diferencia sexuales en el hueso coxal. University Nacional Autonoma de Mexico: Instituto de Historia, Mexico City.

Gibbs, S., Collard, M. and Wood, B. 2002. Soft-tissue anatomy of the extant hominoids: a review and phylogenetic analysis. J Anat, 200(part 1):3-50.

Giesen, E. B. W. Ding, M. Dalstra, M. van Eijden, T. M. G. J. 2003. Architectural measures of the cancellous bone of the mandibular condyle identified by principal components analysis. Calcif Tissue Int, 73(3):225-231.

Goldstein, S.A., Goulet, R. and McCubbrey, D. 1993. Measurement and Significance of Three-Dimensional Architecture to the Mechanical Integrity of Trabecular Bone. Calci Tissue Int, 53 (supp1):S127.

Goodall, C.R. 1991. Procrustes methods and the statistical analysis of shape. J. Royal Statistical Soc (B), 53:285-340.

Gould, S.J. 1966. Allometry and size in ontogeny and phylogeny. Biol Rev Cam Phil Soc, 41:587-640.

Gould, S.J. 1971. Geometric similarity in allometric growth: a contribution to the problem of scaling in the evolution of size. Am Nat, 105:113-136.

Gould, S.J. 1977. Ontogeny and Phylogeny. Cambridge. Mass. Harvard University Press.

Gower, J.C. 1971. A general co-efficient of similarity and some of its properties. Biometrics, 27:857-871.

Gower, J.C. 1975. Generalised Procrustes analysis. Psychometrika, 40:33-50.

Grumbach, M.M., Bin-Abbas, B.S. and Kaplan, S.L. 1998. The Growth Hormone Cascade: Progress and Long-Term Results of Growth Hormone Treatment in Growth Hormone Deficiency. Horm Res, 49(Suppl.2):41-57.

Gugino, L.D., Aglio, L. S., Raymond, S. A., Romero, R., Ramirez, M., Gonzalez, A. and Black, P M. 2001. Intraoperative cortical function localization techniques. Cerebral cortical surgery with functional mapping. Tech Neurosurg, 7(1):19-32.

Hall, B. K. 1991a. Bone matrix and bone-specific products. Boca Raton. CRC Press.

Hall, B. K. 1991b. The Osteoclast .Boca Raton. Boca Raton. CRC Press.

Hall, B. K. 1992a. Bone growth A. Boca Raton. CRC Press.

Hall, B. K.1992b. Bone metabolism and mineralisation. Boca Raton. CRC Press.

Hall, B. K. 1993. Bone Growth B. Boca Raton. CRC Press.

Hager, L.D. 1996. Sex differences in the sciatic notch of great apes and modern humans. Am J Phys Anthropol, 99:287-300.

Hammer, Ø., Harper, D.A.T., and P. D. Ryan, 2001. PAST: Paleontological Statistics Software Package for Education and Data Analysis. Palaeontologia Electronica 4(1): 9pp. http://palaeo-electronica.org/2001_1/past/issue1_01.htm. [Accessed 01.05.06].

Han, Y., Cowin, S.C., Schaffler, M.B. and Weinbaum, S. 2004. Mechanotransduction and strain amplification in osteocyte cell processes. Proc Nat Acad Sci U S A, 101(47):16689-16694.

Hara, T., Tanck, E., Homminga, J. and Huiskes R. 2002. The influence of microcomputed tomography threshold variations on the assessment of structural and mechanical trabecular bone properties. Bone, 31(1):107-109.

Harrigan, T.P. and Mann, R.W. 1984. Characterization of microstructural anisotropy in orthotropic materials using a second rank tensor. J Mat Sci, 19(3):761–767.

Henderson, J. 2005. Ernest Starling and 'Hormones': an historical commentary. J Endocrinol, 184:5–10.

Herring, S.W. 1993a. Epigenetic and functional influences on skull growth. In Hanken J, Hall BK (eds) The Skull, vol 1, pp 153–206. Chicago: University of Chicago Press.

Herring, S.W. 1993b. Formation of the vertebrate face: epigenetic and functional influences. Am Zool, 33: 372-483.

Hotelling, H. 1936. Relations between two sets of variates. Biometrika, 28:321-377

Hott, M., Deloffre, P., Tsouderos, Y. and Marie, P.J. 2003. S12911-2 reduces bone loss induced by short-term immobilization in rats. Bone, 33(1):115-123.

Hou, J.C., Salem, G.J., Zernicke, R.F. and Barnard, R.J. 1990. Structural and mechanical adaptations of immature trabecular bone to strenuous exercise. J Appl Physiol, 69(4):1309-1314.

Hoyle, M.H. 1973. Transformations-An introduction and a bibliography. ISR, 41:203-223.

Hunt, KD. 1991. Mechanical implications of chimpanzee positional behavior Am J Phys Anthropol, 86(4):521-536.

Hunt, K.D. 1992. Positional behaviour of Pan troglodytes in the Mahale Mountains and Gombe Stream National Parks, Tanzania. Am J Phys Anthropol, 87(1):83-105.

Hunt K.D. 1994. Body Size Effects on Vertical Climbing Among Chimpanzees. Int J Primatol, 15(6):855-865.

Hunter, W.S. 1990. Heredity in the craniofacial complex. In Enlow DH (ed), Facial Growth, pp 249–266. Philadelphia: WH Saunders.

Huxley, J.S. 1924. Constant differential growth-ratios and their significance. Nature, 114:895-896.

Huxley, J.S. 1932. Problems of relative growth. Methuen ed. London. Reprinted 1993, John Hopkins University Press.

Huxley, J.C. and Teissier, G. 1936a. Terminology of relative growth. Nature, 137:780-781.

Huxley, J.C. and Teissier, G. 1936b. Terminologie et notation dans la description de la croissance relative. Comptes Rendus Eances Soc Biol Fil, 121:934-937.

Inman, V.T., Ralston, H.J. and Todd, F. 1981. Human walking. Baltimore: Williams and Wilkins.

Ito, M., Nishida, A., Nakamura, T., Uetani, M. and Hayashi, K. 2002. Differences of three dimensional trabecular microstructure in osteopenic rat models caused by ovariectomy and neurectomy. Bone. 30(4):594-598.

Iwamoto, J., Yeh, J.K., Aloia, J.F. 1999. Differential effect of treadmill exercise on three cancellous bone sites in the young growing rat. Bone, 24(3):163-169.

Jacobs, C.R., Yellowley, C.E., Davis, B.R., Zhou, Z., Cimbala, J.M. and Donahue, H.J. 1998. Differential effect of steady versus oscillating flow on bone cells. J Biomech, 31:969-976.

Jaecks G. S. and Carlson, S.J. 2001. How phylogenetic inference can shape our view of heterochrony: examples from thecideide brachiopods Paleobiology, 27(2):205–225.

Jamison, P.L. and Ward, R.E. 1993. Brief communication: Measurement size, precision, and reliability in craniofacial anthropometry: Bigger is better. Am J Phys Anthropol, 90(4):495-500.

Jee, W.S., Li, X.J., Schaffler, M.B. 1991. Adaptation of diaphyseal structure with aging and increased mechanical usage in the adult rat: A histomorphometrical and biomechanical study. Anat Rec, 230(3):332-338.

Jensen, E.B. and Gundersen, H.J.G. 1985. The stereological estimation of moments of particle volume. J Appl Probab, 22(1):82-98.

Jolicoeur, J. 1963. The multivariate generalization of the allometry equation. Biometrics, 19:497-499.

Jolicoeur, P. and Mosimann, J.E. 1960. Size and shape variation in the painted turtle. A principal component analysis. Growth, 24:339-354.

Jungers, W.L. and Hartmann, S.E. 1988. Relative growth of the locomotor skeleton in orang-utans and other large-bodied hominoids. 347–359, In: Schwartz, J.H., ed. Orang-utan Biology, Oxford University Press.

Kamibayashi, L., Wyss, U.P., Cooke, T.D. and Zee, B. 1995. Changes in mean trabecular orientation in the medial condyle of the proximal tibia in osteoarthritis. Calcif Tissue Int, 57(1):69-73.

Kappelman, J. 1996. The evolution of body mass and relative brain size in fossil hominids. J Hum Evol, 30:243–276.

Katz, M.J. 1980. Allometry formula: a cellular model. Growth, 44:89-96.

Keen, M. 1993. Early Development and Attainment of Normal Mature Gait. J Pros Orth, 5:35-38.

Kendall, D.G. 1984. Shape manifolds, procrustean metrics and complex projective spaces. Bull Lond Math Soc, 16:81-121.

Kent, J.T. 1994. The complex Bingham distribution and shape analysis J Roy Statist Soc (B), 56:285-299.

Kleerekoper, M., Villanueva, A.R., Stanciu, J., Rao, D.S. and Parfitt, A.M. 1985. The role of three-dimensional trabecular microstructure in the pathogenesis of vertebral compression fractures. Calcif Tissue Int. 37(6):594-7.

Klingenberg, C.P. 1996a. Individual variation of ontogenies: a longitudinal study of growth and timing. Evol, 50:2412-2428.

Klingenberg, C.P. 1996b. Multivariate allometry. In: L. F. Marcus, M. Corti, A. Loy, G. J. P. Naylor and D. E. Slice, eds. Advances in morphometrics. New York. Plenum Press. 23-49.

Klingenberg, C.P. 1998. Heterochrony and allometry: the analysis of evolutionary change in ontogeny. Biological Reviews, 73:79–123.

Kobayashi, S., Takahashi, H.E., Ito, A., Saito, N., Nawata, M., Horiuchi, H., Ohta, H., Ito, A., Iorio, R., Yamamoto, N. and Takaoka, K. 2003. Trabecular minimodeling in human iliac bone. Bone, 32(2):163-169.

Koch, A.L. 1969. The logarithm in biology. II. Distributions simulating the lognormal. J Theor Biol, 23:251-268.

Kothari, M., Keaveny, T.M., Lin, J.C., Newitt, D.C., Genant, H.K. and Majumdar, S. 1998. Impact of Spatial Resolution on the Prediction of Trabecular Architecture Parameters. Bone, 22:437-443.

Kowalski, C.J. and Guire, K.E. 1974. Longitudinal data analysis. Growth, 38:131-69.

Kuhn, J.L., Goulet, R.W., Pappas, M. and Goldstein, S.A. 1990. Morphometric and anisotropic symmetries of the canine distal femur. J Orthop Res, 8(5):776-780.

Kummer, B. 1972. Biomechanics of bone. In: Fung YC, Perrone N, Anlicker M., eds. Biomechanics: its Foundations and Objectives. Englewood Cliffs, NJ: Prentice Hall. 237–271.

Laird, A.K. 1965. Dynamics of relative growth. Growth, 32:347-354.

Lande, R. 1979. Quantitative genetic analysis of multivariate evolution, applied to brain: body size allometry. Evol, 33:402-416.

Lande, R. 1985. Genetic and evolutionary aspects of allometry. In: W. L. Jungers, ed. Size and scaling in primate biology. New York. Plenum Press 21-32.

Lapicque, L. 1907. Tableau général des poids somatiques et encéphaliques dans les espèces animales. Bull Mém Soc Anthropol Paris, 5e série, 9:248–269.

Larson, S.G. and Stern, J.T. 1986. EMG of scapulohumeral muscles in the chimpanzee during reaching and `arboreal' locomotion. Am J Anat, 176:171-190.

Latash, M.L. 1993. Control of movement. Champaign, Ilinois. Human Kinetics publishers.

Laurenson, R.D. 1964. The primary ossification of the human ilium. Anat Rec, 148:209-217.

Laurenson, R.D. 1965. Development of the acetabular roof in the fetal hip; an arthrographic and histological study. J Bone Joint Surg Am, l(47):975-983.

LaVelle, M. 1995. Natural selection and developmental sexual variation in the human pelvis. Am J Phys Anthropol, 98:59-72.

Le, H. and Kendall, D.G. 1993. The Riemannian structure of Euclidean shape spaces: A novel environment for statistics. Ann. Stat, 21:1225-1271.

Le Gros Clarke, W.E. 1955. The os innominatum of the recent Ponginae with special reference to the Australopithecinae. Am J Phys Anthropol, 13:19-27.

Leigh, S.R. 1992. Cranial capacity evolution in *Homo erectus* and early *Homo sapiens*. Am J Phys Anthropol, 87:1−13.

Leigh, S.R. 1994. Ontogenetic correlates of diet in anthropoid primates. Am J Phys Anthropol, 94:499-522.

Leigh, S.R. and Shea, B.T. 1996a. Ontogeny of body size variation in African apes. Am J Phys Anthropol, 99:43-65.

Leigh, S.R. and Shea, B.T. 1996b. Size and ontogeny in African apes. Am J Phys Anthropol, 101(4):455-474.

Leigh, S.R. 1996. Evolution of human growth spurts. Am J Phys Anthropol, 101(4):455-474.

Lieberman, D.E. 1992. Making behavioral and phylogenetic inferences from hominid fossils: Considering the developmental influence of mechanical forces. Ann Rev Anthropol, 26:185–210.

McHenry, H.M. and Corruccini, R.S. 1975. Distal humerus in hominoid evolution. Folia Primatol, 23:117-44.

Lespessailles, E., Jacquet, G., Harba, R., Jennane, R., Loussot, T., Viala, J.F. and Benhamou, C.L. 1996. Anisotropy measurements obtained by fractal analysis of trabecular bone at the calcaneus and radius. Rev Rhum Engl Ed (Joint Bone Spine Diseases), 63(5):337-343.

Lespessailles, E., Roux, J.P., Benhamou, C.L., Arlot, M.E., Eynard, E., Harba, R., Padonou, C. and Meunier, P.J. 1998. Fractal analysis of bone texture on os calcis radiographs compared with trabecular microarchitecture analyzed by histomorphometry. Calcif Tissue Int, 63(2):121-5.

Leutenegger, W. 1973. Maternal-fetal weight relationships in primates. Folia Primatol, 20:280-293.

Leutenegger, W. 1974. Functional aspects of pelvic morphology in simian primates. J Hum Evol, 3:207-222.

Levington, J. 1988. Genetics, palaeontology and macroevolution. Cambridge. Cambridge University Press.

Lieberman, D.E. 1996. How and why humans grow thin skulls: Experimental evidence for systemic cortical robusticity. Am J Phys Anthropol, 101(2):217-236

Lieberman, D.E. and Crompton, A.W. 1998. Responses of bone to stress. In: Wiebel E, Taylor C , Bolis L, eds. *Principles of biological design: the optimization and symmorphosis debate*. Cambridge: Cambridge University Press. 78-86.

Lovejoy, C.O., Heiple, K.G. and Burstein, A.H. 1973. The gait of Australopithecus. Am J Phys Anthropol, 38(3):757-779.

Loy, A., Corti, M., Marcus, L.F. 1993. Landmark data: size and shape analysis in systematics. A case study on Old World Tapidae (Mammalia, Insectivira). In: L.F. Marcus, E. Bello, A Garcia-Valdecasas, eds. *Contributions to morphometrics*. Museo Nacional de Ciencias Naturales, Madrid. 213-240.

Lumer, H, and Schultz AH (1941) Relative growth of the limb segments and tail in macaques. Hum. Biol, 13:283-305.

Macchiarelli, R., Bondioli, L., Galichon, V. and Tobias, P.V. 1999. Hip bone trabecular architecture shows uniquely distinctive locomotor behaviour in South African australopithecines. J Hum Evol, 36:211-32.

Macchiarelli, R., Rook, L. and Bondioli, L. 2001. Comparative analysis of iliac trabecular architecture in extant and fossil primates by means of digital image processing techniques: implications for the reconstruction of fossil locomotor behaviours. In: L. de Bonis, G. Koufos, P. Andrews, eds. Phylogeny of the Neogene Hominoid Primates of Eurasia. London. Cambridge University Press. 60-101.

Macho, G. A., Abel, R. L., Schutkowski, H. 2005. Age changes in bone microstructure: do they occur uniformly? Int J of Osteoarch. 15(6):421-430.

MacLane, S. 1995. *Homology*. Berlin. Springer.

MacLatchy, L. and Muller, R. 2002. A comparison of the femoral head and neck trabecular architecture of *Galago* and *Perodicticus* using micro-computed tomography (μCT). J Hum Evol, 43(1):89-106.

Majumdar, S., Kothari, M., Augat, P., Newitt, D.C., Link, T.M., Lin, J.C., Lang, T., Lu, Y. and Genant, H.K.1998. High-Resolution Magnetic Resonance Imaging: Three-Dimensional Trabecular Bone Architecture and Biomechanical Properties. Bone, 22(5):445-454.

Manaster, B.J. 1979. Locomotor adaptations within the Cercopithecus Genus: a multivariate approach. Am J Phys Anthropol, 50(2):169-182.

Mardia, K.V. 1970. Measures of multivariate skewness and kurtosis with applications. Biometrika, 57:519-530.

Martin, R.B., Burr, D.B. and Sharkey, N.A. 1998. Skeletal tissue mechanics. New York: Springer-Verlag.

Martinon-Torres, M. 2003. Quantifying trabecular orientation in the pelvic cancellous bone of modern humans, chimpanzees, and the Kebara 2 Neanderthal. Am J Hum Biol, 15(5):647-661.

Mazess, R.B., Whedon. G.D. 1983. Immobilization and bone. Calcif Tissue Int, 35(3):265-267.

McColl, D.J., Abel, R.L., Spears, I.R. and Macho, G.A. 2006. Automated method to measure trabecular thickness from microcomputed tomographic scans and its application. Anat Rec A Discov Mol Cell Evol Biol. 288: 982-8.

McHenry, H.M. and Corruccini, R.S. 1975. Distal humerus in hominoid evolution. Folia Primatol, 23:117-44.

McKinney, M.L. 1990. Trends in body size evolution. In: McNamara, K. J., ed. Evolutionary trends. Tuscon: University of Arizona Press. 75–118.

Mednick, L.W. 1955. The evolution of the human ilium. Am J Phys Anthropol, 13(2):203-216.

Medawar, P.B. 1945. Size, shape and age. In: WE LeGros Clark, PB Medawar, eds. Essays on Growth and Form. Oxford. Clarendon. 157–87.

Meldrum, D.J. 1991. Kinematics of the cercopithecine foot on arboreal and terrestrial substrates with implications for the interpretation of hominid terrestrial adaptations. Am J Phys Anthropol, 84(3):273-289.

von Meyer, G.H. 1867. Die Architektur der Spongiosa. Arch Anat Phys Wiss Med, 34:615-628.

Mitteroecker, P., Gunz, P., Weber, G.W. and Bookstein, F.L. 2004. Regional dissociated heterochrony in multivariate analysis. Ann Anat, 186:463-470.

Mori, T., Okimoto, N., Sakai, A., Okazaki, Y., Nakura, N., Notomi, T. and Nakamura, T. 2003. Climbing exercise increases bone mass and trabecular bone turnover through transient regulation of marrow osteogenic and osteoclastogenic potentials in mice. J Bone Miner Res, 18(11):2002-2009.

Mosimann, J. E. 1970. Size Allometry: Size and Shape Variables with Characterizations of the Lognormal and Generalized Gamma Distributions. ASA, 65(330):930-945.

Mueller, W.H. and Martorell, R. 1988. Reliability and accuracy of measurement. In: TG Lohman, AF Roche and R Martorell, eds. Anthropometric Standardisation Reference Manual. Champaign, IL: Human Kinetics Books. 83–86.

Mueller, R., Hahn, M., Vogel, M., Delling, G. and Rueegsegger, P. 1996. Morphometric analysis of noninvasively assessed bone biopsies: Comparison of high resolution computed tomography and histologic sections. Bone, 18(3):215-220.

Muller, R., Gerber, S.C. and Hayes, W.C. 1998. Micro-compression: a novel technique for the nondestructive assessment of local bone failure. Technol Health Care, 6(5-6):433-444.

Napier, J.R. 1967. Evolutionary aspects of primate locomotion. Am J Phys Anthropol, 27:333-342.

Nilsson, O., Marino, R., De Luca, F., Phillip, M. and Baron, J. 2005. Endocrine Regulation of the Growth Plate. Horm Res, 64:157-165.

Odgaard, A. 1997. Three-dimensional methods for quantification of cancellous bone architecture. Bone 20(4):315-328.

Odgaard, A., Jensen, E.B., Gundersen, H.J. 1990. Estimation of structural anisotropy based on volume orientation. A new concept. J Microsc, 57(2):149-162.

Odgaard, A., Kabel, J., van Rietbergen B, Dalstra M, Huiskes R. 1997. Fabric and elastic principal directions of cancellous bone are closely related. J Biomech. 30(5):487-95.

O'Higgins, P. 1999. Ontogeny and phylogeny: morphometric approaches to the study of skeletal growth and evolution. In Chaplain, M. A. J., Singh, G. D. & McLachlan, J. (Eds) On growth and form: spatio-temporal patterning in biology, 373-393.. London: John Wiley.

O'Higgins, P. and Collard, M. 2002. Sexual dimorphism and facial growth in papionin monkeys. J Zool, 257:255-272.

Ohlsson, C., Nilsson, A., Isaksson, O.G. and Lindahl, A. 1992. Effect of growth hormone and insulin-like growth factor-I on DNA synthesis and matrix production in rat epiphyseal chondrocytes in monolayer culture. J Endocrinol, 133:291-300.

Owan, I., Burr, D.B., Turner, C.H., Qiu, J., Tu, Y., Onyia, J.E. and Duncan, R. 1997. Mechanotransduction in bone: osteoblasts are more responsive to fluid forces than mechanical strain L. Am J Physiol, 273; (3,1):C810-C815.

Oxnard, CE. 1978. One Biologist's View Of Morphometrics. Ann Rev Ecol Syst, 9:219-241.

Oxnard, C.E. 1993. Bone and bones, architecture and stress, fossils and osteoporosis. J Biomech, 26 (suppl. 1):63-79.

Oxnard, C.E. and Yang ,H.C. 1981. Beyond biometrics: studies of complex biological patterns. Symp Zool Soc Lond, 46:127-167.

Pagel, M.D. and Harvey, P.H. 1993. Evolution of the juvenile period in mammals. In: ME Pereira and LA Fairbanks, eds. Juvenile Primates. New York: Oxford University Press. 28-37.

Palastanga, N. 2006. Anatomy and Human Movement (5th edition), Structure and Function. London. Butterworth-Heinemann.

Pauwels, F. 1980. *Biomechanics of the locomotor apparatus*. Berlin: Springer Verlag.

Pearson, O.M. and Lieberman, D.E. 2004. The aging of Wolff's "law": Ontogeny and responses to mechanical loading in cortical bone. Am J Phys Anthropol, (suppl) 39:63-99.

Penin, X. and Berge, C. 2001. Heterochronia via procrustean superimposition: application to the skulls of Homonidae primates. C R Acad Sci III, 324:87-93.

Penin X, Berge C, Baylac M. 2002. Ontogenetic study of the skull in modern humans and the common chimpanzees: neotenic hypothesis reconsidered with a tridimensional Procrustes analysis. Am J Phys Anthropol, 118(1):50-62.

Pezard, A. 1918. Le conditionement physiologique des caracteres sexuels secondaires chez les oiseaux. Bull Biol Fr Belg, 52:1-176.

Ponseti, I.V. 1978a. Morphology of the acetabulum in congenital dislocation of the hip. Gross, histological and roentgenographic studies. J Bone Joint Surg Am, 60 (5):586-599.

Ponseti, I.V. 1978b. Growth and development of the acetabulum in the normal child. Anatomical, histological, and roentgenographic studies. J Bone Joint Surg Am, 60 (5):575-585.

Pontzer, H., Lieberman, D.E., Momin, E., Devlin, M.J., Polk, J.D., Hallgrimsson, B. and Cooper, D.M. 2006. Trabecular bone in the bird knee responds with high sensitivity to changes in load orientation. J Exp Biol, 209 (1):57-65.

Preuschoft, H. 2004. Mechanisms for the acquisition of habitual bipedality: are there biomechanical reasons for the acquisition of upright bipedal posture? J Anat, 204(5):363-84.

Profant, L. 1995. Historical allometric inputs to interspecific patterns of craniofacial diversity in the cercopithecine tribe Papionini. Am J Phys Anthropol (suppl. 20), 175.

Rao, C. R. 1964. The use and interpretation of principal component analysis in applied research. Sankhya A, 26:329-358.

Rasband, W.S., 1997. Image processing and analysis in Java. [online] Research Service Branch, J.U.S. National Institutes of Health, Bethesda, Maryland, USA. Available from: http://rsb.info.nih.gov/ij/, 1997-2006. [Accessed 15.1105].

Ravosa, M.J., David, M., Meyers, K.E. and Glander T.I. 1993. Relative growth of the limbs and trunk in sifakas: Heterochronic, ecological, and functional considerations. Am J Phys Anthropol, 92(4):499-520.

Ravosa, M.J. and Profant, L.P. 2000. Evolutionary morphology of the skull in Old World monkeys. In: P. F. Whitehead & C. J. Jolly, eds. Old World Monkeys. New York: Cambridge University Press. 237–268.

Reiter, E.O. and Grumbach, M.M. 1982. Neuroendocrine control mechanisms and the onset of puberty. Ann Rev Physiol, 44:595-613.

Remis, M. 1995. Effects of body size and social context on the arboreal activities of lowland gorillas in the Central African Republic. Am J Phys Anthropol, 97 (4):413-433.

Reeve, E.C.R. and Huxley, J.S. 1945. Some problems in the study of allometric growth. In: W.E. Le Gros Clarke and P. Medawar eds. Essays on growth and form presented to D'Arcy Wentworth Thompson. Oxford. Clarendon Press. 121-156.

Rice, S.H. 1997. The analysis of ontogenetic trajectories: When a change in size or shape is not heterochrony. Proc Nat Acad Sci U S A, 94(3):907-912.

Richardson, M.K., Chipman, A.D. 2003. Developmental constraints in a comparative framework: A test case using variations in phalanx number during amniote evolution. J Exp Zool Part B: Mol Dev Evol, 296(1):8-22.

Ries, M., Pugh, J., Au, J.C., Gurtowski, J. and Dee, R. 1989a. Cortical pelvic strains with varying size hemiarthroplasty in vitro. J Biomech, 22:775-780.

Ries, M., Pugh, J., Au, J.C., Gurtowski, J. and Dee, R. 1989b. Normal pelvic strain pattern in vitro. J Biomed Eng, 11(5):398-402.

Robson-Brown, K.A., Davies, E.N. and McNally, D.S. 2002. The angular distribution of vertebral trabeculae in modern humans, chimpanzees and the Kebara 2 Neanderthal. J Hum Evol, 43(2):189-205.

Rohlf, F.J. and Slice, D.E. 1990. Extensions of the Procrustes method for the optimal superimposition of landmarks. Syst ZAool, 39:40-59

Rohlf, F.J. 1990a. Morphometrics. Ann Rev Ecol Syst, 21:299-316.

Rohlf, F.J. 1990b. Rotational fit (Procrustes) methods. Proc of the Michigan Morphometrics Workshop, University of Michigan Museums, Ann Arbor: 227-236.

Rohlf, F.J. and Marcus, L. 1993. A revolution in morphometrics. Trends Ecol & Evol, 8:129-132.

Rohlf, F.J. 1993. Relative warp analysis and an example of its application to mosquito wings. In: (ed. L.F. Marcus, E. Bello, A Garcia-Valdecasas eds. Contributions to Morphometrics. Museo Nacional de Ciencias Naturales, Madrid. 131-159.

Rohlf, F.J., Loy, A. and Corti, M. 1996. Morphometric analysis of Old World Talpidae (Mammalia, Insectivora) using partial warp scores. Syst Biol, 45:344-362.

Rohlf, F.J. 1999. Shape statistics: Procrustes superimpositions and tangent spaces. J Classif, 16:197-223.

Rohlf, F.L. 2000. Statistical power comparisons among alternative morphometric methods. Am J Phys Anthrop, 111:463–478.

Rohlf, F.J. 2001. Comparative methods for the analysis of continuous variables: geometric interpretations. Evol, 55:2143-2160.

Rook, L., Bondioli, L., Kohler, M., Moya-Sola, S. and Macchiarelli, R. 1999. Oreopithecus was a bipedal ape after all: evidence from the iliac cancellous architecture. Proc Natl Acad Sci U S A. 96(15):8795-8799.

Rook, L., Bondioli, L., Casali, F., Rossi, M., Kohler, M., Moya-Sola, S. and Macchiarelli, R. 2004. The bony labyrinth of *Oreopithecus bambolii.* J Hum Evol, 46:349-356.

Rosas, A. and Bastir, M. 2002. Thin-plate spline analysis of allometry and sexual dimorphism in the human craniofacial complex. Am J Phys Anthropol, 117:236-45.

Rosenberg, K.R. and Trevathan, W.R. 2001. The evolution of human birth. Sci Am, 285:72-77.

Roux W. 1881. Der züchtende Kampf der Teile, oder die "Teilauslese" im Organismus (Theorie der "Funktionellen Anpassung"). Leipzig: Wilhelm Engelmann.

Ruimerman, R., Hilbers, P., van Rietbergen, B. and Huiskes, R. 2005. A theoretical framework for strain-related trabecular bone maintenance and adaptation. J Biomech, 38(4):931-941.

Russ, J.C. 1990. Surface characterization: Fractal dimensions, Hurst coefficients, and frequency transforms. J Comp-Assist Microsc 2(3):161-183.

Russ, J.C. 1994. Fractal surfaces. New York: Plenum Press.

Ruvolo, M. 1997. Genetic Diversity in Hominoid Primates. Ann Rev Anthropol, 26:515-540.

Ryan, T.M. and Ketcham, R.A. 2002. Femoral head trabecular bone structure in two omomyid primates. J Hum Evol, 43(2):241-263.

Ryan, T.M. and Ketcham, R.A. 2005. Angular orientation of trabecular bone in the femoral head and its relationship to hip joint loads in leaping primates. J Morphol, 265(3):249-263.

Salle, B.L., Rauch, F., Travers, R., Bouvier, R. and Glorieux, F.H. 2002. Human fetal bone development: histomorphometric evaluation of the proximal femoral metaphysis. Bone, 30(6):823-828.

Satta, Y., Klein, J. and Takahata, N. 2000. DNA Archives and Our Nearest Relative: The Trichotomy Problem Revisited. Mol Phyl Evol, 14(2):259-275.

Saunders, J., Inman, V.T., Eberhart, H.D. 1953. The major determinants in normal and pathological gait. Bone Joint Surg Am, 35(A):543-558.

Scally, P. 1999. Medical imaging. Oxford : Oxford University Press

Scheuer, L., Black, S. 2000. Developmental Juvenile Osteology. London. Academic Press.

Uhthoff, H.K. 1990. The embryology of the human locomotor system. Berlin Heidelberg New York : Springer.

Scheuer, L. and Black, S. 2000. Developmental Juvenile Osteology. London. Academic Press.

Schultz, A. 1930. The skeleton of the trunk and limbs of higher primates. Hum Biol, 2:203-438.

Schultz, A.1930. The skeleton of the trunk and limbs of higher primates. Hum Biol, 2:203-438.

Schultz, A. 1936. Characters common to higher primates and characters specific for man. Q Rev Biol, 11:259-283 and 425-459.

Schultz, A. 1940. Growth and development of the chimpanzee. Contrib Embryol, 170:1-63.

Schultz, A. 1949. Sex differences in the pelves of higher primates. Am J Phys Anthropol. 7:401-423.

Schwenk, K. and Wagner, G.P. 2001. Function and the evolution of phenotypic stability: Connecting pattern to process. Am Zool, 41(3):552-563.

Segebarth-Orban, R. 1980. An evaluation of the sexual dimorphism of the human innominate bone. J Hum Evol, 9:601–607.

Seeman, E. 2003 Reduced bone formation and increased bone resorption: rational targets for the treatment of osteoporosis. Osteoporos Int. (suppl 3):S2-8.

Shea, B.T. 1981. Relative growth of the limbs and trunk in the African apes. Am J Phys Anthropol, 56:179-201.

Shea, B.T. 1983b. Allometry and heterochrony in the African apes. Am J Phys Anthropol, 62:275-289.

Shea, B.T. 1985a. Bivariate and multivariate growth allometry: statistical and biological considerations. J Zool, 206:367–390.

Shea, B.T. 1985b. Ontogenetic allometry and scaling: A discussion based on the growth and form of the skull in African apes. In: Jungers, W. L. ed. Size and scaling in primate biology. New York. Plenum. 175-205.

Shea, B.T. 1985c. On aspects of skull form in African apes and orangutans, with implications for hominoid evolution. Am J Phys Anthropol, 68:329-342.

Shea, B.T. 1985d. Bivariate and multivariate growth allometry: statistical and biological considerations. J Zool Lond A, 206:367-390.

Shea, B.T.1986. Scapula form and locomotion in chimpanzee evolution. Am J Phys Anthropol, 70(4):475-488.

Shea, B.T. 1988 Heterochrony in primates. In: ML McKinney ed. Heterochrony in Evolution. New York: Plenum. 237-266.

Shefelbine, S.J., Tardieu, C. and Carter, D.R. 2002. Development of the femoral bicondylar angle in hominid bipedalism. Bone, 30(5) 765-770

Sholl, A.D. 1950. The theory of differential growth analysis. Proc R Soc Lon B, 137:470-474.

Slice, D.E., Rohlf, F. J. and Bookstein, F.L. 1996. In: Marcus, L. F., M. Corti, A. Loy, G. Naylor, and D. E. Slice, eds. Advances in Morphometrics. Proceedings of the 1993 NATO Advanced Studies Institute on Morphometrics in Il Ciocco, Italy. New York. Plenum Publishing Corp. 531-551.

Slice, D.E. 1998. Morpheus et al.: software for morphometric research. Revision 01-30-98. Department of Ecology and Evolution, State University of New York, Stony Brook, New York.

Slomianka, L., 2004. Blues histology. School of Anatomy and Human Biology - The University of Western Australia. Available from: http://www.lab.anhb.uwa.edu.au/mb140/CorePages/Bone/Bone.htm. [Accessed 01.05.06.]

Smit, T. H., Odgaard, A. and Schneider, E. 1997. Structure and function of vertebral trabecular bone. Spine, 22:2823-2833.

Smit, T.H., Schneider, E. and Odgaard, A. 1998. Star length distribution: a volume-based concept for the characterization of structural anisotropy. J Microsc, 191(3):249-257.

Smith, R.J. 1980. Rethinking allometry. J Theor Biol, 87:97-111.

Smith, R.J. 1984a. Allometric scaling in comparative biology: problems of concept and method. Am J Physiol, 246:152-160.

Smith, R.J. 1984b. Determination of relative size: the "criterion of subtraction" problem in allometry. J Theor Biol, 108:131-142.

Smith, R.J. 1993. Logarithmic transformation bias in allometry. Am J Phys Anthropol, 90:215-228.

Smith, R.J. 1998. Sexual dimorphism in primate neonatal body mass. J Hum Evol, 34:173-201.

Smith, R.J. and Jungers, W.L. 1997. Body mass in comparative primatology Journal of Human Evolution, 32(6):523-559

Smith, B. H. 1989. Dental development as a measure of life history in primates. Evol B, 43(3):683-688

Smith, B.H. 1991. Dental development and the evolution of life history in Hominidae Am J Phys Anthropol, 86:157–174.

Smith, B.H. 1994. Patterns of dental development in Homo, Australopithecus, Pan, and Gorilla. Am J Phys Anthropol, 94(3):307-325.

Spoor, C.F., Zonneveld, F.W. and Macho, G.A. 1993. Linear measurements of cortical bone and dental enamel by computed tomography: applications and problems. Am J Phys Anthropol, 91(4):469-484.

Stern, J. and Susman, R.L. 1983. The locomotor anatomy of *Australopithecus afarensis*. Am J Phys Anthropol, 60:279-317.

Steudel, K. 1978. A multivariate analysis of the pelvis of early Hominids. J Hum Evol, 7:583-595.

Steudel, K. 1981. Functional aspects of primate pelvic structure: a multivariate approach. Am J Phys Anthropol, 55:399-410.

Steudel, K. 1982. Patterns of intraspecific and interspecific allometry in Old World primates. Am J Phys Anthropol, 59(4):419-430.

Stones, H.H., Lawton, F.E., Bransby, E.R. and Hartley, H.O. 1951. Time of eruption of permanent teeth and time of shedding of deciduous teeth. Br Dent J, 90(1):1-7.

Straus, W. 1927. The human ilium: sex and stock. Am J Phys Anthropol, 11:1-28.

Straus, W. 1929. Studies on primate ilia. Am J Anat, 43:403-460.

Styne, D.M. 2003. The Regulation of Pubertal Growth. Horm Res, 60 (suppl 1):22–26.

Svenningsen, S., Apalset, K., Terjesen, T. and Anda, S. 1989. Osteotomy for femoral anteversion. complications in 95 children. Acta Orthop Scand, 60(4):401-405.

Swartz, S.M., Parker, A. and Huo, C. 1998. Theoretical and empirical scaling patterns and topological homology in bone trabeculae. J Exp Biol, 201(4):573-590.

Swindler, D.R. and Wood, C.D. 1982. Atlas of Primate Gross Anatomy: Baboon, Chimpanzee, and Man. Florida: Robert E. Krieger Publishing Company.

Tague, R.G. 1991. Commonalities in dimorphism and variability in the anthropoid pelvis, with implications for the fossil record. J Hum Evol, 21:153-176.

Tague, R.G. 2005. Big-bodied males help us recognize that females have big pelves. Am J Phys Anthropol, 127:392-405.

Takata, S. and Yasui, N. 2001. Disuse osteoporosis. J Med Invest, 48(3-4):147-156.

Tanck, E., Homminga, J., van Lenthe, G.H. and Huiskes, R. 2001. Increase in bone volume fraction precedes architectural adaptation in growing bone. Bone, 28(6):650-654.

Tanner, J.M. 1955. Growth at adolescence. With a general consideration of the effects of hereditary and environmental factors upon growth and maturation from birth to maturity, 2nd ed. Oxford: Blackwell Scientific.

Tanner, J.M. 1962. Growth at Adolescence. Oxford: Blackwell Scientific Publications.

Tanner, J.M., Whitehouse, R.H. and Takaishi, M. 1966. Standards from birth to maturity for height, weight, height velocity, and weight velocity: British children, 1965. Arch Dis Child. I. 41(219):454-471.

Teissier, G. 1938. Un essai d'analyse factorielle, les variants sexuels de Maja squinada. Biotypologie, 7:73–96.

Thieme, F.P. and Schull, W.J. 1957. Sex determination form the skeleton. Hum Biol, 29:242-273.

Thompson, D'A.W. 1917. On growth and form. Cambridge: Cambridge University press.

Thompson, D'A.W. 1942. On Growth and Form. Cambridge: Cambridge University Press.

Trevathan, W.R. 1988. Fetal emergence patterns an evolutionary perspective. Am Anthropol, 90:19-26.

Tsutakawa, R.K. and Hewett J.E. 1977. Quick test for comparing two populations with bivariate data. Biometrics. 33:215-219.

Turner, C.H., Cowin, S.C., Rho, J.Y., Ashman, R.B. and Rice, J.C. 1990. The fabric dependence of the orthotropic elastic constants of cancellous bone. J Biomech, 23:549-561.

Turner, C.H. 1998. Three rules for bone adaptation to mechanical stimuli. Bone, 23(5):399-407.

Ulijaszek, S.J. and Lourie, J.A. 1994. Intra- and inter-observer error in anthropometric measurement. In: SJ Ulijaszek and CGN Mascie-Taylor, eds. Anthropometry: the Individual and the Population. Cambridge: Cambridge University Press. 30–55.

Ulrich, D., van Rietbergen, B., Laib, A. and Ruegsegger, P. 1999. Load transfer analysis of the distal radius from in-vivo high-resolution CT-imaging. J Biomec, 32:821-828.

Vaananen, H. K., Zhao, H., Mulari, M. and Halleen, J. M. 2000. The cell biology of osteoclast function. J Cell Sci, 113(3):377-382.

Vogl, C. Atchley, W.R. Cowley, D.E. Crenshaw, P. 1993. The epigenetic influence of growth hormone on skeletal development. Growth Development and Aging, 57(3):163-182.

Wagner, G.P. 1989. The biological homology concept. Annu. Rev. Ecol. Syst, 20:51-69.

Wagner, G.P.1994. Homology: The Hierarchical Basis of Comparative Biology,

Walker, J.A. 1996. Principal components of body shape variation with an endemic radiation of threespine stickleback. In: ed. L. F. Marcus, M. Corti, A. Loy, G. Naylor and D. E. Slice, eds. Advances in morphometrics. New York: Plenum Press. 321-334.

Waterman, H. 1929 Studies on the evolution of the pelvis of man and other primates. Bull Am Mus Nat Hist, 12:585-642.

Weidenreich, F. 1913. Ueber das Hüftbein und das Becken der Primaten und ihre Umformung durch den aufrechten Gang. Anat Anz, 44S:497-513.

Weinbaum, S., Cowin, S.C. and Zeng, Y. 1994. A model for the excitation of osteocytes by mechanical loading-induced bone fluid shear stresses. J Biomech, 27:339–360.

Weinreb, M., Rodan, G.A. and Thompson, D.D. 1989. Osteopenia in the immobilized rat hind limb is associated with increased bone resorption and decreased bone formation. Bone, 10(3):187-194.

Wheeler, M.D. 1991. Physical changes of puberty. Endocrinol Metab Clin North Am, 20(1):1-14.

Whitehouse, W.J. 1974. The quantitative morphology of anisotropic trabecular bone. J Microsc, 101:153-168.

Whitehouse, W.J. and Dyson, E.D. 1974. Scanning electron microscope studies of trabecular bone in the proximal end of the human femur. J Anat, 118:417-444.

Witte, H., Eckstein, F. and Recknagel, S. 1997. A calculation of the forces acting on the human acetabulum during walking. Based on in vivo force measurements, kinematic analysis and morphometry. Acta Anat (Basel), 160(4):269-80.

Wolff, J. 1892. Das Gesetz der Transformation der Knochen. Berlin: Hirschwald Verlag.

Wolff, J. 1996. The law of bone remodelling [translated from 1892 original, Das Gesetz der Transformation der Knochen, by P. Maquet and R. Furlong] Berlin: Springer Verlag.

Zander, G. 1943. Os acetabuli and other bone nuclei: periarticular calcifications at the hip joint. Acta Radiol, 24:317-327.

Zelditch, M.L., Sheets, H.D. and Fink, W.L. 2000. Spatiotemporal reorganization of growth rates in the evolution of ontogeny. Evol, 54:1363–1371.

Zonneveld, F.W. 1987. Computed tomography of the temporal bone and orbit. Munich. Urban and Schwarzenberg.

Zuckerman, S., Ashton, E.H., Flinn, R.M., Oxnard, C.E. and Spence, T.F. 1973. Some locomotor features of the pelvic girdle in primates. Symp Zool Soc Lond, 33:71-165.

Appendix

Published papers submitted in support of the thesis.

International Journal of Osteoarchaeology
Int. J. Osteoarchaeol. **15**: 421–430 (2005)
Published online 16 August 2005 in Wiley InterScience (www.interscience.wiley.com). DOI: 10.1002/oa.797

Age Changes in Bone Microstructure: Do They Occur Uniformly?

G. A. MACHO,[a]* R. L. ABEL[a] AND **H. SCHUTKOWSKI[b]**

[a] *Hominid Palaeontology Research Group, Department of Human Anatomy and Cell Biology, University of Liverpool, Sherrington Buildings, Ashton Street, Liverpool L69 3GE, UK*

[b] *Biological Anthropology Research Centre, Department of Archaeological Sciences, Phoenix Building, University of Bradford, Bradford BD7 1DP, UK*

ABSTRACT Age estimations based on conventional multifactorial methods were compared with trends observed in the internal morphology of bones obtained from high-resolution μCT. Specifically, average trabecular thickness and number of trabeculae/mm transect were determined in the non-load-bearing capitate (hand) and the load-bearing navicular (foot). The μCT findings reveal age-related trends but—surprisingly—these correspond only loosely with the ages assigned by conventional ageing methods, and are also not in accordance with what would be predicted from biomechanical considerations: trabeculae tend to be thinner in the (habitually) load-bearing navicular than in the (habitually) non-load-bearing capitate. While the statistically significant correlation between trabecular thickness and number of trabeculae would suggest a compensatory mechanism between these two aspects of microanatomy, they are not correlated with the assigned ages and, importantly, may differ between sexes. Only in females is there an unequivocal trend towards trabecular thickness increase with age. These findings, although unexpected, can be reconciled with recent histological evidence and assumed average activity levels in historical populations. Conversely, changes in trabecular number are less clear-cut and may be due to the lack of very old individuals in the sample. Nevertheless, the trends observed for trabecular thickness, as well as for trabecular number, seem to imply that the higher incidence of osteoporosis in women could be explained from a structural point of view alone.

Key words: μCT; bone microstructure; trabeculae; age; sex; osteoporosis; osteopenia

Introduction

Ascertainment of age at death in archaeological populations is fraught with problems, and the confounding factors are many. Firstly, biological processes of skeletal maturation and degeneration are generally poorly correlated with chronological age and vary between bones. Secondly, the genetic and biological processes underlying skeletal ageing are not well understood and are influenced by environment, lifestyle and activity. For example, synovial joints are particularly susceptible to activity-related degenerative processes, whereas normal ageing processes as well as inactivity (which may, in part, be correlated with age) would lead to a thinning of cortical bone (e.g. Maggio *et al.*, 1997; Mays, 2000; Malkin *et al.*, 2002) and loss of trabeculae (e.g. Thomsen *et al.*, 2002a) without affecting joint surfaces. This interplay between intrinsic (i.e. genetically determined, biological) and extrinsic (i.e. environmentally induced) factors confounds age estimation and hampers contextual archaeological research, such as palaeodemography (e.g. Bocquet-Appel & Masset, 1996).

Identification of osteoporosis and osteopenia is a major concern in palaeoanthropological enquiry (e.g. Roberts & Wakely, 1992; Brickley & Howell, 1999), but a prerequisite for any such enquiry is the documentation of normal variation in trabecular architecture and changes with age. Such heuristic studies are relatively rare, however

* Correspondence to: Hominid Palaeontology Research Group, Department of Human Anatomy and Cell Biology, University of Liverpool, Liverpool L69 3GE, UK.
e-mail: gama1@liverpool.ac.uk

Received 17 *November* 2003
Revised 8 *November* 2004
Accepted 22 *November* 2004

(Ding & Hvid, 2000; Thomsen *et al.*, 2002b,c; Vijayapalan *et al.*, 2003), especially with regard to historical populations (Agarwal *et al.*, 2004). In a medieval skeletal assemblage, Agarwal *et al.* (2004) found increased trabecular maintenance in females and suggested that this trend may be the result of higher activity levels and reproductive strategies in this population. While reasonable, it cannot be ruled out that directional morphological changes with age may have been obscured. As is common in skeletal studies, age groups were broad and only three categories were defined. To bypass such limitations inherent in osteoarchaeology, and to contribute to a better understanding of the interrelationships between skeletal ageing processes, seriation of morphological trends may be more useful. This was undertaken in the present study and the covariation of ageing processes was determined. Specifically, the present study analysed μCT images of one weight-bearing (i.e. navicular) and one non-weight-bearing (i.e. capitate) bone and contrasted the results with the ages derived from conventional methods. The aim was to establish whether: (a) changes in trabecular microstructure correspond with traditional macro-morphological methods of ageing; (b) structural changes in trabecular architecture (number of trabeculae and trabecular thickness) follow the same trends; and (c) load-bearing and non-load-bearing bones behave in a comparable manner.

Material and methods

Twenty well-preserved skeletons from the Anglo-Saxon cemetery at Raunds Furnells, Northamptonshire (Boddington, 1996), were aged and sexed [HS] using conventional criteria (Table 1). One navicular (tarsal bone) and one capitate (carpal bone), preferably from the same side, were chosen for scanning with high-resolution μCT at the University of Liverpool. The specimens were scanned using a BIR Inc. ACTIS 420/600 system equipped with a tungsten x-ray target, a 250 μm thick columnar caesium iodide scintillator and a Toshiba AI5877 JP dual field image intensifier. The bones were scanned at a slice thickness of 100 μm with 100 μm increments and angular intervals of 0.3°. Voltage and current ranged from 45 kV to 55 kV and 160 μA to 200 μA respectively, giving an effective monochromatic x-ray energy of between 22.5–27.5 keV. Focal spot size was 50 μm and contrast resolution was approximately 0.5%. Matrix size was 512 × 512 pixels, while voxel size was typically 100 × 100 × 100 μm. Given the adopted protocol for determining the thickness of each trabecula individually (see below), and bearing in mind that the average trabecular thickness reported in the published literature tends to be around 150–250 μm (e.g. Whitehouse, 1974) with a range of 50–750 μm (Chappard *et al.*, 1999; Byers *et al.*, 2000), the resolution chosen was considered sufficient. As the orientation of joint surfaces indicates a predominantly proximo-distal loading direction, the long axes of the bones were oriented perpendicularly to the beam, thus ensuring maximum resolution (Kothari *et al.*, 1998). Images were reconstructed using VG Studio MAX 1.1 (maximum intensity projection reconstruction algorithm) (Figure 1), provided to the Hominid Palaeontology Research Group on a trial basis. Image analysis was carried out using ImageJ (http://rsb.info.nih.gov/ij/).

Two sets of measurements were taken for each bone [RA]. Firstly, trabecular thickness was measured along six transects close to midline (Figure 2) using the half-maximum-height (HMH) method (Spoor *et al.*, 1993). Rather than applying a global threshold value, the HMH was determined for each trabecula individually in order to minimise problems associated with beam hardening and partial volume effects. More than 3600 trabeculae were thus analysed. As the length of each transect as well as the number of trabeculae along this transect was recorded also, the average number of trabeculae per mm was calculated for each bone separately. This measure, albeit crude, may allow an assessment of bone (trabecular) loss with age and could thus also provide an indication of osteoporosis. Relationships between age, sex and trabecular micro-architecture were tested using rank-order correlations.

Results

Raw data are shown in Table 2. Data were ranked to determine (a) whether trabecular thickness

Table 1. Sex and age distribution of the individuals analysed from Raunds Furnells

Specimen	Sex	Age range	Age (mean)	Ageing criteria
5002	M	30–39	32	Pubic symphysis III-IV, auricular surface III, sternal rib end IV-V, S1/S2
5006	M	18–22	20	Medial clavicle, sternal rib end I-II
5007	M	50–60	55	Auricular surface VII-VIII
5008	F	40–44	42	Sternal rib end V, auricular surface V [pubic symphysis VI]
5009	M	40–50	45	Auricular surface V, sternal rib end V-VI
5015	M	18–22	20	Pubic symphysis I-II, epiphyseal lines visible at Caput humeri and ischial tuberosity
5018	F	35–39	37	Auricular surface IV-V, sternal rib end V
5019	F	30–40	35	Pubic symphysis III-IV, sternal rib end IV-V
5025	M	50–60	55	Auricular surface VII [sternal rib end younger]
5026	M	35–39	37	Pubic symphysis IV, auricular surface IV
5028	F	25–39	32	Pubic symphysis II-III, auricular surface IV
5031	F	30–34	32	Auricular surface III, pubic symphysis II-III, S1/S2
5033	M	35–39	37	Auricular surface IV
5036	F	43–58	50	Pubic symphysis V, sternal rib end VI
5040	F	50–55	52	Auricular surface VII
5042	F	35–39	37	Auricular surface IV
5044	M	35–55	45	Pubic symphysis IV-V, sternal rib end V-VI, auricular surface VI-early VII
5045	M	60+	60	Pubic symphysis VI, auricular surface VIII
5181	M	22–29	24	Pubic symphysis II, auricular surface II, sternal rib end III
5257	F	50–60	55	Pubic symphysis VI, auricular surface VII

Ages are given with rounded figures; age ranges were calculated from published means of the respective age groups of all features used; remarks refer to ageing criteria available and the respective stages of trait expressions. Assessment of sex was carried out using morphological criteria. For methods of age and sex diagnosis see Brooks & Suchey (1990), Herrmann *et al.* (1990), İşcan & Loth (1986) and Lovejoy *et al.* (1985).

and number of trabeculae/mm transect change systematically with estimated age, and (b) whether these changes might affect load-bearing and non-load-bearing bones differently (Figure 3). With few exceptions, trabecular thickness in the capitate always exceeded that in the navicular (Figure 3A), but trabecular number per mm transect was almost always higher in the navicular than in the capitate (Figure 3B). Surprisingly, there was no clear correspondence with the ages assigned by conventional osteological methods, although some trends were apparent (Table 3). Rank-order correlations revealed a statistically significant relationship between estimated age and average trabecular thickness increase. However, bones are affected differently, such that trabecular thickness increase was statistically significant only for the navicular, but not the capitate. The number of trabeculae did not decrease statistically with age, although there appears to be a statistically significant, inverse relationship between trabecular thickness and trabecular number in both bones (Table 3). This trend is not apparent within each sex and may be the result of the small sample size (Table 4).

Discussion

Although medical CT scanners have been used in (palaeo)anthropological research for over a decade (e.g. Macho & Thackeray, 1992), high-resolution μCT scanners with a larger field of view and/or no gantry, which enable the scanning of larger pieces of bone or complete small bones, have become available only recently (Kappelman, 1998). This new technology has already been adopted for anthropological research (Fajardo & Müller, 2001; Fajardo *et al.*, 2002; MacLatchy & Müller, 2002; Ryan & Ketcham, 2002a,b) and promises to become an invaluable tool which will enable the formulation and testing of sharper research questions related to functional adaptations in primate bones (Huiskes, 2000). A prerequisite for between-species comparisons is a sound understanding of normal variation within species and changes associated with age, sex and activity. To contribute towards this overall goal was the aim of this study. Specifically, this study was designed to test whether ages assigned largely on the basis of maturational/degenerative alterations of joint

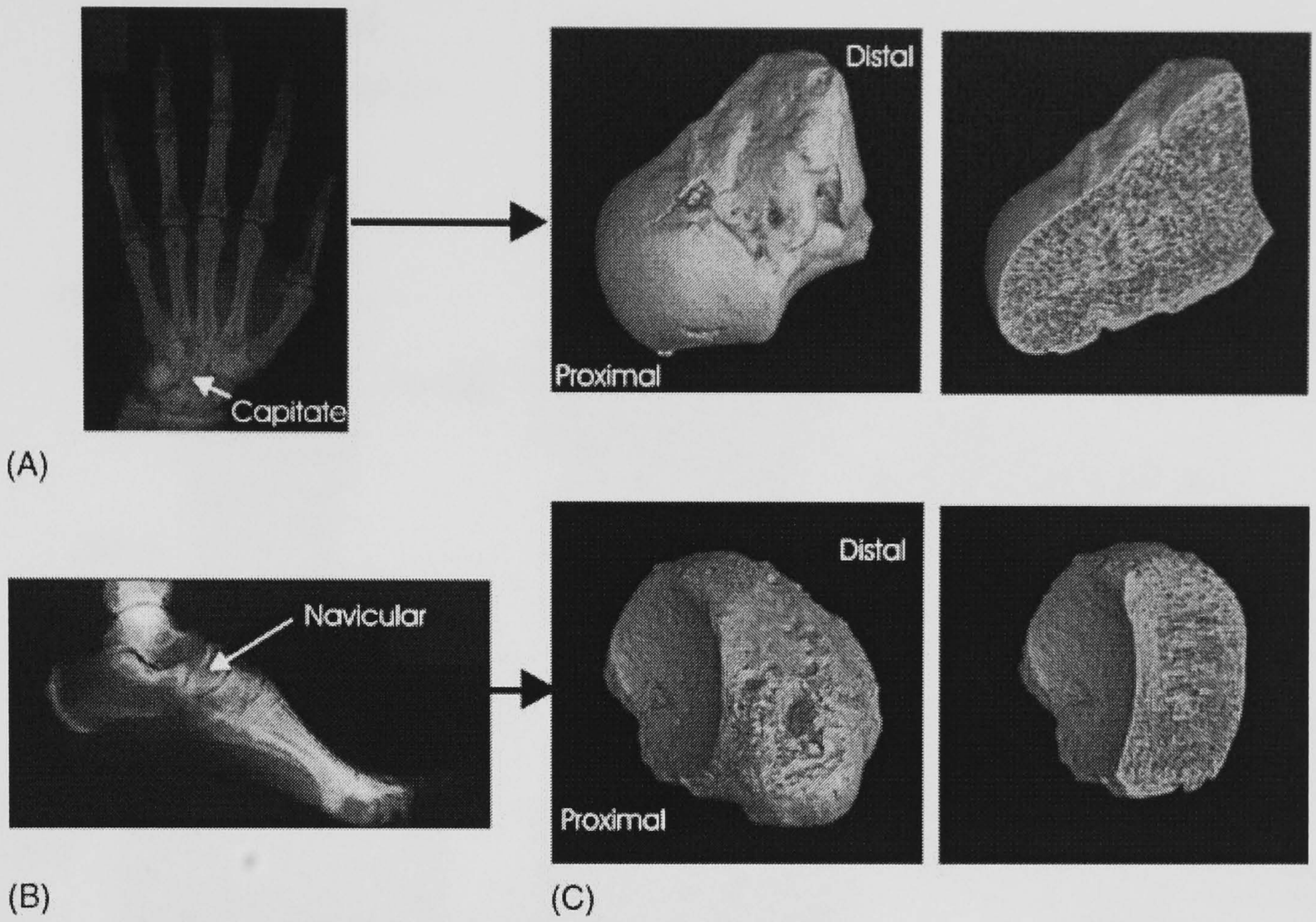

Figure 1. Illustration of bones used for analysis. Radiographs (left) show positions of the capitate within the hand (A) and the navicular within the foot (B). In (C) CT reconstructions of the whole bones (middle), as well as the trabecular architecture within each bone (right) are shown. Bones are not to scale and are for illustrative purposes only.

surfaces, such as the pubic symphysis and the auricular surface (Table 1), correspond with trends independently observed in the internal structure of bone. Secondly, it was enquired whether age changes in the load-bearing (navicular) and the non-load-bearing (capitate) bone are comparable. Although it should be borne in mind that sample size is relatively small, that age-at-death of the sample is unknown, and that data derived from imaging techniques may be prone to error (e.g. due to partial volume-averaging), the protocol adopted here ensures that the trends observed in the present study may reflect reality, albeit in an unexpected way. In particular, the results appear to shed new light on commonly assumed mechanisms underlying bone adaptation and homeostasis, while at the same time casting doubt on the validity of macroscopic morphological ageing techniques in osteoarchaeology, and some of its assumptions.

Reliable age-at-death estimation of archaeological human remains is considered imperative for interpreting osteological data within a biocultural framework. Conventional osteological ageing methods of adult skeletons are fraught with problems, however, and the present findings further highlight such difficulties. Not only are there discrepancies between ages assigned on the basis of macro-morphology (Table 1) and observed changes in trabecular micro-architecture (Figures 3 and 4), but also among different aspects of internal morphology (Table 3). As regards the latter, it appears that there are opposite directional changes in trabecular thickness and number of trabeculae/mm transect, implying a compensatory mechanism between these two variables. Although a decrease in average trabecular number, particularly in the non-load-bearing capitate, is expected, the trends observed for trabecular thickness are surprising (Table 3). These findings highlight the importance of taking into account localised changes in bone architecture with age (i.e. capitate *versus* navicular).

Based on theoretical considerations, Frost (1990) suggested that trabeculae, unlike cortical bone, may retain their ability to model

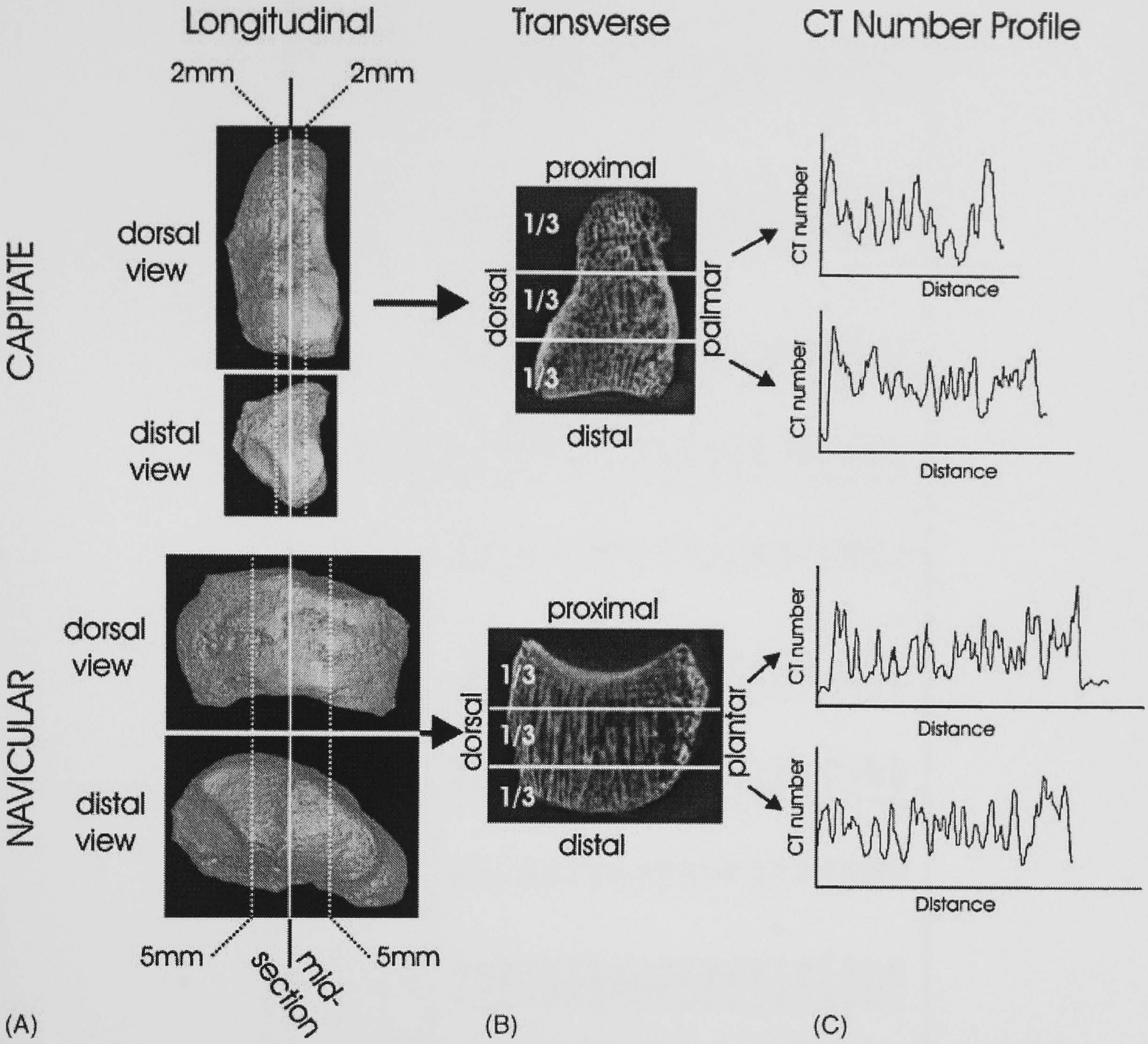

Figure 2. Planes of sections through the images of the captitate and navicular, reconstructed from μCT images, are shown. (A) depicts the three virtual longitudinal cuts; bones are scaled to approximately the same size to indicate the relative positions of the planes. (B) shows how each of the slices is cut in the transverse plane for calculation of trabecular thickness using the HMH-method. (C) displays examples of CT number profiles. Images in (B) and (C) are not to scale.

throughout life. This has recently been confirmed histologically (Kobayashi *et al.*, 2003). Given that Anglo-Saxon populations probably had higher activity levels than are encountered today, the increase in trabecular thickness with age could thus be explained (Agarwal *et al.*, 2004). The clear-cut trends shown in Figure 3 and Table 3 are therefore biologically meaningful, and the discrepancies with the presumed ages of the individuals (Table 1) are probably due to problems associated with conventional ageing techniques. It is further noteworthy that females show a directional, statistically significant trend in trabecular size, whereas men do not. Given that sample sizes are equal between men and women, this finding is unlikely to be an artefact of sample size, and requires further explanation.

Recent histological observations indicate that there may be sex differences in ageing processes, whereby trabecular thickness decreases with age in men, but increases, or remains stable, in women (Aaron *et al.*, 1987; Vijayapalan *et al.*, 2003) The biological mechanisms underlying these differential changes are still poorly

Table 2. Average trabecular thicknesses and trabecular number per mm transect for each bone of each individual analysed

Specimen	Age	Sex	Trabecular thickness									Density	
			Capitate			Navicular			Total			Capitate Trab. No/mm	Navicular Trab. No/mm
			n	Mean (mm)	std	*n*	Mean (mm)	std	*n*	Mean (mm)	std		
5006	18–22	M	85	0.347	0.179	122	0.413	0.233	207	0.386	0.215	1.917	1.142
5015	18–22	F	93	0.367	0.208	133	0.330	0.155	226	0.346	0.179	1.473	1.455
5019	20–25	F	69	0.431	0.193	110	0.339	0.141	179	0.374	0.168	1.036	1.130
5181	22–29	M	73	0.469	0.188	148	0.401	0.181	221	0.423	0.186	1.059	1.306
5028	25–39	F	61	0.500	0.246	101	0.350	0.129	162	0.407	0.195	1.064	1.385
5031	30–34	F	67	0.432	0.219	106	0.324	0.153	173	0.366	0.188	1.231	1.437
5002	30–35	M	63	0.484	0.252	107	0.385	0.202	170	0.422	0.226	1.011	1.287
5044	30–40	M	70	0.543	0.249	109	0.510	0.244	179	0.523	0.246	0.920	1.069
5026	35–39	M	59	0.534	0.301	105	0.402	0.240	164	0.450	0.270	0.825	1.016
5033	35–39	M	79	0.535	0.244	133	0.428	0.207	212	0.468	0.227	0.994	1.199
5042	35–39	F	82	0.401	0.220	133	0.329	0.162	215	0.357	0.189	1.348	1.552
5018	35–40	F	58	0.428	0.166	113	0.400	0.222	171	0.409	0.204	1.165	1.367
5008	34–46	F	51	0.454	0.249	78	0.458	0.224	129	0.456	0.233	1.037	1.163
5009	40–44	M	51	0.521	0.245	111	0.431	0.250	162	0.459	0.251	0.929	1.209
5036	43–58	F	63	0.472	0.205	113	0.368	0.183	176	0.405	0.197	1.090	1.399
5040	50–55	F	82	0.399	0.194	92	0.418	0.187	174	0.409	0.190	1.314	1.235
5007	50–60	M	63	0.463	0.244	110	0.404	0.187	173	0.425	0.211	0.980	1.206
5025	50–60	M	36	0.656	0.294	122	0.364	0.191	158	0.430	0.250	0.911	1.419
5257	50–60	F	66	0.503	0.227	139	0.436	0.251	205	0.458	0.245	0.970	1.202
5045	60+	M	53	0.438	0.172	99	0.452	0.276	152	0.447	0.244	1.070	1.038

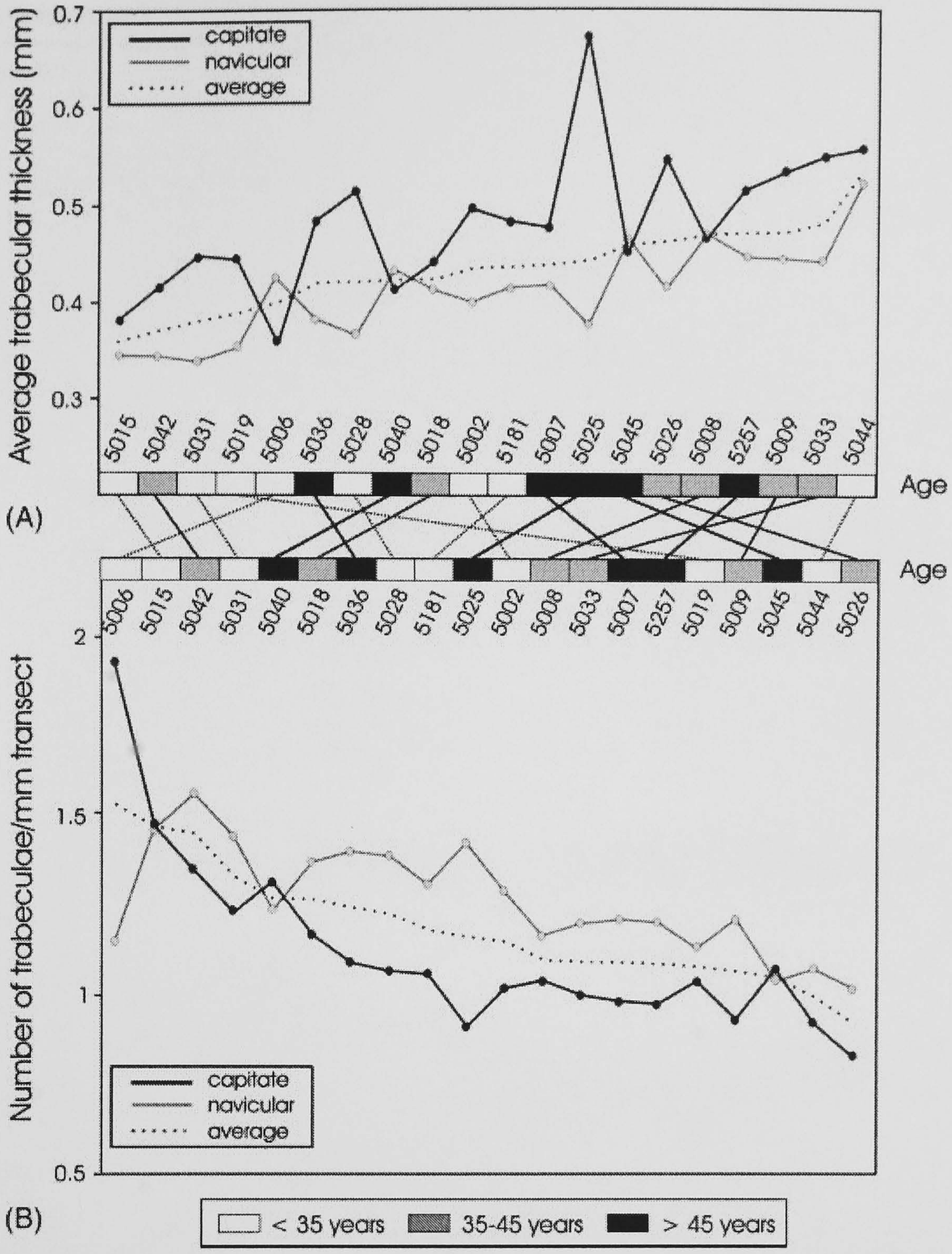

Figure 3. Average trabecular thickness is ranked in ascending order (A), while number of trabeculae per mm transect (B) is ranked in decreasing order. In both instances, data for the navicular and the capitate are shown and the presumed ages are indicated in the respective boxes below and above the graphs. Although there appears to be a trend with age for both analyses, these are not concordant: individuals are linked between graphs to highlight the unstructured relationship.

understood and subject to ongoing research. Regardless, if correct, such patterns of change between sexes could have obscured any obvious trends in the present analyses. To test whether this is the case, average trabecular thickness was ranked and overlain with trabecular number/mm transect, sex and age (Figure 4). Surprisingly, women (with two exceptions) tend to have generally thinner trabeculae than men, but the increase in thickness with age seems to be more pronounced (Figure 4). These findings thus support (or are supported by) published histological evidence (Aaron *et al.*, 1987; Vijayapalan *et al.*, 2003), even though they are unexpected and raise a number of questions. Specifically, if the data are correct and reflect reality, why are

Table 3. Rank-order correlations (ρ) between age and microstructural variables

Rank-order correlations	ρ
Capitate thickness increase—navicular thickness increase	0.453*
Capitate volume decrease—navicular volume decrease	0.135
Average age—average thickness increase	0.516*
Average age—capitate thickness increase	0.332
Average age—navicular thickness increae	0.474*
Average age—average trabecular number decrease	0.352
Average age—trabecular number (capitate) decrease	0.334
Average age—trabecular number (navicular) decrease	0.083
Average trabecular thickness increase—average trabecular number decrease	0.774**
Trabecular thickness increase (capitate)—trabecular number decrease (capitate)	0.886**
Trabecular thickness increase (navicular)—trabecular number decrease (navicular)	0.728**

*$p < 0.05$; **$p < 0.01$.

Table 4. Rank-order correlations (ρ) between microstructural variables for each sex

Rank-order correlations (with age)	ρ males	ρ females
Average trabecular thickness increase	0.039	0.564*
Capitate trabecular thickness increae	0.115	0.394
Navicular trabecular thickness increase	0.200	0.770**
Average trabecular number decrease	0.515	0.309
Capitate trabecular number decrease	0.346	0.333
Navicular trabecular number decrease	0.127	0.333

*$p < 0.05$; **$p < 0.01$.

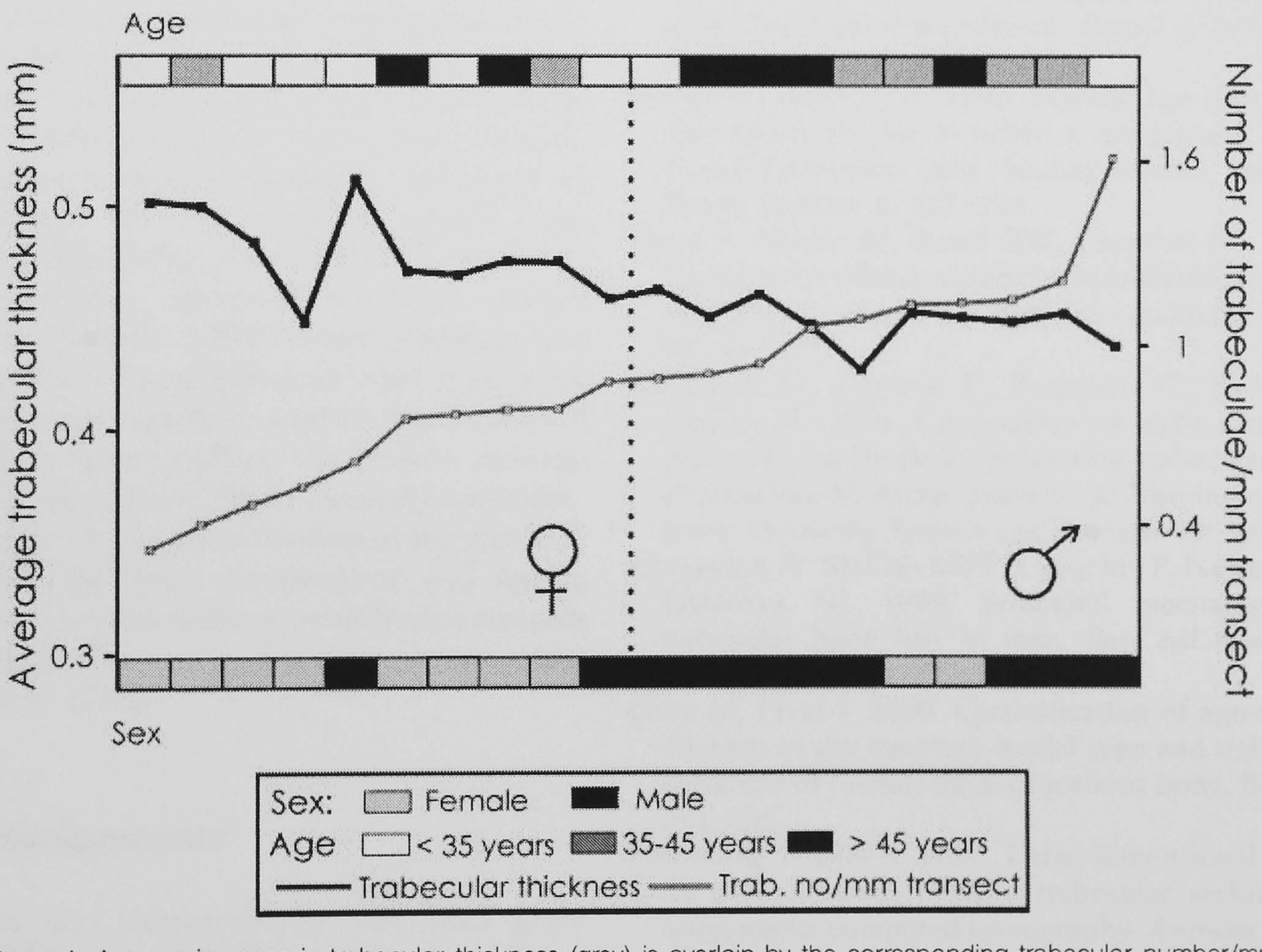

Figure 4. Average increase in trabecular thickness (grey) is overlain by the corresponding trabecular number/mm transect (black) of the respective individual. Age categories are highlighted on top of the graph, whereas presumptive sex is indicated at the bottom. There appears to be a good correspondence between sex and trabecular thickness. Even when bearing in mind the apparent lack of old individuals, there appears to be a decrease in relative number of trabeculae in females, but not in males.

women more prone to osteoporosis and bone failure than men? The observation that trabeculae are thinner in woman than in men may provide some clue.

Clinical studies have cast doubt on the assumed key-role of bone mineral density for the development of osteoporosis (e.g. Hordon *et al.*, 2000). Rather, structural differences in trabecular architecture and loss of connectivity may be the main cause underlying osteoporosis (Bertram & Swartz, 1991; Aaron *et al.*, 2000; Guo & Kim, 2002; Link *et al.*, 2002). When the data are analysed according to increasing age for each sex separately (Table 4, Figure 4) such propositions appear reasonable. In women, the data suggest a more marked compensatory mechanism between trabecular thickness increase and trabecular loss with age. From these observations it further follows that the higher incidence of osteoporosis may not necessarily be the result of loss in overall bone mass. Instead, it is conceivable that women will experience a higher rate of loss in connectivity (and trabeculae) than men, simply because their trabeculae are thinner. In other words, any reduction in trabecular thickness will have a greater, potentially more damaging effect in women than in men. Consequently, the risk of osteoporosis will be increased irrespective of homoeostatic, hormonally mediated or activity-related processes, and/or overall bone density (e.g. Compston *et al.*, 1989). The relatively longer trabeculae observed in older women (Brickley & Howell, 1999) could therefore also be explained as a consequence of interconnections getting lost more rapidly in women than in men. If confirmed in future studies, the present findings have wider implications (both clinically and methodologically) for an understanding of the mechanisms underlying bone maintenance and ageing techniques, and may make a contribution towards addressing questions related to osteoporosis in the past (Ortner, 2003).

Acknowledgements

This work was supported by the JREI grant (JR99LICREQ) to GM. RA is supported by a Natural Environment Research Council studentship (NER/S/A/2001/06485).

References

Aaron JE, Makins NB, Sagreiya K. 1987. The microanatomy of trabecular bone loss in normal aging men and women. *Clinical Orthopaedics and Related Research* **215**: 260–271.

Aaron JE, Shore PA, Shore RC, Beneton M, Kanis JA. 2000. Trabecular architecture in women and men of similar bone mass and with and without vertebral fracture: II. Three-dimensional histology. *Bone* **27**: 277–282.

Agarwal SC, Dimitriu M, Tomlinson GA, Grynpas MD. 2004. Medieval trabecular bone architecture: the influence of age, sex, and lifestyle. *American Journal of Physical Anthropology* **124**: 33–44.

Bertram JEA, Swartz SM. 1991. The 'Law of Bone Transformation': a case of crying Wolff? *Biological Review* **66**: 245–273.

Bocquet-Appel J, Masset C. 1996. Palaeodemography: expectancy and false hope. *American Journal of Physical Anthropology* **99**: 571–583.

Boddington A. 1996. *Raunds Furnells: The Anglo Saxon Church and Churchyard*. English Heritage: London.

Brickley M, Howell PGT. 1999. Measurement of changes in trabecular bone structure with age in an archaeological population. *Journal of Archaeological Science* **26**: 151–157.

Brooks S, Suchey JM. 1990. Skeletal age determination based on the os pubis: a comparison of the Acsádi-Nemeskéri and Suchey-Brooks methods. *Human Evolution* **5**: 227–238.

Byers S, Moore AJ, Byard RW, Fazzalari NL. 2000. Quantitative histomorphometric analysis of the human growth plate from birth to adolescence. *Bone* **27**: 495–501.

Chappard D, Legrand E, Pascaretti C, Basle MF, Audran M. 1999. Comparison of eight histomorphometric methods for measuring trabecular bone architecture by image analysis on histological sections. *Microscopy Research and Technique* **45**: 303–312.

Compston JE, Mellish RWE, Croucher P, Newcobe R, Garrahan NJ. 1989. Structural mechanisms of trabecular bone loss in man. *Bone and Mineral* **6**: 339–350.

Ding M, Hvid I. 2000. Quantification of age-related changes in the structure model type and trabecular thickness of human tibial cancellous bone. *Bone* **26**: 291–295.

Fajardo RJ, Müller R. 2001. Three-dimensional analysis of nonhuman primate trabecular architecture using micro-computed tomography. *American Journal of Physical Anthropology* **115**: 327–336.

Fajardo RJ, Ryan TM, Kappelman J. 2002. Assessing the accuracy of high-resolution X-ray computed

tomography of primate trabecular bone by comparisons with histological sections. *American Journal of Physical Anthropology* **118**: 1–10.

Frost HM. 1990. Skeletal structural adaptations to mechanical usage (SATMU): 1. Redefining Wolff's Law: The bone modeling problem. *Anatomical Record* **226**: 403–413.

Guo XE, Kim CH. 2002. Mechanical consequence of trabecular bone loss and its treatment: a three-dimensional model simulation. *Bone* **30**: 404–411.

Herrmann B, Grupe G, Hummel S, Piepenbrink H, Schutkowski H. 1990. *Prähistorische Anthropologie. Leitfaden der Feld- und Labormethoden*. Springer-Verlag: Berlin.

Hordon LD, Raisi M, Aaron JE, Paxton SK, Beneton M, Kanis JA. 2000. Trabecular architecture in women and men of similar bone mass and with and without vertebral fracture: I. Two-dimensional histology. *Bone* **27**: 271–276.

Huiskes R. 2000. If bone is the answer, then what is the question? *Journal of Anatomy* **197**: 145–156.

İşcan MY, Loth SR. 1986. Estimation of age and determination of sex from the sternal rib. In *Forensic Osteology*, Reichs KJ (ed.). CC Thomas: Springfield, IL; 68–89.

Kappelman J. 1998. Advances in three-dimensional data acquisition and analysis. In *Primate Locomotion. Recent Advances*, Strasser E, Fleagle J, Rosenberger A, McHenry H (eds). Plenum Press: New York; 205–222.

Kobayashi S, Takahashi HE, Ito A, Saito N, Nawata M, Horiuchi H, Ohta H, Ito A, Iorio R, Yamamoto N, Takaoka K. 2003. Trabecular minimodeling in human iliac bones. *Bone* **32**: 163–169.

Kothari M, Keaveny TM, Lin JC, Newitt DC, Genant HK, Majumdar S. 1998. Impact of spatial resolution on the prediction of trabecular architecture parameters. *Bone* **22**: 437–443.

Link TM, Saborowski O, Kisters K, Kempkes M, Kosch M, Newitt D, Lu Y, Waldt S, Majumdar S. 2002. Changes in calcaneal trabecular bone structure assessed with high-resolution MR imaging in patients with kidney transplantation. *Osteoporosis International* **13**: 119–129.

Lovejoy C, Meindl RS, Pryzbeck TR, Mensforth RP. 1985. Chronological metamorphosis of the auricular surface of the ilium: a new method for the determination of adult skeletal age at death. *American Journal of Physical Anthropology* **68**: 15–28.

Macho GA, Thackeray JF. 1992. Computed tomography and enamel thickness of maxillary molars of Plio-Pleistocene hominids from Sterkfontein, Swartkrans and Kromdraai (South Africa): an exploratory study. *American Journal of Physical Anthropology* **89**: 133–143.

MacLatchy L, Müller R. 2002. A comparison of the femoral head and neck trabecular architecture of *Galago* and *Perodicticus* using micro-computed tomography (CT). *Journal of Human Evolution* **43**: 89–105.

Maggio D, Pacifici R, Cherubini A, Simonelli G, Luchetti M, Aisa MC, Cucinotta D, Adami S, Senin U. 1997. Age-related cortical bone loss at the metacarpal. *Calcified Tissue International* **60**: 94–97.

Malkin I, Karasik D, Livshits G, Kobyliansky E. 2002. Modelling of age-related bone loss using cross-sectional data. *Annals of Human Biology* **29**: 256–270.

Mays S. 2000. Age-dependent cortical bone loss in women from 18th and early 19th century London. *American Journal of Physical Anthropology* **112**: 349–361.

Ortner DJ. 2003. *Identification of Pathological Conditions in Human Skeletal Remains* (2nd edn). Academic Press: London.

Roberts C, Wakely J. 1992. Microscopical findings associated with the diagnosis of osteoporosis in palaeopathology. *International Journal of Osteoarchaeology* **2**: 23–30.

Ryan TM, Ketcham RA. 2002a. The three-dimensional structure of trabecular bone in the femoral head of strepsirrhine primates. *Journal of Human Evolution* **43**: 1–26.

Ryan TM, Ketcham RA. 2002b. Femoral head trabecular bone structure in two omomyid primates. *Journal of Human Evolution* **43**: 241–263.

Spoor F, Zonneveld FW, Macho GA. 1993. Linear measurements of cortical bone and dental enamel by computed tomography: applications and problems. *American Journal of Physical Anthropology* **91**: 469–484.

Thomsen JS, Ebbesen EN, Mosekilde LI. 2002a. Age-related differences between thinning of horizontal and vertical trabeculae in human lumbar bone as assessed by new computerized method. *Bone* **31**: 136–142.

Thomsen JS, Ebbesen EN, Mosekilde L. 2002b. Static histomorphometry of human iliac crest and vertebral trabecular bone: a comparative study. *Bone* **30**: 267–274.

Thomsen JS, Ebbesen EN, Mosekilde L. 2002c. Zone-dependent changes in human vertebral trabecular bone: clinical implications. *Bone* **30**: 664–669.

Vijayapalan V, Sutton-Smith P, Parkinson IH, Martin RB, Fazzalari NL. 2003. Trabecular rod thickness by direct measurement from 3D SEM analysis. *Anatomical Record* **271A**: 286–290.

Whitehouse WJ. 1974. The quantitative morphology of anisotropic trabecular bone. *Journal of Microscopy* **101**: 153–168.

THE ANATOMICAL RECORD PART A 288A:982–988 (2006)

Automated Method to Measure Trabecular Thickness From Microcomputed Tomographic Scans and Its Application

DANIEL J. MCCOLL,[1,2] RICHARD L. ABEL,[1,3] IAIN R. SPEARS,[2] AND GABRIELE A. MACHO[1*]

[1]Palaeoanthropology Research Group, Centre for Research in Evolutionary Anthropology, Roehampton University, London, United Kingdom
[2]Sport and Exercise Subject Group, School of Social Sciences and Law, University of Teesside, Middlesbrough, United Kingdom
[3]Department of Human Anatomy and Cell Biology, University of Liverpool, Liverpool, United Kingdom

ABSTRACT

Trabeculae form the internal bony mesh work and provide strength to the bone; interconnectivity, overall density, and trabecular thickness are important measures of the integrity of the internal architecture. Such strength is achieved only gradually during ontogeny, whereby an increase in trabecular thickness precedes an increase in mineralization. Loss of bone mass later in life may be compensated for by thickening of the remaining trabeculae. These facts, and the role of trabeculae in mineral homeostasis, highlight the importance of investigating trabecular thickness within and between species. While nondestructive imaging techniques (i.e., μCT and MRI) are becoming increasingly popular, quantification of trabecular thickness using nondestructive techniques has proved difficult owing to limitations imposed by scanning parameters, uniform thresholding, and partial volume averaging. Here we present a computer application, which aims to overcome these problems. Validation is carried out against a phantom and against trabecular thickness measured in corresponding histological sections. Good agreement was found between these measurements. Furthermore, when trabecular thickness is recorded for modern human fetal ilia, a trend toward trabecular thickness increase is found and is in line with reports of ontogenetic morphometric changes using histological sections. However, there are discrepancies. These may in part be due to partial volume effects of obliquely oriented structures. More crucial, however, are problems inherent in histological sections, e.g., shrinkage and distortion, especially where differences in mineralization are concerned; this may affect biological interpretations. Anat Rec Part A, 288A: 982–988, 2006.

Key words: trabecular thickness; μCT; pelvis; ontogenetic changes

Grant sponsor: Leverhulme Trust; Grant number: F00569C; Grant sponsor: Natural Environment Research Council; Grant number: NER/S/A/2001/06485; Grant sponsor: Joint Research Equipment Initiative; Grant number: JR99LIREQ.

*Correspondence to: Gabriele A. Macho, Centre for Research in Evolutionary Anthropology, Roehampton University, Holybourne Avenue, London SW15 4JD, United Kingdom.
Fax: 44-20-8392-3610. E-mail: g.macho@roehampton.ac.uk

Received 18 March 2006; Accepted 16 June 2006
DOI 10.1002/ar.a.20371
Published online 7 August 2006 in Wiley InterScience (www.interscience.wiley.com).

The internal architecture of bone is made up of a mesh work of bony trabeculae, which confers strength to the bone while minimizing overall bone mass. The mechanical properties of trabecular bone depend, at least in part, on trabecular thickness (Tb.Th.) (Kleerekoper et al., 1985; Swartz et al., 1998; Ulrich et al., 1999), as will, to a certain extent, physiological processes such as mineral homeostasis (Swartz et., 1998). To this end, several studies have compared Tb.Th. across extinct and extant species (Swartz et al., 1998; Fajardo and Müller, 2001; Ryan and Ketcham, 2002a, 2002b), between bones (Mullender et al., 1996; Swartz et al., 1998; Fajardo and Müller, 2001; Macho et al., 2005), during early development (Glorieux et al., 2000; Salle et al., 2002; Mulder et al., 2005; Mulder and Koolstra, 2006), and as part of the aging process (Rehman et al., 1994; Thomsen et al., 2002a, 2002b; Cvijanovic et al., 2004; Macho et al., 2005). It would appear that a minimum thickness must be attained prenatally before mineralization commences (Mulder et al., 2005; Mulder and Koolstra, 2006), while failure to achieve this minimum bone maturity before birth may result in long-term effects on bone structure and density (Backström et al., 2005). Conversely, loss of bone mass in adulthood may be compensated for by an increase in thickness of the remaining trabeculae (Frost, 1999; Macho et al., 2005; Stauber and Müller, 2006a).

Histological techniques are commonly regarded the method of choice to obtain accurate measures of trabecular architecture, despite their time-consuming and invasive nature. Alternatively, over the last few years, nondestructive visualization tools, especially μCT, have become increasingly popular for an assessment of trabecular bone morphology (Fajardo and Müller, 2001; Ryan and Ketcham, 2002a, 2002b). In order to display the trabecular arrangement and to measure Tb.Th., such studies commonly employ uniform (often arbitrary) thresholds to distinguish the bone-air boundaries. However, differences in mineralization within and between bones will result in different average CT values and uniform thresholding will thus lead to differential display of trabeculae and hence over- or underestimation of structures (Ding et al., 1999; Hara et al., 2002). Scanning parameters and voxel size (i.e., resolution), and their effects on partial volume averaging, similarly result in inaccurate measurements (Kothari et al., 1998; Banse et al., 2002; Hara et al., 2002; Kim et al., 2004). In an attempt to distinguish accurately between rods and plates, more complex algorithms have recently been developed (Stauber and Müller, 2006b), but these have not been adequately validated and the authors were content the results looked "reasonable" (p. 479) and were "intuitively correct" (p. 481). The need for an objective and repeatable method to determine trabecular measures from nondestructive techniques is thus as great as ever.

Zonneveld (1987) outlined the full-width, half-maximum-height (HMH) principle to determine the boundaries between structures. This was subsequently validated on biological specimens (Spoor et al., 1993) and the limitations, specifically with regard to the resolution of the images, were discussed. Recently, Prevrhal et al. (1999, 2003) reevaluated the protocol (referred to as 50% method by them) on a phantom and similarly demonstrated that the main confounding factor for obtaining accurate measures is the resolution. Given the high resolution of modern μCT (i.e., below the average thickness of trabeculae), it should now be possible to overcome this major limitation and to apply the HMH principle to the measurement of thin structures such as trabeculae. Here we present a computer program that automatically calculates the HMHs and trabecular thicknesses within a CT slice. The results are validated against a phantom and histological sections. Subsequently, a biological structure is evaluated and the usefulness of the technique is discussed.

MATERIALS AND METHODS

An in-house automated computer program was written in C^{++}. The program was used to collect measurements of Tb.Th. from CT slices sectioned in the plane of the original CT scan and utilized the full range of CT values (0–65,536). Pixel size/field of view was entered into the program and a transect was then sampled across the slice and subjected to a number of mathematical algorithms. First, in order to identify the peaks representing the external cortical surfaces, the difference in CT numbers between the presumptive air and the subsequent voxels along the transect were calculated. When this peak reached a level substantially higher (i.e., at least three times) than what could be considered artifact/noise, the external surfaces were identified. Second, the CT numbers between these external landmarks were searched for all maxima and minima, representing bone and nonbone, respectively (Fig. 1). Third, between adjacent peaks and troughs, the CT numbers were fitted to a cubic piecewise third-order polynomial spline. The bone-nonbone boundary was then identified using interpolation, whereby the halfway point between the maximum and minimum CT values was determined (Spoor et al., 1993). Trabecular thickness was measured as the distance along the transect between the two bone-nonbone boundaries of a single trabecula as adjusted to the spline, then outputted to an ASCII file. It was possible

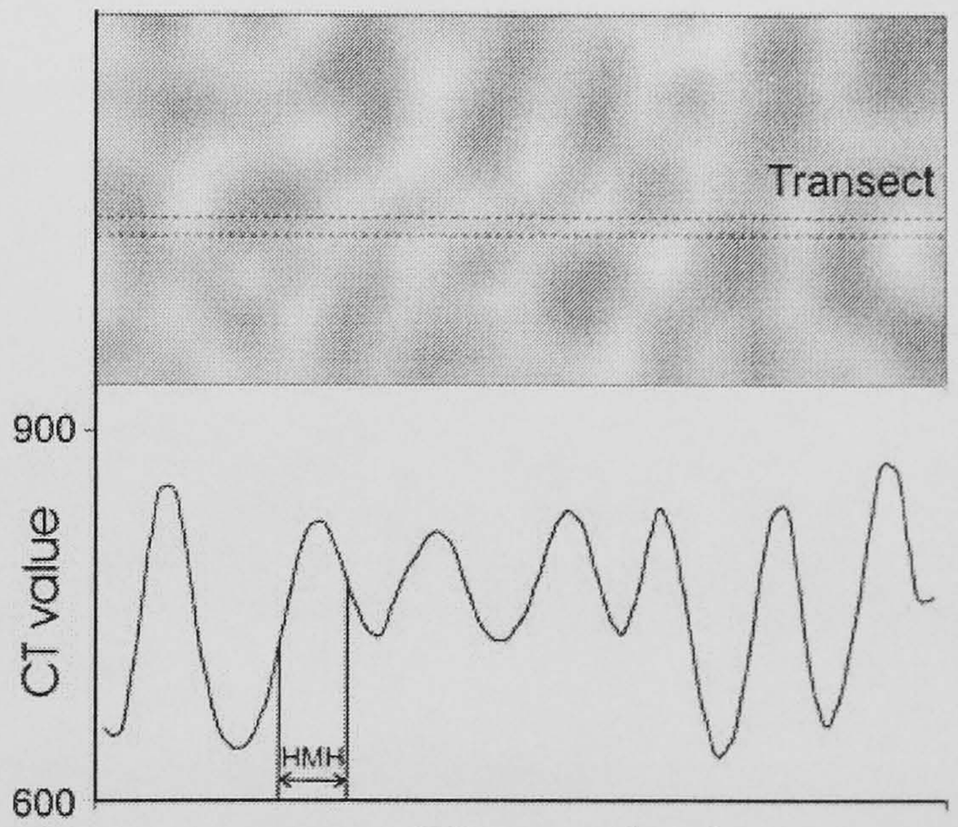

Fig. 1. A section of a typical CT image of trabecular bone is shown (top) and the CT value profile for the transect indicated above is given (bottom). For one trabecula, the HMH is identified and the width given.

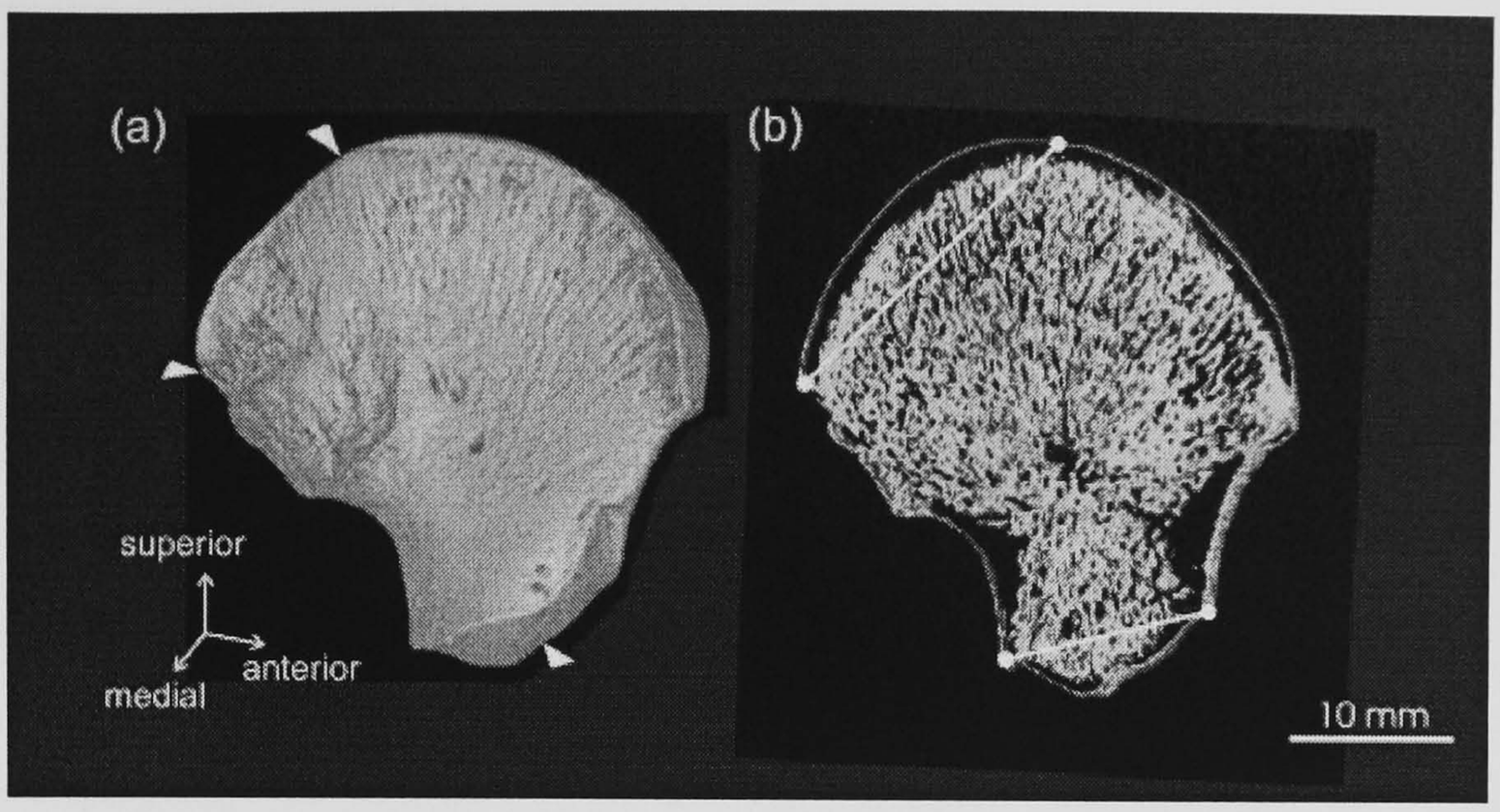

Fig. 2. Reconstruction of a fetal ilium from CT slices (**a**). Triangles denote the landmarks used to define the plane of sectioning. In **b**, a thin slice through the ilium is shown as well as the transects used for obtaining Tb.Th. measurements.

to calculate linear measurements within a single pixel width.

Microcomputed Tomography

For validation purposes, a hairbrush with synthetic bristles and an adult pig calcaneus were scanned at the University of Liverpool using an ACTIS 420/600 system (BIR, IL) equipped with a tungsten X-ray target, a 250 μm thick columnar caesium iodide scintillator, and a Toshiba AI5877 JP dual-field image intensifier. Voltage was set at 60 kV and current at 200 mA, giving an effective monochromatic X-ray energy of 30 kV. Focal spot size was 50 μm and contrast resolution was ~ 0.5%. Slice thickness and slice increment were 100 μm with a 44.91 mm field of view and a matrix size of 512 × 512, resulting in a voxel size of 80 μm × 80 μm × 100 μm. This voxel size is below the average adult trabecular thickness and below the resolution considered critical for the accurate representation of trabeculae (Kothari et al., 1998; Ding, 1999); it is also below the size of the bristles. The bristles of the brush and the presumed long axes of trabecular bones were oriented perpendicularly to the beam, thus ensuring maximum resolution in the section analyzed (Kothari et al., 1998). Stacks made up of two-dimensional μCT slices were used to produce a three-dimensional reconstruction of the bristles and the calcaneus using VGStudio MAX v1.1 (employing a maximum-intensity projection reconstruction algorithm).

In order to test the usefulness of the automated measures further, the program was subsequently applied to a cross-sectional series of modern human fetal ilia. Thirty-eight specimens of known sex, aged 16–36 weeks at 4-week intervals, originated from a Liverpool workhouse at the turn of the 19th–20th century and are held in the Department of Human Anatomy and Cell Biology, Liverpool. The specimens were stillbirths and the age was originally ascertained to the nearest months according to the mother's testimony. Specimens had been defleshed using bicuspid beetles and stored wrapped in newspaper without further treatment. All specimens were kept under the same conditions and, although postmortem alterations cannot be ruled out, these biases would be internally consistent across specimens. All bones were available for study, but the ilia were chosen because of their unusual principal alignment of trabeculae, i.e., fan-shaped, and because of the great interest in the ilium in clinical research, i.e., biopsies. The principal orientation of trabeculae was established through radiographs, although in more mature specimens it can always be predicted from the main direction of load transfer, bearing in mind that trabeculae align along the main axis of stress (Biewener et al., 1996; Gefen and Seliktar, 2004). Scan parameters for the ilia were effectively the same as those stated above for the pig calcaneus except for voltage (40–60 kV), current (140–200 mA), effective monochromatic X-ray energy (20–30 kV), and voxel size of 40 μm × 40 μm × 100 μm for smaller (younger) specimens and 60 μm × 60 μm × 100 μm for larger (older) specimens. The resolution chosen was considered sufficient given that fetal trabeculae were reported to range from 45 to 118.2 μm in thickness (Salle et al., 2002; Nuzzo et al., 2003). Measures of Tb.Th. were collected from two transects, one superior and one inferior (Fig. 2) in a plane defined by the posterior superior iliac spine, the point where the iliac crest meets the posterior iliac buttress and the acetabular notch; these landmarks are commonly used in the anthropological literature (Scheuer and Black, 2000). These transects were chosen to ascertain the average Tb.Th. (i.e., close to the primary ossification center and toward the epiphysis at the iliac crest) rather than to answer a specific biological question.

Histomorphometric Analysis

Ten slices of 50 μm thickness were cut from the previously scanned calcaneus in the coronal plane using a diamond saw. A mark made at the level of the first scan was used as a guide for obtaining the first histological section; this should ensure minimal difference in plane of section between scans and histology. Sections were

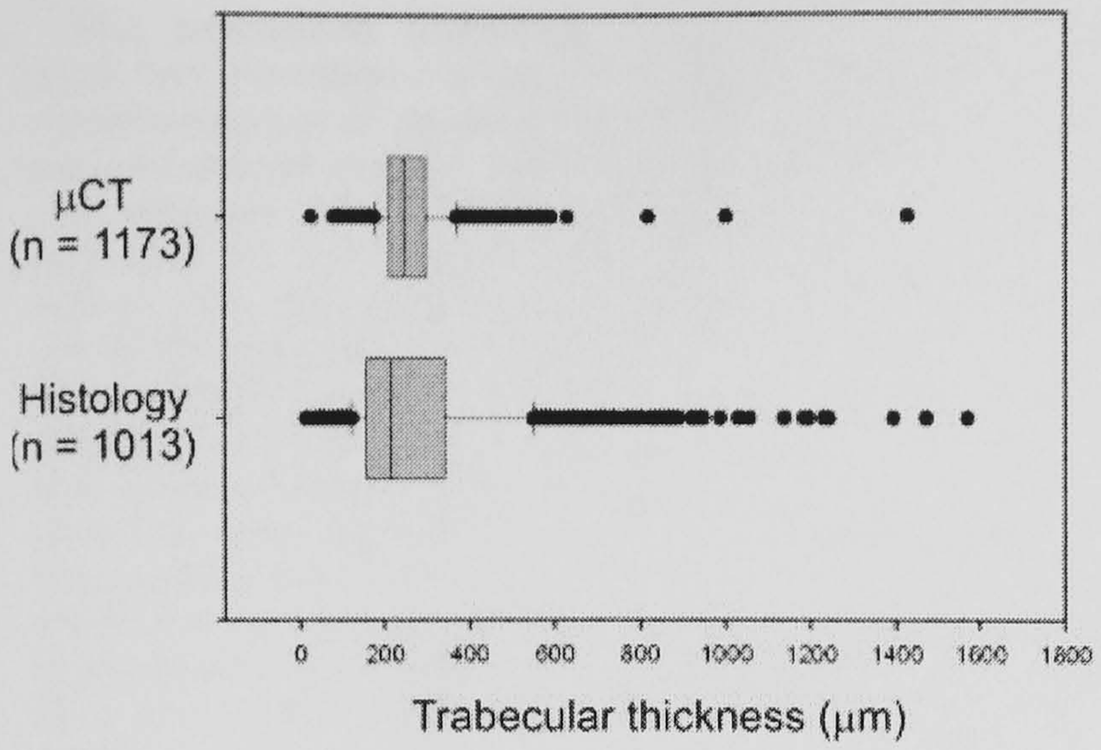

Fig. 3. Box plot of trabecular thicknesses obtained by different methods (black line = mean value; box = 50% of data; bars = 75% of data; additional points are considered outliers).

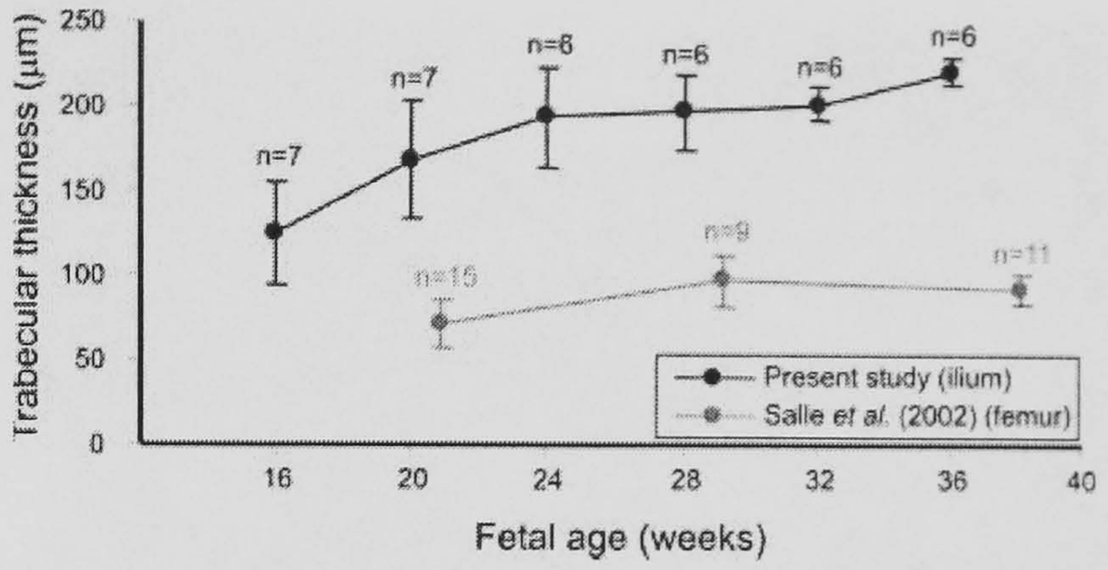

Fig. 4. Data of average trabecular thickness are given for human fetal ilia (present study) and for femora (Salle et al., 2002).

then removed with minimal bone loss. Sections were decalcified and stained with eosin red (1% solution) for 15 min. Subsequently, sections were washed in distilled water to remove any loose particles and were dehydrated in 70% ethanol. The stained specimens were immediately photographed before further shrinkage could occur with a slide scale using a Nikon Coolpix 990 camera (Nikon, Tokyo, Japan) mounted on an Olympus SZH-ILLO microscope (Olympus Optical, Tokyo, Japan). Linear measurements of Tb.Th. were taken from photos of the histological region of interest (pixel size = 5 μm) following the line-intercept method (Underwood, 1970). Ten transects were taken through each of the 10 histological slices analyzed. Statistical analyses were carried out using SPSS version 12.

RESULTS

The accuracy of measurements taken by the computer program was first assessed against the phantom with known dimensions. Forty bristles of the brush were measured with digital callipers, resulting in an average thickness of 0.468 ± 0.013 mm. The average thickness obtained by the automated method was 0.464 ± 0.036 and deviated from the actual measurements by less than 1%; these differences are not statistically significant. While this good correspondence between results is encouraging, it needs to be considered that biological specimens differ in material properties and geometry and may display less well-defined boundaries. To validate the automated program, comparisons were first carried out between automated HMH measurements taken from transects through a pig calcaneus and histomorphometric measures taken from comparable histological slices of the same specimen.

Variation in Tb.Th. was higher when histomorphometric techniques were employed ($t = 3.286$; $P = 0.001$). The statistically significant difference between the samples is reflected in the histomorphometrically derived data being 13% lower than those taken automatically from CT images (Fig. 3).

In order to test for the applicability of the automated method for biological purposes, the program was applied to a cross-sectional series of modern human fetal ilia. No statistically significant differences in mean Tb.Th. were found between sexes or between transects for each subset. However, there is a trend for trabecular thickness to increase from an average of 99 μm in the youngest specimens to 240 μm in the oldest (Fig. 4). These results are statistically significant ($F = 11.850$; $P = 0.000$), mainly due to the youngest and, to a lesser extent, the oldest group according to the Tukey HSD postdoc test. When compared with similar-aged data presented for histological sections of femora (Salle et al., 2002), the trends are comparable, but the absolute values differ considerably.

DISCUSSION

Although nondestructive techniques are becoming increasingly popular in addressing biological questions with regard to bone structure and integrity, an accurate appraisal of Tb.Th. is problematic due to limitations associated with uniform thresholding, partial volume averaging, and voxel size (Kothari et al., 1998; Ding et al., 1999; Hara et al., 2002, Kim et al., 2004). For many biological investigations, and especially for clinical applications, researchers tend to be satisfied with high correlations between histological measures and those taken from CT images (Thomsen et al., 2004; Chappard et al., 2005), rather than accurate measures. However, even though the errors may be regarded systematic if the correlation coefficients are relied on, further biological investigations, such as structural and biomechanical assessments, may be hampered (Tabor, 2006). The present study aimed to overcome these fundamental problems and explored the usefulness of the HMH method (Zonneveld, 1987; Spoor et al., 1993; Prevrhal et al., 1999) for the determination of Tb.Th. Owing to the high resolution of present-day μCT, this should no longer be a problem.

When the data collected are compared with the results of a phantom, whose width has been measured manually, good agreement was found and the error was less than 1%. This would argue for the accuracy and applicability of the software presented here. The somewhat higher standard deviation for the CT measurements could be the result of slight obliquity of the bristles with regard to the transect in some instances; in contrast, the physical measurements are always perpendicular to the long axis of the bristle shaft. However, when examining biological structures, the findings are more complex.

The automated technique consistently gave higher (and less variable) values for Tb.Th. compared to the histomorphometric measurements. For example, the lowest histomorphometric measurement of Tb.Th. was 16 μm, whereas that of the automated computer program was only 27 μm (Fig. 3). Previous studies have highlighted the effects of partial volume averaging on an overestimation of structures (Müller et al., 1996; Kothari et al., 1998). Although the high resolution of the images employed in this study would generally argue against this having been a major problem here, it is recognized that this may have affected the measurements of very thin structures. Perhaps more important, though, the thickness measurements made in this study are one-dimensional and, despite attempts to align the bones so that the predominant orientation of trabecular is perpendicular to the scan, this is not possible for the ilium. This bone exhibits a fanned distribution of trabeculae (Fig. 2), and the obliquity in measurements may have led to an overestimation of dimensions. Trabeculae of the pig calcaneus are aligned more parallel and the automated measurement was therefore probably less affected by this one-dimensional error. Nonetheless, deviation in measurements obtained remain between the techniques. On initial inspection, this casts doubts on the usefulness of the automated method presented here, especially as regards the measures taken for the ilia (Fig. 4).

Trabecular thickness in the ilia appears to be substantially higher in the cross-sectional fetal sample than it is for similar-aged femora (Salle et al., 2002). To explain these discrepancies, a number of issues should be considered. First, it needs to be borne in mind that trabeculae differ in thickness between bones, even within the same individual (Macho et al., 2005). Such differences are probably functionally related, and it is conceivable that muscular-related biomechanical constraints experienced intrauterine could similarly account for differences in Tb.Th. between femora and ilia. Second, and probably of greater significance, the method employed for collecting Tb.Th. differed between the present study and that of Salle et al. (2002). While the former took direct measurements of individual trabeculae, the latter employed the parallel-plate model (Parfitt et al., 1983) to obtain trabecular dimensions. It has, however, been long known that the parallel-plate model consistently, and considerably, underestimates trabecular thickness (Birkenhager-Frenkel et al., 1988; Ding and Hvid, 2000). Third, problems associated with histological sections may have further exacerbated the trends toward overall thinner trabeculae reported for the histological sections, both for the pig calcaneus measured here for validation and the Tb.Th. of the fetal sample presented in Figure 4.

Preparation of histological sections involves a number of processes, e.g., cutting, embedding, decalcification, staining, and dehydration, which will lead to alterations of the tissue. As a case in point, Uchiyama et al. (1997) reported 25% shrinkage perpendicular to and about 6% parallel to the cutting knife, while the figures given in the older literature are even higher (Lane and Ralis, 1983). Fixation, dehydration, and embedding will have an additional effect (Ferguson et al., 1999). Perhaps even more problematic for the present investigation (or any study that involves immature bone) are reports that

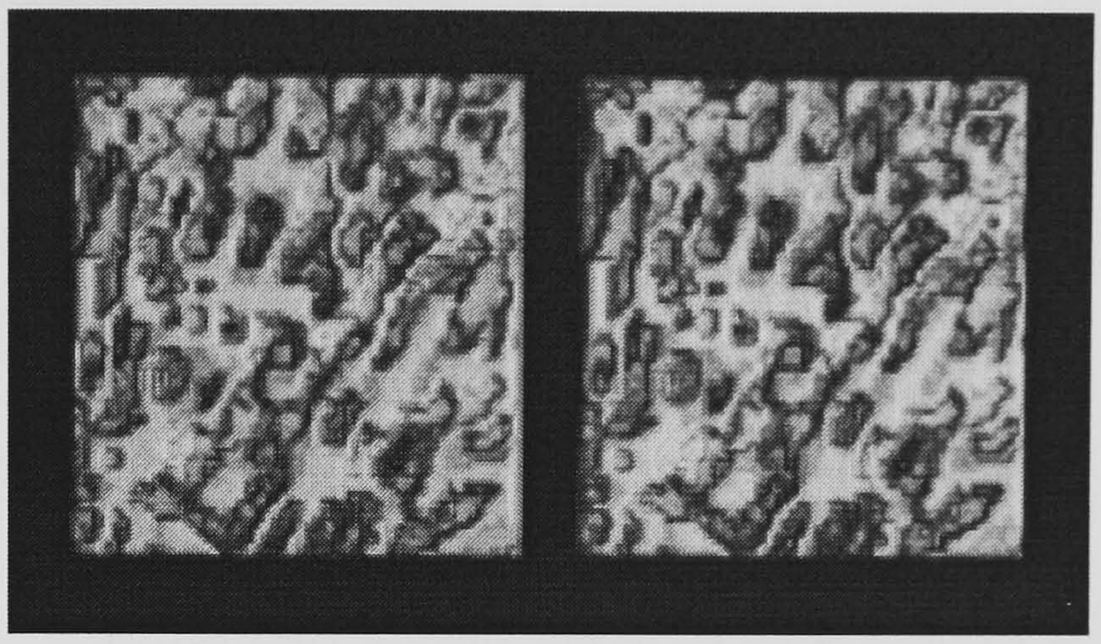

Fig. 5. Stereoimages of trabecular architecture at the iliac crest of a 36-week-old fetus.

cartilaginous tissue may shrink to up to 50% (Ferguson et al., 1999). In light of these considerations, the 13% differences between CT-derived Tb.Th. and those derived histologically for the pig calcaneus seem negligible and may be the result of histological preparation rather than the potential inaccuracies of our automated technique. This discrepancy could probably have been reduced, or even eliminated, if the tissue had not been decalcified (Buesche et al., 2006). Hence, while the discrepancies can be explained and do not invalidate the program presented here, more fundamental issues are raised by the present findings, especially when histological sections are used as the gold standard.

For ontogenetic studies, the lower mineralization of bone (Mulder et al., 2005; Mulder and Koolstra, 2006) would be expected to lead to greater shrinkage (and artifacts) in histological sections compared with measures taken from μCT. This may lead to an inaccurate assessment of the maturity of the specimens. Where clinical studies are concerned, the incompatibility of measures taken from biopsies vis-à-vis those obtained through imaging techniques (Fox et al., 2005) may render invalid any appraisal of the functional properties of the tissue investigated. The same argument may apply to functional analyses of bone from extant and extinct species (Ryan and Ketcham, 2005). In other words, without due regard of the limitations inherent in histological techniques (either preparation or measuring), the results obtained may not be comparable between studies while rendering some of the functional interpretations questionable. Histological sections provide invaluable information, which cannot be gleaned by other methods, but caution must be exercised when using histological data for purposes for which they were not intended (e.g., biomechanical assessment). Conversely, the method presented here has the advantage that structural measures of trabeculae can be obtained accurately (and noninvasively), irrespective of differences in the properties of the tissue. Provided the resolution of the images is high and below that of the average structure to be measured, the HMH method appears suitable for the determination of trabecular thickness. However, this is only the first step toward analyses of bone structure.

Although Tb.Th. is of paramount importance for an assessment of trabecular architecture and bony integrity, it constitutes only one aspects. Interconnectivity,

overall density, and structural characteristics, such as plates and rods, are of similar or even greater significance. While the program presented here was specifically designed to obtain Tb.Th. measures, it can also be used to create a more realistic representation of the trabecular architecture. By determining the HMH values across every row of pixels, the appropriate bone-specific threshold can be determined easily and efficiently, while areas of very disparate average HMH values can be easily found and excluded from the area of interest. This allows the entire bone structure to be visualized and analyzed further. Figure 5 shows the trabecular architecture in a small block of the fetal ilium; transverse trabeculae can be seen clearly, although plates have not yet developed. This further highlights the usefulness of the technique presented here and, with further modification, may provide an effective tool for three-dimensional analysis of irregular trabeculae.

ACKNOWLEDGMENTS

This study was supported by a Joint Research Equipment Initiative (JREI) grant (JR99LIREQ; to G.A.M.), a Leverhulme Trust grant (F00569C; to G.A.M. and I.R.S.), and a Natural Environment Research Council studentship (NER/S/A/2001/06485; to R.L.A.). The help of Professor J.A. Gallagher and Mrs. Brenda Wlodarski with the histological sections is greatly appreciated. The comments of two anonymous reviewers improved an earlier version of the manuscript.

LITERATURE CITED

Backström MC, Kuusela AL, Koivisto AM, Sievänen H. 2005. Bone structure and volumetric density in young adults born prematurely: a peripheral quantitative computed tomography study. Bone 36:688–693.

Banse X, Devogelaer JP, Grynpas M. 2002. Patient-specific microarchitecture of vertebral cancellous bone: a peripheral quantitative computed tomographic and histological study. Bone 30:829–835.

Biewener AA, Fazzalari NL, Konieczynski DD, Baudinette RV. 1996. Adaptive changes in trabecular architecture in relation to functional strain patterns and disuse. Bone 19:1–8.

Birkenhager-Frenkel DH, Courpron P, Hupscher EA, Clermonts E, Coutinho MF, Schmitz PI, Meunier PJ. 1988. Age-related changes in cancellous bone structure: a two-dimensional study in the transiliac and iliac crest biopsy sites. Bone Miner. 4:197–216.

Buesche G, Georgii A, Kreipe H-H. 2006. Diagnosis and quantification of bone marrow fibrosis are significantly biased by the prestaining processing of bone marrow biopsies. Histopathology 48: 133–148.

Chappard D, Guggenbuhl P, Legrand E, Baslé MF, Audran M. 2005. Texture analysis of X-ray radiographs is correlated with bone histomorphometry. J Bone Miner Metab 23:24–29.

Cvijanovic O, Bobinac D, Zoricic S, Ostojic Z, Maric I, Crncevic-Orlic Z, Kristofic I, Ostojic L. 2004. Age- and region-dependent changes in human lumbar vertebral bone: a histomorphometric study. Spine 29:2370–2375.

Ding M, Odgaard A, Hvid I. 1999. Accuracy of cancellous bone volume fraction measured by micro-CT scanning. J Biomech 32:323–326.

Ding M, Hvid I. 2000. Quantification of age-related changes in the structure model type and trabecular thickness of human tibila cancellous bone. Bone 26:291–295.

Fajardo RJ, Müller R. 2001. Three-dimensional analysis of nonhuman primate trabecular architecture using micro-computed tomography. Am J Phys Anthropol 115:327–336.

Ferguson SJ, Bryant JT, Ito K. 1999. Three-dimensional computational reconstruction of mixed anatomical tissues following histological preparation. Med Eng Phys 21:111–117.

Fox J, Miller MA, Recker RR, Bare SP, Smith SY, Moreau I. 2005. Treatment of postmenopausal osteoporotic women with parathyroid hormone 1-84 for 18 months increases cancellous bone formation and improves cancellous architecture: a study of iliac crest biopsies using histomorphometry and micro computed tomography. J Musculoskelet Neuronal Interact 5:356–357.

Frost HM. 1999. On the trabecular "thickness"-number problem. J Bone Min Res 14:1816–1821.

Gefen A, Seliktar R. 2004. Comparison of the trabecular architecture and the isostatic stress flow in the human calcaneus. Med Eng Phys 26:119–129.

Glorieux FH, Travers R, Taylor A, Bowen JR, Rauch F, Norman M, Parfitt AM. 2000. Normative data for iliac bone histomorphometry in growing children. Bone 26:103–109.

Hara T, Tanck E, Homminga J, Huiskes R. 2002. The influence of microcomputed tomography threshold variations on the assessment of structural and mechanical trabecular bone properties. Bone 31:107–109.

Kim DG, Christopherson GT, Dong XN, Fyhrie DP, Yeni YN. 2004. The effect of microcomputed tomography scanning and reconstruction voxel size on the accuracy of stereological measurements in human cancellous bone. Bone 35:1375–1382.

Kleerekoper M, Villanueva AR, Stanciu J, Rao DS, Parfitt AM. 1985. The role of three-dimensional trabecular microstructure in the pathogenesis of vertebral compression fractures. Calcif Tissue Int 37:594–597.

Kothari M, Keaveny TM, Lin JC, Newitt DC, Genant HK, Majumdar S. 1998. Impact of spatial resolution on the prediction of trabecular architecture parameters. Bone 22:437–443.

Lane J, Ralis ZA. 1983. Changes in dimensions of large cancellous bone specimens during histological preparation as measured on slabs from human femoral heads. Calcif Tissue Int 35:1–4.

Macho GA, Abel RL, Schutkowski H. 2005. Age changes in bone microstructure: do they occur uniformly? Int J Osteoarch 15:421–430.

Mulder L, Koolstra JH, Weijs WA, van Eijden TM. 2005. Architecture and mineralization of developing trabecular bone in the pig mandibular condyle. Anat Rec 285A:659–667.

Mulder L, Koolstra JH. 2006. Architecture and mineralization of developing cortical and trabecular bone of the mandible. Anat Embryol 211:71–78.

Mullender MG, Huiskes R, Versleyen H, Buma P. 1996. Osteocyte density and histomorphometric parameters in cancellous bone of the proximal femur in five mammalian species. J Orthop Res 14: 972–979.

Müller R, Koller B, Hildebrand T, Laib A, Gianolini S, Ruegsegger P. 1996. Resolution dependency of microstructural properties of cancellous bone based on three-dimensional mu-tomography. Technol Health Care 4:113–119.

Nuzzo S, Meneghini C, Braillon P, Bouvier R, Mobilio S, Peyrin F. 2003. Microarchitectural and physical changes during fetal growth in human vertebral bone. J Bone Miner Res 18:760–768.

Parfitt AM, Mathews CHE, Villanueva AR, Kleerekoper M, Frame B, Rao DS. 1983. Relationships between surface, volume, and thickness of iliac trabecular bone in aging and in osteoporosis. J Clin Invest 72:1396–1409.

Prevrhal S, Engelke K, Kalender W. 1999. Accuracy limits for the determination of cortical width and density: the influence of object size and CT imaging parameters. Phys Med Biol 44:751–764.

Prevrhal S, Fox JC, Shepherd JA, Genant HK. 2003. Accuracy of CT-based thickness measurement of thin structures: modeling of limited spatial resolution in all three dimensions. Med Phys 30:1–8.

Rehman MT, Hoyland JA, Denton J, Freemont AJ. 1994. Age related histomorphometric changes in bone in normal British men and women. J Clin Pathol 47:529–534.

Ryan TM, Ketcham RA. 2002a. The three-dimensional structure of trabecular bone in the femoral head of strepsirrhine primates. J Hum Evol 43:1–26.

Ryan TM, Ketcham RA. 2002b. Femoral head trabecular bone structure in two omomyid primates. J Hum Evol 43:241–263.

Ryan TM, Ketcham RA. 2005. Angular orientation of trabecular bone in the femoral head and its relationship to hip joint loads in leaping primates. J Morphol 265:249–263.

Salle BL, Rauch F, Travers R, Bouvier R, Glorieux FH. 2002. Human fetal bone development: histomorphometric evaluation of the proximal femoral metaphysis. Bone 30:823–828.

Scheuer L, Black S. 2000. Developmental juvenile osteology. Academic Press: London.

Spoor CF, Zonneveld FW, Macho GA. 1993. Linear measurements of cortical bone and dental enamel by computed tomography: applications and problems. Am J Phys Anthropol 91:469–484.

Stauber M, Müller R. 2006a. Age-related changes in trabecular bone microstructures: global and local morphometry. Osteoporos Int 17:616–626.

Stauber M, Müller R. 2006b. Volumetric spatial decomposition of trabecular bone into rods and plates: a new method for local bone morphometry. Bone 38:475–484.

Swartz SM, Parker A, Huo C. 1998. Theoretical and empirical scaling patterns and topological homology in bone trabeculae. J Exp Biol 201:573–590.

Tabor Z. 2006. Estimating structural properties of trabecular bone from grey-level low-resolution images. Med Eng Phys (in press).

Thomsen JS, Ebbesen EN, Mosekilde L. 2002a. Static histomorphometry of the human iliac crest and vertebral trabecular bone: a comparative study. Bone 30:267–274.

Thomsen JS, Ebbesen EN, Mosekilde L. 2002b. Zone-dependent changes in human vertebral trabecular bone: clinical implications. Bone 30:664–669.

Thomsen JS, Laib A, Koller B, Prohaska S, Mosekilde LI, Gowin W. 2004. Stereological measures of trabecular bone structure: comparison of 3D micro computed tomography with 2D histological sections in human proximal tibial bone biopsies. J Microscopy 218: 171–179.

Uchiyama T, Tanizawa T, Muramatsu H, Endo N, Takahashi HE, Hara T. 1997. A morphometric comparison of trabecular structure of human ilium between microcomputed tomography and conventional histomorphometry. Calcif Tissue Int 61:493–498.

Ulrich D, van Rietbergen B, Laib A, Ruegsegger P. 1999. The ability of three-dimensional structural indices to reflect mechanical aspects of trabecular bone. Bone 25:55–60.

Underwood E. 1970. Quantitative stereology. Reading, MA: Addison-Wesley.

Zonneveld FW. 1987. Computed tomography of the temporal bone and orbit. München: Urban und Schwarzenberg.